PB90-226960
UILU-ENG-89-2006

CIVIL ENGINEERING STUDIES
STRUCTURAL RESEARCH SERIES NO. 552

ISSN: 0069-4274

TORSIONAL EFFECTS IN STRUCTURES SUBJECTED TO STRONG GROUND MOTION

By

Shi Lu
and
William J. Hall

A Technical Report of Research
Supported by the
NATIONAL SCIENCE FOUNDATION
Under Grant Nos. DFR 84-19191, CES 88-03920
and BCS 88-03920
and
THE DEPARTMENT OF CIVIL ENGINEERING

DEPARTMENT OF CIVIL ENGINEERING
UNIVERSITY OF ILLINOIS
AT URBANA-CHAMPAIGN
URBANA, ILLINOIS

APRIL 1990

TORSIONAL EFFECTS IN STRUCTURES SUBJECTED TO STRONG GROUND MOTION

by

SHI LU
and
WILLIAM J. HALL

A Technical Report of Research Supported by the

NATIONAL SCIENCE FOUNDATION
Under Grant Nos. DFR 84-19191, CES 88-03920 and BCS 88-03920

and

THE DEPARTMENT OF CIVIL ENGINEERING

Department of Civil Engineering
University of Illinois at Urbana-Champaign
Urbana, Illinois
April 1990

50272-101

REPORT DOCUMENTATION PAGE	1. REPORT NO. UILU-ENG-89-2006	2.	3. Recipient's Accession No.
4. Title and Subtitle TORSIONAL EFFECTS IN STRUCTURES SUBJECTED TO STRONG GROUND MOTION			5. Report Date April 1990
			6.
7. Author(s) Shi Lu and William J. Hall			8. Performing Organization Rept. No. SRS 552
9. Performing Organization Name and Address University of Illinois at Urbana-Champaign Department of Civil Engineering 205 N. Mathews Avenue Urbana, Illinois 61801			10. Project/Task/Work Unit No.
			11. Contract(C) or Grant(G) No. (C) DFR 84-19191 (G) CES 88-03920 BCS 88-03920
12. Sponsoring Organization Name and Address National Science Foundation, Washington, D.C., 20550 and The Department of Civil Engineering, UIUC Urbana, Illinois 61801			13. Type of Report & Period Covered
			14.

15. Supplementary Notes

16. Abstract (Limit: 200 words)

The purpose of this study was to increase the understanding of torsional behavior in low-rise frame buildings and to assess its importance in the gross response of such buildings.

One aspect of this investigation centered on understanding the strong coupling between translational and torsional response with closely spaced frequencies (including the beating phenomenon arising from modal instability); this study is believed to be the first conclusive theoretical demonstration of the beating phenomenon arising in the manner noted. It was found that the dynamic amplification factor in torsion (as measured by static eccentricity) was about 2.5.

With the use of a theoretical model encompassing nonlinear material behavior, it was possible to predict the torsional effects in two low-rise buildings and to compare such results with response data recorded in these buildings in the 1987 Whittier Narrows Earthquake. The low-rise moment-resisting frame-building studies indicated that the fundamental frequencies identified earlier herein are usually not well separated, and if possible, to prevent damage arising from torsion (usually late in the response process), the translational frequency should be kept smaller in relation to the torsional frequency, to ensure that the fundamental translational mode is dominant.

17. Document Analysis a. Descriptors

Seismic, Earthquake Resistant Design, Torsion, Dynamic Response

b. Identifiers/Open-Ended Terms

c. COSATI Field/Group

18. Availability Statement	19. Security Class (This Report)	21. No. of Pages
Release Unlimited	Unclassified	201
	20. Security Class (This Page) Unclassified	22. Price A10

(See ANSI-Z39.18) See Instructions on Reverse

OPTIONAL FORM 272 (4-77)
(Formerly NTIS-35)
Department of Commerce

ABSTRACT

TORSIONAL EFFECTS IN STRUCTURES SUBJECTED TO STRONG GROUND MOTION

Shi Lu, Ph.D.
Department of Civil Engineering
University of Illinois at Urbana–Champaign, 1990
Professor William J. Hall, Advisor

The dynamic characteristics and torsional behavior of structures during strong ground motion were investigated; both linear and nonlinear material behavior were considered. Emphasis was placed on the strong torsional coupling associated with the beating phenomenon in the seismic response of structures with small static eccentricity and closely spaced frequencies. In order to study the response of structures subjected to complex loading histories, structural models were analyzed through the use of a numerical procedure (Newmark's β method) combined with a generalized nonlinear material model in the force–displacement space. Parametric studies were made for the dynamic amplification of the torsional response of simple structural systems. An amplification factor of about 2.5 was observed for static eccentricity in structural response arising from earthquake ground excitation.

To further comprehend the torsional effects in low–rise structures, two buildings that were extensively instrumented during the 1987 Whittier Narrows Earthquake were analyzed in the light of the seismic requirements in the current building codes. The theoretical demonstration of the beating phenomenon was confirmed by the field recordings in the symmetric steel moment–resisting–frame structure with closely spaced frequencies; similar confirming results were obtained for the other structure. The behavior and response of the two structures were observed to be somewhat different from that envisioned and assumed by the direct design procedure employed by the codes. Some suggestions for improvement in building code provisions are offered.

ACKNOWLEDGEMENTS

This report was prepared as a doctoral dissertation by Mr. Shi Lu and submitted to the Graduate College of the University of Illinois at Urbana-Champaign in partial fulfillment of the requirements for the degree of Doctor of Philosophy in Civil Engineering. The thesis was completed under the supervision of Professor William J. Hall.

This research study was made possible through the research grants sponsored by the National Science Foundation (NSF). The financial support from NSF under Grants DFR 84-19191, "Studies Towards New Seismic Design Approaches," and CES-8803920 and BCS 8803920, "Torsional Response of Low-Rise Buildings during the 1987 Whittier Narrows Earthquake" is gratefully appreciated. Any findings or recommendations in this report are those of the authors and do not necessarily reflect the views of the sponsor.

The authors are especially appreciative to the contributions, advice and comments provided by Professor Arthur R. Robinson throughout the study. Also the authors wish to express the sincere thanks to Professors David A. W. Pecknold and Mete A. Sozen for their continuous interest, constructive assistance, suggestions and comments. Special acknowledgement is given to Drs. J. Bonacci, S. Schiff and D. Segal, Messrs. C-H Chen, C. Deel and C-J Xu, and many others in the Department of Civil Engineering for the valuable discussions at various stages of this research.

The numerical results and graphical plots were obtained using the Apollo Work-station Network of the Department of Civil Engineering. The authors gratefully acknowledges the usage of these computer facilities and the technical support provided by M. A. Berg, M. Keppel, L. Ray and S. Warsaw.

TABLE OF CONTENTS

LIST OF TABLES

LIST OF FIGURES

CHAPTER 1

INTRODUCTION

1.1 General Observations and Objectives of Research

In spite of the extensive research on engineered buildings subjected to strong ground motion, the role of torsional effects in the response and its significance in practical design have received limited study. The relatively small amount of research has been, in part, a result of the difficulty in studying this complex topic. Research results, as well as observations from recent earthquakes, have suggested that seismic ground motion often causes structures to respond torsionally, and that building damage has been associated to some degree with the torsional mode of response in some cases. In addition to structural response estimated by using the conventional planar analysis procedures, a significant amount of deformation and accompanying force in individual members may develop as a result of the torsional motion experienced by structures subjected to earthquake loadings, should it occur.

Numerous references [21, 29, 42, 59] in earthquake observations reported obvious torsion in structural response. For example, Dr. A. Zeevaert Wolff's commentary [59] on the 1985 Earthquake in Mexico City, stated the following.

> *"During the inspection of damaged buildings that I performed after the earthquake, all kinds of failure were observed: ground failure, pile failure, foundation failure, column, beam and torsion failures, and the general torsion of structures even though symmetrical in both orthogonal directions. Symmetrical buildings experience torsion. We felt a torsion movement of the LAT (Latino Americana Tower) during the earthquake of September 19. ...... In my opinion the possible movement of the center of torsional resistance should be carefully studied. Many of Mexico City's failures were in this mode."*

Although coupled torsional motion with translational motions has been the topic of limited research on structures for many years, the effects of structural torsion are not well understood from an analytical or design point of view. The role of torsion in the gross structural response to strong ground motion still is not clear. Thus far there has not been evidence that torsion is the initial causative source for structural failures. Nevertheless in examining buildings after major seismic events observers seem to believe they see evidence of torsional response that may have occurred during ground excitation. Thus it is important to increase our understanding of the torsional behavior of structures.

In the light of the aforementioned observations it was decided that this investigation should concentrate study on: (1) strong torsional coupling in the beating phenomenon, (2) development of a generalized nonlinear material model, (3) parametric studies of dynamic effects of torsion and static eccentricity, and (4) analysis of two low–rise buildings that were extensively instrumented during The 1987 Whittier Narrows Earthquake. The underlying goal of this study was to provide suggestions for design and analysis of low–rise buildings subjected to strong seismic motion.

The general effects of torsional response can be pictured rather easily. Structural torsion can occur as a result of the physical eccentricities in structures and asymmetric strength changes or damage to structural members. Torsion produces its most severe effects on the structural members far away from the centers of rigidity. On the one hand, torsion will increase the shear force in the peripheral members in addition to the lateral shear arising from seismic ground motion. On the other hand, excessive rotation of stiff floor diaphragms could result in large deformation in the peripheral members and damage those with relatively low strength. Thus, such damage reduces not only the torsional stiffness but also the lateral stiffness of the structural system. If the intensity of the earthquake shaking continues for some time, more deformation and damage of structural members and contents of the building can be expected. This progressive, torsionally–induced loss of stiffness is dangerous and should be prevented.

In the response of buildings subjected to ground motion, structural torsion can arise from many different sources. The most obvious cause is that there exists physical eccentricity between centers of mass and rigidity on any floor diaphragm of a structure. As a consequence, equivalent torsional moments exist within the floor diaphragms. When the structure responds dynamically to ground excitation, torsional effects could be amplified. On the other hand, even a structure with coincident centers of mass and rigidity, after several cycles of motion, may start to experience significant torsional response resulting from slight strength asymmetry as a consequence of light damage (yielding) of some of the structural resisting elements. As will be shown in Chapter 2, a structure may undergo unavoidable torsional vibration when the lateral and torsional frequencies of the structure are very close, through the transfer of part of the imparted energy to torsional motion from translational motions.

In addition, other parameters can contribute to strong torsional response in structures as well, e.g., the difference in yield strength of structural members, the elongation and shifting of fundamental frequencies of a structure, the torsion in one story due to the torsional response of other stories, nonuniform soil–structure interaction, etc. Other causes, such as phase differences in translational ground motions, the torsional component in ground motion input, or the uncertainties in determining the strength and stiffness of structural elements, also can lead to torsional vibration of structures. The latter effects are commonly handled through provision for "accidental" torsion as opposed to "computed or calculated" torsional effects accounting for off center masses.

Now, the question to answer is whether or not these effects are properly accounted for in design through the provisional regulations. Other equally important questions concern the significance of torsional response. Will the torsional vibration be so strong that it may be the direct cause of failure of a building? Does the current design practice provide enough margin of safety to cover the occurrence of torsional phenomena in structures? If new and better design approaches are to be developed, it is necessary for the profession to gain understanding of the torsional effects in the total response of buildings subjected to seismic ground motion.

1.2 Background

In the last twenty years, many investigators have undertaken research on the coupled lateral–torsional elastic response of structures subjected to earthquakes. Numerous studies have been conducted to investigate the linear–elastic response of asymmetric systems. Many of the parameters responsible for strong structural response in these linear–elastic systems have been identified.

In seismic design, however, the practicing engineer is required to design a structure to be strong enough to withstand the dynamically induced forces and deformations (to protect the contents), and yet to provide a structure to be flexible enough to minimize the design forces and the design costs. The present design philosophy may be summarized as follows: (1) structures are able to survive a strong earthquake without life–endangering collapse while allowing structural damage; (2) structures are able to sustain a moderate earthquake without structural damage; and (3) structures are able to resist small earthquakes without any damage. These criteria are based partly on economics, partly on the concept of controlled deformation (and energy absorption), and with consideration of acceptable risk. The idea is to allow the structure to deform beyond the linear–elastic range and to absorb energy hysteretically in the nonlinear range, which requires considerable ductility in the structural members.

In the Tentative Provisions for the Development of Seismic Regulations for Buildings (ATC 3–06) [1] and NEHRP Recommended Provisions for the Development of Seismic Regulations for New Buildings (1985) [6], the following statement is made:

> *"Dynamic analyses assuming linear behavior indicate that the torsional moment due to eccentricity between centers of mass and resistance may significantly exceed M (the design torsional moment). However, such dynamic magnification is not included in these design provisions, partly because its significance is not well understood for buildings designed to perform well beyond the range of linear behavior."*

Since the behavior of most structural systems under moderate to strong earthquake excitation involves some degree of nonlinearity, a thorough understanding of elastic and inelastic torsional response in structures is needed.

1.2.1 Building Code Provisions

Traditional design procedures often assume linear elastic behavior of structural systems. Building code provisions usually call for planar analysis of independent load–resisting systems in the principal directions of a building, but do not address directly many issues pertaining to torsion. The equivalent lateral force procedures found in many building codes normally start by having the analyst obtain a design base shear. This design base shear in turn is distributed as the lateral forces to each of the stories. A planar analysis is employed to determine the member forces and interstory drifts resulting from the statically applied story forces. The story deflections calculated from this pseudo–static analysis must be less than the drift limits imposed by the code. Also, for each applicable loading combination a strength check of the members is required to confirm the adequacy of the design.

The code provisions are established for "regular" buildings only. The current equivalent lateral force procedures account for the torsional response of buildings through use of a highly simplified procedure. For each story, (1) the "calculated" torsion is computed as a result of the story shear force and the physical eccentricity between centers of mass and stiffness of that story; (2) the "accidental" torsion is estimated in association with an assumed relocation of the mass center on the floor plane from its actual location by a distance equal to five percent of the dimension of the building perpendicular to the direction of the applied forces; and (3) the "calculated" (known) torsion plus the "accidental" (unknown) torsion are converted to shear forces in individual members, which in turn are to be added to the shear forces resulting from the design base shear. These total shear forces then are used in the design of the corresponding individual members. The "accidental" torsion is intended to account for ground motion phasing differences, unforeseeable distributions of live load, as well as unidentified sources of eccentricities in the building. These additional torsional forces must be included in the checking of the member forces and stresses; however in a "regular" structure these forces and effects were not considered in checking story drifts before the 1988 Edition of the Uniform Building Code. Thus it is quite possible that the torsional effects may be large and not fully accounted for in the design.

The 1988 Edition of the Uniform Building Code focuses slightly more attention on the torsional effects than has been the case in the past. The story deformation due to torsion must be considered in drift calculation. An amplification factor for the "accidental" torsion is devised to account for the effects of having torsional irregularity in a structure with shear–beam type of diaphragms (floors). This is a major step forward in proper consideration of the torsional aspects of seismic design of structures having torsional irregularity.

1.2.2 Review of Previous Analysis Works

Selected literature on torsional response of structures has been evaluated by the investigator. Excellent summaries of older and more general work can be found in references by Batts, Berg, and Hanson [4], Hoerner [16], and Kan and Chopra [22]. The development of research work on this topic by these investigators and others is reviewed and summarized next.

Early studies on building torsion undertaken by Ayre [2] showed the strong coupling between lateral and torsional motions. A shear beam model was used in the analyses. The author noted that the mode shapes could be coupled if the centers of mass and resistance do not coincide.

Although Shiga [45] observed that with large eccentricities strong coupling between translational and torsional motions is likely to occur, Newmark [33] and Morgan, Hall, and Newmark [31] showed that a structure with regular layout but without large eccentricity may exhibit torsional response if the horizontal ground motion shows uneven spatial propagation over the base. This torsional response even occurs in buildings with coincident centers of mass and resistance. Stochastic ground motion models were employed by Kung and Pecknold [28] to investigate the effects of ground motion variations on the response of elastic systems.

Recognizing that the closeness of structural modal frequencies is important in the accuracy of results by modal analysis, Rosenblueth and Elorduy [41] developed a method of combining modal maxima to estimate the maximum value of a response quantity when the modal frequencies are close. Hoerner [16] used a continuous three-dimensional shear beam model to investigate the modal coupling between the two translational and one rotational degrees of freedom. Hoerner's study showed that the amount of modal coupling was related to the eccentricity between the center of mass and the center of stiffness divided by the difference of the uncoupled translational-torsional frequency.

In addition to confirming the research results mentioned above, forced vibration tests by Jennings, Matthiesen, and Hoerner [21] also displayed strong coupling between lateral and torsional motions of buildings with close low natural frequencies.

Kan and Chopra [22, 23, 24] undertook a series of research studies on the coupled lateral-torsional response of structures to earthquakes. A wide range of basic structural parameters affecting the coupled torsional response of linear systems was identified. The investigators modeled a N-story torsionally coupled structure as a N-story torsionally uncoupled counterpart having N planar degrees of freedom along with an associated single-story three-degree-of-freedom torsionally coupled system with equivalent properties and an equivalent single yield surface. Through use of the approximation that any lower vibration mode of a torsionally coupled building may be expressed as a linear combination of three vibrational modes of the corresponding torsionally uncoupled systems, they provided a modal analysis procedure for estimating the maximum responses of elastic systems from the response spectra.

Hejal and Chopra [15] suggested that the beam-to-column stiffness ratio which characterizes the frame action also affects the response of torsionally-coupled systems.

This ratio influences the member forces in individual elements in the system, and it affects the higher mode participation in the system response.

In dynamic structural analysis, there are two major types of analyses, time–domain and frequency–domain analysis. The choice of analysis method depends partially on the philosophy of the analyst. The majority of the research studies have been in the time domain, a response history analysis. A simple frequency domain analysis was outlined by Irvine and Kountouris [19]. A parametric study also was undertaken by these authors [20] in an attempt to identify trends in the peak ductility demand. They claimed that eccentricity does not appear to be a particularly significant parameter in the response of torsionally unbalanced one–story buildings. This conclusion is apparently in opposition to opinions held by earlier investigators; its validity needs to be investigated further.

The torsional analysis approaches summarized above are valid in the linear–elastic range. The studies have shown that strong modal coupling between translational and torsional responses can result in significant increases in response unaccounted for in usual design practice. The modal coupling depends strongly on the ratio of natural frequencies for the corresponding uncoupled system. From the research results, many investigators have come to the conclusion that when the translational response is coupled with the torsional motion, the horizontal story shears decrease while the induced torque increases. The combined shear forces in (peripheral) structural members from both the reduced story shear forces and the induced torque, however, can reach significant magnitude. It is not clear from these studies as to the phasing of these modes of response. As indicated later herein this topic deserves intensive study.

While much of the research efforts have been directed to the linear–elastic torsional response of structures, Tso's work [49] shows the importance of nonlinear coupling between the rotational and translational motions resulting from the nonlinear force–deformation characteristics of the structure. Veletsos, Erdik, and Kuo [53] investigated the nonlinear, lateral–torsional response of the three–dimensional shear–beam type structures subjected to asynchronous excitation of the base during the passage of an earthquake wave. Their results indicate that the maximum column deformation induced in the structure by a propagating ground motion significantly exceeds those corresponding to conventional analysis for high–frequency systems.

Batts, Berg, and Hanson [4] used Monte–Carlo methods to study the peripheral response of perimeter shear wall structures. The results of the probabilistic analysis show that the increase in the elastic peripheral response is on the order of 50 percent, arising from both the eccentricity and ground rotations. They then assumed that the material model for the shear walls was bilinear. Their results show the peripheral response of unsymmetric structures to be only marginally greater than that for symmetric structures.

Kan and Chopra's studies [25] show that the structural lateral response in the inelastic range is affected by torsional coupling to a lesser degree than in the elastic range. The nonlinear response of a structure is strongly influenced by the yielding properties of the system. However, the authors did not correlate the coupled lateral–torsional response with the system parameters in the inelastic range because of few apparent systematic trends in the results.

Most of the previous studies were concerned with systems subjected to single-component ground motion. Yamazaki [57] used a single–story structure to model systems subjected to double–component ground motion. He also investigated the effect of force interaction during yielding on the coupled translational–torsional response of structures. The author concluded that the excessive torsional response due to eccentricities can be controlled by increasing the yield level of shear forces appropriately.

The majority of the research on the nonlinear lateral–torsional response of structures has centered on single–story models. The generality and applicability of these results to practical design of multi–story structures remain unanswered. It is certain that further investigation is needed.

1.3 Scope of The Report

This report centers on the torsional behavior of structures subjected to strong ground motion. An overview of this study has been presented in this first chapter. The presentation of some background information and a brief review of previous research enabled the formulation of the specific objectives for the study reported herein, as briefly described next.

It is well known that if two modes of a linear vibrating system have equal frequencies, any linear combination of the corresponding mode shapes is also a mode with the same frequency. In a sense, then, for equal frequencies a pair of mode shapes is indeterminate. If, however, there are two mode shapes having close frequencies, a small change in the parameters of the system can result in very large changes in the (now unique) mode shapes. It is with reference to this last phenomenon, which will be termed "modal instability," that we shall explain the presence of unexpected yet significant torsional motions in the absence of large torsional excitation.

For a long time it has been a concern of many researchers that severe coupling between translational and torsional response can arise from closely spaced fundamental frequencies, even in structures with relatively small eccentricity. It is theoretically demonstrated in Chapter 2, perhaps for the first time in the literature, that such coupling is the result of modal instability which leads to the beating phenomenon in structural response, a form of behavior observed by many previous investigators. Through the examination of energy transfer from the primary translational motion to the torsional motion, as well as response of single–mass systems during free vibration and harmonic base excitation, this study provides unique analytical solution for the phenomenon of amplified torsional response in structures. Attention also is given to structural response to earthquake ground motion. The findings in that chapter are confirmed by some of the field recordings presented later in Chapter 5. Although the study is performed on linear–elastic systems, the conclusions regarding the effects of nearly equal fundamental frequencies also are applicable to nonlinear structural response because of the changing of structural frequencies.

In most cases a building's response to severe earthquakes involves a certain degree of inelastic behavior. Under current design philosophy, inelastic behavior, including limited hysteretic action, is viewed as an important energy absorption mechanism. Modeling techniques of the inelastic behavior are an important element of meaningful analysis. A generalized mathematical model in the force–displacement space is formulated and documented in Chapter 3, based on the theories of classical plasticity to account for the force interactions and material strength hardening in the lateral load–resisting members. The integration procedure employing Newmark's β method also is presented there for completeness.

In Chapter 4 limited yet comprehensive parametric studies of simple models are performed, using the generalized model in Chapter 3, to understand the effect of static eccentricity on the system response. A wide range of structural systems with an uncoupled frequency ratio of 1.225 are subjected to harmonic base excitation and several selected earthquake ground motions. The development, results and conclusions of the parametric studies are presented and discussed. Relations between eccentricity and the envelopes of various response quantities, e.g., the dynamic torsional response, are examined.

Two low–rise buildings extensively instrumented during the 1987 Whittier Narrows Earthquake are studied in Chapter 5. Several parameters are considered in the modeling of the buildings. The analysis procedure described in Chapter 3 is used to calculate the structural response in both the elastic and inelastic domains. The analysis results are reported along with the recorded data for comparison purposes. The field recordings are examined to identify the building fundamental frequencies and to understand the performance and behavior of these low–rise buildings during seismic ground motion, in the light of the seismic requirements in the current building codes. The analysis results are extrapolated to estimate the building response if by any chance they were subjected to stronger earthquakes.

A brief overview of this study and a summary of the major observations are contained in Chapter 6.

1.4 Notation

For reference purpose a list of the important symbols is given below. The notations and symbols used in this study are defined where they are first introduced in the text. All units of the quantities in this report are consistent units of mass, length, and time. The quantities are used in this manner throughout the report.

A = amplitude or "envelope" of vibration with beating characteristics

a = amplitude of the harmonic base excitation

$\{B_{ij}\}$ = vector of back–force used in the kinematic hardening material model

$[C]$ = proportional damping matrix

C = numerical coefficient in determining design base shear

C_s = numerical coefficient in determining design base shear

D = building dimension

$\{\dot{D}_{ij}\}$ = vector of deformation rate of element i of story j

$\{\dot{D}^e_{ij}\}$ = vector of elastic deformation rate of element i of story j

$\{\dot{D}^p_{ij}\}$ = vector of plastic deformation rate of element i of story j

$d_eD^p_{ij}$ = equivalent plastic deformation increment

d_eQ_{ij} = equivalent force increment

e = static eccentricity between the centers of mass and stiffness

e_d = dynamic eccentricity

e_{eq} = equivalent eccentricity

$\{F\}$ = vector of external force applied to the structural system

f = structural natural frequency

g = acceleration of gravity

I = importance factor in determining design base shear

i = index for structural members, also used for number of iterations

J = rotational mass moment of inertia with respect to mass center

j = index for structural members indicating the j^{th} story

$[K]$ = stiffness matrix

${}^t[K]$ = tangent stiffness matrix at time t

$[K^e_{ij}]$ = elastic stiffness matrix of element i of story j

$[K^{ep}_{ij}]$ = elasto–plastic stiffness matrix of element i of story j

$[K^*]$ = effective stiffness matrix in dynamic analysis

k = stiffness of the weak spring connecting the two–pendulum system

k = plastic modulus of element i of story j

k_u = translational stiffness

k_x = uniaxial elastic stiffness of element i of story j

k_θ = torsional stiffness with respect to the center of mass

l_i = length of pendulum

$[M]$ = diagonal mass matrix

$\{M^p_{ij}\}$ = vector of plastic moments of element i of story j in all directions

m = mass

N = number of stories in the structure

$\{n_{ij}\}$ = unit normal vector of the yield surface at the current force state

$\{P\}$ = external force vector applied to the structural system

${}^{t+\Delta t}\{P\}$ = external force vector applied to the system at time $t + \Delta t$

${}^{t+\Delta t}\{Q\}$ = restoring force vector at time $t + \Delta t$

${}^{t+\Delta t}\{Q_{ij}^{T}\}$ = trial state of the restoring force vector at time $t + \Delta t$

R_W = system quality factor used in determining design base shear

r = radius of gyration

$\{S_{ij}\}$ = shifted–force vector used in the kinematic hardening material model

T_I = torsional moment existing at mass center

T_i = kinetic energy possessed by the i^{th} pendulum mass

T_u = kinetic energy associated with the translational motion

$\{T_R\}$ = vector of maximum torsional moment at rigidity center

T_θ = kinetic energy associated with the rotational motion

t = time

$\{U\}$ = displacement vector

${}^{t+\Delta t}\{U\}$ = displacement vector at time $t + \Delta t$

u = translational displacement relative to the base

$\{\ddot{U}_g\}$ = vector of ground motion acceleration

$\ddot{u}_g$ = acceleration input of the base excitation

$\{u_m\}$ = vector of maximum translational displacement at mass center

$[V]$ = modal transformation matrix

V = design base shear

V_I = inertial force applied at mass center

$\{V_m\}$ = vector of maximum force applied at the floor levels

W = total design weight of building

x = Cartesian coordinate axis

Y_{ij} = uniaxial yield force of element i of story j

y = Cartesian coordinate axis

Z = seismic zone factor used in determining design base shear

a_n = variable defined in Equation 2.3

a_x = strength–hardening coefficient in uniaxial test

β = integration coefficient in Newmark's β method

γ = integration coefficient in Newmark's β method

Δ = incremental quantity

$\{\Delta D_{ij}\}$ = vector of deformation increment of element i of story j

$\{\Delta D_{ij}^p\}$ = vector of plastic deformation increment of element i of story j

$\{\Delta P^*\}$ = effective load vector in dynamic analysis

$\{\Delta Q\}$ = incremental restoring force vector during the time interval Δt

$\{\Delta U\}$ = incremental displacement vector during the time interval Δt

ϵ = measure of the difference of the uncoupled frequencies ω_θ^2 and ω_u^2

ζ = variable defined in Equation 2.8

η = scalar indicating the pre–yield portion of the total force increment

θ = rotational displacement relative to the base

θ_i = pendulum displacement

$\{\theta_m\}$ = vector of maximum rotational displacement at mass center

$\dot{\lambda}$ = proportional scalar for plastic deformation rate

ϱ = ratio of energy transfer

Φ_{ij} = yield surface in the force space for element i of story j

Ω = circular frequency of the harmonic base excitation

ω_n = undamped natural circular frequency

ω_u = uncoupled translational circular frequency

ω_θ = uncoupled rotational circular frequency

$|\ |$ = absolute value of a quantity

A dot above a symbol denotes the derivative of the variable with respect to time

CHAPTER 2

BEHAVIOR OF LINEAR-ELASTIC SYSTEMS WITH CLOSE FUNDAMENTAL FREQUENCIES

2.1 Definition of Systems

It has been pointed out by several previous investigators that the torsional response of a structure possibly could exhibit beating phenomena when the fundamental translational and torsional frequencies of a structure are nearly equal, even with very small eccentricity. Accordingly, study was undertaken in order to look further into the phenomena. In Chapter 5, as will be noted later herein, such phenomena were observed to occur in building structures with recorded motion.

The structural systems considered for study are simple linear–elastic systems. For the purpose of demonstration and simplicity, the system model is defined as a one–story structure with eccentricity in only one principal direction. The system therefore has two coupled degrees of freedom when subjected to base excitation in the y–direction, i.e., the translational and the torsional degrees of freedom, as shown in Figure 2–1. The small shaded circular area and the black square box in the figure represent the locations of the centers of mass and rigidity, respectively. The translational response in the x–direction (of eccentricity) is not coupled with response in the orthogonal y–direction, nor with the

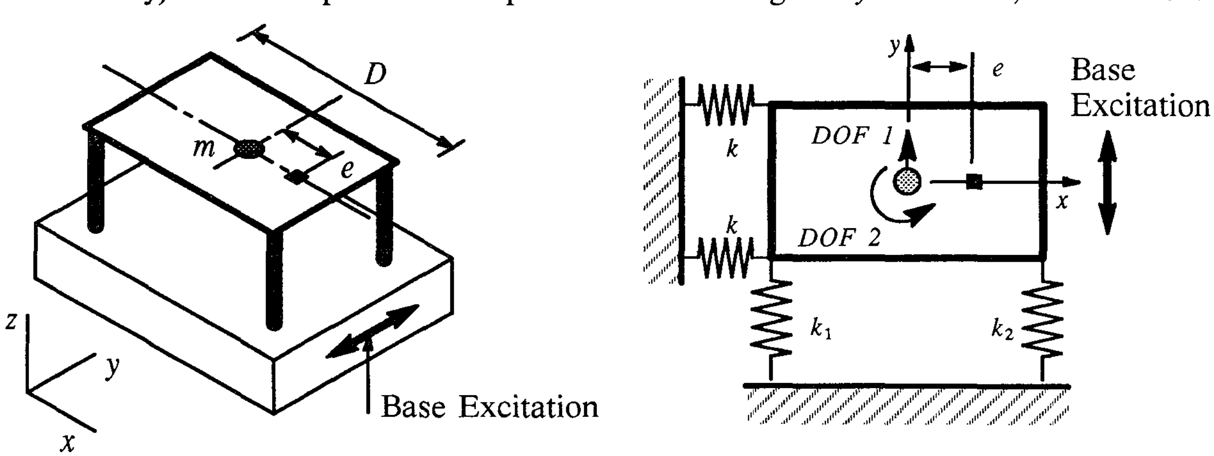

(a) 3–D View (b) Plan View

Figure 2–1 Model of Linear–Elastic System rotational response. When subjected to translational base excitation in the y–direction, the response in the x–direction is not excited.

2.2 Coupled Translational and Torsional Response

Physical eccentricity between the centers of mass and rigidity serves as a link between the translational and the torsional response of a structure. When the eccentricity is very small, the mathematical model of the system resembles that of a two–pendulum system connected by a weak spring.

For a system of two separate pendulums (without a spring connecting the two masses) shown in Figure 2–2(a), the natural frequencies of the system are $\sqrt{g/l_1}$ and $\sqrt{g/l_2}$, where l_1 and l_2 are the respective lengths of the pendulums. As long as the two frequencies are separated, in order words, the lengths of the pendulums are different, there exist two definite mode shapes namely $\{1, 0\}$ and $\{0, 1\}$. If the two frequencies are the same, any two different 2–dimensional vectors could serve as the mode shapes of the system. In a sense, then, the pair of mode shapes is indeterminate.

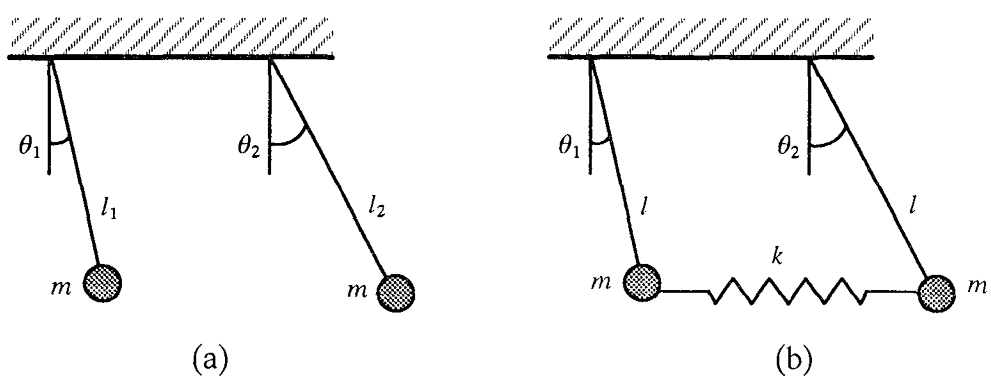

Figure 2–2 Two–Pendulum Systems

If the two pendulums with equal length are connected by a spring k as shown in Figure 2–2(b), the configuration of the system is completely changed from the system in Figure 2–2(a), even when the spring is very weak. The natural frequencies of the two–pendulum system are close together, namely $\sqrt{g/l}$ and $\sqrt{g/l + (2k)/m}$. By virtue of a small change in the system parameter (k changes from zero to a non–zero value), the mode shapes now change to $\{1, 1\}$ and $\{1, -1\}$ as compared to the indeterminate pair described above. This phenomenon is termed "modal instability."

The motions of the two pendulums are coupled, in other words, the oscillations of the two masses in the system shown in Figure 2–2(b) become coupled. If the two frequencies are nearly equal (the stiffness of the spring k is quite small), a beating phenomenon will occur and the transfer of motion from one pendulum to another can be observed. That is to say, if one of the masses is set in motion, the energy it possesses will transfer to, and excite, the other one during the beating process. An example is given in Figure 2–3, in which the frequency of the system f is *0.5 Hz*, and the ratio of the spring stiffness k and the mass m, (k/m), is $(40\pi^2/361)$. In Figure 2–3(a), θ_1 and θ_2 represent the displacements of the pendulums respectively, θ_0 is the initial displacement of the first pendulum while the other one starts from the vertical position, and ω_1 and ω_2 are the natural circular frequencies of the system. As shown in Figure 2–3(b), the energy flows from one pendulum to the other. T_1 and T_2 represent the kinetic energy possessed by the two masses, respectively. In the process the transfer medium is the small spring connecting the two pendulums; it transfers energy in the form of storing and releasing strain energy.

The single–story structure shown in Figure 2–1 has two degrees of freedom. Without any eccentricity, the system is analogous to that of two separate pendulums. The response of the structure along the two degrees of freedom can be calculated independently. However, with even very small eccentricity, the system configuration changes to that similar to the two pendulums connected by a spring. The eccentricity here plays the role of the spring, coupling and transferring energy between the two motions. The two degrees of freedom in the single–story structure are coupled through the eccentricity; therefore there exists energy transfer from the primary translational motion to the torsional motion, and back. If the eccentricity is in a certain range with respect to other parameters in the system, a beating phenomenon with periodically varying amplitudes can be observed. The torsional response will be excited by the translational ground motion through modal instability.

One method for investigating the coupled response is by modal analysis for the linear–elastic systems. The coordinates originate from the mass center as depicted in Figure 2–1. Since the system has eccentricity only in the x–direction and the ground motion is assumed to input in the perpendicular y–direction, the degree of freedom in the x–direction, perpendicular to the base motion direction, will not be excited. Therefore, only one translational, u, and the torsional, θ, degrees of freedom are considered herein.

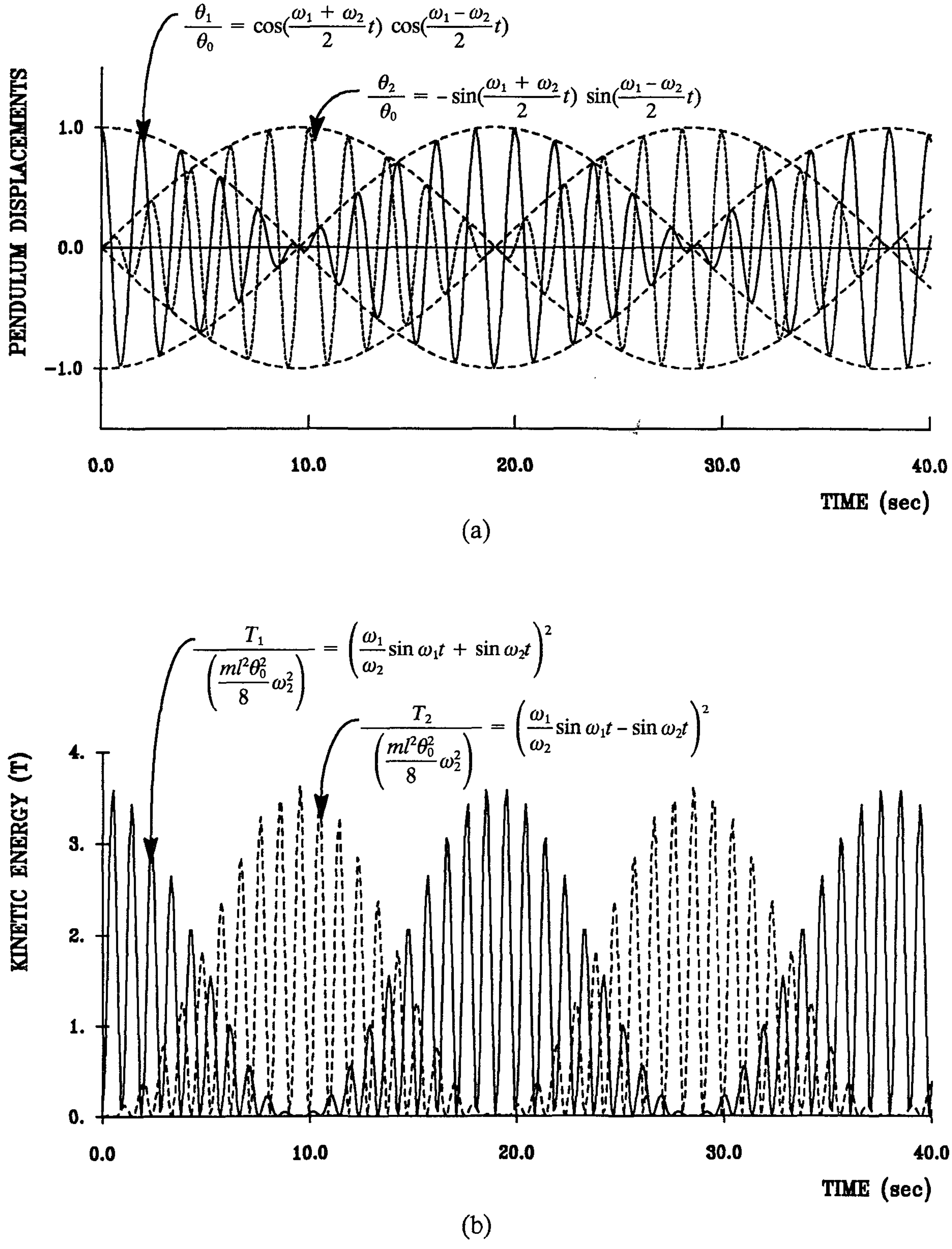

Figure 2-3 Free Oscillation of A Two-Pendulum System

For illustrative purposes, the structure in later examples will have the properties listed in Table 2–1, in which the eccentricity is ten percent of the radius of gyration, r, defined as $\sqrt{J/m}$.

Table 2–1 Structural Parameters of Model

Translational Frequency (Hz)	Translational Stiffness (#/in.)	Mass (#–in/s^2)	Rotational Mass Moment of Inertia (#–in^3/s^2)	Eccentricity (in.)
0.75	$4*10^5$	$1.8*10^4$	$5*10^3$	0.10 r

2.2.1 Equations of Motion

For the purpose of simplicity, damping is not considered in the following derivation. The effects of damping will be addressed in a later section.

The equations of motion of the system shown in Figure 2–1 may be written in the following matrix form:

$$[M]\ \{\ddot{U}\} + [K]\ \{U\} = \{F\}, \tag{2.1}$$

where $[M]$ = diagonal mass matrix of the system,
$[K]$ = stiffness matrix of the system,
$\{U\}$ = displacement vector of the degrees of freedom,
$\{F\}$ = external force vector applying onto the system, and
the dots represent the derivative of the variables with respect to time.

The modal analysis of the system is carried out in Appendix A. If the uncoupled translational and torsional frequencies are $\sqrt{k_u/m}$ for ω_u and $\sqrt{k_\theta/J}$ for ω_θ, respectively, the frequencies of the system are given by Equation A.2 in Appendix A, namely

$$\omega_{\substack{1\\2}}^{\ 2} = \frac{1}{2}(\omega_u^{\ 2} + \omega_\theta^{\ 2}) \mp \sqrt{\frac{1}{4}(\omega_u^{\ 2} - \omega_\theta^{\ 2})^2 + \frac{k_u^{\ 2}\ e^2}{mJ}}, \tag{2.2}$$

and the mode shapes are expressed in following equation,

$$\begin{Bmatrix} u \\ \theta \end{Bmatrix} = \begin{Bmatrix} 1 \\ a_1 \end{Bmatrix} = \begin{Bmatrix} 1 \\ \frac{1}{e}(\frac{\omega_1^{\ 2}}{\omega_u^{\ 2}} - 1) \end{Bmatrix} \quad \text{and} \quad \begin{Bmatrix} u \\ \theta \end{Bmatrix} = \begin{Bmatrix} 1 \\ a_2 \end{Bmatrix} = \begin{Bmatrix} 1 \\ \frac{1}{e}(\frac{\omega_2^{\ 2}}{\omega_u^{\ 2}} - 1) \end{Bmatrix}, \tag{2.3}$$

where k_u = translational stiffness of the system,

k_θ = torsional stiffness with respect to the center of mass,

e = static eccentricity between the centers of mass and stiffness,

m = mass,

J = rotational mass moment of inertia with respect to the center of mass,

ω^2 = square of circular natural frequency, and

a_1 and a_2 are variables defining mode shapes.

The equations of motion are then transformed into the uncoupled generalized coordinates. The solution for free vibration of the generalized degrees of freedom is readily available, and the results are summed up to obtain the system response. With the initial conditions of $\{U\}$ being $\{u_0, \theta_0\}$ and $\{\dot{U}\}$ being $\{\dot{u}_0, \dot{\theta}_0\}$, the system responses are given by Equation A.6 in Appendix A, namely

$$\begin{Bmatrix} u \\ \theta \\ \dot{u} \\ \dot{\theta} \end{Bmatrix} = \begin{bmatrix} \sin\omega_1 t & \cos\omega_1 t & \sin\omega_2 t & \cos\omega_2 t \\ a_1 \sin\omega_1 t & a_1 \cos\omega_1 t & a_2 \sin\omega_2 t & a_2 \cos\omega_2 t \\ \omega_1 \cos\omega_1 t & -\omega_1 \sin\omega_1 t & \omega_2 \cos\omega_2 t & -\omega_2 \sin\omega_2 t \\ a_1\omega_1 \cos\omega_1 t & -a_1\omega_1 \sin\omega_1 t & a_2\omega_2 \cos\omega_2 t & -a_2\omega_2 \sin\omega_2 t \end{bmatrix} \begin{Bmatrix} (a_2\dot{u}_0 - \dot{\theta}_0)/(a_2 - a_1)\omega_1 \\ (a_2 u_0 - \theta_0)/(a_2 - a_1) \\ (-a_1\dot{u}_0 + \dot{\theta}_0)/(a_2 - a_1)\omega_2 \\ (-a_1 u_0 + \theta_0)/(a_2 - a_1) \end{Bmatrix}. \tag{2.4}$$

2.2.2 Translational Free Vibration of Asymmetric Systems

For purpose of demonstration but without losing generality, let the initial conditions of a system be $\{U\} = \{u_0, 0\}$ and $\{\dot{U}\} = \{0, 0\}$. The free vibration of the asymmetric system is represented as

$$\begin{Bmatrix} u \\ \theta \\ \dot{u} \\ \dot{\theta} \end{Bmatrix} = \begin{bmatrix} \cos\omega_1 t & \cos\omega_2 t \\ a_1 \cos\omega_1 t & a_2 \cos\omega_2 t \\ -\omega_1 \sin\omega_1 t & -\omega_2 \sin\omega_2 t \\ -a_1\omega_1 \sin\omega_1 t & -a_2\omega_2 \sin\omega_2 t \end{bmatrix} \begin{Bmatrix} a_2 u_0/(a_2 - a_1) \\ -a_1 u_0/(a_2 - a_1) \end{Bmatrix}. \tag{2.5}$$

From Equation 2.5, the translational vibration becomes

$$u = u_0 \left[\cos(\frac{\omega_1 + \omega_2}{2} t) \cos(\frac{\omega_1 - \omega_2}{2} t) + \frac{a_1 + a_2}{a_1 - a_2} \sin(\frac{\omega_1 + \omega_2}{2} t) \sin(\frac{\omega_1 - \omega_2}{2} t) \right]. \tag{2.6}$$

Let us define

$$\omega_\theta^2 = \omega_u^2 + \epsilon \ , \tag{2.7}$$

in which $|\epsilon| \ll \omega_u^2$ is a measure of the difference of the uncoupled frequencies ω_θ^2 and ω_u^2. Further, let ζ represent the percentage of the second term in the total translational vibration. From Equations 2.2 and 2.3 in the modal analysis,

$$\zeta = \frac{(a_2 + a_1)}{(a_2 - a_1)} = \frac{(\omega_2^2 + \omega_1^2 - 2\omega_u^2)}{(\omega_2^2 - \omega_1^2)} = \frac{(\omega_\theta^2 - \omega_u^2)}{(\omega_2^2 - \omega_1^2)}, \tag{2.8}$$

in which the value of ζ ranges from −1 to 1. Then Equation 2.6 becomes

$$u = u_0 \left[\cos(\frac{\omega_1 + \omega_2}{2} t) \cos(\frac{\omega_1 - \omega_2}{2} t) - \zeta \ \sin(\frac{\omega_1 + \omega_2}{2} t) \sin(\frac{\omega_1 - \omega_2}{2} t) \right]. \tag{2.9}$$

Or, in another form,

$$u = A \cos\left(\frac{\omega_1 + \omega_2}{2} t + \psi \right), \tag{2.10}$$

in which A is the amplitude or so-called "envelope" of the translational vibration being a function of time, and defined as

$$\begin{aligned} A &= u_0 \sqrt{\cos^2(\frac{\omega_1 - \omega_2}{2} t) + \zeta^2 \ \sin^2(\frac{\omega_1 - \omega_2}{2} t)} \\ &= u_0 \sqrt{\frac{1 + \zeta^2}{2} + \frac{1 - \zeta^2}{2} \cos(\omega_1 - \omega_2) t} \ , \quad \text{and} \end{aligned} \tag{2.11}$$

ψ is the phase angle due to the effect of ζ, as defined by

$$\tan \psi = \zeta \ \tan\left(\frac{\omega_1 - \omega_2}{2} t \right) .$$

If the uncoupled frequencies of the system are equal (i.e., $\epsilon = 0$ and $\zeta = 0$) in Equation 2.11, the envelope of the translational vibration forms complete beats. This beating phenomenon is depicted in Figure 2–4, in which the structural system is defined in Table 2–1 with equal uncoupled frequencies. The period of the beating envelope is $2\pi/(\omega_2 - \omega_1)$. At the valleys of the beating envelope, the energy associated with the translational motion is transferred totally to the torsional motion, resulting from modal instability. This phenomenon will be discussed further later.

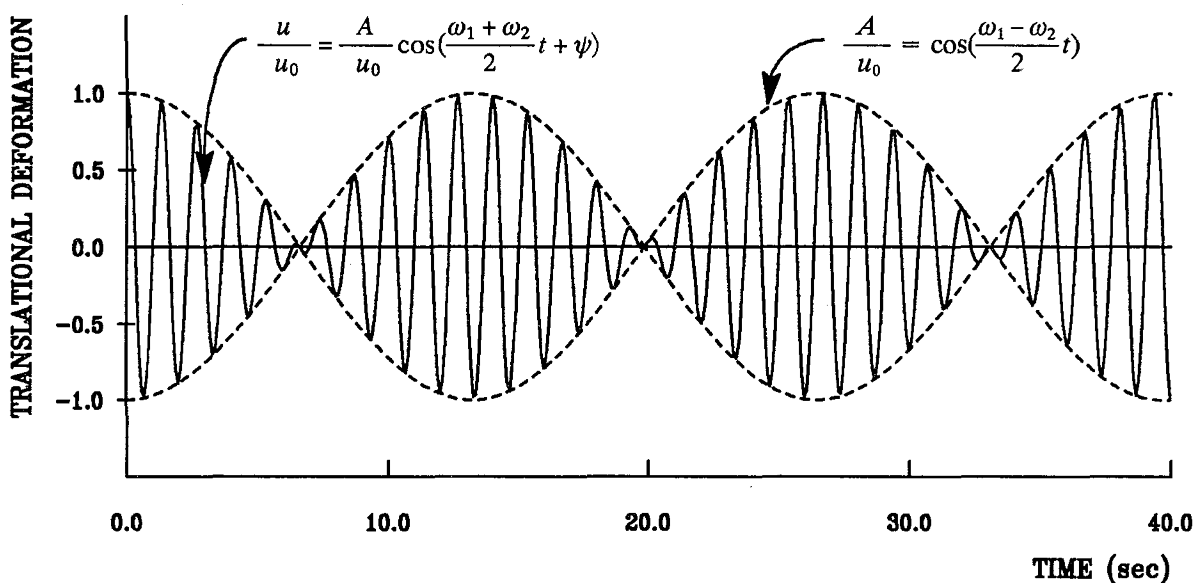

(a)

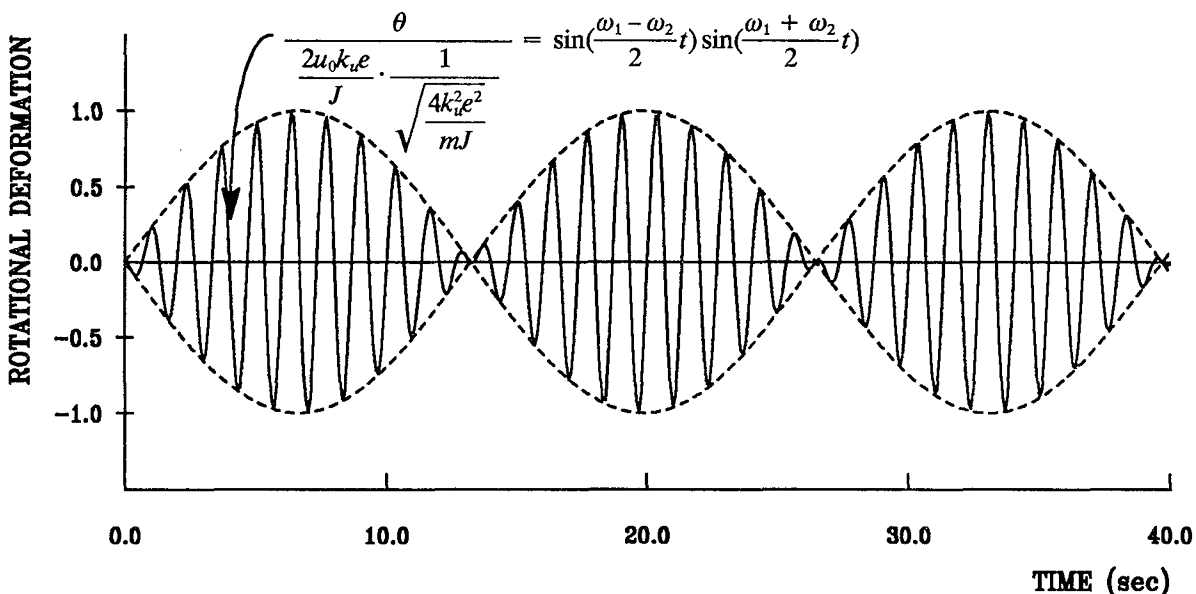

(b)

Figure 2–4 Free Vibration of System with Equal Frequencies

In the cases of systems having different uncoupled frequencies, i.e., relatively small but non–zero ϵ, the occurrence of the beating phenomenon depends upon the value of ζ. The variation of response amplitude with respect to time is defined in Equation 2.11, and its form is similar to sinusoidal types of functions. The free vibration of the structural

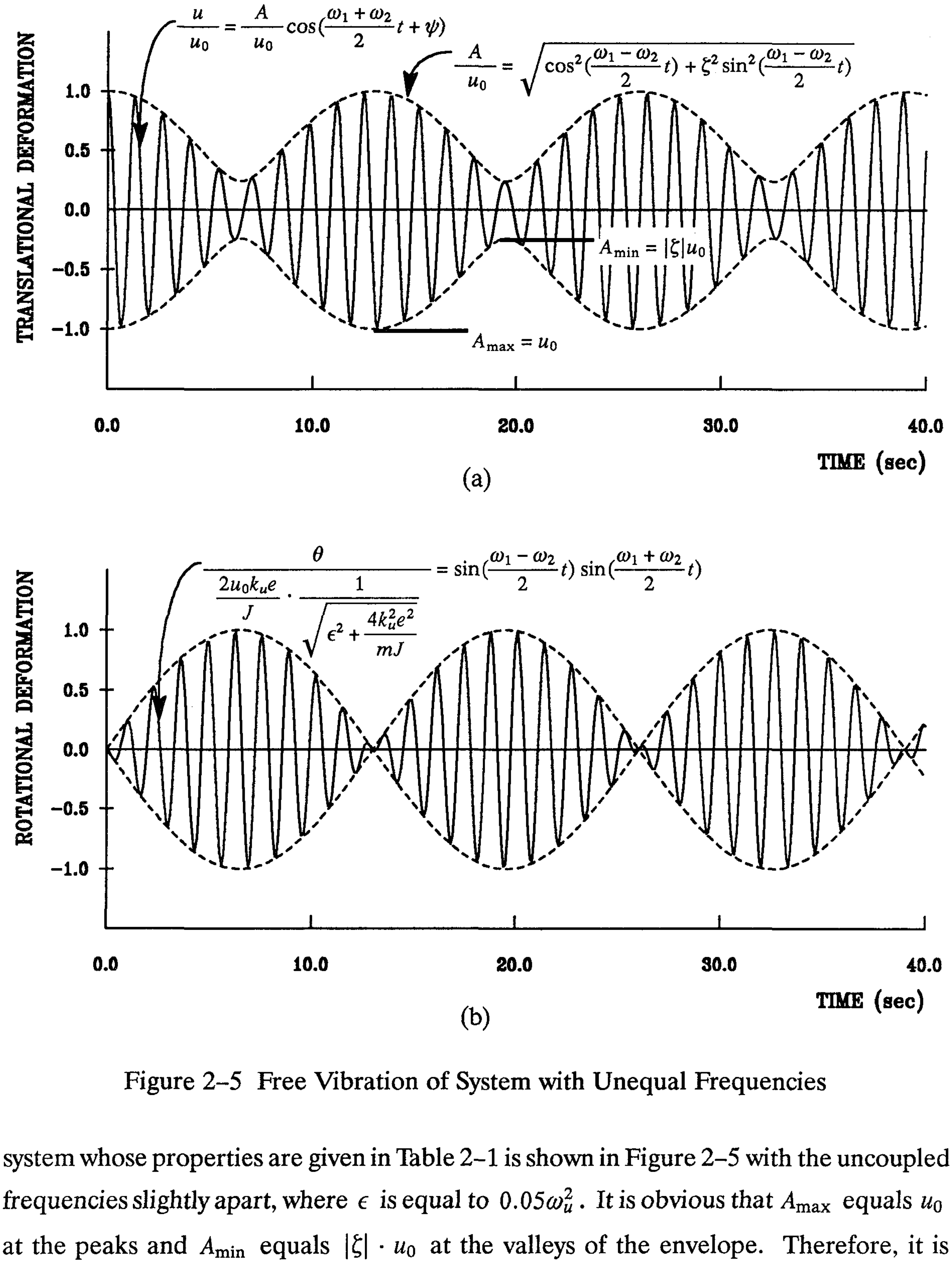

Figure 2–5 Free Vibration of System with Unequal Frequencies

system whose properties are given in Table 2–1 is shown in Figure 2–5 with the uncoupled frequencies slightly apart, where ϵ is equal to $0.05\omega_u^2$. It is obvious that A_{max} equals u_0 at the peaks and A_{min} equals $|\zeta| \cdot u_0$ at the valleys of the envelope. Therefore, it is observed that the translational motion does not exhibit much beating behavior, especially if the absolute value of ζ is near unity, and there will be only a small change from $A_{\max}$ to $A_{\min}$. In that case, the torsional motion is excited by the translational motion because of the coupling effect resulting from the eccentricity between the centers of mass and resistance. Only part of the energy associated with the translational motion will be transferred to the torsional motion. The remaining energy stays primarily in the translational motion. The ratio of amplitude of the translational response at the valleys to that of the maximum translational motion is $|\zeta|$.

2.2.3 Torsional Free Vibration

Similar to the translational response, the torsional vibration is examined with the initial conditions of $\{U\}$ being $\{u_0, 0\}$ and $\{\dot{U}\}$ being $\{0, 0\}$. From Equation 2.5,

$$\theta = \frac{2\ u_0\ k_u\ e}{J} \cdot \frac{1}{\sqrt{\epsilon^2 + \dfrac{4k_u^2\ e^2}{m\ J}}} \cdot \sin\left(\frac{\omega_1 - \omega_2}{2} t\right) \cdot \sin\left(\frac{\omega_1 + \omega_2}{2} t\right) , \tag{2.12}$$

in which ϵ is defined in Equation 2.7. It is apparent that the torsional response exhibits the beating characteristic, as shown in Figures 2–4 and 2–5. The influence of torsional response on the overall vibration, including the translational and torsional vibration, depends largely on the difference of the uncoupled frequencies and the amount of eccentricity. If the uncoupled frequencies are nearly equal, the additional displacement caused by the torsional vibration is of the same order as the translational displacement. Thus, structural members could experience large displacements, possibly larger than the translational displacement, depending on the location of the members with respect to the rigidity center in the structure.

Shown in Figure 2–6 is the plot of the maximum displacements versus the ratio of the square of uncoupled frequencies for systems with eccentricity ranging from 0.5 to 10 percent of the radius of gyration. The basic structural properties are listed in Table 2–1. It is noticed that the maximum translational displacement is not affected by the difference of the uncoupled frequencies and the amount of eccentricity in the system. Curves of the maximum rotational displacements are normalized by the largest value among the resulting rotational displacements. They are so modified simply for data presentation, because the relative positions and trends of the curves are most important in later

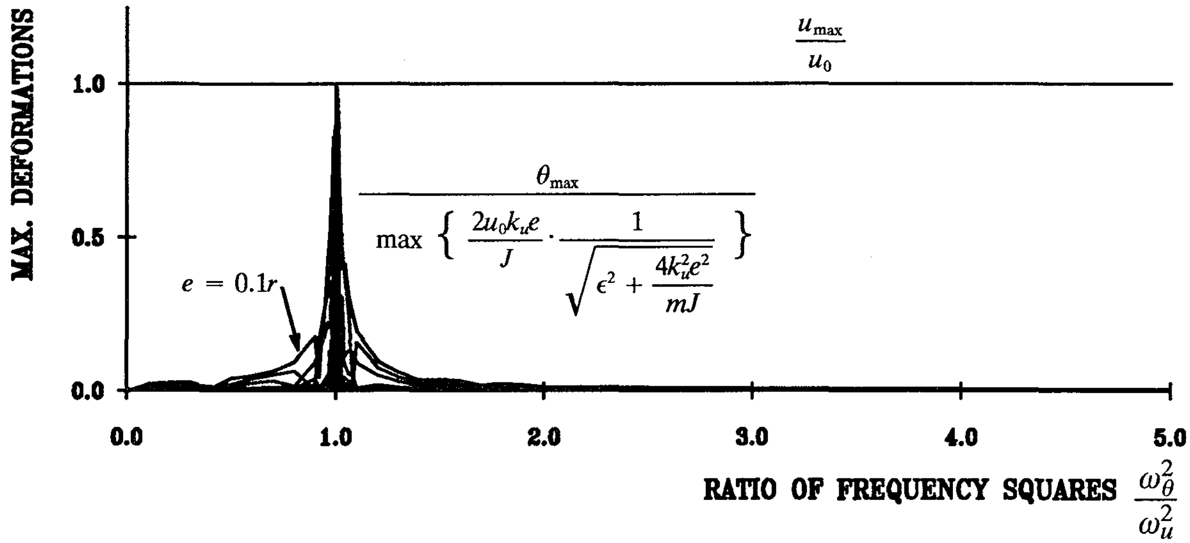

Figure 2–6 Maximum Displacements During Free Vibration

discussion. These curves of maxima reach the peak when the uncoupled frequencies are equal, i.e., $\epsilon = 0$. Centered around this peak, the maximum rotational displacements in systems with various eccentricities decrease quickly as the two frequencies separate. When the uncoupled frequencies are well separated, then the coupling effects of torsion with translation depend primarily on the amount of eccentricity in the structure.

2.2.4 Energy Transfer During Coupled Free Vibration

Based on the principle of conservation of energy, the total energy in a conservative system at any time should be the same, and should be equal to the energy possessed by the system at the beginning of the analysis. An undamped linear–elastic system possesses energy in the forms of kinetic and strain energy. As can be perceived for the one–story, one–directional unbalanced system, it is sufficient to examine the kinetic energy associated with the translational and torsional motions to understand the transfer of energy between the two motions, because the kinetic energy reaches its maximum while the strain energy decreases to zero.

For the purpose of easy visualization and simplicity, a closer examination of motions, not modes, will illustrate more clearly the transfer of energy. Let us first consider the modes in the modal analysis. Without any eccentricity, the translational and rotational motions in a structure are not coupled, so the motions can be treated independently. With even a very small amount of eccentricity, however, the two mode shapes of the system change from $\{1, 0\}$ and $\{0, 1\}$ to those given in Equation 2.3. Each of the modes involves translational and torsional motions because of the existence of a small eccentricity in the system. The modes do not correspond to the "natural" coordinates of translation and rotation of the structural system, so they are relatively difficult to visualize. In terms of modes, the energy remains constant in each mode. It is only when the natural coordinates, translation and rotation, are considered that there appears to have an exchange of energy from translational motion to rotational motion and back. Therefore, it is meaningful to examine energy flow associated with motions along the natural coordinates in the system. The main objective is to identify the flow of energy within the system from one primary motion to another, and to correlate the percentage of energy transfer with the difference of natural fundamental frequencies.

The two obvious parameters affecting the energy flow are the difference of frequencies and the eccentricity. The function of the eccentricity here resembles that of a weak spring in the case of the two–pendulum system. It serves as a medium to couple the two motions and to transfer energy among the motion components. Only systems with relatively small eccentricity are considered in the following.

From Appendix C, the energy associated with the translational and torsional motions of the system is given below, respectively

$$T_u = \frac{m\ u_0^2}{2}\ \frac{a_2^2}{(a_1 - a_2)^2}\left[(\omega_1^2 + \frac{a_1^2}{a_2^2}\omega_2^2) - 2\omega_1\omega_2\frac{a_1}{a_2}\cos(\omega_1 - \omega_2)t\right]\sin^2\left(\frac{\omega_1 + \omega_2}{2}t + \psi_u\right) \quad (2.13)$$

and

$$T_\theta = \frac{J\ u_0^2}{2}\ \frac{a_1^2\ a_2^2}{(a_1 - a_2)^2}\left[(\omega_1^2 + \omega_2^2) - 2\omega_1\omega_2\cos(\omega_1 - \omega_2)t\right]\sin^2\left(\frac{\omega_1 + \omega_2}{2}t + \psi_\theta\right). \quad (2.14)$$

Shown in Figure 2–7 are the levels of kinetic energy possessed by the system, whose free vibration is shown in Figure 2–5, with respect to time. The flow of energy from the primary translational motion to the torsional motion and back is presented graphically. The similarity between this figure and Figure 2–3 can be observed.

The ratio of energy transfer is defined in Appendix C by the maxima of the kinetic energy envelopes for the translational and torsional motions, namely

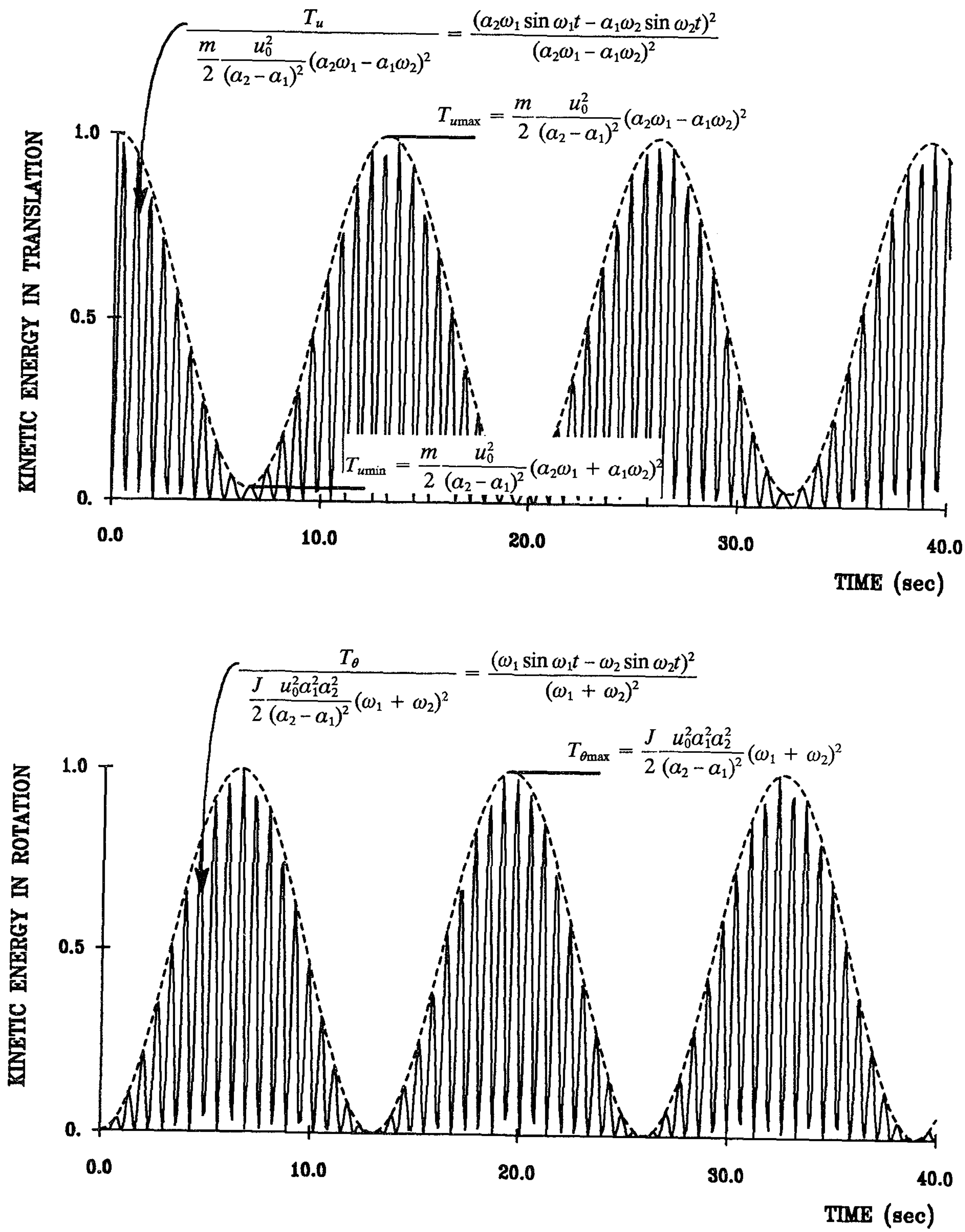

Figure 2–7 Kinetic Energy in Free Vibration

$$\varrho = \frac{J}{m}\, a_1^2 a_2^2 \,\frac{(\omega_1+\omega_2)^2}{(\omega_1 a_2 - a_1\omega_2)^2}$$

$$= \frac{m\ e^2}{J} \cdot \frac{1}{\left(1+\sqrt{1-\dfrac{m\ e^2}{J}+\dfrac{\epsilon}{\omega_u^2}}\right)^2} \cdot \frac{\left(2+\dfrac{\epsilon}{\omega_u^2}\right)+2\sqrt{1-\dfrac{m\ e^2}{J}+\dfrac{\epsilon}{\omega_u^2}}}{\left(2+\dfrac{\epsilon}{\omega_u^2}\right)-2\sqrt{1-\dfrac{m\ e^2}{J}+\dfrac{\epsilon}{\omega_u^2}}}\ , \tag{2.15}$$

which describes the percentage of energy flow from translational motion to torsional motion in the system. As may be ascertained from this expression, regardless of the magnitude of the static eccentricity the ratio is 100 percent in the case of equal uncoupled frequencies (i.e., $\epsilon = 0$ and $\zeta = 0$) due to the effect of modal instability, or

$$\varrho = \frac{m\ e^2}{J} \cdot \frac{1}{\left(1+\sqrt{1-\dfrac{m\ e^2}{J}}\right)^2} \cdot \frac{2+2\sqrt{1-\dfrac{m\ e^2}{J}}}{2-2\sqrt{1-\dfrac{m\ e^2}{J}}}$$

$$= \frac{m\ e^2}{J} \cdot \frac{1}{\left(1+\sqrt{1-\dfrac{m\ e^2}{J}}\right)} \cdot \frac{1}{\left(1-\sqrt{1-\dfrac{m\ e^2}{J}}\right)}$$

$$= 1\ .$$

In Figure 2–8, the transfer ratio is plotted versus the ratio of square of uncoupled frequencies. The curves represent the transfer ratios in systems with eccentricity ranging from 0.5 to 10 percent of the radius of gyration. It is shown clearly that ϱ equals one when the two frequencies are equal (i.e., $\epsilon = 0$) and that the larger the eccentricity, the more effect it has on the energy transfer from translational motion to torsional motion. For eccentricity less than ten percent of the radius of gyration, however, the effect of nearly equal uncoupled frequencies is limited to a relatively narrow band. As also shown in Figure 2–6, outside of this band only some portion of the kinetic energy in translation is transferred to the torsional motion, depending on the amount of eccentricity.

2.2.5 Response During Harmonic Base Motion

The solution of the free vibrating system with the specified initial conditions is expressed in Equation 2.4. The solution reveals the behavior of one–directional

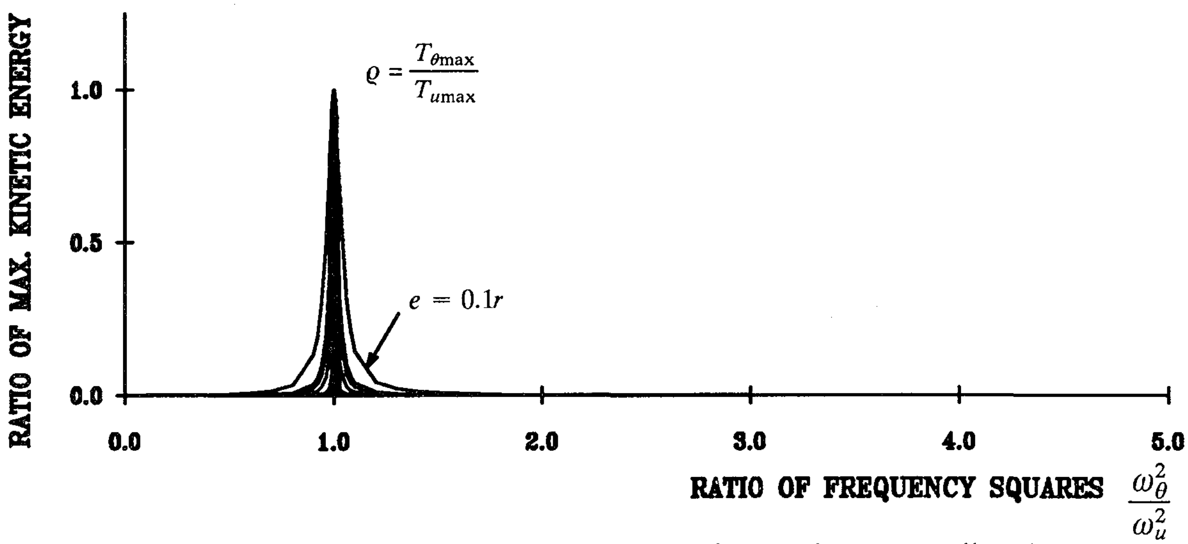

Figure 2–8 Ratio of Kinetic Energy Transfer During Free Vibration

unbalanced systems after any base motion. To comprehend the response of the system, it is necessary to examine its response during ground excitation as well.

The base motion considered in this section is assumed to be harmonic and only imparted to the system in the y–direction in Figure 2–1. The frequencies of the input base motions are so chosen that they are away from the natural frequencies of the system to avoid the influence of resonance. As was demonstrated in the free vibration of a system with close frequencies, the torsional response could reach an unexpectedly high magnitude because of the beating effect from the coupled translational and torsional motions. In this section, it will be shown that the beating phenomenon also occurs in the forced vibration of systems with close fundamental frequencies. The structural model is the same one–directional unbalanced system as shown in Figure 2–1, and the structure in the following examples, for illustration, is the system with the uncoupled frequencies slightly apart ($\epsilon = 0.05\omega_u^2$), whose free vibration is shown in Figures 2–5 and 2–7.

The system response during harmonic base motion ($\ddot{u}_g = \text{a} \sin \Omega t$, where a and Ω are the amplitude and circular frequency of the base motion) is derived in Appendix B. The responses are a function of the modal frequencies, and in turn a function of the uncoupled frequencies and the static eccentricity. The objective here is to show the dynamic amplification of the response, especially the rotational displacement and torsional moment at the center of mass. The responses are given by Equations B.1 and B.2 in Appendix B as,

$$u = \frac{m\ a}{m_1^*\ (\Omega^2 - \omega_1^2)}(\sin \Omega t - \frac{\Omega}{\omega_1}\sin \omega_1 t) + \frac{m\ a}{m_2^*\ (\Omega^2 - \omega_2^2)}(\sin \Omega t - \frac{\Omega}{\omega_2}\sin \omega_2 t)$$

$$\theta = \frac{m\ a\ a_1}{m_1^*\ (\Omega^2 - \omega_1^2)}(\sin \Omega t - \frac{\Omega}{\omega_1}\sin \omega_1 t) + \frac{m\ a\ a_2}{m_2^*\ (\Omega^2 - \omega_2^2)}(\sin \Omega t - \frac{\Omega}{\omega_2}\sin \omega_2 t) \tag{2.16}$$

and

$$V_I = m\ a\left[\frac{m}{m_1^*}\frac{\omega_1^2}{(\Omega^2 - \omega_1^2)}(-\sin \Omega t + \frac{\Omega}{\omega_1}\sin \omega_1 t) + \frac{m}{m_2^*}\frac{\omega_2^2}{(\Omega^2 - \omega_2^2)}(-\sin \Omega t + \frac{\Omega}{\omega_2}\sin \omega_2 t)\right]$$

$$T_I = m\ J\ a\left[\frac{a_1\ \Omega^2}{m_1^*(\Omega^2 - \omega_1^2)}(-\sin \Omega t + \frac{\omega_1}{\Omega}\sin \omega_1 t) + \frac{a_2\ \Omega^2}{m_2^*(\Omega^2 - \omega_2^2)}(-\sin \Omega t + \frac{\omega_2}{\Omega}\sin \omega_2 t)\right], \tag{2.17}$$

in which u and θ are the displacements relative to the base, measured at the center of mass; V_I and T_I are, respectively, the inertial force applied to, and the torsional moment existing at, the center of mass. It is apparent from these equations that the responses exhibit beating characteristic when similar terms are collected. The beating phenomenon in the translational and torsional responses is illustrated by the example in Figure 2–9. The system in the example has equal uncoupled frequencies, and it is subjected to harmonic base excitation with Ω being 10π radians, or $5\ Hz$. The jags on the curves are the result of transient response in the system. In damped systems, these are supposed to vanish rather quickly. When the example system is subjected to harmonic base motion of other frequencies, the shapes of the beats may be distorted depending on the ratio of the base motion frequency with respect to the structural frequencies, but the beating characteristic in the response is retained.

The response maxima are plotted versus the ratio of frequency squares in Figures 2–10 and 2–11 for systems with eccentricity ranging from 0.5 to 10 percent of the radius of gyration. It is shown that maximum translational response is not affected by either the difference of the uncoupled frequencies or the amount of eccentricity, because of the phase difference between the maximum translational and torsional response. However, maximum torsional response is influenced by the difference of the frequencies, especially in systems with higher eccentricity. The effect of nearly equal uncoupled frequencies is most pronounced on systems of various eccentricities with equal frequencies, i.e., when $\epsilon = 0$. The curves in these plots are normalized by the largest values among the absolute

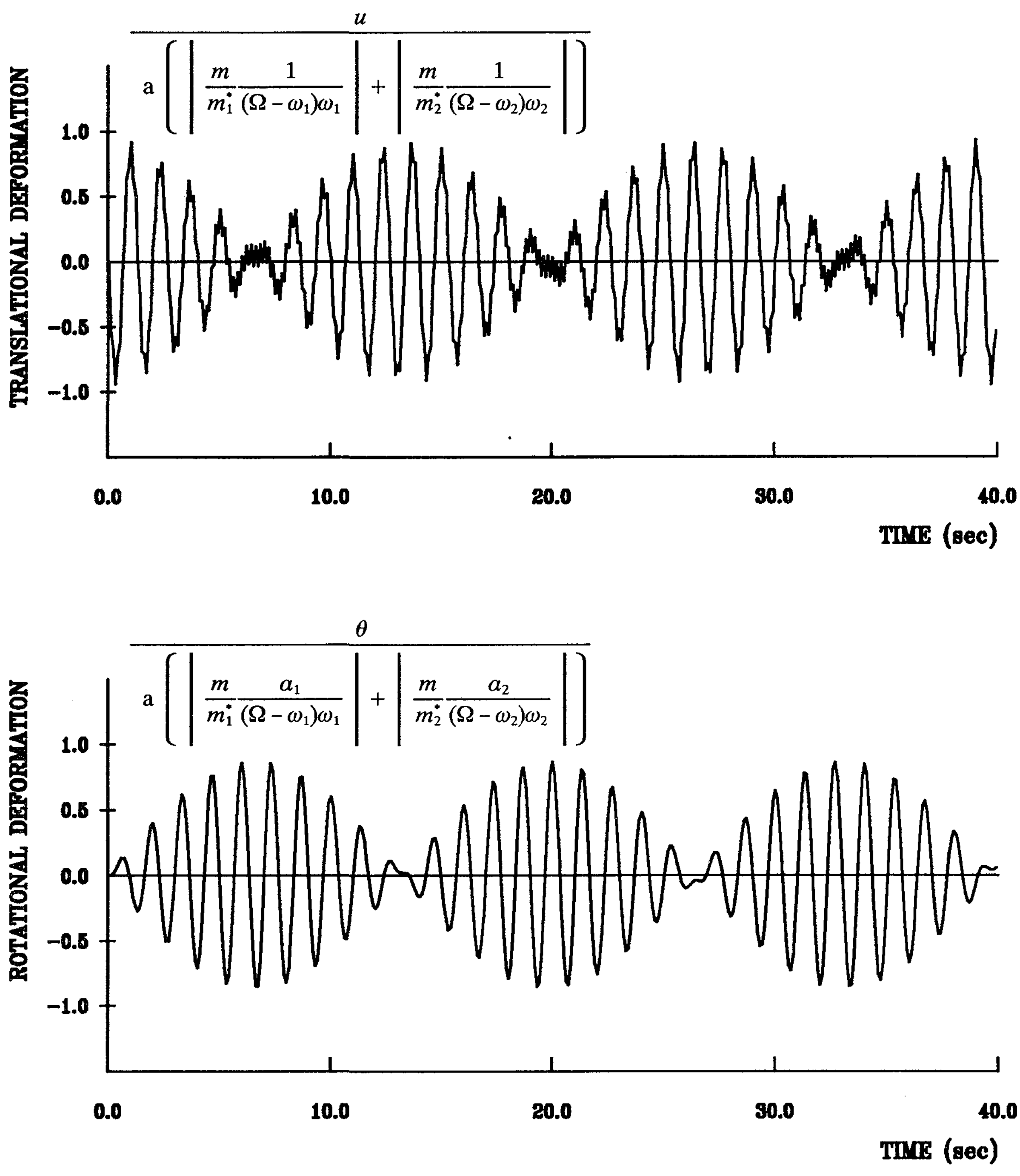

Figure 2–9 Response to Harmonic Base Excitation

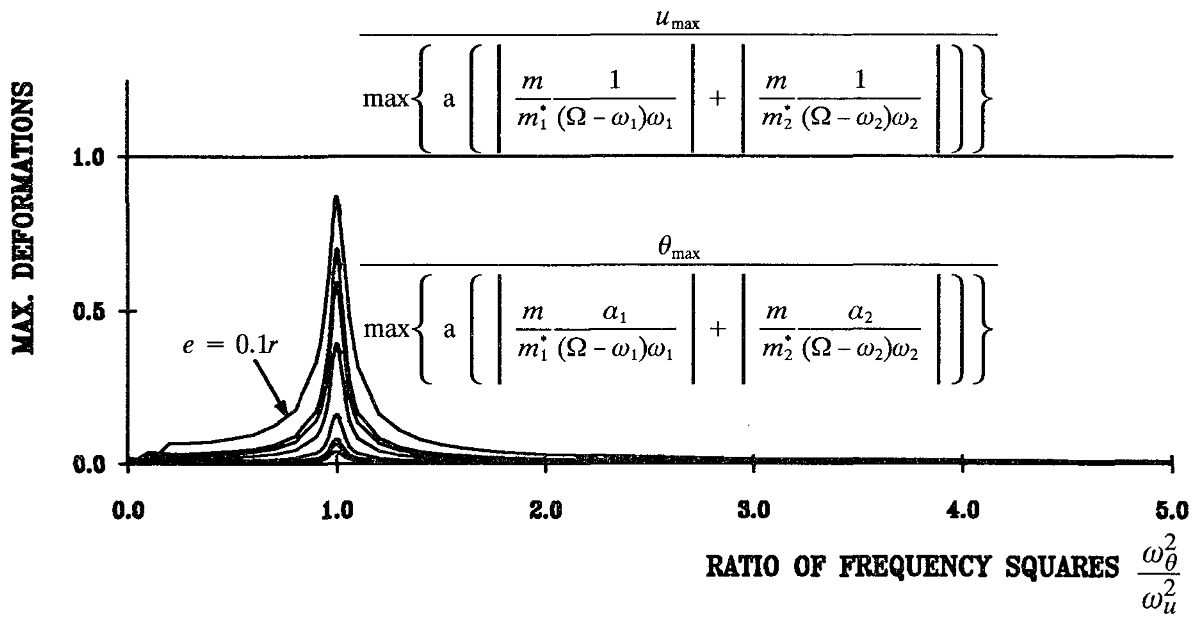

Figure 2–10 Maximum Response During Harmonic Base Excitation

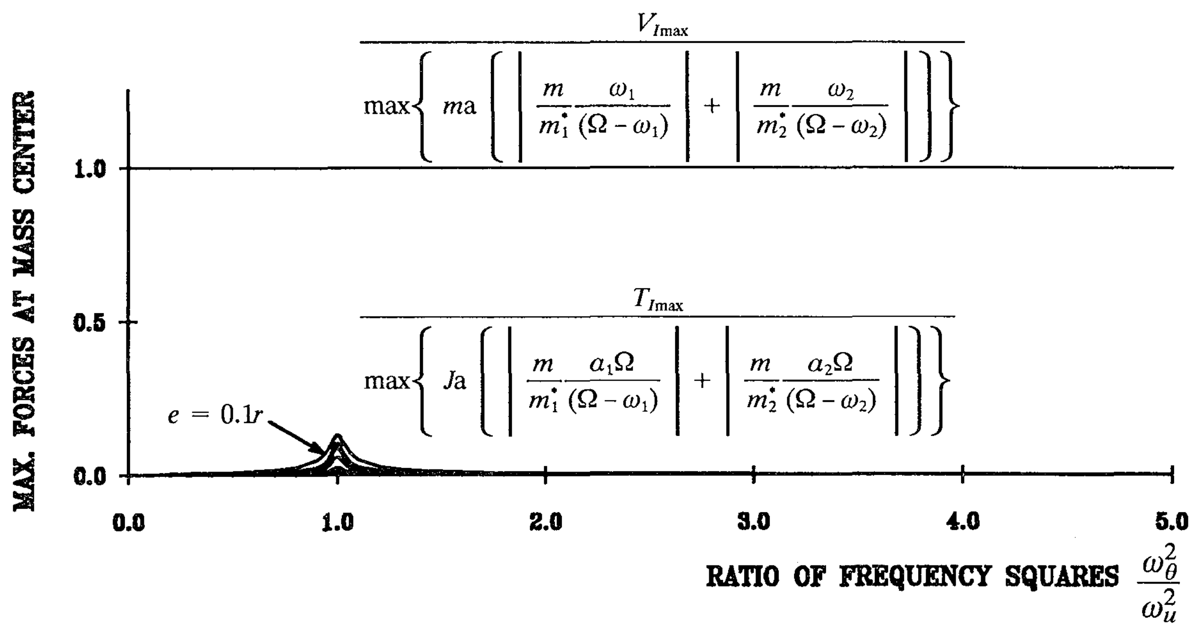

Figure 2–11 Maximum Force Response During Harmonic Base Excitation

sum of the coefficients in the respective expressions. This modification is employed only for convenience in presentation of data.

Since the inertial force acting at the center of mass is the product of mass and acceleration, these equations also can be normalized so that the normalization factors will demonstrate the dynamic amplifications of response caused by the modal instability resulting from close uncoupled frequencies. The torsional moment at the mass center, defined in Equation 2.17, can be expressed in terms of the pseudo–inertia force (the product of mass and ground acceleration) and an equivalent eccentricity,

$$\begin{aligned} T_I &= m \;\; J \;\; \mathrm{a} \left[\frac{a_1 \; \Omega^2}{m_1^*(\Omega^2 - \omega_1^2)} (- \sin \Omega t + \frac{\omega_1}{\Omega} \sin \omega_1 t) + \frac{a_2 \; \Omega^2}{m_2^*(\Omega^2 - \omega_2^2)} (- \sin \Omega t + \frac{\omega_2}{\Omega_2} \sin \omega_2 t) \right] \\ &= (\; m \;\; \ddot{u}_g(t) \;) \cdot e_{eq} \end{aligned} \tag{2.18}$$

in which

$$\begin{aligned} e_{eq} &= e + J \;\Omega^2 \left[\frac{a_1}{m_1^* \;(\omega_1^2 - \Omega^2)} + \frac{a_2}{m_2^* \;(\omega_2^2 - \Omega^2)} - \frac{e}{J \;\Omega^2} \right] \\ &- \frac{J \;\Omega}{\sin \Omega t} \left[\frac{a_1 \;\omega_1}{m_1^* \;(\omega_1^2 - \Omega^2)} \sin \omega_1 t + \frac{a_2 \;\omega_2}{m_2^* \;(\omega_2^2 - \Omega^2)} \sin \omega_2 t \right] . \end{aligned} \tag{2.19}$$

The equivalent eccentricity is so defined that the product of pseudo–inertia and this eccentricity matches the torsional moment, which is the product of the torsional moment of inertia and the angular acceleration about the center of mass. This equivalent eccentricity can be decomposed into the sum of two parts, the static eccentricity and the complemental eccentricity, as indicated in Equation 2.19. The equivalent eccentricity may reach an unexpectedly high value resulting from the beating characteristic in systems with nearly equal frequencies, as illustrated in Figure 2–12.

2.3 Effects of Frequency Shrift on The Response

It has been illustrated in the previous sections that the torsional response can be amplified as a result of nearly equal fundamental frequencies. The effects of close frequencies and structural eccentricity are demonstrated in Figures 2–6, 2–8, 2–10, and 2–11. Therefore, it is expedient to examine how to prevent the beating phenomenon from happening.

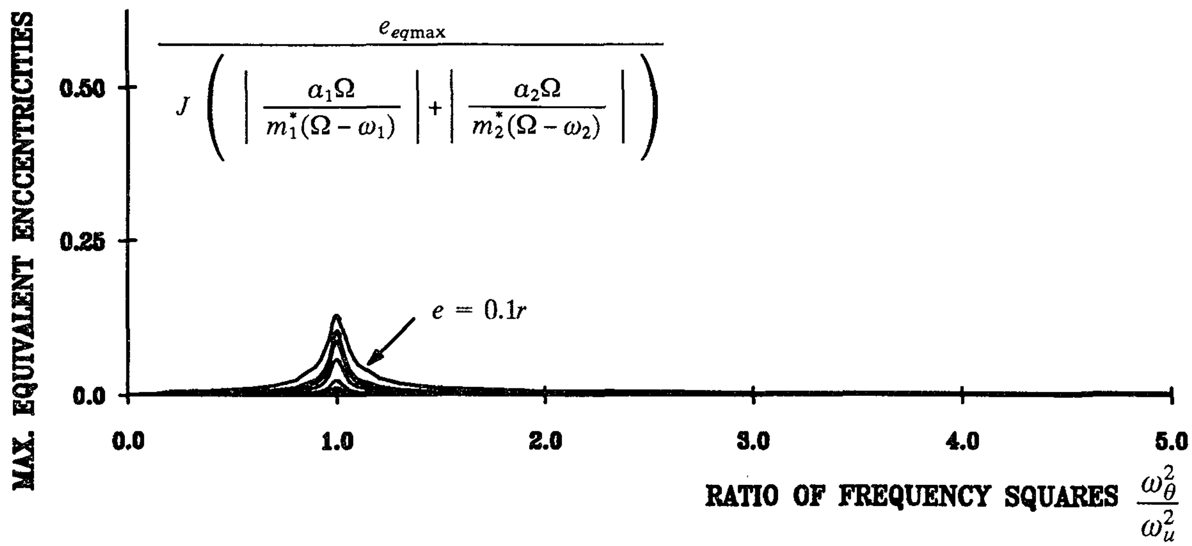

Figure 2–12 Maximum Equivalent Eccentricity During Harmonic Base Excitation

There are many uncertainties that can be cited in determining the system properties, for instance, assessment and distribution of mass, stiffness, and damping; estimate of structural frequencies; interaction between structure and foundation; and soil properties. The fundamental translational periods of vibration of a building are usually increased during strong ground motion, as a result of cracking and yielding of some nonstructural and structural members, as well as by rocking of the foundation underneath the buildings. The translational periods are commonly associated with the fundamental modes and are longer than the fundamental torsional periods. Because of the changing of building frequencies, especially the lengthening of fundamental periods in the translational direction, it is possible in the case of nearly equal fundamental frequencies to separate the lower frequencies to avoid the effects of modal instability.

When the fundamental frequencies are well separated from each other, the effect of close frequencies on structural response will vanish for structures with relatively small eccentricity, as discussed in the previous sections, because of the narrowly confined nature of modal instability.

2.4 Implications in Structural Response During Earthquakes

The foregoing discussions and observations serve to place in perspective the trends in response of undamped structures with close fundamental frequencies and small eccentricity. The investigation into response in free vibration and response to harmonic base excitation provides a basis for the study of structural response to actual earthquake excitation. It is expected that structural response during an earthquake will be more complicated because many more parameters will be involved.

In this section the effects of several parameters on structural response to earthquake ground motion are discussed in the light of the observations made in the previous sections.

2.4.1 Effects of Damping

Damping limits the magnitude of structural response both in the translational and torsional motions. The magnitude of steady–state response both in the translational and torsional motions decreases progressively as a result of damping. However, damping does not eliminate the occurrence of the beating phenomenon. The energy associated with the translational motion is partly dissipated through damping and partly transferred into the torsional motion. For systems with equal or nearly equal fundamental frequencies and small eccentricity, the transferred energy to the torsional motion might be higher than usually expected as a result of modal instability. The torsional displacements and forces may reach unexpectedly high values. This situation can be extremely harmful to the structural members located far away from the center of rigidity.

The effect of torsional coupling decreases as damping increases. The magnitudes of the beating envelopes of translational and torsional response decrease rather rapidly with the presence of damping. Therefore the proper amount of damping in a structural system may be an effective measure to control the response amplitude during beating.

2.4.2 Effects of Earthquake Ground Excitation

Earthquake–types of base excitations contain various frequencies. A ground motion input could be decomposed into harmonic base motions by means of a Fourier transformation. As mentioned in Section 2.2.5, the occurrence of beating is associated with the nature of the system, and the magnitude of the structural response is affected by the amplitude of the base motion and the relative ratios of excitation frequency to the frequencies of the system. Regardless of the frequency content of an earthquake, the beating phenomenon could occur when the fundamental frequencies are relatively close, as will be shown in Chapter 5 by the recorded response of one of the buildings during the 1987 Whittier Earthquake. Energy flow to torsional motion from translational motion imparted to the structure by ground motion through modal instability can be observed clearly in one case. It also has been demonstrated by Lin and Papageorgiou [29] that structural response to earthquake ground motion exhibits a strong beating effect, as shown by the records at the Santa Clara County Office Building during the 1984 Morgan Hill Earthquake. Since the torsional component was not significant in the incoming wave field, such a strong coupling of vibrational motions is attributed to the closely spaced fundamental translational and torsional frequencies in the building.

2.4.3 Effects of Eccentricity and Nonlinearity

From the equations of motion for linear–elastic systems, it is known that the coupling of motions in a one–directional unbalanced systems is affected strongly by eccentricities. As concluded by some, but not all, previous investigators, the translational response seems insensitive to eccentricity, but the torsional response about the center of mass increases almost linearly with increasing values of the eccentricity.

For the systems studied here with small eccentricities, the torsional response and the coupling of motions through eccentricity should not be a major concern in analysis and design. However, through modal instability in the beating phenomenon, torsional response may be excited by the translational motion in a structure only subjected to strong ground motion. As discussed and observed in this chapter the torsional response, in addition to the translational motion, increases the deformations and forces in individual members, especially the peripheral elements in the structure. Shearing forces in the members at distances away from the center of rigidity can become quite appreciable if the fundamental translational and torsional frequencies of the structure are close enough. When the response of the structure reaches a certain level then some elements may yield and go into the inelastic range. In such a case, even though the structure as a whole unit responds to the ground motion elastically, the structural eccentricities will become significant owing to the unsymmetric yielding of members, which in turn affects the total response of the structure and thus causes progressive damage to the structural assemblage.

Thus, it may be expected that geometric nonlinearity and material inelasticity in structures will change the natural characteristics of structural response to ground motion.

Changes in mass and stiffness distribution may lead to separation of fundamental frequencies of the system, so the shift of frequencies may prevent the beating phenomenon from happening. In addition, the inelastic mechanism is able to absorb imparted energy hysteretically.

2.5 Summary

The main objective of this chapter was to demonstrate the strong coupling effect in structural systems with equal or nearly equal fundamental translational and rotational frequencies. It is the slight difference in frequency that causes beating in vibration. On the contrary, if this were a case of static response to a static load, nothing of interest would be observed.

Analytical solutions for the one–directional unbalanced systems were presented for both free–vibration and forced vibration to harmonic base excitation. Trends can be observed in system responses exhibiting obvious beating phenomena as a result of modal instability associated with equal or nearly equal frequencies. Both the rotational deformation and the torsional moment could reach unexpectedly high values, even in systems with very small eccentricities. The energy in the translational motion can be transferred to the rotational motion as the result of the coupling effect not only from eccentricity but also from modal instability. Then, an inevitable question follows: what is a practical measure in design and analysis to account for such torsional amplification effect to prevent its occurrence?

An attempt was made to identify the dynamic eccentricity, which commonly is defined as the torque occurring at the center of rigidity divided by the lateral force applied at the center of mass, as expressed by

$$e_{dy} = \frac{(T_I - V_I e)}{V_I} \quad . \tag{2.20}$$

One physical interpretation is that the dynamic eccentricity defines a point in the horizontal diaphragm through which the lateral force resultant should be applied so that the diaphragm only experiences lateral translational motion without any rotational deformation. As can be perceived, the dynamic eccentricity so defined varies markedly with time, because both the torque and the lateral force are functions of time. Upon careful examination of the analytical solutions, it is concluded that the dynamic eccentricity thus defined is not a meaningful parameter. Its value could become unrealistically high, especially in structural systems showing strong beating behavior when the torsional moment and the lateral force are out of phase.

Another often used parameter is the equivalent eccentricity, without respect to time considerations, defined as the maximum torque at the center of rigidity (the numerator in Equation 2.20) divided by the maximum lateral force (the denominator in Equation 2.20). In the same manner, as being out of phase for dynamic eccentricity, the equivalent eccentricity is not able to fully account for the amplified torsional effect in structural systems with equal or nearly equal fundamental frequencies. Therefore these definitions of eccentricity are considered not to be fully complete, nor fully adequate, in dealing with dynamic effects resulting from modal instability.

On the basis of the foregoing investigation, it can be observed from Figures 2-6, 2-8, 2-10, and 2-11 that the amplified torsional effect resulting from beating behavior is limited to a relatively narrow band of frequency ratios. For practical purpose, structures should be so designed that their fundamental translational and torsional frequencies neither coincide with, nor are very close to, each other. The fundamental translational periods should be longer than the fundamental torsional period. For structures with eccentricity less than ten percent of the radius of gyration, the differences among the translational frequencies and the torsional frequency should be on the order of 10 percent to avoid strong beating effects.

Although the studies were made on the one-story one-directional unbalanced system, the results and observations are believed to be equally applicable to systems with asymmetry in the two principal directions, a subject that also deserves study in the future. Special attention should be paid to the possible strong beating and coupling effects of the two translational motions through torsion.

CHAPTER 3

MODELING OF INELASTIC BEHAVIOR

3.1 Introduction

Modeling techniques of structural behavior are an important element of accurate and meaningful analysis. As a part of the process of developing a better understanding of torsional behavior in the seismic response of buildings, there is a need for analytical models that are able to analyze in a reasonable manner the inelastic response of structures, to account for force–interaction in load–resisting elements, and to consider various models of material with strength hardening. The work presented in this chapter is part of that effort.

In structural analysis, especially in response–history analysis of structures during earthquakes, it is convenient and economical to work with quantities in the force–displacement space rather than quantities in the stress–strain space. Based on the theory of classical plasticity, a general theory of yielding is formulated in the following in terms of forces and displacements of lateral resisting members. The purpose of this chapter is to develop an extended mathematical model for elastic and inelastic behavior of simple structures under earthquake excitation, a model that will provide better comprehension of torsional effects arising from seismic base motion. This model is used in the analysis that follows in Chapters 4 and 5.

3.2 Dynamic Inelastic Response of Structures

In reality, a building's response to severe earthquakes almost always exhibits a certain degree of inelastic behavior. Moreover it has been observed that the inelastic behavior of structures plays an important role during earthquakes. Despite the simplicity and the relatively small amount of time required for thorough analysis, only a small number of buildings can be modeled linear–elastically to observe and study the structural behavior and response under the effects of strong ground motion. In modern design practice, hysteresis as a result of inelastic nonlinearity is an energy dissipation mechanism which may help structures to sustain strong seismic motion without suffering severe structural damage. A better understanding of the inelastic behavior of structures subjected to strong ground motion should aid in leading to improvement in seismic design provisions, to selecting proper seismic loadings, and to providing practical guidelines for design. It may be well to point out that the amount of nonlinear behavior considered herein is small. Moreover the hysteretic model is a simple one, reasonably representative for steel members, but not representative of the "degradation and pinching" type hysteretic models that more accurately represent inelastic behavior in concrete members that undergo extensive deformation.

3.2.1 Equations of Motion

The analytical model defined here is a shear–beam type of structure with rigid floors resting on axially inextensible weight-bearing members. A multi–story, lumped mass, rigid–floor structural idealization, as shown in Figure 3–1, is employed. The chosen degrees of freedom are the displacements at the mass center of each floor including the two translational (u_x, u_y) and one rotational (θ) motions relative to the base. The floors are interconnected by a number of columns or shear resisting elements. Each such

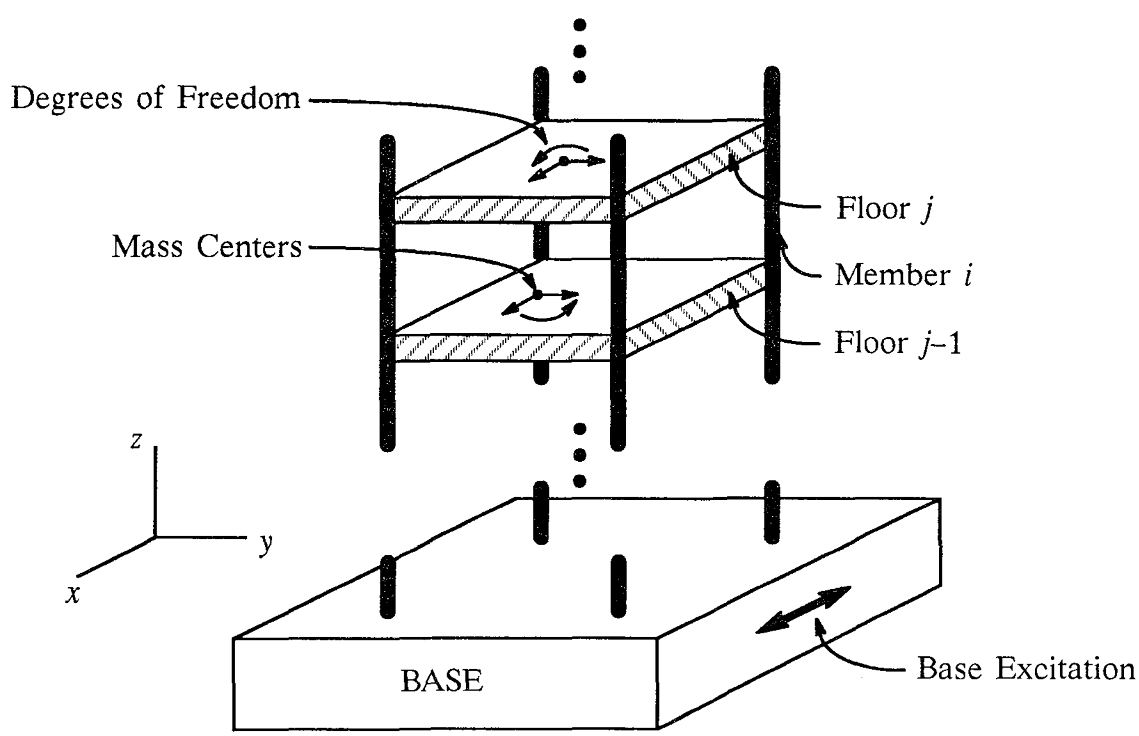

Figure 3–1 Idealized Structural Model

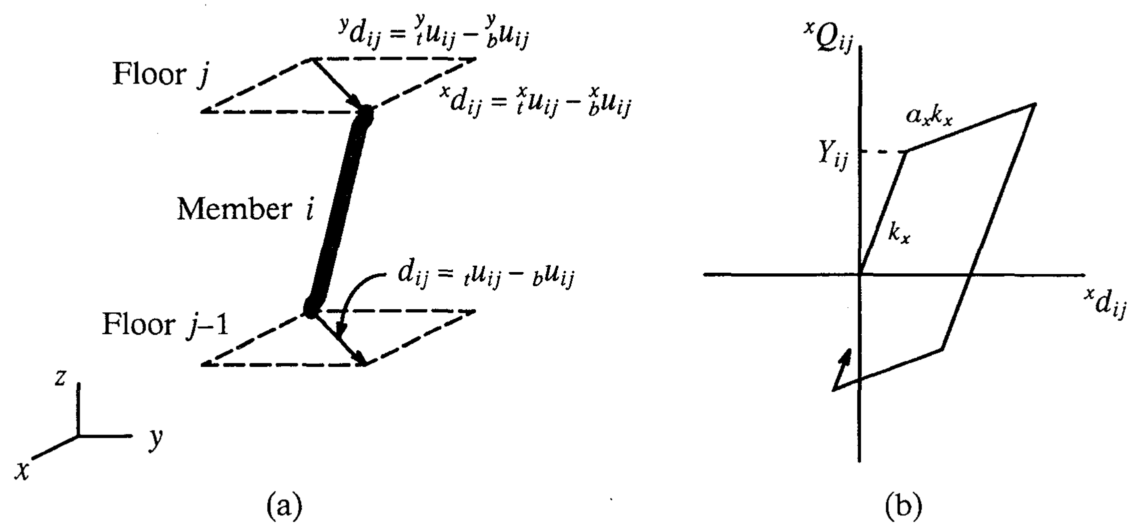

Figure 3–2 Uniaxial Material Model for Member i of Story j

element has its corresponding uniaxial or one–dimensional shear–displacement relation as shown in Figure 3–2. The yielding zones are assumed to be confined exclusively to the top and bottom of these shear resisting elements, so that each member has the same yield surface for each of its end nodes.

The equations of motion for the system are established in terms of the incremental displacements and the lumped forces at the degrees of freedom. From equilibrium, the external applied force at any time instant should be balanced by the inertial force, the damping force, and the restoring force in the system. In order to integrate the dynamic equations, it is assumed that the response quantities at the previous time step are known. The restoring force could be estimated by summing up the restoring force at the previous time step and the approximate tangential increment during the current time interval. In other words,

$$
\begin{aligned}
{}^{t+\Delta t}\{P\} &= [M]\ {}^{t+\Delta t}\{\ddot{U}\} + [C]\ {}^{t+\Delta t}\{\dot{U}\} + {}^{t+\Delta t}\{Q\} \\
&= [M]\ {}^{t+\Delta t}\{\ddot{U}\} + [C]\ {}^{t+\Delta t}\{\dot{U}\} + {}^{t}\{Q\} + \{\Delta Q\} \\
&= [M]\ {}^{t+\Delta t}\{\ddot{U}\} + [C]\ {}^{t+\Delta t}\{\dot{U}\} + {}^{t}\{Q\} + {}^{t}[K]\{\Delta U\}\ , \qquad (3.1)
\end{aligned}
$$

where ${}^{t+\Delta t}\{P\}$ = external force vector applying onto the system at time $t+\Delta t$,

${}^{t+\Delta t}\{Q\}$ = restoring force vector of the system at time $t+\Delta t$,

${}^{t+\Delta t}\{U\}$ = displacement vector of the degrees of freedom at time $t+\Delta t$,

$\{\Delta Q\}$ = incremental restoring force vector during the time interval Δt,

$\{\Delta U\}$ = incremental displacement vector during the time interval Δt,

$[M]$ = diagonal mass matrix of the system,

$[C]$ = proportional damping matrix of the system,

${}^{t}[K]$ = tangent stiffness matrix of the system at time t, and

the dots represent the derivative of variables with respect to time.

If the number of stories in the structure is N, the number of equations and the order of variable vectors are $3N$ with three degrees of freedom per story.

By means of Newmark's β method [32], the set of equations of motion for lumped–mass systems is readily converted into the familiar incremental form of static equilibrium equations in Appendix D,

$$[K^*]\{\Delta U\}^{(i)} = \{\Delta P^*\} \ , \tag{3.2}$$

where $[K^*] = \dfrac{1}{\beta \Delta t^2}[M] + \dfrac{\gamma}{\beta \Delta t}[C] + {}^{t}[K]$,

$$\begin{aligned}
\{\Delta P^*\} &= {}^{t+\Delta t}\{P\} - {}^{t+\Delta t}\{Q\}^{(i-1)} \\
&\quad - [M]\left[\frac{1}{\beta \Delta t^2}\left({}^{t+\Delta t}\{U\}^{(i-1)} - {}^{t}\{U\} \right) - \frac{1}{\beta \Delta t}{}^{t}\{\dot{U}\} - \left(\frac{1}{2\beta} - 1\right){}^{t}\{\ddot{U}\}\right] \\
&\quad - [C]\left[\frac{\gamma}{\beta \Delta t}\left({}^{t+\Delta t}\{U\}^{(i-1)} - {}^{t}\{U\} \right) + \left(1 - \frac{\gamma}{\beta}\right){}^{t}\{\dot{U}\} + \left(1 - \frac{\gamma}{2\beta}\right)\Delta t \ {}^{t}\{\ddot{U}\}\right] ,
\end{aligned}$$

$${}^{t+\Delta t}\{U\}^{(i)} = {}^{t+\Delta t}\{U\}^{(i-1)} + \{\Delta U\}^{(i)} \ ,$$

$${}^{t+\Delta t}\{Q\}^{(i)} = {}^{t+\Delta t}\{Q\}^{(i-1)} + {}^{t}[K]\{\Delta U\}^{(i)} \ ,$$

$${}^{t+\Delta t}\{U\}^{(0)} = {}^{t}\{U\} \ , \text{ and}$$

$${}^{t+\Delta t}\{Q\}^{(0)} = {}^{t}\{Q\} \ . \tag{3.3}$$

The effective stiffness matrix $[K^*]$ in dynamic analysis involves the mass and damping matrices, and it corresponds to the stiffness matrix in static analysis. By the same token, the effective load vector $\{\Delta P^*\}$ in dynamic analysis contains the response quantities at the beginning of the time step and the property matrices of the system. It is observed that no iteration is needed for solutions to linear systems. It generally requires some number of iterations for solutions to a nonlinear system in order to achieve certain accuracy within the desired tolerance(s), simply because the method approximates system response during the time interval. The Modified Newton–Raphson's method or the quasi–Newton methods [3] can be used to solve Equation 3.2.

When the response of a structural system is required during and after strong ground motion, the external force applied to the system is generated only from base excitation. The force vector ${}^{t+\Delta t}\{P\}$ in Equations 3.1 and 3.2 at any time instant becomes

$$\{P(t)\} = -[M]\ [1]\ \{\ddot{U}_g\}\ , \tag{3.4}$$

where $[1]$ is a $3N$x3 rectangular matrix filled by N number of stacking 3x3 unity matrices, and

$\{\ddot{U}_g\}$ is the ground motion vector, in which only the translational components of the ground motion is considered in this study,

$$\{\ddot{U}_g\} = \begin{Bmatrix} {}^x\ddot{U}_g \\ {}^y\ddot{U}_g \\ {}^\theta\ddot{U}_g \end{Bmatrix} = \begin{Bmatrix} {}^x\ddot{U}_g \\ {}^y\ddot{U}_g \\ 0 \end{Bmatrix}. \tag{3.5}$$

3.2.2 Deformations and Restoring Forces in Individual Members

It is convenient to let $\{\Delta U_j\}$ represent the global incremental displacements of story j relative to the ground; it is a sub–vector of the incremental displacement vector $\{\Delta U\}$ in Equation 3.2. Also $\{\Delta U_{ij}\}$ is defined as the local relative displacement in element i of story j with respect to the ground. The relations for transformation between the local element quantities and the global structural quantities are given below,

$$\{\Delta U_{ij}\} = \begin{Bmatrix} \Delta_t U_{ij} \\ \Delta_b U_{ij} \end{Bmatrix} = \begin{bmatrix} {}_tZ_{ij} & 0 \\ 0 & {}_bZ_{ij} \end{bmatrix} \begin{Bmatrix} \Delta U_j \\ \Delta U_{(j-1)} \end{Bmatrix} . \tag{3.6}$$

In this expression $[{}_tZ_{ij}]$ and $[{}_bZ_{ij}]$ are the transformation matrices for displacements at the column top and bottom, respectively, namely

$$[{}_tZ_{ij}] = \begin{bmatrix} 1 & 0 & -({}_tY_{ij} - {}_mY_j) \\ 0 & 1 & ({}_tX_{ij} - {}_mX_j) \end{bmatrix} \quad \text{and} \quad [{}_bZ_{ij}] = \begin{bmatrix} 1 & 0 & -({}_bY_{ij} - {}_mY_{(j-1)}) \\ 0 & 1 & ({}_bX_{ij} - {}_mX_{(j-1)}) \end{bmatrix},$$

in which $\{{}_tX_{ij}, {}_tY_{ij}\}$ and $\{{}_bX_{ij}, {}_bY_{ij}\}$ are the respective coordinates of the top and bottom of element i of story j, and $\{{}_mX_j, {}_mY_j\}$ are the coordinates of the mass center of story j. The terms $\{\Delta_tU_{ij}\}$ and $\{\Delta_bU_{ij}\}$ are the incremental lateral displacements relative to the base at the top and bottom, respectively, of element i of story j, namely

$$\{\Delta_tU_{ij}\} = \begin{Bmatrix} \Delta_t^x u_{ij} \\ \Delta_t^y u_{ij} \end{Bmatrix} \quad \text{and} \quad \{\Delta_bU_{ij}\} = \begin{Bmatrix} \Delta_b^x u_{ij} \\ \Delta_b^y u_{ij} \end{Bmatrix}.$$

The global displacement increments of story j and story $(j-1)$ relative to the ground include

$$\{\Delta U_j\} = \begin{Bmatrix} \Delta^x U_j \\ \Delta^y U_j \\ \Delta\theta_j \end{Bmatrix} \quad \text{and} \quad \{\Delta U_{(j-1)}\} = \begin{Bmatrix} \Delta^x U_{(j-1)} \\ \Delta^y U_{(j-1)} \\ \Delta\theta_{(j-1)} \end{Bmatrix},$$

in which $\Delta^x U_j$, $\Delta^y U_j$ and $\Delta\theta_j$ are the incremental lateral displacements in the x– and y–direction and the incremental rotational displacement, respectively, relative to the base at the mass center of story j. The deformation increment $\{\Delta D_{ij}\}$ of element i of story j is defined as the difference of top and bottom displacement increments of the element, as illustrated in Figure 3–2(a),

$$\{\Delta D_{ij}\} = \{\Delta_tU_{ij}\} - \{\Delta_bU_{ij}\} \; . \tag{3.7}$$

In the equations of motion, Equation 3.1 or 3.2, the resistance ${}^{t+\Delta t}\{Q\}$ is a function of deformations in the structure. The restoring force vector contains the story shear forces and torsional moments at the mass center of each story. By the incremental step–by–step numerical procedure, the equations of motion are solved for the displacements of the degrees of freedom. This set of incremental displacements then is transformed by Equations 3.6 and 3.7 into the deformations in each lateral shear resisting member. Based on the computed deformations, the shear forces $\Delta^x Q_{ij}$ and $\Delta^y Q_{ij}$ are computed for each member as follows (neglecting the element torsional stiffness),

$$\{\Delta Q_{ij}\} = [K_{ij}^{ep}]\{\Delta D_{ij}\} \; . \tag{3.8}$$

In order to account for inelastic behavior in the members, the stiffness matrix $[K_{ij}^{ep}]$ should be an approximation to the tangent stiffness matrix, which will be derived in the next section. Finally, the possible inelastic restoring forces in relevant individual elements are assembled into the total restoring force vector ${}^{t+\Delta t}\{Q\}$. As a check, this total restoring force vector with the current inertia and damping force should balance the external applied forces.

3.3 Modeling of Inelastic Behavior in Force Space

A stable inelastic material is defined by Drucker's postulate,

$$\oint_{\{Q_s^a\}} (\{Q_s\} - \{Q_s^a\}) \cdot \{dq_s\} \;\; \geq \;\; 0 \;, \tag{3.9}$$

where $\{Q_s\}$ is the generalized stress, $\{q_s\}$ is the generalized strain, and $\{Q_s^a\}$ is the stress state at the beginning of any deformation process during which only positive work is done. The force–deformation characteristic of the resisting members in this study falls into this category. This postulate governs the force–deformation relationships of the elements.

This study assumes initial elasticity during the loading or elastic unloading in the lateral load–resisting elements of a structural system, and neglects time–dependent and thermal effects on the strength and stiffness of the members. With the assumption of linearized response during a typical time step, a proper definition of a consistent tangent operator is developed to maintain convergence of the Newton–type solution schemes [47] used in solving Equation 3.2. For elastic displacement, the solution of a nonlinear problem is achieved by solving a sequence of linear problems with the consistent tangent operator. For inelastic displacement, the response solution is calculated in an incremental process which must be characterized by solving the rate constitutive equations. Accordingly, the application of the solution procedure for elastic systems to inelastic response requires the numerical integration of the rate constitutive equations over a discrete sequence of time intervals. Thus, the integration algorithm enables one to formally treat the elasto–plastic problems over a typical time step as an equivalent elastic problem, with a modified tangent stiffness in Equation 3.1 to account for the inelastic behavior.

It is assumed that the inelastic response quantities of a structural system at the beginning of a time step ($t = t$) are already known, and the response at the end of the time step ($t = t + \Delta t$) are required during the plastic or neutral loading. In the following derivation, the pre-superscript $t + \Delta t$ is omitted in the equations for conciseness.

3.3.1 Associated Flow Rule and Deformation Rates

The response of a structural system subjected to strong ground motion usually involves elastic and plastic deformations. A flow rule is necessary for decomposing the deformations into elastic and plastic parts during neutral or plastic loadings in an individual shear resisting member. The associated flow rule is adopted here because of its generality and simplicity. It is assumed that the plastic deformation increment $\{\Delta D_{ij}^p\}$ lies in the outer direction normal to the selected yield surface, resulting in a symmetrical stiffness matrix defined by the force–deformation relationship.

As research in the theory of plasticity has demonstrated, the decomposition of total deformation into elastic and plastic deformations is at best a crude approximation in inelastic analysis, especially in systems with relatively large deformation. On the contrary, solutions expressed in terms of deformation rates with respect to time give a fairly good estimate in describing the state of most systems. Thus, deformation rates are chosen in decomposing the deformations into elastic and plastic parts. Let $\{\dot{D}_{ij}\}$ represent the deformation rate, $\{\dot{D}_{ij}^e\}$ be the elastic deformation rate, and $\{\dot{D}_{ij}^p\}$ be the plastic deformation rate. With the assumption that the current state of the member is already on the interaction yield surface (which is capable of accounting for strength hardening), the decomposition is expressed as

$$\{\dot{D}_{ij}\} = \{\dot{D}_{ij}^e\} + \{\dot{D}_{ij}^p\} \ . \tag{3.10}$$

Given a yield surface $\Phi_{ij} = 1$ in the force space, the direction of the plastic deformation rate is defined as being normal to the yield surface by the associated flow rule,

$$\{\dot{D}_{ij}^p\} = \dot{\lambda} \ \{n_{ij}\} \ , \tag{3.11.a}$$

where $\dot{\lambda}$ = proportional scalar to be determined in the following, and

$\{n_{ij}\}$ = unit vector normal to the yield surface at the current force state,

$$\{n_{ij}\} = \frac{\left\{\frac{\partial \Phi}{\partial Q_{ij}}\right\}}{\sqrt{\left\{\frac{\partial \Phi}{\partial Q_{ij}}\right\} \cdot \left\{\frac{\partial \Phi}{\partial Q_{ij}}\right\}}} \quad . \tag{3.11.b}$$

During the neutral or plastic loading, the proportional scalar $\dot{\lambda}$ will be computed through use of the plastic hardening rules by satisfying the consistency condition that the final state of the member remains on the yield surface (${}^{t+\Delta t}\Phi_{ij} = 1$).

Two variables are defined here, the equivalent plastic deformation increment $d_eD^p_{ij}$ and the equivalent force increment d_eQ_{ij}. The equivalent plastic deformation increment $d_eD^p_{ij}$ is defined as the norm of the plastic deformation, representing the length of the plastic deformation increment $\{\dot{D}^p_{ij}\}dt$ in Equation 3.11,

$$d_eD^p_{ij} = \| \{\dot{D}^p_{ij}\}dt \| = \sqrt{\{\dot{D}^p_{ij}\}dt \cdot \{\dot{D}^p_{ij}\}dt} = \dot{\lambda}\ dt\ \sqrt{\{n_{ij}\} \cdot \{n_{ij}\}} = \dot{\lambda}\ dt \ . \tag{3.12}$$

The equivalent force increment is expressed as the projection of the incremental element force onto the normal direction of the yield surface,

$$d_eQ_{ij} = \{dQ_{ij}\} \cdot \{n_{ij}\} \ . \tag{3.13}$$

In terms of the energy dissipated during the time interval, the work done in the equivalent space defined by the two variables should be equal to the work done in the multi–dimensional space ($d_eQ_{ij} \cdot d_eD^p_{ij} = \{dQ_{ij}\} \cdot \{dD^p_{ij}\}$).

The equivalent deformation increment is related to the equivalent force increment through a plastic modulus k. This plastic modulus is assumed to be a constant throughout the time step. It can be calculated from the pre–defined uniaxial force–deformation relation given for element i of story j in Figure 3–2(b) which is similar to Figure 3–3. For members with bilinear uniaxial force–deformation relationship as shown in Figure 3–3, the modulus k is derived in Appendix E,

$$k = \frac{d_eQ_{ij}}{d_eD^p_{ij}} = \frac{a_x\ k_x}{(1 - a_x)} \ , \tag{3.14.a}$$

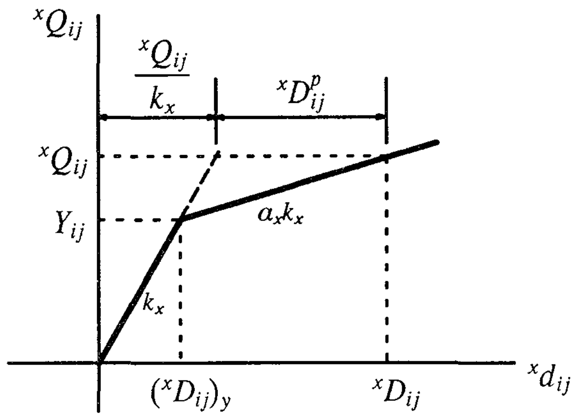

Figure 3–3 Bilinear Shear Resisting Member i of Story j

in which k_x is the elastic stiffness of the member i of story j in the x–direction and a_x is the hardening coefficient. The symbols in Figure 3–3 are defined as follows: Y_{ij} is the yield force, $({}^{x}D_{ij})_y$ represents the yield deformation in the x–direction, ${}^{x}Q_{ij}$ and ${}^{x}D_{ij}$ are the current shear force level and deformation in the x–direction, respectively, and ${}^{x}D^{p}_{ij}$ equals the plastic deformation in the x–direction.

For members with nonlinear behavior in the uniaxial force–deformation relation, the plastic modulus k is expressed as

$$k = \frac{d_e Q_{ij}}{d_e D^{p}_{ij}} \ . \tag{3.14.b}$$

To calculate the proportional scalar $\dot{\lambda}$ in Equation 3.11 for the plastic deformation rate, it can be done conveniently by examining the equivalent force increment $d_e Q_{ij}$. As exemplified in Figure 3–4 for a uniaxial test, the force increment is related to the elastic deformation through a consistent tangent operator by the rate equation,

$$\begin{aligned} \{\dot{Q}_{ij}\} &= [K^{e}_{ij}]\ \{\dot{D}^{e}_{ij}\} \\ &= [K^{e}_{ij}]\ (\ \{\dot{D}_{ij}\} - \{\dot{D}^{p}_{ij}\}\ ) \\ &= [K^{e}_{ij}]\ (\ \{\dot{D}_{ij}\} - \dot{\lambda}\ \{\ n_{ij}\ \}\ )\ , \end{aligned} \tag{3.15}$$

where $[K^{e}_{ij}]$ is the elastic stiffness matrix of element i of story j. From the definition of the equivalent force increment in Equation 3.13, and from Equations 3.12 and 3.14, the projection of the force increment onto the normal direction gives

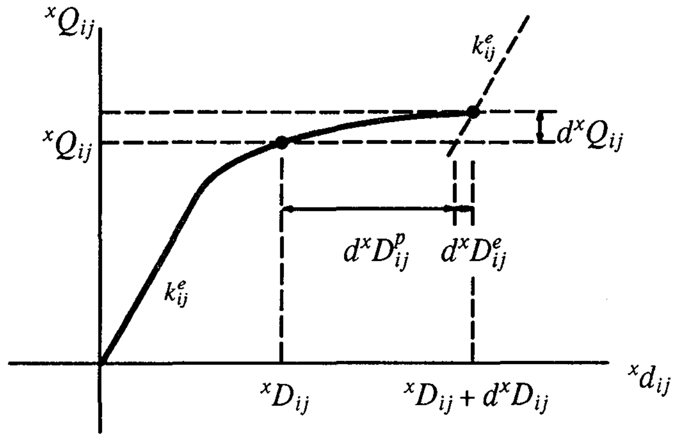

Figure 3–4 Uniaxial Force–Deformation Curve for Member $i\,j$

$$\begin{aligned}\{dQ_{ij}\} \cdot \{n_{ij}\} &= \{n_{ij}\} \cdot \{\dot{Q}_{ij}\}\ dt \\ &= \{n_{ij}\}^T[K^e_{ij}]\{\dot{D}_{ij}\}\ dt - \dot{\lambda}\ dt\ \{n_{ij}\}^T[K^e_{ij}]\{n_{ij}\} \\ &= k\ \dot{\lambda}\ dt\ .\end{aligned}$$

Hence, the proportional scalar is given by

$$\dot{\lambda} = \frac{\{n_{ij}\}^T[K^e_{ij}]\{\dot{D}_{ij}\}}{k + \{n_{ij}\}^T[K^e_{ij}]\{n_{ij}\}}\ . \tag{3.16}$$

By substituting this scalar back to the rate equation, Equation 3.15 becomes

$$\{\dot{Q}_{ij}\} = \left([K^e_{ij}] - \frac{[K^e_{ij}]\{n_{ij}\}\{n_{ij}\}^T[K^e_{ij}]}{k + \{n_{ij}\}^T[K^e_{ij}]\{n_{ij}\}} \right) \{\dot{D}_{ij}\}\ . \tag{3.17}$$

Comparing this expression with Equation 3.8 reveals that

$$[K^{ep}_{ij}] = [K^e_{ij}] - \frac{[K^e_{ij}]\{n_{ij}\}\{n_{ij}\}^T[K^e_{ij}]}{k + \{n_{ij}\}^T[K^e_{ij}]\{n_{ij}\}}\ . \tag{3.18}$$

From the proceeding equations, the following observations are made. In ideal plasticity, i.e., for elastic–perfectly–plastic materials, once a member reaches its ultimate strength, it no longer contributes any additional stiffness or strength to the entire structural system except in the case of elastic unloading. This may be represented in the generalized coordinates by the fact that once the state of the member gets onto the yield surface, the tangent stiffness of the member becomes singular until the member is elastically unloaded. The plastic deformation increment (rate) of the member, as defined by the associated flow rule, lies in the direction normal to the yield surface. Since the plastic modulus k equals zero, the inelastic stiffness matrix becomes a singular matrix while on the yield surface.

3.3.2 Strength Hardening of Structural Members

Following the theory of plasticity, strength hardening of materials generally is specified in two ways: kinematic and isotropic hardening. For the kinematic type of hardening, the yield surface translates without changing its shape or size in the force space. In the isotropic hardening model the yield surface expands isotropically every time the material is reloaded beyond yielding. The combination of these two hardening models leads to a model that exhibits reasonably realistic behavior of many structural materials [12, 47]. The combined hardening model can be used to account for the Bauschinger effect if desired.

3.3.2.a Kinematic Hardening Model

The kinematic hardening model assumes that the total force $\{Q_{ij}\}$ is composed of the back–force component $\{B_{ij}\}$ and the shifted–force component $\{S_{ij}\}$, i.e.,

$$\{Q_{ij}\} = \{B_{ij}\} + \{S_{ij}\} \ . \tag{3.19}$$

The back–force $\{B_{ij}\}$ is used to account for strength hardening and to locate the center of the yield surface. The behavior of the shifted–force $\{S_{ij}\}$ resembles that of the force component in the elasto-plastic material model. In Figure 3–5(a) the locations of the back–force ${}^{x}B_{ij}$ are illustrated by the dashed base line in the bilinear uniaxial $Q - D$ plot. Also shown in Figure 3–5(b) is the manner by which the back–force $\{B_{ij}\}$ locates the center of the yield surface in the case of two–dimensional force interaction.

The yield surface for kinematic hardening can be expressed in the form

$$\Phi(\{S_{ij}\}) = \Phi(\{Q_{ij}\} - \{B_{ij}\}) = 0 \ . \tag{3.20}$$

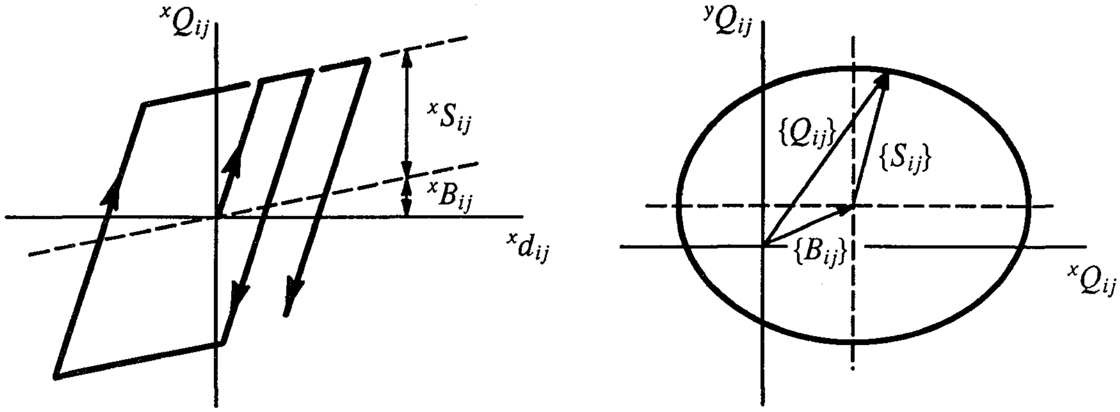

(a) (b)

Figure 3–5 Kinematic Hardening Model

As may be observed, certain rules are required in order to define how the yield surface translates as a result of kinematic hardening. Prager's rule is used in this study; it assumes that the surface translates in the normal direction at the current force state $\{Q_{ij}\}$, as shown in Figure 3–6. The increment of the back–force $\{\Delta B_{ij}\}$ grows in the normal direction by Prager's rule,

$$\{dB_{ij}\} = dB^P \{n_{ij}\} \ , \tag{3.21}$$

where dB^P is a scalar and the superscript P stands for Prager's rule. As was defined for the equivalent force, the magnitude of the back–force increment is the projection of the force increment onto the normal direction, defined in Equations 3.13 and 3.14, or

$$dB^P = d_eQ_{ij} = k \ d_eD^p_{ij} = k \ \dot{\lambda} \ dt \ . \tag{3.22}$$

The shifted–force exhibits the elasto–plastic behavior on the yield level, so the shifted–force increment $\{\Delta S_{ij}\}$ is perpendicular to the normal [37, 57].

3.3.2.b Isotropic Hardening Model

Isotropic hardening is a straight forward strain–hardening model. If it is assumed that the shape of the yield surface does not change during material hardening and that the ratios of the yield forces in different directions are constants, there exists one parameter in

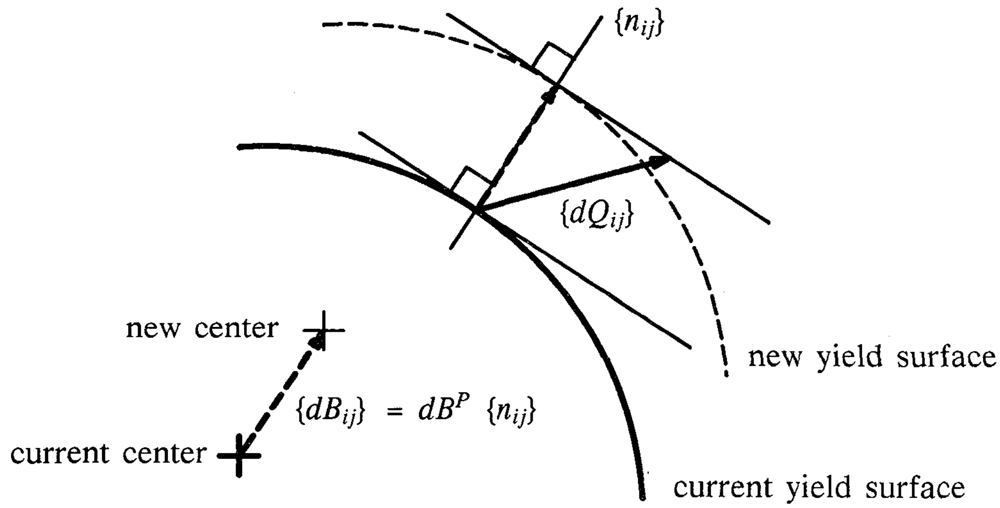

Figure 3–6 Prager's Rule in Kinematic Hardening

controlling the hardening process. This is similar to the von Mises type yielding criterion dictated by one parameter. Therefore one can assign

$$r_x = 1 \ , \qquad r_y = \frac{{}^yY_{ij}}{Y_{ij}} \ , \qquad \cdots \ , \tag{3.23}$$

in which Y_{ij} and ${}^yY_{ij}$ are the uniaxial yield forces in the x– and y–direction, respectively, and r_x and r_y are the constant ratios of the yield forces in different directions.

Figure 3–7(a) exemplifies the changing of yield–force–level in the uniaxial $Q-D$ plot, and Figure 3–7(b) shows the expanding of the yield surface for two–dimensional force–interaction.

The general form of the yield function for isotropic hardening is $\Phi(\{Q_{ij}\}, \{Y_{ij}\})$ being zero where $\{Y_{ij}\}$ is the uniaxial yield force vector containing Y_{ij}, ${}^yY_{ij}$, etc. in the respective directions. According to the consistency condition in plasticity, the new point in the force space must still satisfy the yield criterion after any deformation and/or force increment, i.e., the new point must stay on the expanded yield surface, defined by the expression $\Phi(\{Q_{ij} + dQ_{ij}\}, \{Y_{ij} + dY_{ij}\}) = 0$.

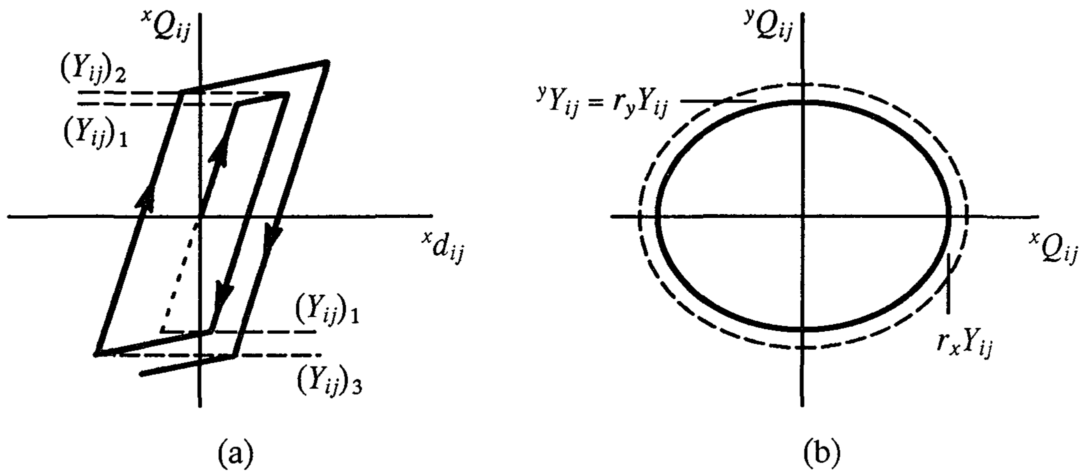

Figure 3–7 Isotropic Hardening Model

For the von Mises type of yielding criterion, the expansion of yield surface in isotropic hardening is controlled by one parameter Y_{ij} for the element being considered. The yield function can be expressed then as

$$\Phi(\{Q_{ij}\}, Y_{ij}) = 0 \ . \tag{3.24}$$

During any deformation and/or force increment as the yield surface expands,

$$d\Phi(\{Q_{ij}\}, Y_{ij}) = \left\{\frac{\partial \Phi}{\partial Q_{ij}}\right\} \cdot \{dQ_{ij}\} + \frac{\partial \Phi}{\partial Y_{ij}} \, dY_{ij} = 0 \ . \tag{3.25}$$

Hence, from Equations 3.11, 3.13, and 3.14

$$\begin{aligned} dY_{ij} &= - \left\{\frac{\partial \Phi}{\partial Q_{ij}}\right\} \cdot \{dQ_{ij}\} \Bigg/ \frac{\partial \Phi}{\partial Y_{ij}} \\ &= - \sqrt{\left\{\frac{\partial \Phi}{\partial Q_{ij}}\right\} \cdot \left\{\frac{\partial \Phi}{\partial Q_{ij}}\right\}} \ (\{n_{ij}\} \cdot \{dQ_{ij}\}) \Bigg/ \frac{\partial \Phi}{\partial Y_{ij}} \\ &= - \sqrt{\left\{\frac{\partial \Phi}{\partial Q_{ij}}\right\} \cdot \left\{\frac{\partial \Phi}{\partial Q_{ij}}\right\}} \ (k \ \dot{\lambda} \ dt) \Bigg/ \frac{\partial \Phi}{\partial Y_{ij}} \ . \end{aligned} \tag{3.26}$$

In summary, a force increment in the force space in the tangent direction on the yield surface represents the elastic–perfectly–plastic behavior $\{\Delta S_{ij}\}$ [37, 57], and the force

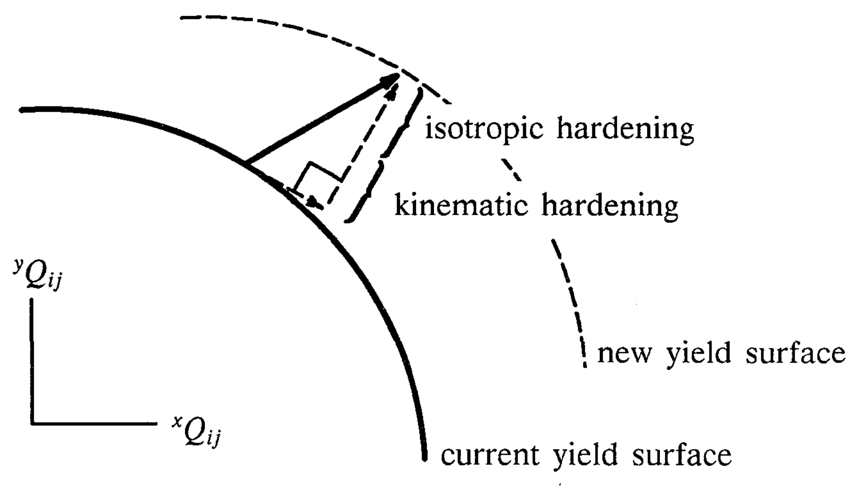

Figure 3–8 Decomposition of Strength Hardening

increment in the normal direction represents the strength hardening behavior $\{\Delta B_{ij}\}$ + $\{\Delta Y_{ij}\}$. Any strength hardening characterization can be decomposed into two components through shifting and expanding of the yield surface, as illustrated in Figure 3–8.

In strength hardening the kinematic and isotropic hardening models are combined to account for the Bauschinger effect. From Equations 3.21 and 3.26, the plastic hardening rules consistent with the von Mises yield criterion are,

$$\begin{aligned} \{dB_{ij}\} &= (1-\xi)\; k\; \dot{\lambda}\; dt\; \{n_{ij}\}\ , \text{ and} \\ dY_{ij} &= -\,\xi \sqrt{\left\{\frac{\partial\Phi}{\partial Q_{ij}}\right\}\cdot\left\{\frac{\partial\Phi}{\partial Q_{ij}}\right\}}\;(k\;\dot{\lambda}\;dt) \bigg/ \frac{\partial\Phi}{\partial Y_{ij}}\ , \end{aligned} \tag{3.27}$$

where the parameter ξ defines the portion of isotropic hardening in the total amount of strength hardening.

3.3.3 Yield Surface of Shear Failure Members

When estimating the restoring forces in the lateral load–resisting members, interaction between the shear forces on a cross section is considered in this study. The interaction is represented by the strength hardening models described in the proceeding sections, and occurs through the construction of a yield surface for each member. The coordinate axes of the shifted forces ($\{S_{ij}\} = \{Q_{ij}\} - \{B_{ij}\}$) in Equation 3.19 are designated to coincide with the axes of the deformation variables $\{D_{ij}\}$. From the Drucker's postulate, therefore, it can be concluded that a yield surface must be convex [8], and that the yield surface has to be bounded within limits.

If the generalized forces are normalized by the element ultimate strength with the assumption of identical behavior in tension and compression, the maximum value of the normalized forces on respective axes cannot exceed unity. The lower limit for a yield surface then is bounded by the surface planes defined by

$$\left| \frac{{}^xQ_{ij} - {}^xB_{ij}}{Y_{ij}} \right| + \left| \frac{{}^yQ_{ij} - {}^yB_{ij}}{{}^yY_{ij}} \right| + \cdots = 1 \tag{3.28.a}$$

in which the absolute values of the fractions enclosed by vertical bars are required, and the upper limit is bounded by the surface planes defined by

$$\left| \frac{{}^xQ_{ij} - {}^xB_{ij}}{Y_{ij}} \right| = 1 , \qquad \left| \frac{{}^yQ_{ij} - {}^yB_{ij}}{{}^yY_{ij}} \right| = 1 , \qquad \cdots . \tag{3.28.b}$$

A yield surface must fall within the area enclosed by these bounds. It should be reasonable for practical purpose to use a circular yield surface in analysis. Thus the normalized yield function defined in Equations 3.20 and 3.24 can be expressed as

$$\overline{\Phi}(\{S_{ij}\}, Y_{ij}) = \frac{\Phi(\{S_{ij}\}, Y_{ij})}{Y_{ij}^2} = \left\{ \frac{Q_{ij} - B_{ij}}{r_s Y_{ij}} \right\} \cdot \left\{ \frac{Q_{ij} - B_{ij}}{r_s Y_{ij}} \right\} - 1 = 0, \tag{3.28.c}$$

where the r_s represents the constant ratios of yield forces in the respective directions, as given in Equation 3.23.

In the current investigation, only the shear forces ${}^xQ_{ij}$ and ${}^yQ_{ij}$ in the x– and y–direction are included in the force space for element i of story j. This situation constitutes a special case of the general yield function specified by Equation 3.28. Figure 3–9 depicts the limits for a yield surface in two–dimensional normalized force coordinates. The lower bound is defined by the lines connecting the unity points on the coordinate axes, while the upper bound is enclosed by the lines passing through the unity points and parallel to the axes.

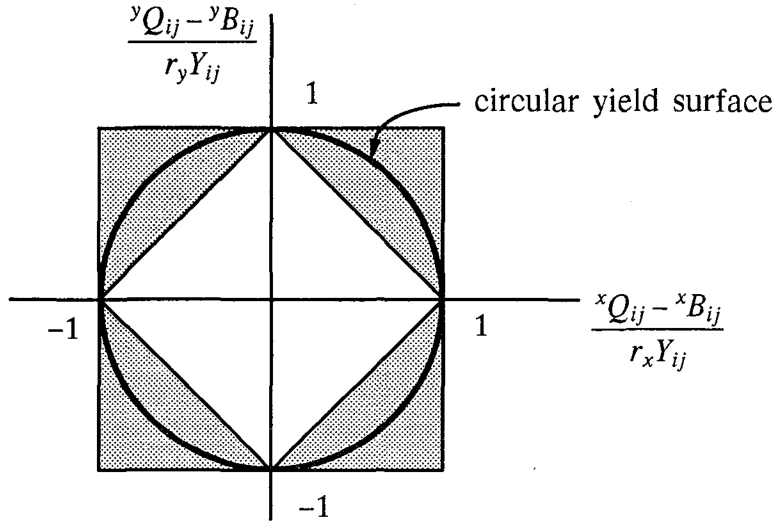

Figure 3–9 Bounds for Yield Surface in 2–D

The simplest smooth surface allowing different yield levels in the x– and y–direction is an ellipse. In turn an ellipse becomes a circle in the normalized coordinates,

$$\overline{\Phi}(\{S_{ij}\}, Y_{ij}) = \frac{\Phi(\{S_{ij}\}, Y_{ij})}{Y_{ij}^2} = \left(\frac{{}^xQ_{ij} - {}^xB_{ij}}{Y_{ij}} \right)^2 + \left(\frac{{}^yQ_{ij} - {}^yB_{ij}}{r_y Y_{ij}} \right)^2 - 1 = 0, \quad (3.29)$$

as shown in Figure 3–9. The unit normal vector in Equation 3.11.b for this particular surface is

$$\{n_{ij}\} = \frac{\left\{ \frac{\partial \Phi}{\partial Q_{ij}} \right\}}{\sqrt{\left\{ \frac{\partial \Phi}{\partial Q_{ij}} \right\} \cdot \left\{ \frac{\partial \Phi}{\partial Q_{ij}} \right\}}} = \left\{ \begin{array}{c} \dfrac{({}^xQ_{ij} - {}^xB_{ij})}{\sqrt{({}^xQ_{ij} - {}^xB_{ij})^2 + \frac{1}{r_y^4}({}^yQ_{ij} - {}^yB_{ij})^2}} \\ \dfrac{({}^yQ_{ij} - {}^yB_{ij})}{r_y^2 \sqrt{({}^xQ_{ij} - {}^xB_{ij})^2 + \frac{1}{r_y^4}({}^yQ_{ij} - {}^yB_{ij})^2}} \end{array} \right\} . \quad (3.30)$$

For the purpose of determining the yield force level, or, the ultimate strength of the shear–resisting members, it is a fair approximation to assume equal and opposite moments at the top and bottom of any member. The moment reflection points are at mid–height of the columns. The lateral loading on the elements is negligible between the floors. The most severely loaded zones in columns are at the top and bottom in each story. Because fracture type failures should be prevented in structural design, the shear strength of any member should be higher than its lateral capacity associated with its expected flexural strength. Further, it should be insured that the failure mode of any structural component is ductile. More precisely, damage should be kept to a minimum. Therefore, the ultimate strength of a member is determined from its flexural strength instead of by its shear strength, or

$$\{Y_{ij}\} = \frac{2}{H_{ij}} \{M_{ij}^{p}\} , \tag{3.31}$$

where $\{Y_{ij}\}$ = the uniaxial yield shear forces for element i of story j in all directions,

H_{ij} = the height of element i of story j, and

$\{M_{ij}^{p}\}$ = the plastic moments of the member in all directions.

3.3.4 State of Structural Members

The yield surface partitions the normalized force space. The yield function that $\Phi(\{S_{ij}\}, Y_{ij})$ is less than zero ($\Phi(\{S_{ij}\}, Y_{ij}) < 0$) encloses the elastic region, while the plastic region is defined on the yield surface ($\Phi(\{S_{ij}\}, Y_{ij}) = 0$). As can be perceived, the function $\Phi(\{S_{ij}\}, Y_{ij}) > 0$ defines the inaccessible domain. The state of a structural component therefore is decided according to the position of its yield function in the normalized force space. When $\Phi(\{S_{ij}\}, Y_{ij}) < 0$, the structural member is either elastic, or in a state of elastic unloading. Once the yield function for the member reaches the yield surface ($\Phi(\{S_{ij}\}, Y_{ij}) = 0$), the state of the member is considered plastic or neutral loading

3.4 Integration Procedure

The procedure used here to estimate the inelastic restoring forces is the elastic predictor–radial return algorithm, which is unconditionally stable and is exact for deformation increments in the radial direction [12]. The model in this study is able to account for the strength hardening with shear-force–interactions in the resisting members, and the Bauschinger effect can be incorporated using a mixed kinematic–isotropic hardening model with a constant plastic modulus. Accordingly, it is different from the plasticity models used by other previous researchers [19, 26, 37, 50, 52, 57].

The algorithm employed in computation consists of two steps: the first step involves calculating the elastic predictor, and the second step involves locating the true state of element behavior on the expanded and shifted yield surface. Based on the previous computed response (at $t = t$) and the displacement increment $\{\Delta U\}$ from Equation 3.2 with the current tangent stiffness, the elastic trial restoring force ${}^{t+\Delta t}\{Q_{ij}^T\}$ (at $t = t + \Delta t$) is calculated for each member, where the superscript T stands for a trial test from the computed deformation increment $\{\Delta D_{ij}\}$ during the time interval Δt. The state of the trial force ${}^{t+\Delta t}\{Q_{ij}^T\}$ is decided next according to its position with respect to the yield surface $\Phi_{ij} = 0$. If ${}^{t+\Delta t}\{Q_{ij}^T\}$ falls within the elastic region, the trial force is considered as the true final state of the member with an ordinary elastic loading or unloading step. If the resulting state of structural element i of story j defined by ${}^{t+\Delta t}\{Q_{ij}^T\}$ lies outside of the elastic region enclosed by the yield surface $\Phi_{ij} = 0$, the final state is then the projection of the plastic part of this trial state ${}^{t+\Delta t}\{Q_{ij}^T\}$ onto the shifted or expanded yield surface. From a geometric standpoint, this procedure maintains the consistency condition at the end of each time step [54]. From a mathematical standpoint, it can be shown that the algorithm defines a contraction mapping in a suitable Hilbert space, and thus produces unconditionally stable results [38].

It is obvious that in order to calculate the concurrent hardening strength and stiffness of a member, this procedure must be an iterative type algorithm. The variables in the following equations (at $t = t + \Delta t$) are understood to correspond to the n^{th} iteration within the time interval Δt. Because the values at the previous $(n\text{–}1)^{\text{th}}$ iteration plays no explicit role here, the concurrent values are computed solely based on the response quantities at the beginning of the time step (at $t = t$). The trial state of the forces for element i of story j has the form

$$\begin{aligned}
\{\Delta Q_{ij}^T\} &= [K_{ij}^e]\{\Delta D_{ij}\} \ , \\
{}^{t+\Delta t}\{Q_{ij}^T\} &= {}^{t}\{Q_{ij}\} + \{\Delta Q_{ij}^T\} \ , \ \text{and} \\
{}^{t+\Delta t}\{S_{ij}^T\} &= {}^{t+\Delta t}\{Q_{ij}^T\} - {}^{t}\{B_{ij}\} \ ,
\end{aligned} \tag{3.32}$$

in which the trial force increment $\{\Delta Q_{ij}^T\}$ is the elastic predictor depending on the elastic stiffness matrix.

If the state of the structural member defined by ${}^{t+\Delta t}\{S_{ij}^T\}$ is within the yield surface ($\Phi({}^{t+\Delta t}\{S_{ij}^T\}, {}^{t}Y_{ij}) < 0$) specified in Equation 3.29, then this calculated force vector represents the true state of the member. The member is either in a state of elastic loading or elastic unloading. The updated response quantities are

$$
\begin{aligned}
{}^{t+\Delta t}\{Q_{ij}\} &= {}^{t+\Delta t}\{Q_{ij}^T\} \ , \\
{}^{t+\Delta t}\{B_{ij}\} &= {}^{t}\{B_{ij}\} \ , \\
{}^{t+\Delta t}\{Y_{ij}\} &= {}^{t}\{Y_{ij}\} \ , \quad \text{and} \\
{}^{t+\Delta t}\{S_{ij}\} &= {}^{t+\Delta t}\{Q_{ij}\} - {}^{t+\Delta t}\{B_{ij}\} \ ,
\end{aligned}
\tag{3.33}
$$

in which the updated back–force increment is based on the inelastic stiffness matrix.

If the trial force state lies outside of the yield surface ($\Phi({}^{t+\Delta t}\{S_{ij}^T\}, {}^{t}Y_{ij}) > 0$), it is necessary to decouple the ordinary elastic loading increment from the total increment. This operation is needed in order to avoid "overshoot" of the yield surface caused by the finite time step in the numerical computation. The force increment from the present state (at $t = t$) to the original yield surface involves no plastic deformation, thus this part of the force increment should be treated in the same way as a elastic step outlined in Equations 3.32 and 3.33. If one excludes the ordinary elastic increment, the remaining force increment involves post–yield deformation from the original yield surface to the current position. If one uses a variable η to represent the pre–yield portion of the total force increment, then the intersection point can be defined by the trial force vector on the original surface. Further, if for the consistency condition one notes that the new state is on the original yield surface at the end of this elastic loading increment, then a quadratic equation for η is formed for a von Mises type of material model. As was expressed in Equation 3.32, the state of the intersection point on the surface is given by

$$
{}^{t+\Delta t}\{S_{ij}^T\} = {}^{t}\{Q_{ij}\} + \eta \ \{\Delta Q_{ij}^T\} - {}^{t}\{B_{ij}\} \ . \tag{3.34.a}
$$

The consistency condition ($\Phi({}^{t+\Delta t}\{S_{ij}^T\}, {}^{t}Y_{ij}) = 0$) expressed in Equation 3.28.c becomes

$$
\left(\frac{{}^{x}S_{ij}^T}{Y_{ij}} \right)^2 + \left(\frac{{}^{y}S_{ij}^T}{r_y Y_{ij}} \right)^2 + \cdots = 1 \ . \tag{3.34.b}
$$

It is derived easily from this expression that

$$C_1\,\eta^2 + 2C_2\,\eta + C_3 = 0\ , \tag{3.34.c}$$

where $C_1 = \left(\ \Delta^x Q_{ij}^2 + \frac{1}{r_y^2}\Delta^y Q_{ij}^2 + \cdots\ \right)$,

$$C_2 = \left[\ (\ {}^{t,x}Q_{ij} - {}^{t,x}B_{ij}\ )\Delta^x Q_{ij} + \frac{1}{r_y^2}(\ {}^{t,y}Q_{ij} - {}^{t,y}B_{ij}\ )\Delta^y Q_{ij} + \cdots\ \right]\ , \text{ and}$$

$$C_3 = -\,Y_{ij}^2 + \left[\ (\ {}^{t,x}Q_{ij} - {}^{t,x}B_{ij}\ )^2 + \frac{1}{r_y^2}(\ {}^{t,y}Q_{ij} - {}^{t,y}B_{ij}\ )^2 + \cdots\ \right].$$

Hence, the solution to Equation 3.34.c gives

$$\eta = -\frac{C_2}{C_1} \pm \sqrt{\left(\frac{C_2}{C_1}\right)^2 - \frac{C_3}{C_1}}\ , \tag{3.34.d}$$

from which the positive value of η should be taken because the negative value shows the intersection point on the yield surface along the negative direction of the trial force increment.

In Figure 3–10 of the graphical presentation, the elastic trial force increment $[K_{ij}^e]\{\Delta D_{ij}\}$ is computed and added to the current force state ${}^t\{Q_{ij}\}$ in order to locate the contact point $\mathbf{P_c}$ on the current yield surface. From this point, the plastic loading step,

$$\{\Delta Q_{ij}^{ep}\} = (1-\eta)\ [K_{ij}^{ep}]\{\Delta D_{ij}\}, \tag{3.35}$$

is calculated and the yield surface is updated to the new position, based on the plastic modulus k and the hardening models. The final state then is determined by adding the correction drift $\{\Delta Q_{ij}^{corr}\}$ in the radial direction.

The state of force at the contact point ${}_c\{Q_{ij}\}$ is described by

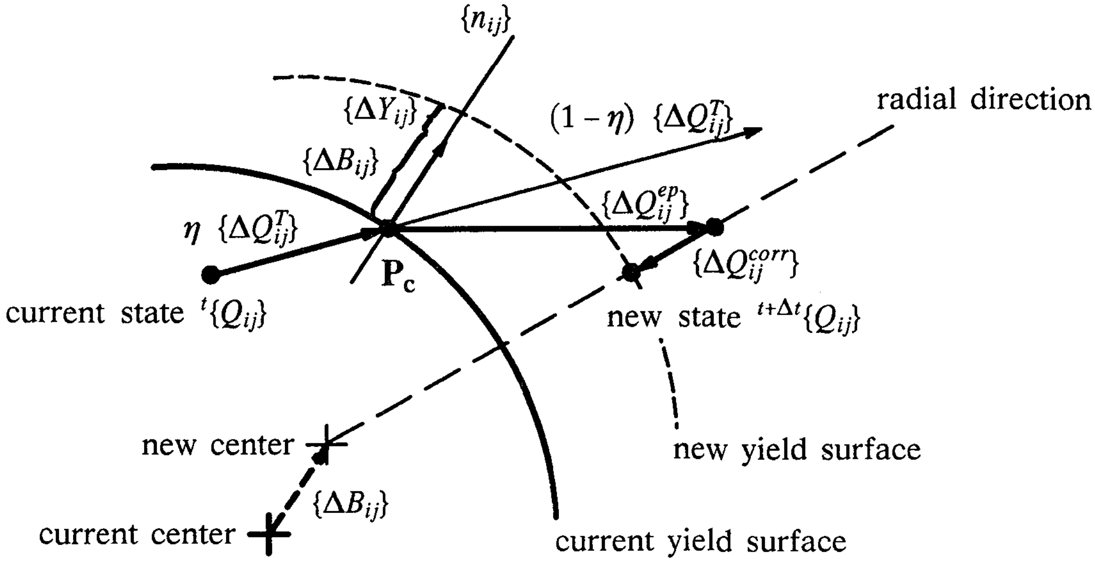

Figure 3–10 Elastic Predictor–Radial Return Algorithm

$$
\begin{aligned}
{}_c\{Q_{ij}\} &= {}^{t}\{Q_{ij}\} + \eta\ [K_{ij}^{e}]\{\Delta D_{ij}\} , \\
{}_c\{B_{ij}\} &= {}^{t}\{B_{ij}\} , \\
{}_c\{Y_{ij}\} &= {}^{t}\{Y_{ij}\} , \quad \text{and} \\
{}_c\{S_{ij}\} &= {}_c\{Q_{ij}\} - {}_c\{B_{ij}\} , \qquad (3.36)
\end{aligned}
$$

in which the parameter η is determined in Equation 3.34.d. The final state is defined by

$$
\begin{aligned}
{}^{t+\Delta t}\{Q_{ij}\} &= {}_c\{Q_{ij}\} + \{\Delta Q_{ij}^{ep}\} + \{\Delta Q_{ij}^{corr}\} , \\
{}^{t+\Delta t}\{B_{ij}\} &= {}_c\{B_{ij}\} + \{\Delta B_{ij}\} , \\
{}^{t+\Delta t}\{Y_{ij}\} &= {}_c\{Y_{ij}\} + \{\Delta Y_{ij}\} , \quad \text{and} \\
{}^{t+\Delta t}\{S_{ij}\} &= {}^{t+\Delta t}\{Q_{ij}\} - {}^{t+\Delta t}\{B_{ij}\} , \qquad (3.37)
\end{aligned}
$$

where the material hardening terms $\{\Delta B_{ij}\}$ and $\{\Delta Y_{ij}\}$ are given by Equation 3.27, $\{\Delta Q_{ij}^{ep}\}$ is the plastic loading increment given in Equation 3.35, and the correction drift $\{\Delta Q_{ij}^{corr}\}$ in the radial direction is determined by satisfying the consistency condition on the new yield surface. The radial direction is defined by the vector pointed towards the new center ${}^{t+\Delta t}\{B_{ij}\}$ from the final state ${}^{t+\Delta t}\{Q_{ij}\}$ on the new yield surface. The correction drift then becomes

$$\{\Delta Q_{ij}^{corr}\} = s\left[{}^{t+\Delta t}\{B_{ij}\} - \left({}_{c}\{Q_{ij}\} + \{\Delta Q_{ij}^{ep}\}\right)\right], \tag{3.38.a}$$

where the parameter s indicates the amount of drift along the direction vector. From the consistency condition ($\Phi({}^{t+\Delta t}\{S_{ij}^{T}\}, {}^{t}Y_{ij}) = 0$) of Equation 3.28.c and the expressions in Equations 3.36, 3.37, and 3.38.a, s can be derived and is noted to be,

$$s = 1 - \frac{1}{\sqrt{\left(\dfrac{{}_{c}^{x}Q_{ij} + \Delta^{x}Q_{ij}^{ep} - {}^{t+\Delta t,x}B_{ij}}{{}^{t+\Delta t}Y_{ij}}\right)^2 + \left(\dfrac{{}_{c}^{y}Q_{ij} + \Delta^{y}Q_{ij}^{ep} - {}^{t+\Delta t,y}B_{ij}}{r_y\ {}^{t+\Delta t}Y_{ij}}\right)^2 + \cdots}} . \tag{3.38.b}$$

The value of s is substituted back to Equations 3.38.a and 3.37 to compute the final force state.

When incorporating the inelastic material models into the dynamic analysis of structures, the following issues are important to notice. Inelastic analysis is generally path–dependent, i.e., the accuracy of results at the end of a time interval is dictated by the response quantities at the beginning of the time step and the accuracy of the response in the previous time steps. In solving the dynamic equations of motion, Newmark's β method contains certain approximations of system response as defined in Equations 3.2 and 3.3. Therefore, on the basis of the above considerations the numerical computations generally require a relatively small time step to assure stability, and several iterations to achieve convergence within a desired tolerance.

One of the approaches for increasing the efficiency of solving equations is to make use of the concept of residual force. At time t, if the reaction force $[K^{*}]\{\Delta U\}$ in Equation 3.2 is not in equilibrium with the applied force $\{\Delta P^{*}\}$, there exists an unbalanced residual force $\{\Delta R\}$. Through use of an iterative procedure one recalculates the response of the system until this residual vanishes before proceed to the next time step. The equilibrium state always exists at every time step. However, the analysis results may not be accurate because of the inelastic behavior. In contrast, a noniterative procedure accepts the unequilibrium state of the system and the existence of the residual force $\{\Delta R\}$. The algorithm then adds this $\{\Delta R\}$ to the applying force $\{\Delta P^*\}$ as a corrector in the next time step (at $t = t + \Delta t$).

In a dynamic analysis, the structural restoring force ${}^{t+\Delta t}\{Q\}$ balances only a small portion of the applied load ${}^{t+\Delta t}\{P\}$. The inertial force plays a major role in balancing the structural motion during dynamic excitation. The mass matrix $[M]$ contributes significantly to the effective stiffness matrix $[K^*]$ in Equation 3.2, especially when the time interval Δt is very small. The effective stiffness matrix $[K^*]$ becomes quite well–conditioned because of the dominance of diagonal terms from the mass matrix $[M]$. In addition, change of tangent stiffness ${}^t[K]$ has little effect on behavior of the effective stiffness matrix $[K^*]$. The convergence rate in dynamic analysis is much faster than in static analysis. The efficiency of solving the equations of motion can be increased by updating the tangent stiffness matrix ${}^t[K]$ after several time steps instead of every time step.

3.5 Summary

This chapter has focused on the development of a generalized material model that can reflect linear and nonlinear behavior representative of certain materials. A general theory of yielding of structural elements based on the theories of classical plasticity has been formulated herein in terms of quantities in the force–displacement space. The mathematical model for inelastic behavior, and the integration procedure, have been described for structural systems subjected to strong ground motion. Parametric studies on the effects of eccentricity on simple model systems with torsional response will be performed in the next chapter using this extended material model and the analysis procedure.

CHAPTER 4

PARAMETRIC STUDIES OF ECCENTRICITIES IN ASYMMETRIC SYSTEMS

4.1 Introduction

Many factors play some role in the response of structural systems subjected to dynamic loadings such as base excitation. Foreseeable and nonforeseeable parameters all affect the responding deformations and forces in individual members. Torsion is one of the important factors that should be considered. If new and better design approaches are to be developed, it is necessary to gain understanding of the origin, role and influence of torsion on the behavior and overall response of buildings.

In structures with potential torsionally-induced loss of stiffness, slight modifications of certain parameters could result in drastic changes in the structural response. Because of the coupling of the conventional translational deformations through torsion, the behavior of structures subjected to ground motion can become complex and difficult to study, especially in asymmetric systems. One of the most obvious parameters causing structural torsion and consequently amplified member deformations is the structural eccentricity between the centers of mass and stiffness. The parametric studies in this chapter, employing the analysis procedure and the inelastic material model for structural members developed in Chapter 3, are centered on studies of the effects of dynamic amplification of eccentricity on structural behavior.

The dynamic amplification of torsional moments (torques) at floor levels, arising from ground motion excitation and the physical (static) eccentricities, is considered to come from two sources: dynamic amplification of lateral forces at the mass centers caused by the base excitation; and the dynamic effect of the torsional moments at the rigidity centers resulting from the dynamic lateral forces at the mass centers. The former normally is accounted for routinely when computing the base shear and the lateral forces at floor levels. The latter, which can lead to somewhat more complex design or analysis situations, will be investigated in this chapter for structural models shown in Figure 4–1 with a specific uncoupled frequency ratio of 1.225 for each story.

With the existence of structural eccentricity, the rotational movement of a structure as a whole unit adds at least one additional independent degree of freedom per story to the structure. The additional deformations and forces in individual structural members, generated by torsion, depend largely on the distance from the location of concern to the center of rigidity. Thus far no one has found it possible to devise a single index that will permit evaluation of the overall response accounting for both translational and rotational deformations over a broad range of conditions. Thus at present separate considerations in design are needed for the familiar planar analysis and the torsional analysis. The parametric study herein investigates the torsional coupling, arising from structural eccentricity, in the response caused by selected ground motion excitations.

To understand the behavior of more complex systems, it is useful to study the response characteristics of one–story to two–story structures. Therefore the analyses in this chapter are performed on simple structural models, more specifically, one-directional unbalanced (torsional coupling in one direction) one–story and two–story systems as shown in Figure 4–1 subjected to uniaxial input of selected ground motions. Then the analysis results are evaluated and are used to identify the trends in structural response with respect to the effects of dynamic amplification of eccentricity in linear-elastic and inelastic systems.

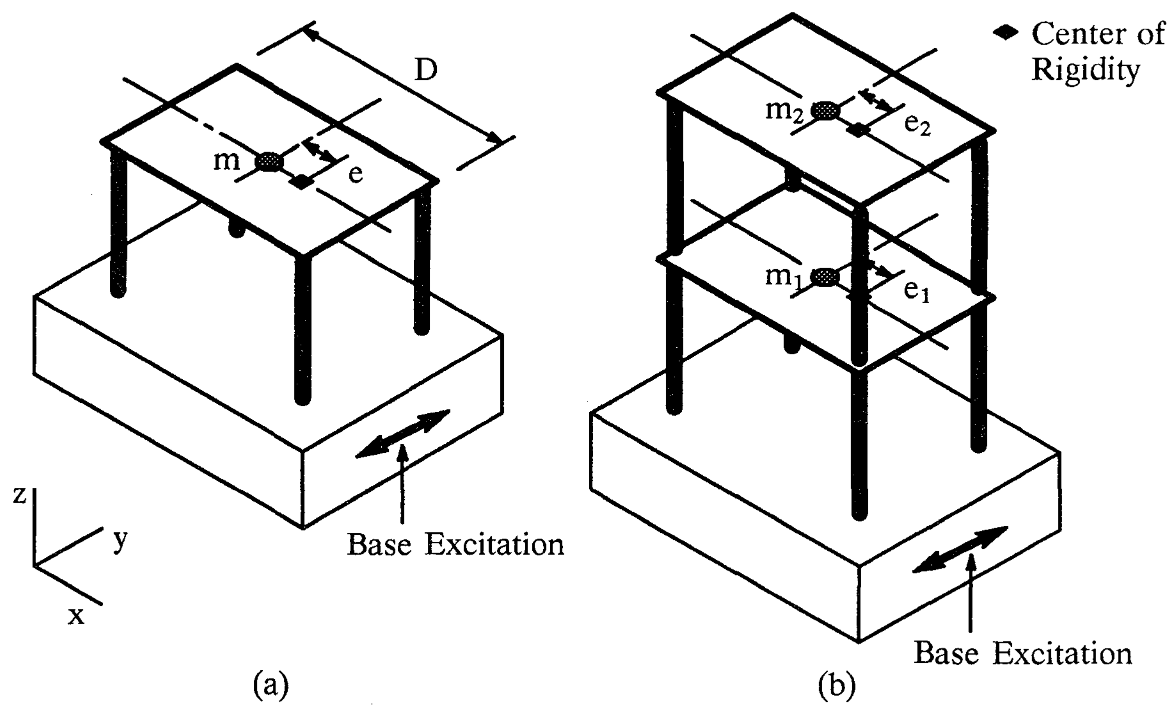

Figure 4–1 Structural Models for Parametric Studies

4.2 One–Directional Asymmetric Systems

Parametric studies were conducted on structural systems with eccentricity in only one of their principal directions. The structural models of these one–story and two–story systems, presented in Figure 4–1, are composed of rigid floor decks resting on lateral load–resisting elements. The base excitation is input in the principal y–direction in which the eccentricity exists. The translational motion in the other principal x–direction is not coupled with the system response, and thus not excited. With this in mind, only two degrees of freedom per story, one translational and one rotational, are considered for purpose of investigation.

In this study, the masses are assumed to be concentrated at the floor levels. Columns are used as the lateral load–resisting elements. The effects of dynamic amplification of eccentricity are studied by considering a series of structural systems with five percent of viscous damping in each mode. The one–story models are designed, respectively, to have the specified translational frequencies of 0.2, 0.8, 3.75, and 10.0 *Hz* to cover a full range of structures. For the two–story models, the second story has the same properties as the first story. Eccentricity in the models is created by placing the mass center away from the rigidity center. The values of eccentricity in the analyses range from zero to ten percent of the structural dimension *D*. The properties of the models, including the uncoupled torsional frequencies with zero eccentricity, are listed in Table 4–1.

Table 4–1 Structural Properties for One–Story Systems

Translational Frequency (*Hz*)	Translational Stiffness (#/in.)	Mass (#–in/s^2)	Rotational Mass Moment of Inertia (#–in^3/s^2)	Torsional Frequency (*Hz*)
0.200	$4.0*10^5$	$2.531*10^5$	$6.075*10^8$	0.245
0.800	$4.0*10^5$	$1.583*10^4$	$3.799*10^7$	0.980
3.750	$4.0*10^5$	$7.205*10^2$	$1.729*10^6$	4.593
10.00	$4.0*10^5$	$1.013*10^2$	$2.431*10^5$	12.25

4.3 Description of Selected Ground Motion Excitations

To study the dynamic amplification of eccentricity in structures responding to ground motion excitation, it was deemed desirable to investigate the linear–elastic and inelastic behavior of structural systems subjected to a wide range of ground motions. The selected ground motions, with 30 seconds duration, were employed to excite the structural models in order to observe the effects of eccentricity on structural response. These ground motions generated lateral loadings in only one principal direction of the models in which any eccentricity exists, and no input of base excitation was considered in the other principal direction, as described earlier.

For systems with linear–elastic response only, two types of base excitations were employed. Harmonic base excitations with the frequency of 1, 2, 4, and 8 *Hz* were used to excite the models. The intention was to compare the results from numerical integration with the known closed form solution, and to observe any trends in the model response caused by simple harmonic excitations. Then six earthquake ground motion records were selected as ground input in the analyses. Some records needed to be scaled down to insure only linear–elastic behavior during the analysis.

The first 30 seconds of the following earthquake records were employed in this study: El Centro, Melendy Ranch, Pacoima Dam, Taft, 1985 Mexico, and 1985 Chile. They were selected from the following standpoint. The El Centro record is of the type of sustained strong shaking ground motion; the Melendy Ranch record represents the near–field type ground motion with a short burst of energy; the Pacoima Dam record exhibits strong pulse–type excitation with large acceleration amplitudes in the middle of the record; the Taft record and the Mexico record show long duration, relatively severe and symmetric type cyclic ground excitation; and the Chile record contains a significantly long duration of strong shaking with high peak accelerations. These earthquakes are generally considered as representative of a full range of ground motion excitations. Information about these six earthquakes has been extensively documented in the literature related to earthquake engineering, and excellent summaries can be found in References [30], [42], [55], [56], and [58].

In dynamic analysis of structures responding to strong ground motion, the ratio of the uncoupled torsional frequency to the uncoupled translational frequency, as well as the frequency content of a specific earthquake, is an important factor in determining the amplitudes of response. In this chapter, however, the focus is centered on the effects of static eccentricity on the structural responses caused by earthquake ground motion. The uncoupled frequency ratio for the one–story systems is specified as 1.225, and the effects of earthquake motion frequency content is not considered in depth herein.

To examine the various degrees of inelastic behavior in asymmetric systems, the six earthquake records then were anchored so as to have peak accelerations of 0.1g, 0.2g, and 0.4g, respectively. These are representative of effective maximum accelerations for elastic response envisioned by building codes for the corresponding seismic zones 3, 5, and 7 (ATC and NEHRP), or zones 1–2A, 2B, and 4 (UBC–88). The ductility experienced by the columns responding to these scaled ground motions is in the intermediate range of three to six, on the upper side of that believed to be acceptable, especially if the structure is to be reusable. The resulting data serve to place in perspective the general trends in the inelastic response of the class of asymmetric systems studied for earthquake type of base excitations.

4.4 Organization and Presentation of Results

Any numerical computation of response history of structures can generate a vast amount of output. The analysis of such a massive volume of data constitutes a major task. It is understood that presenting a long list of numbers or a huge table full of data gives the reader a tremendous job to assess and comprehend the analysis results, much less their significance. On the other hand, a graphical presentation makes the assessment of the analysis data much easier. In this chapter, therefore, the analysis results are presented graphically for the structural models subjected to the ground excitations.

The plots are made to show the effects of static eccentricity on the maximum responses of the models. The maximum response quantities include the translational displacement, the deck rotation, the lateral force at the mass centers of the models, and the torsional moment at the centers of rigidity. In each of the following figures, three out of the four plots present the maximum responses at the mass center versus eccentricity ratio. The fourth plot shows the change of maximum torques with respect to eccentricity ratio. The eccentricity ratio e/D, defined as the static eccentricity over the building dimension, ranges from 0.00 to 0.10.

The results presented in this chapter are the envelopes of maximum overall response for each story in the models. Although these plots gave an indication of the maximums, they did not reveal the complicated nature of the structural response caused by strong ground motion, especially the number of times that some members had reached the corresponding yielding levels in the case of inelastic response. However, the information and conclusions contained here can be directly interpreted in relationship to the design procedures adopted in the current building codes.

In the following, the variables to be plotted are normalized by respective quantities for easier assessment and comprehension of the response data of the models.

The maximum translations in the y–direction, $\{u_m\}$, at the mass centers, when subjected to a specific ground excitation, are normalized by the maximum translation at the first level, $u_{m1}|_{e=0}$, in the corresponding model with no structural torsion involved (i.e., eccentricity is zero). The plots are placed in the upper–left corner of the following figures. This type of plots indicates the amplification or de–amplification of the maximum lateral displacements with respect to the amount of physical eccentricities in structures.

The maximum rotations, $\{\theta_m\}$, of the model with different values of eccentricities, when subjected to a specific ground excitation, are normalized by the maximum deck rotation of the first level, $\theta_{m1}|_{e=0.1D}$, in the corresponding model with ten percent eccentricity ratio ($e = 0.10D$). The plots are placed in the upper–right corner of the following figures. The purpose of this normalization is simply for data organization and easy plotting. The general trends of variations of the maximum floor rotation exhibited in these plots are the same even without this normalization. The effect of static eccentricity on the maximum floor rotation can be observed in these plots.

Similar to the plots for the maximum translations in the models, the maximum lateral forces, $\{V_m\}$, applying at the floor levels are normalized by the maximum lateral force at the first level, $V_{m1}|_{e=0}$, in the corresponding model subjected to an identical ground motion without torsion involved. These plots are placed in the lower–left corner of the following figures. Plots of this type show the amplification or de–amplification of the maximum lateral forces in structures as a function of eccentricity. In the response of the two–story models, the lateral forces at a designated eccentricity in these plots depict the vertical distribution of lateral forces caused by the selected ground excitations.

The maximum torques, $\{T_R\}$, generated at the rigidity centers, when subjected to a selected ground excitation, are normalized by the product of the maximum lateral force at the first level without torsion, $V_{m1}|_{e=0}$, and the building dimension perpendicular to the base motion direction, D. By way of further explanation, the ratio of the maximum torque

T_R at the rigidity center and the maximum lateral force without torsion, $V_{m1}|_{e=0}$, provides a measure of dynamic eccentricity for that floor level i $\left(e_{di} = \dfrac{T_{Ri}}{V_{m1}|_{e=0}} \right)$, which then is normalized by the building dimension D to become the dynamic eccentricity ratio e_d/D. This dynamic eccentricity ratio (which is dependent on the selected ground motion) is plotted against the physical (static) eccentricity ratio e/D. These plots are placed in the lower-right corner of the following figures. The division of the dynamic eccentricity ratio by the corresponding static eccentricity ratio $(\frac{e_d/D}{e/D} = \frac{e_d}{e})$, indicates the dynamic amplification factor for the static eccentricities in seismic design of structures. This ratio is obviously the average slope of the curves in these particular plots.

4.5 Influence of Eccentricity on Linear-Elastic Systems

In this section the analysis results of the models in Section 4.2, subjected to the selected ground motions described in Section 4.3, are plotted in Figures 4–2 through 4–17 for systems with linear-elastic behavior. The results then are examined to determine the influence of various amounts of eccentricity on the seismic response envelopes in linear-elastic systems.

The plots in Figures 4–2 through 4–9 are for the one-story systems with the uncoupled frequency ratio of 1.225. Figures 4–2 through 4–5 show the results of systems subjected to the harmonic base motions, and Figures 4–6 through 4–9 show the analysis results during the earthquake ground motions. The plots in Figures 4–10 through 4–17 are for the two-story systems; Figures 4–10 through 4–13 show the results for harmonic base motions and Figures 4–14 through 4–17 show the maximum response for the earthquake ground motions.

The following are a few of the most significant observations on the trends displayed by the results of the parametric studies. As shown in Figures 4–2 through 4–17, the maximum values of translational displacements and lateral shear forces at the mass centers of corresponding floor levels remain essentially constant for different amounts of static eccentricities in the models. It will be noted that in the plots for translational responses that as the exciting frequency approaches the natural frequency of the systems, there is a change (decrease in most cases) as a result of the near resonance excitation. The reason for this decrease is in part that near resonance the denominator term becomes quite large, and as the eccentricity ratio increases, the torsional frequency shifts away from the exciting frequency so that the response decreases, as exemplified in Figure 4–4. For the two–story systems it is observed that for large e/D values where the excitation is close to the fundamental torsional frequencies there are large excursions. For example, in the upper–left plot in Figure 4–16 it will be observed that for the 1985 Mexico record (of which the dominant frequency is about 0.5 *Hz*) the excursion is extreme; the fundamental torsional frequency of the system is close to be 0.7 *Hz*. In summary, careful study reveals that the translational response caused by ground excitation in the class of systems studied (with the specific frequency ratio of 1.225 for each story) is not very sensitive to the torsional coupling effect except near resonance.

Different observations on the effects of torsional coupling were presented by Kan and Chopra [22] and Kung and Pecknold [28]. These investigators noticed that when the uncoupled frequency ratio ω_θ/ω_u was close to one, there was a reduction of translational response (deformation and force) as a result of torsional coupling. However, the results of this study do not show the same coupling characteristics. One possible explanation is that the model systems in this investigation have only one fixed frequency ratio of 1.225 which may be a value of frequency ratio where the torsional coupling effect is not as pronounced. Another possible explanation is that the results presented by these investigators are the mean square response values which involves certain rules for modal combinations, as opposed to the maximum response (involving torsion) plotted herein. Also when the uncoupled frequency ratio is equal to one $(\omega_\theta/\omega_u = 1)$, this lack of sensitivity of translational response to torsional coupling may be attributed to the phase difference between the occurrence of the peak translational and torsional responses. On the basis of studies reported herein it is believed that this latter topic deserves further detailed investigation.

In the static analysis of linear–elastic systems subjected to lateral loadings, the rotational displacements of floor decks are linearly proportional to the respective static eccentricities in the structures. Similarly, as shown in the upper–right plots in Figures 4–2 through 4–17, the maximum rotational displacements of floor decks vary nearly linearly with respect to the values of eccentricity in the models.

It can be concluded from the analysis results displayed in the lower–right plot in Figures 4–2 through 4–17, that significant amounts of dynamic torques can be generated during ground excitation at the rigidity centers of the models with eccentricity. As shown in the analysis results for one–story models, the dynamic torque at the rigidity center is generally larger than the "static torsional moment" defined as the product of lateral force at the mass center and the static eccentricity (leading to a slope greater than one). Structural systems should be designed to withstand such dynamic torsional loadings. The dynamic amplification factor for structural eccentricity, defined by the ratio of dynamic eccentricity ratio and static eccentricity ratio (depicted as the average slope of the curves in the plots), falls generally into the range of two to three with few exceptions for the one–dimensional asymmetric one–story systems. The dynamic amplification factor ranges from 0.5 to two for the two–story systems.

To examine how the column arrangements affect the overall linear structural response of systems subjected to ground motion, model configurations of two columns and four columns per story were used. The corresponding two–column and four–column models have the same uncoupled translational and torsional frequencies. Because the respective results for corresponding two–column and four–column model configurations are identical, the calculational results are not shown but brief comments follow. With the same values of eccentricity, the overall response of a model caused by ground motion is not affected by the different arrangements of columns, so long as its translational and torsional frequencies are maintained. Thus, it is valid to use a "stick– model" of a complex yet fairly "regular" structure (in which the mass and stiffness are lumped to the respective centers at the corresponding floor levels with a single column) to estimate its response at the centers of mass. The resulting data of this computation then can be transformed into the response at the location of interest in the original structure. The obvious advantage of employing a "stick–model" is in the considerable saving of computational effort when calculating the response–history in the original structures, especially for complex structures with a large number of lateral resisting members, subjected to ground motions of relatively small magnitude.

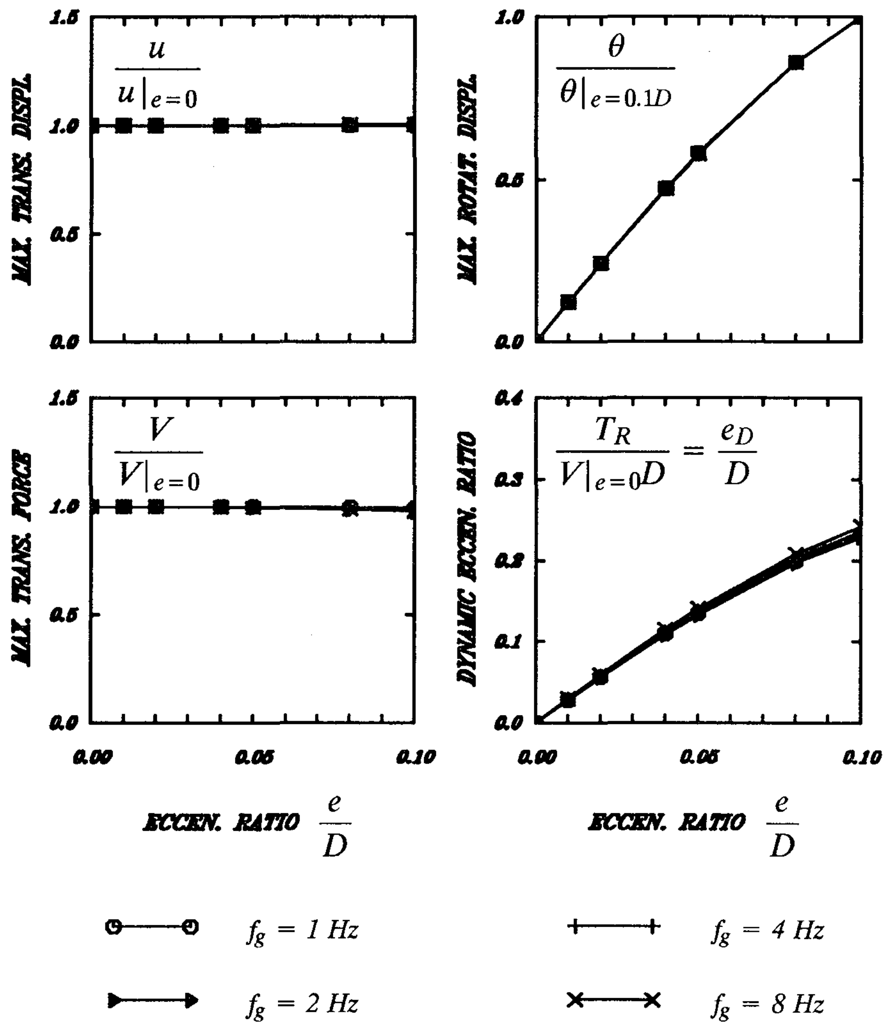

Figure 4–2 Maximum Response of One–Story 0.2 *Hz* System Subjected to Harmonic Base Motion

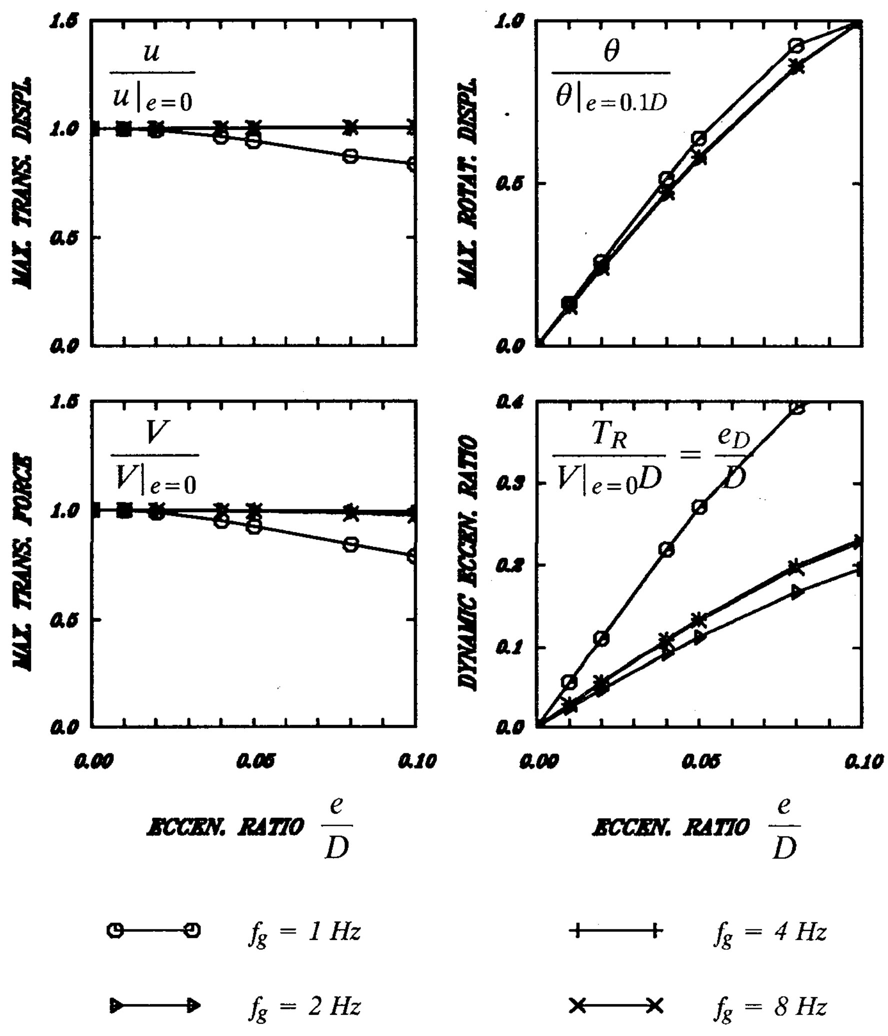

Figure 4–3 Maximum Response of One–Story 0.8 *Hz* System Subjected to Harmonic Base Motion

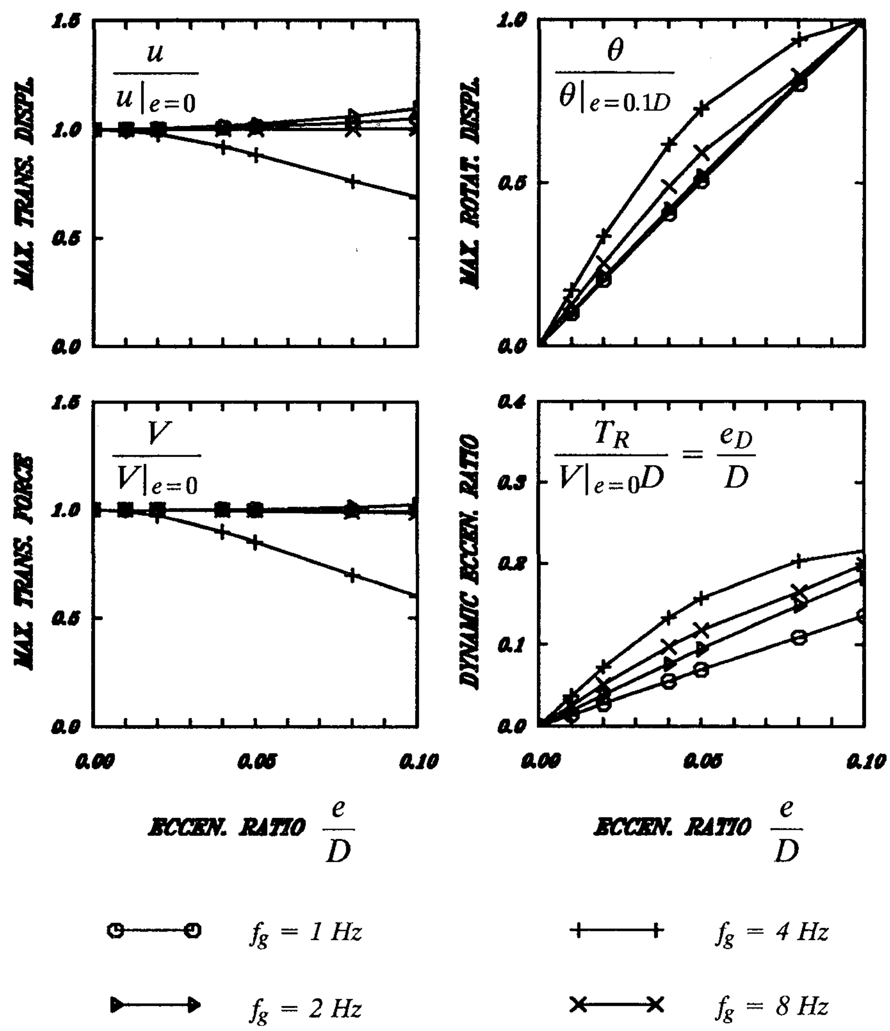

Figure 4–4 Maximum Response of One–Story 3.75 *Hz* System Subjected to Harmonic Base Motion

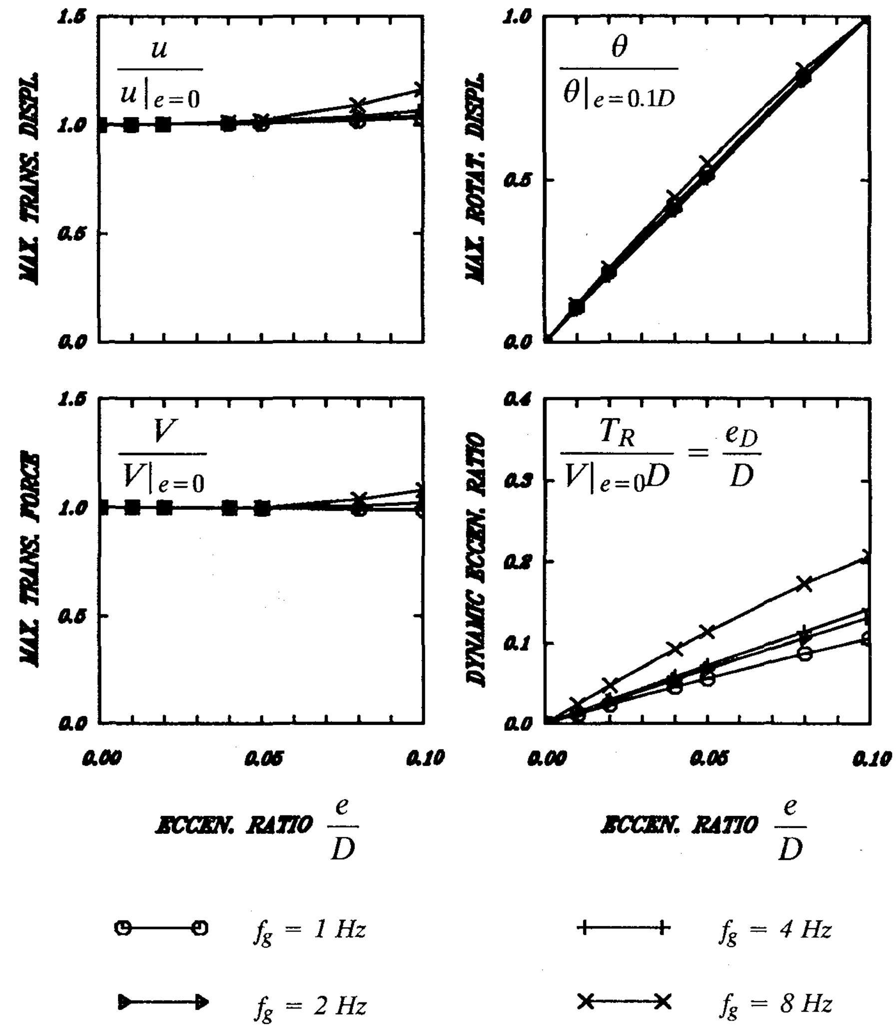

Figure 4–5 Maximum Response of One-Story 10.0 *Hz* System Subjected to Harmonic Base Motion

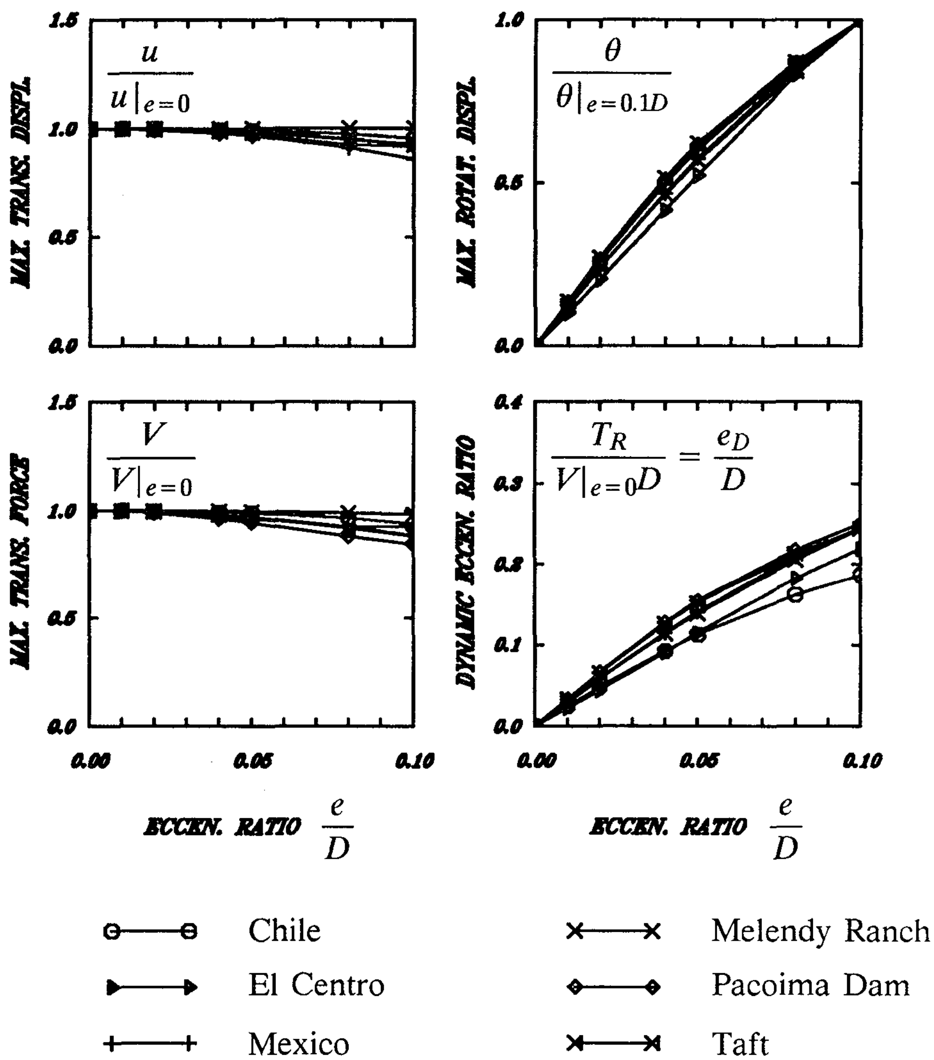

Figure 4–6 Maximum Response of One–Story 0.2 *Hz* System Subjected to Earthquake Ground Motion

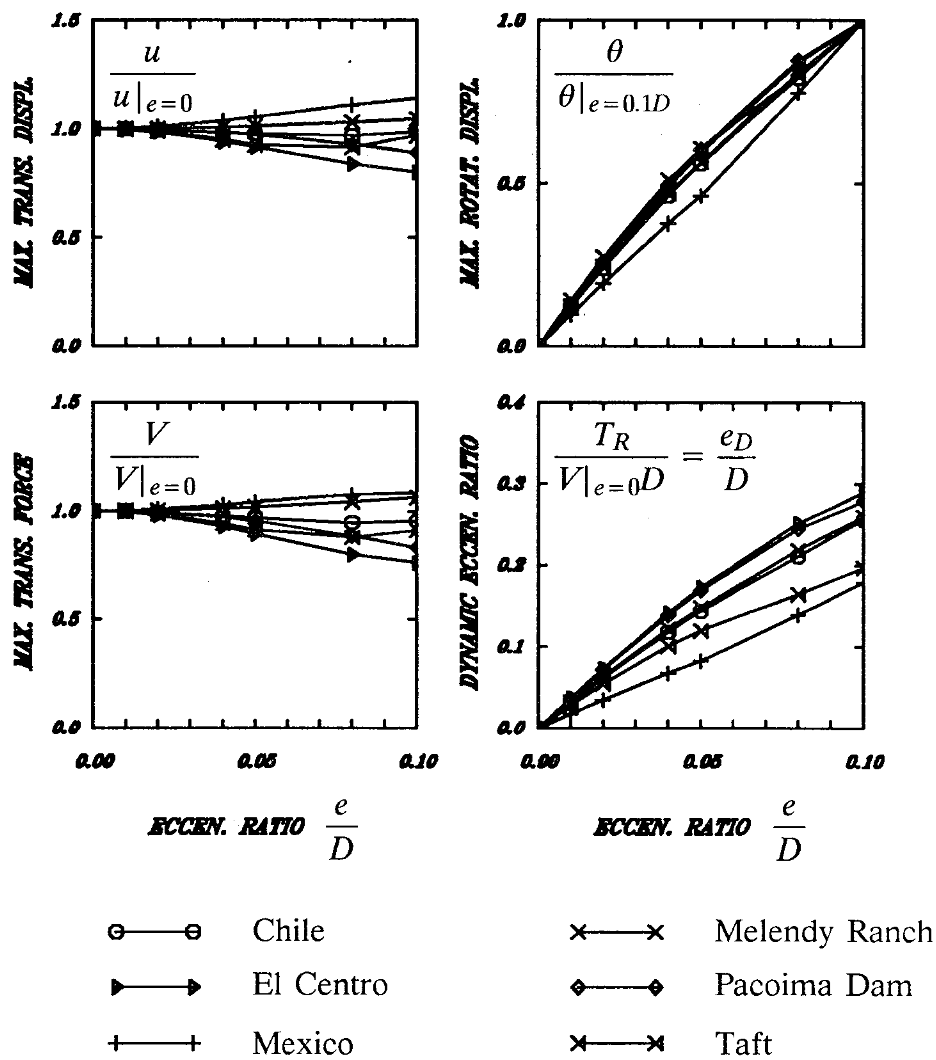

Figure 4–7 Maximum Response of One–Story 0.8 *Hz* System Subjected to Earthquake Ground Motion

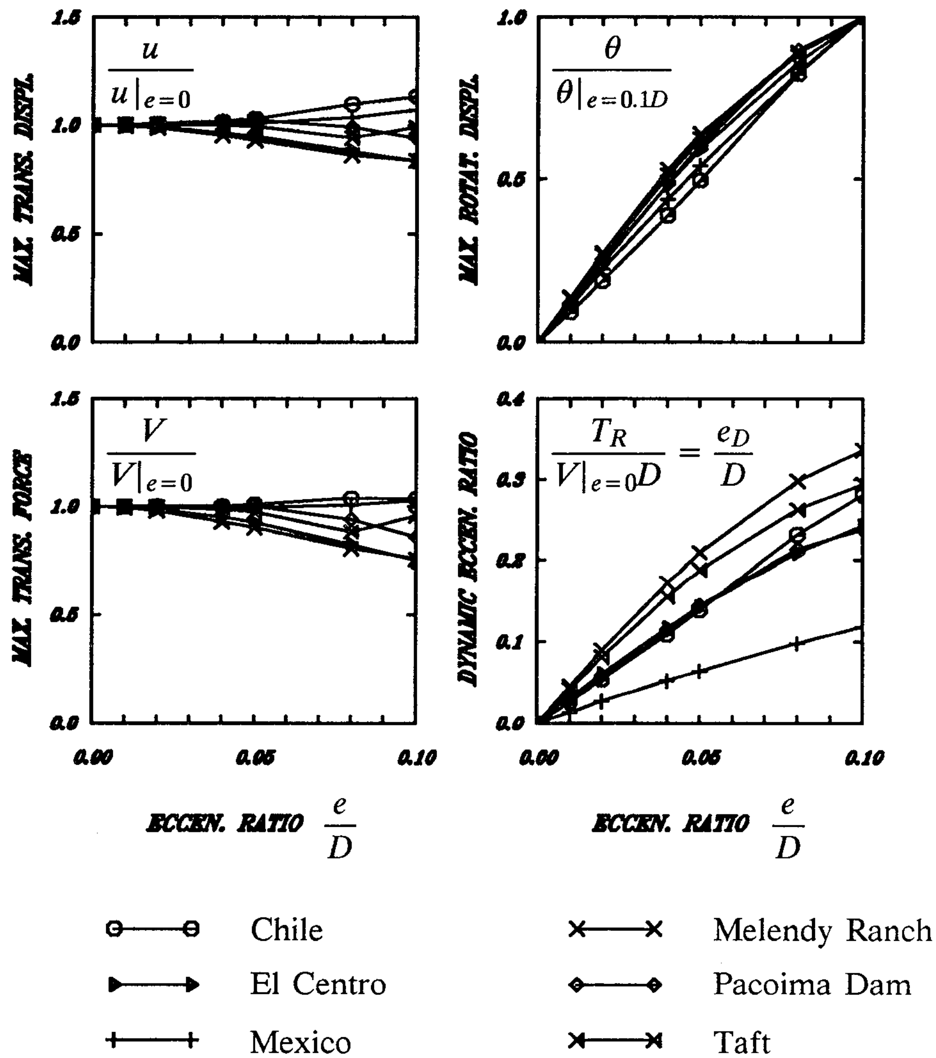

Figure 4–8 Maximum Response of One–Story 3.75 *Hz* System Subjected to Earthquake Ground Motion

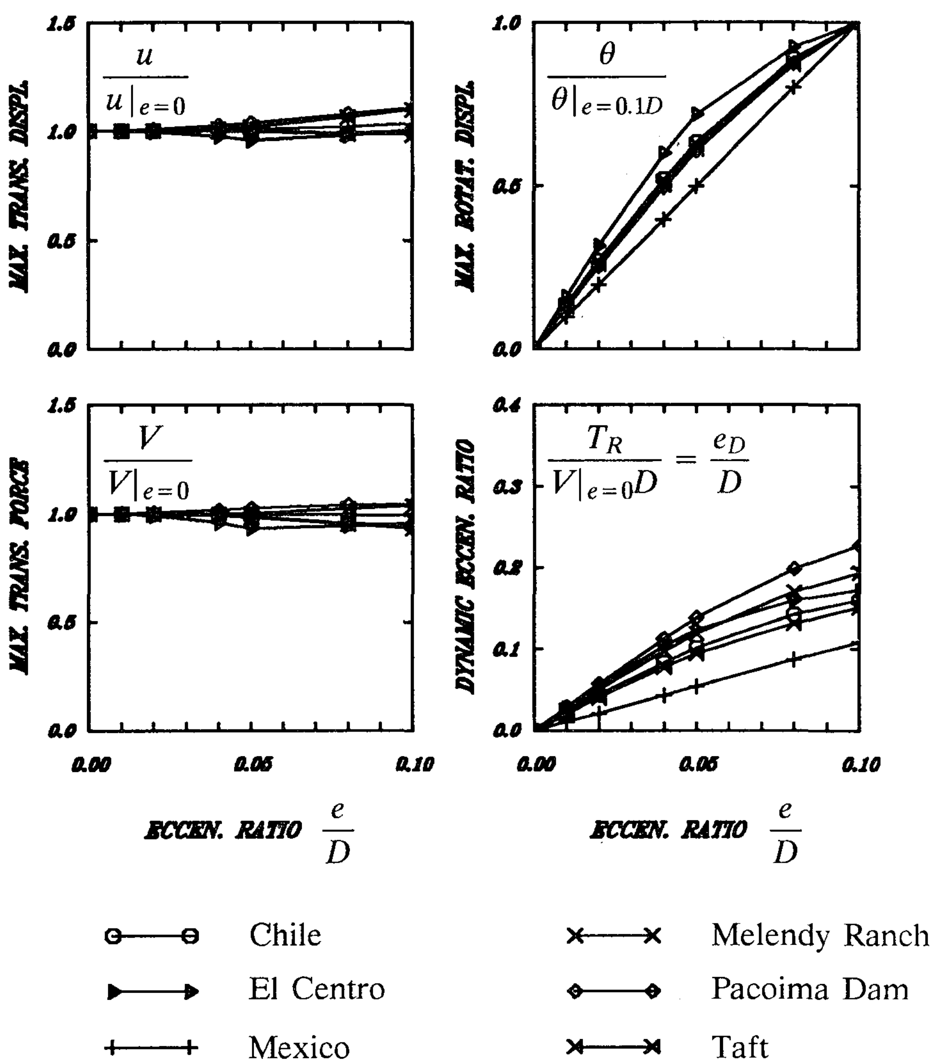

Figure 4–9 Maximum Response of One–Story 10.0 *Hz* System Subjected to Earthquake Ground Motion

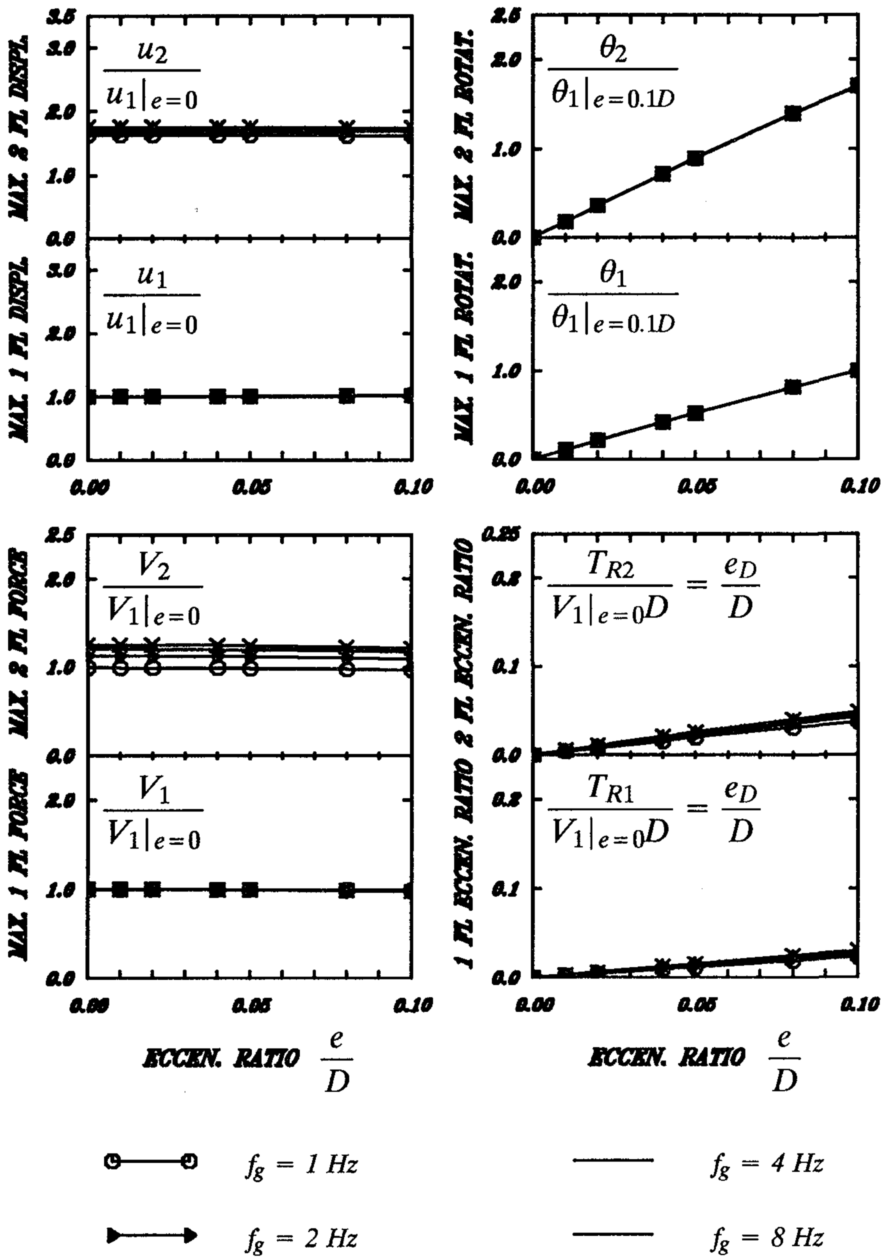

Figure 4–10 Maximum Response of Two-Story 0.2 *Hz* System Subjected to Harmonic Base Motion

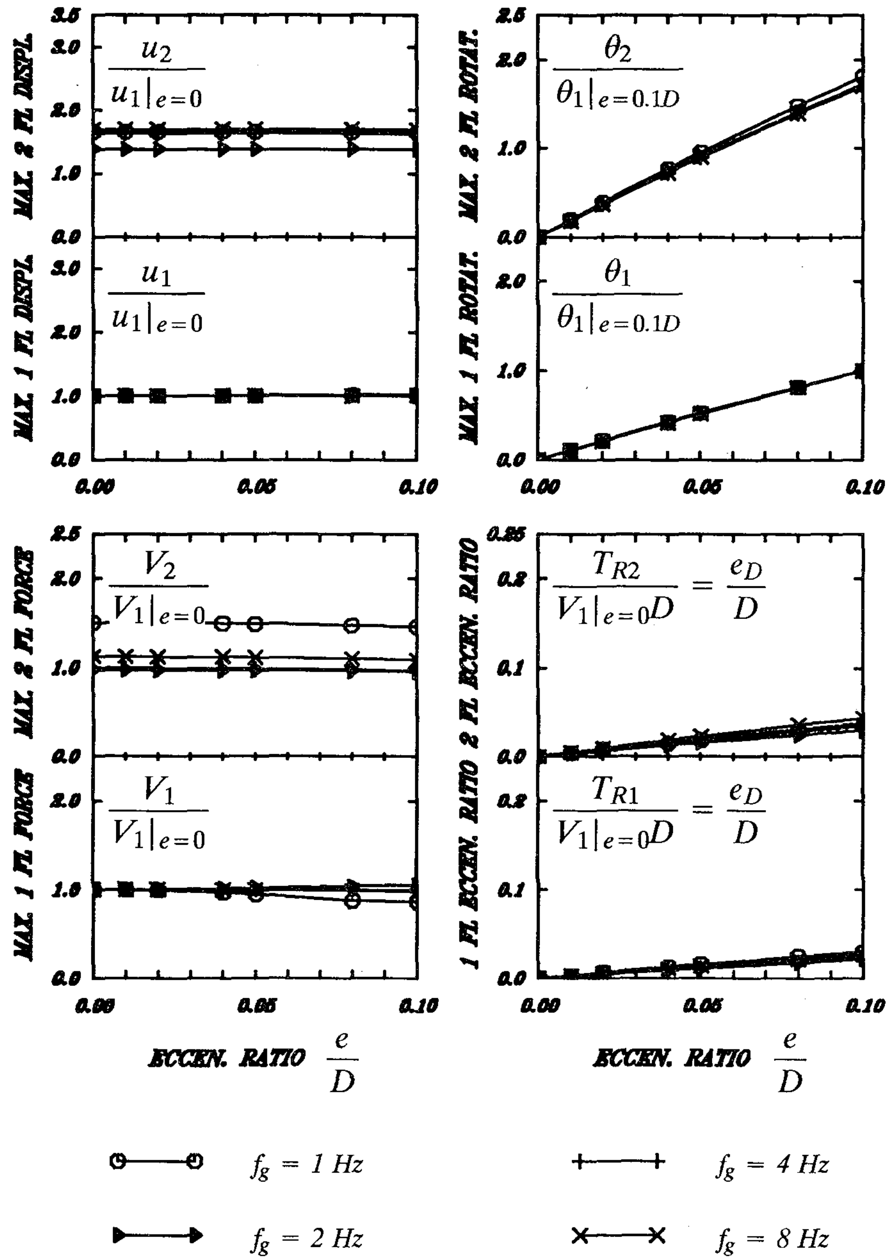

Figure 4–11 Maximum Response of Two-Story 0.8 Hz System Subjected to Harmonic Base Motion

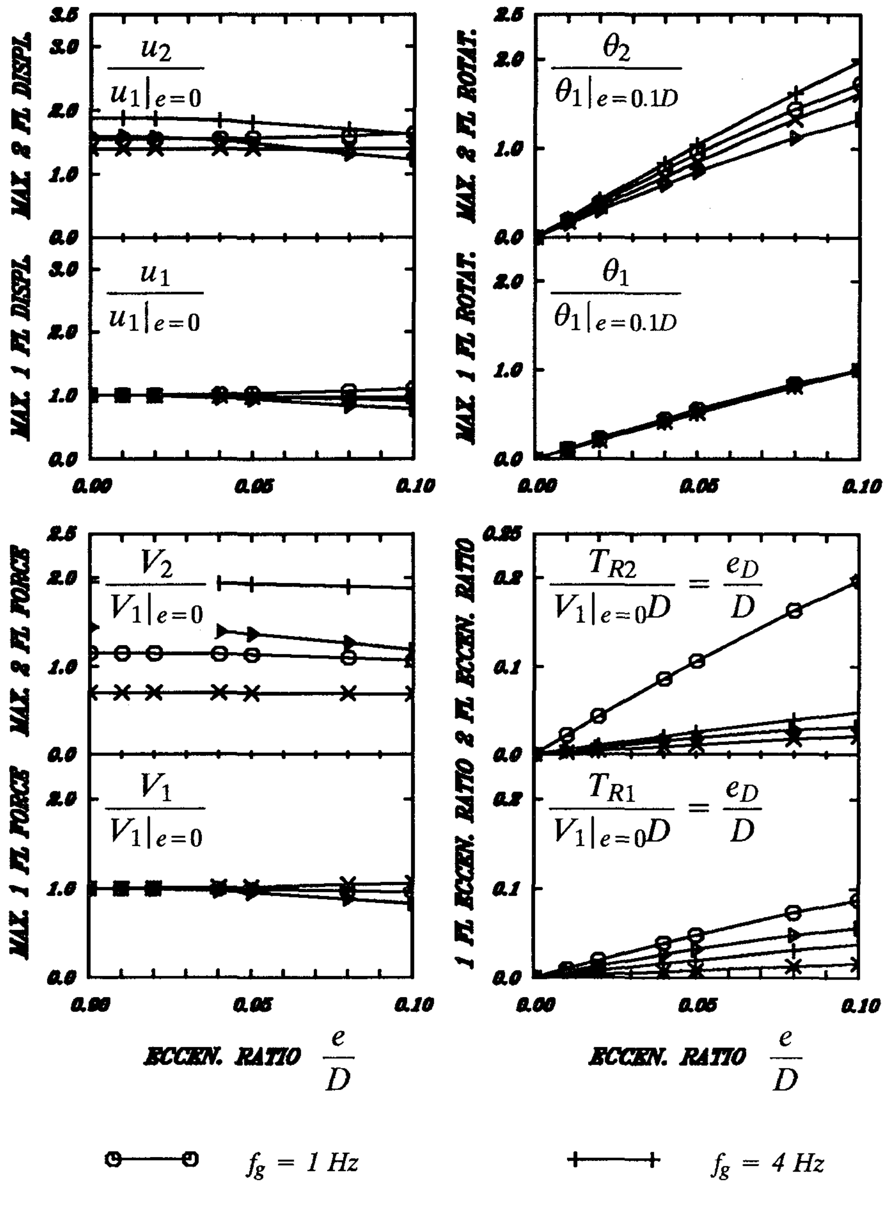

Figure 4–12 Maximum Response of Two–Story 3.75 *Hz* System Subjected to Harmonic Base Motion

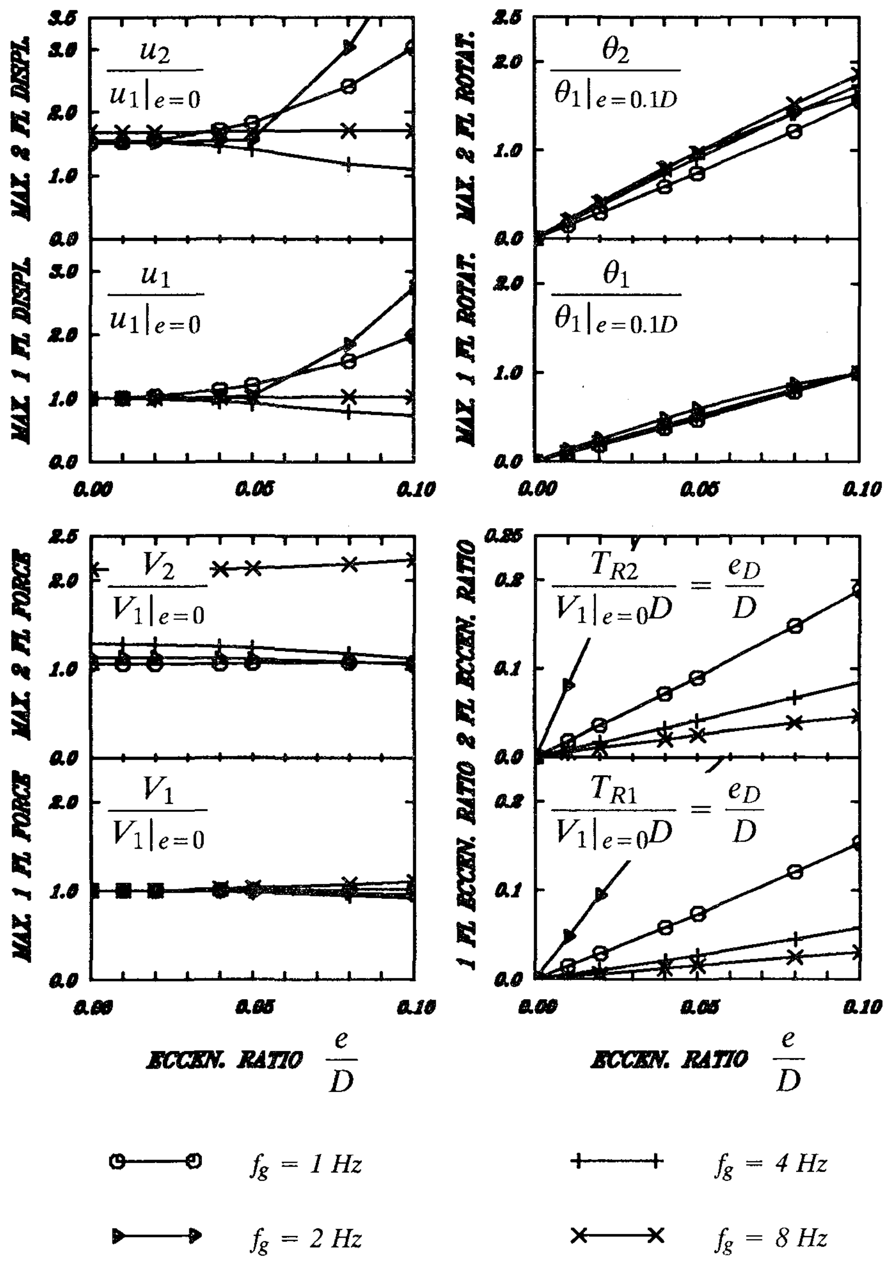

Figure 4–13 Maximum Response of Two–Story 10.0 *Hz* System Subjected to Harmonic Base Motion

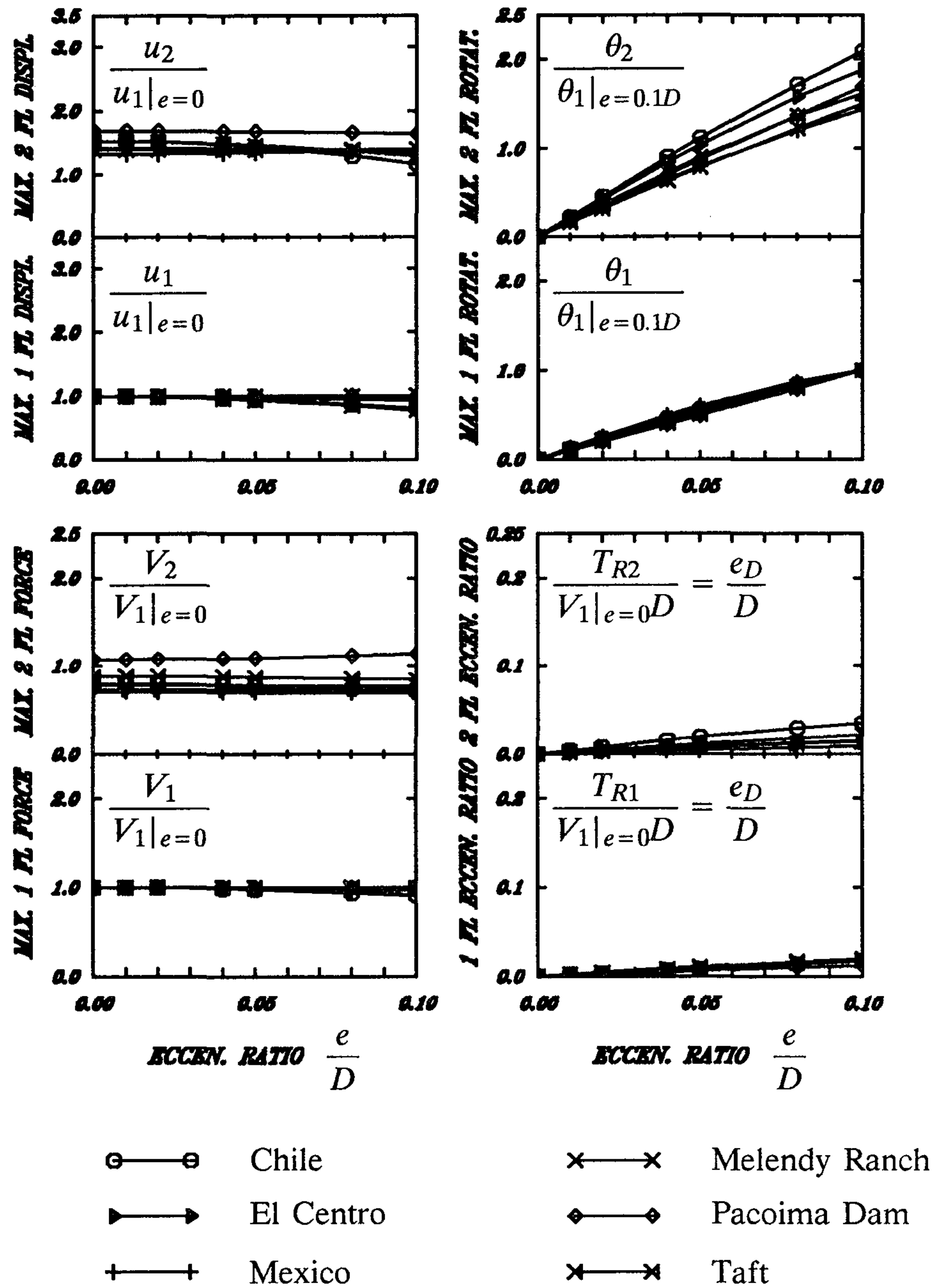

Figure 4–14 Maximum Response of Two-Story 0.2 *Hz* System Subjected to Earthquake Ground Motion

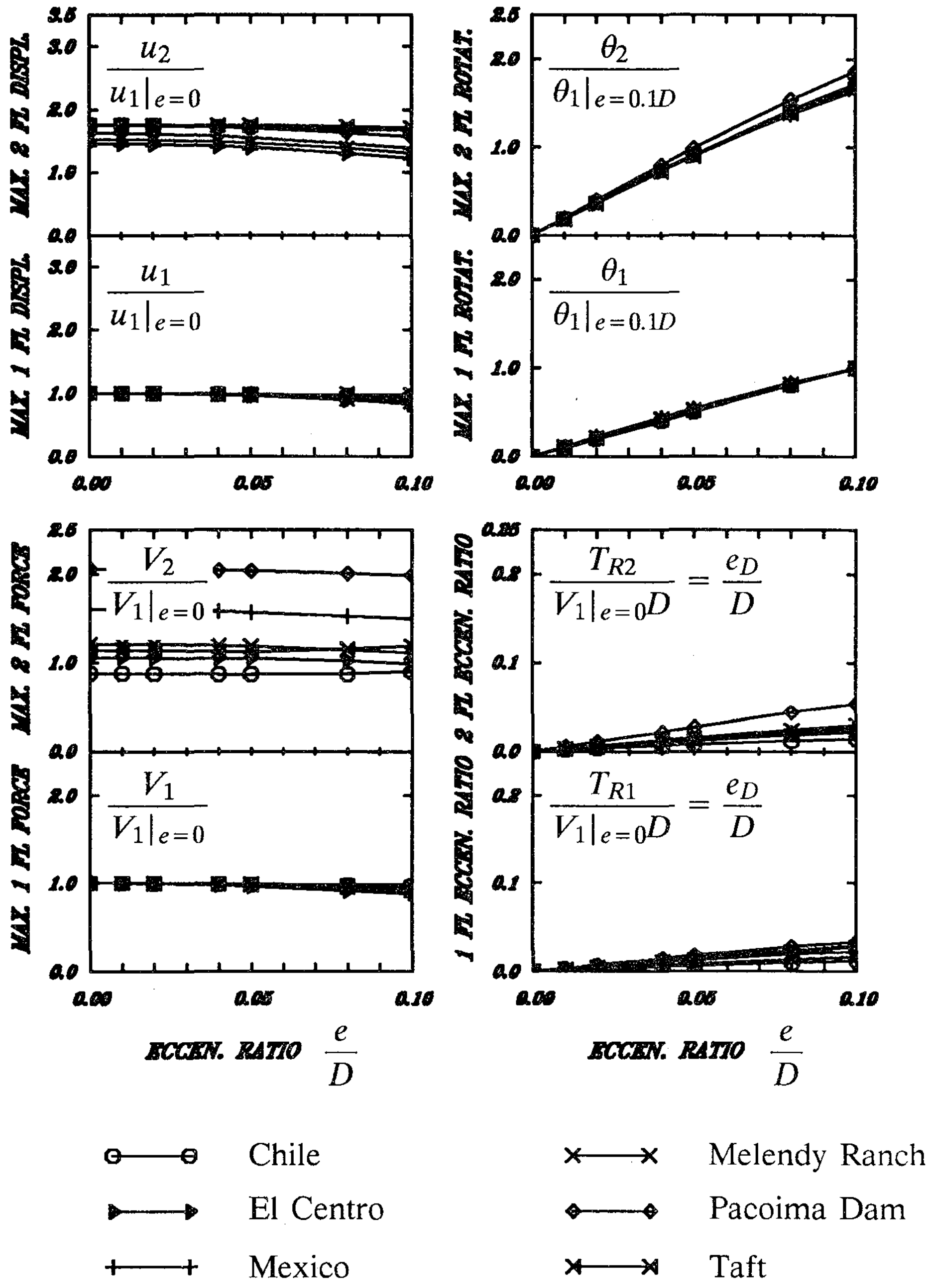

Figure 4–15 Maximum Response of Two-Story 0.8 *Hz* System Subjected to Earthquake Ground Motion

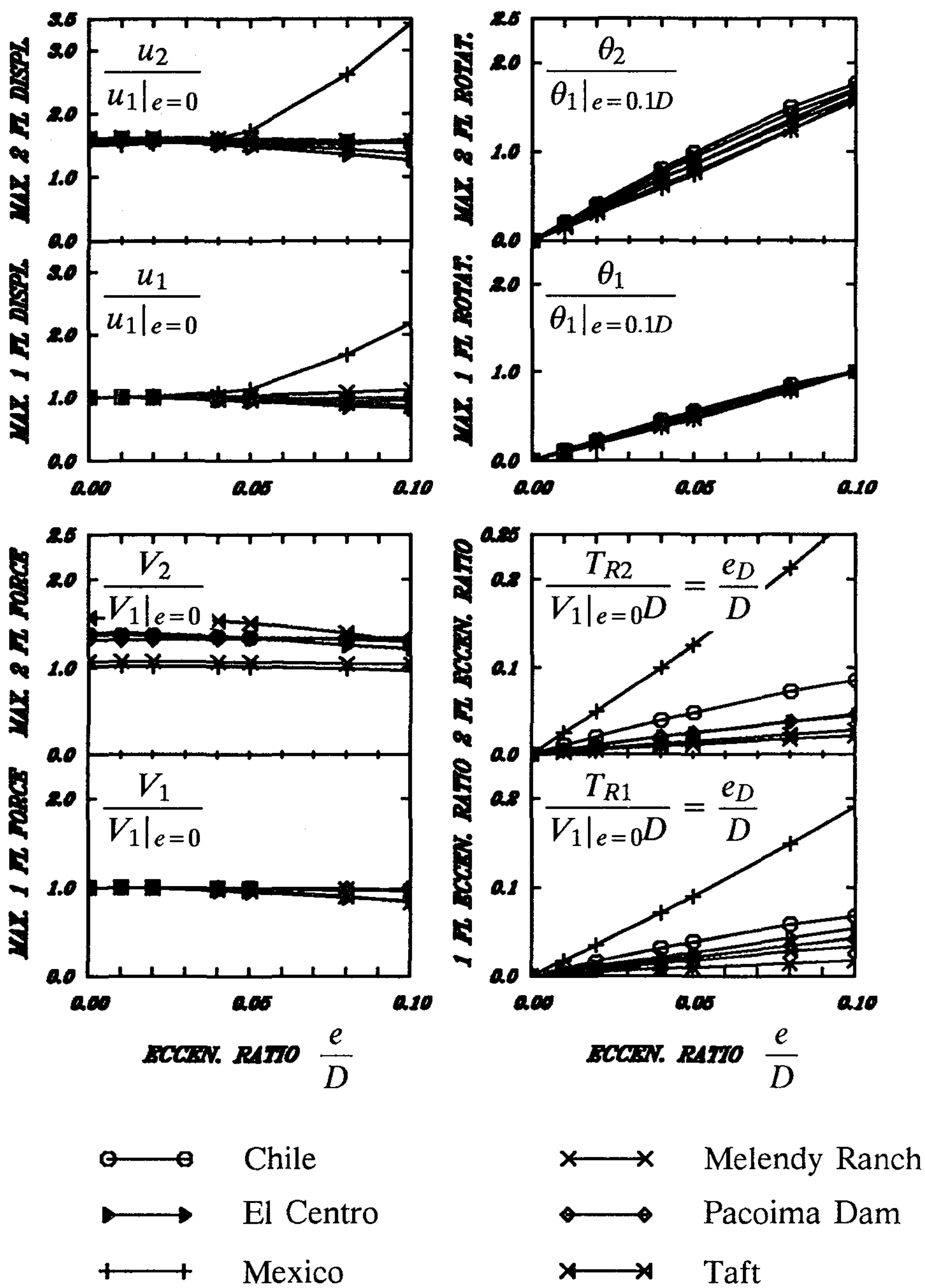

Figure 4–16 Maximum Response of Two–Story 3.75 *Hz* System Subjected to Earthquake Ground Motion

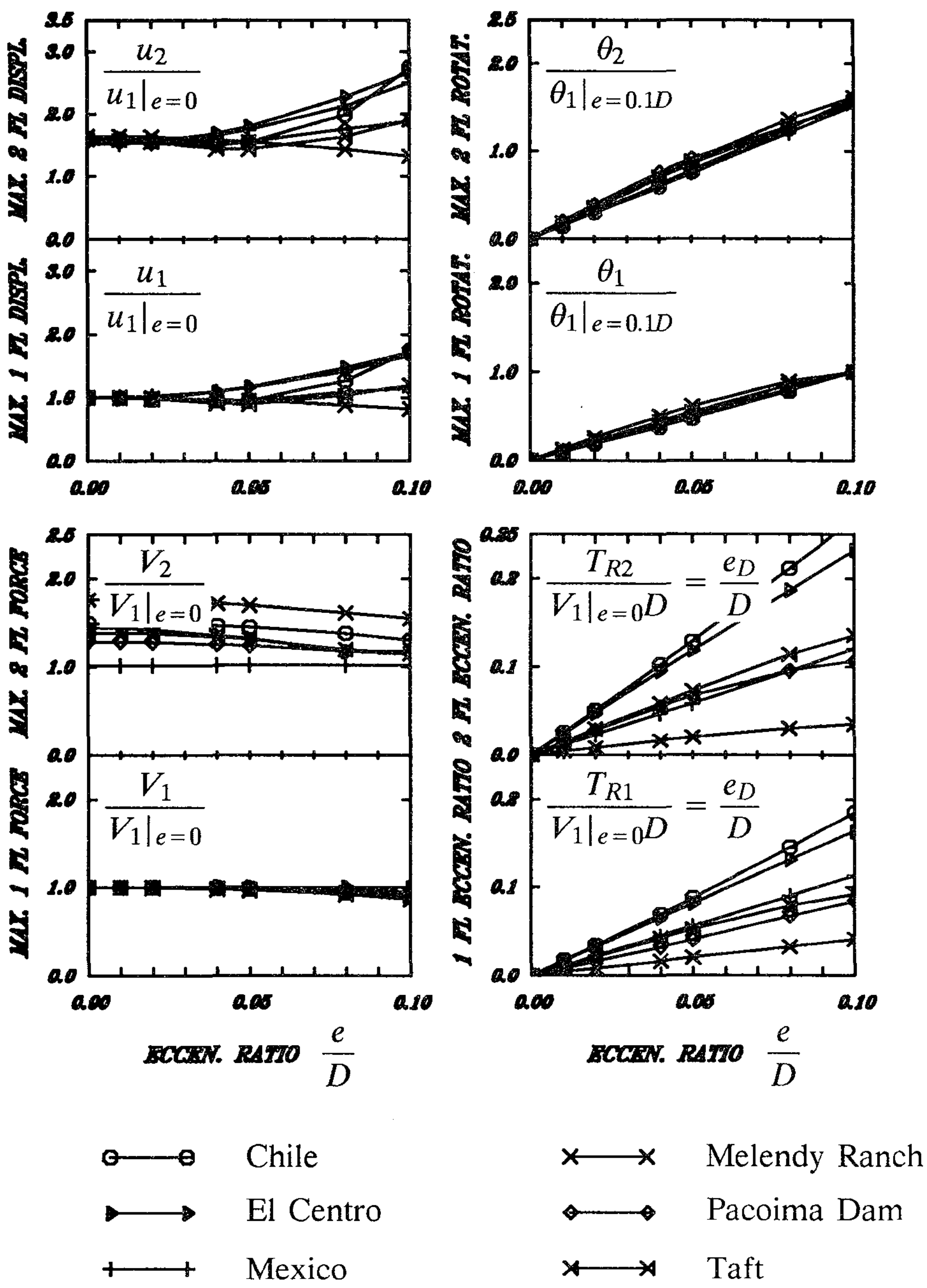

Figure 4–17 Maximum Response of Two-Story 10.0 *Hz* System Subjected to Earthquake Ground Motion

4.6 Influence of Eccentricity on Systems with Inelastic Response

Observations and discussions in the previous section have concentrated on the influence of structural eccentricity on the response envelopes of linear–elastic one–directional asymmetric systems subjected to harmonic and earthquake ground motion. During intensive strong ground motion, however, the response of most well–designed structures inevitably will go beyond the linear–elastic range of the load–resisting members in order to absorb the input energy hysteretically. Yet the performance and behavior of asymmetric structures responding inelastically to strong ground motion, as well as the rationale behind any effective measures to prevent torsionally–induced loss of stiffness from becoming a major factor in causing excessive structural damage, are not well understood by the profession. In the following, observations are presented on the analysis of results of the models subjected to the scaled earthquake ground motions described in Section 4.3.

The plots in Figures 4–18 through 4–29 are for the one–story systems with the frequency ratio of 1.225. The plots in Figures 4–30 through 4–41 are for the two–story systems. Both of the one–story and two–story model systems were subjected to the six selected earthquake ground motions with the maximum acceleration scaled to 0.1g, 0.2g, and 0.4g, respectively. The ductility experienced by the columns responding to these scaled ground motions is in the intermediate range of three to six. The resulting envelopes of inelastic response in each case exhibit the expected general trends in the response of one–directional asymmetric systems to earthquake ground motion, with the exception of the torsional response as discussed next.

As shown in the upper–left and lower–left plots of these figures, the maximum translational response in the model systems studied (with the specific frequency ratio of 1.225 for each story) with inelastic behavior is not severely affected by the presence of torsional response, which is similar to the observation made earlier for the translational response in linear–elastic systems.

Torsional response can result from structural eccentricity when a structure is only subjected to translational ground motion input. In structures with symmetric distribution of mass and stiffness, however, torsional response can be a result of damage to the lateral load–resisting members with relatively lower strength. After the uneven yielding of some members, the member stiffness will be changed. As shown in the upper–right plots of these figures, symmetric systems with zero structural eccentricity experienced some rotational deformation when the ground motion intensity was high enough to cause the members to yield. In the analyses with zero static eccentricity only, the strength of the columns on one side of a symmetric system was 33 percent higher than that on the other side; for all other e/D eccentricity ratios the column strengths were equal. The rotational displacement in symmetric systems arose because of yielding of the weaker columns which in turn led to redistribution of the lateral stiffness and consequently a dynamic eccentricity. The dips in those same plots arose because of the foregoing reason, namely differences in column strength at eccentricity ratio of zero. The dynamic eccentricity in some of the asymmetric systems was not as large as that created in the corresponding symmetric systems, thus the rotational displacement of the asymmetric systems with small eccentricity ratios was less than the rotation experienced by the symmetric systems.

It can be concluded that physical eccentricity between the centers of mass and stiffness can be generated during earthquake ground excitation. If the intensity of the strong ground motion shaking is sustained, the rigidity center will shift away from the damaged elements as their stiffness decreases. Thus the eccentricity may increase, and in turn will affect the deformation and force in the elements away from the rigidity center. Torsionally–induced loss of stiffness of this type is the most dangerous, because of its progressive nature. Therefore it should be prevented to the extent possible.

The effect of eccentricity on torsional moments in inelastic systems is generally the same as in linear systems. The dynamic amplification factor for eccentricity ratios greater than 0.01 for this study, for both the one–story and the two–story inelastic systems, ranges from 1.5 to 3, as shown by the slopes in the lower–right plots of these figures.

When dealing with inelastic behavior in the planar analysis of structural systems, the term “ductility” is commonly used to describe the ductility demand for a load–resisting system. With torsion involved, however, the term “ductility” seems inappropriate as a single index for measuring the plastic capacity of the lateral load–resisting system because ductility is usually defined in terms of linear deformations. Conversion of the rotational response to translational response requires the use of a quantity with units of length. In order to measure the degree or extent of inelasticity in a structure, therefore, it is necessary to address the inelastic deformations in specific members, instead of estimating the ductilities from overall gross structural response.

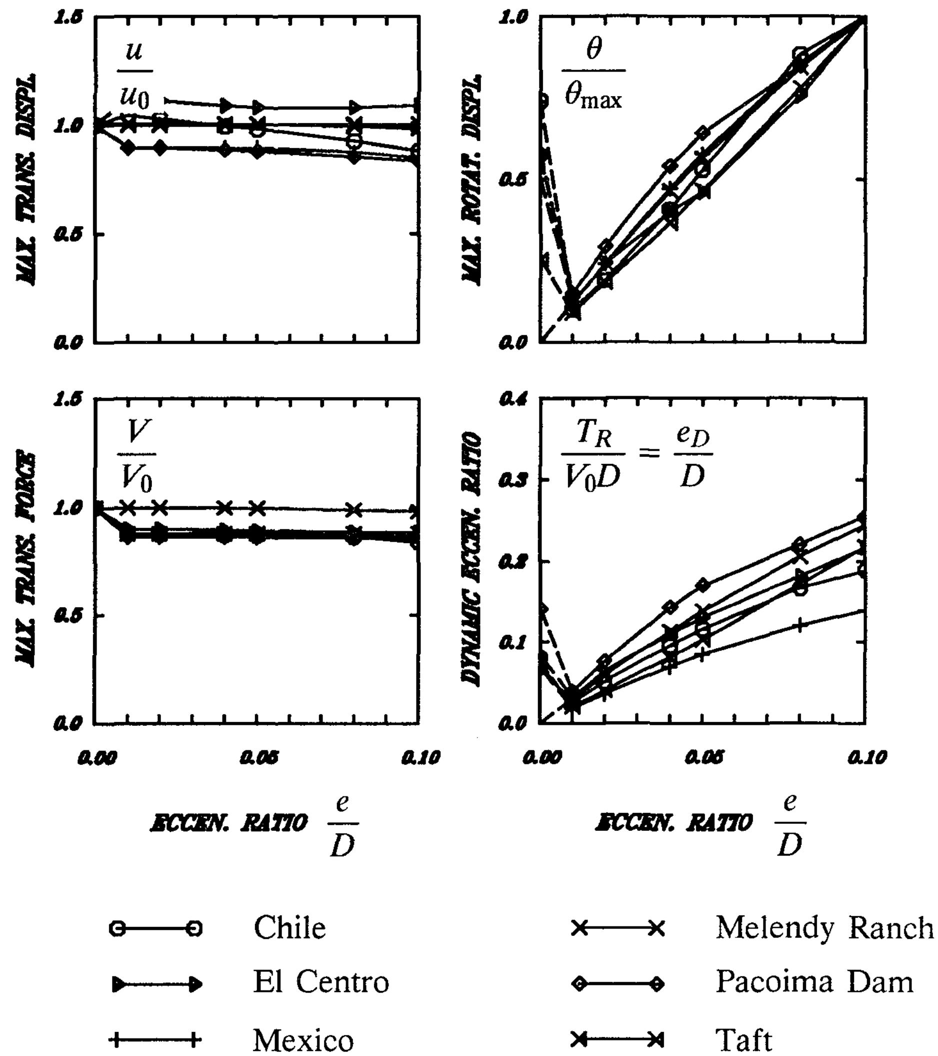

Figure 4–18 Maximum Response of One–Story 0.2 *Hz* System Subjected to Earthquake Ground Motion of 0.1g

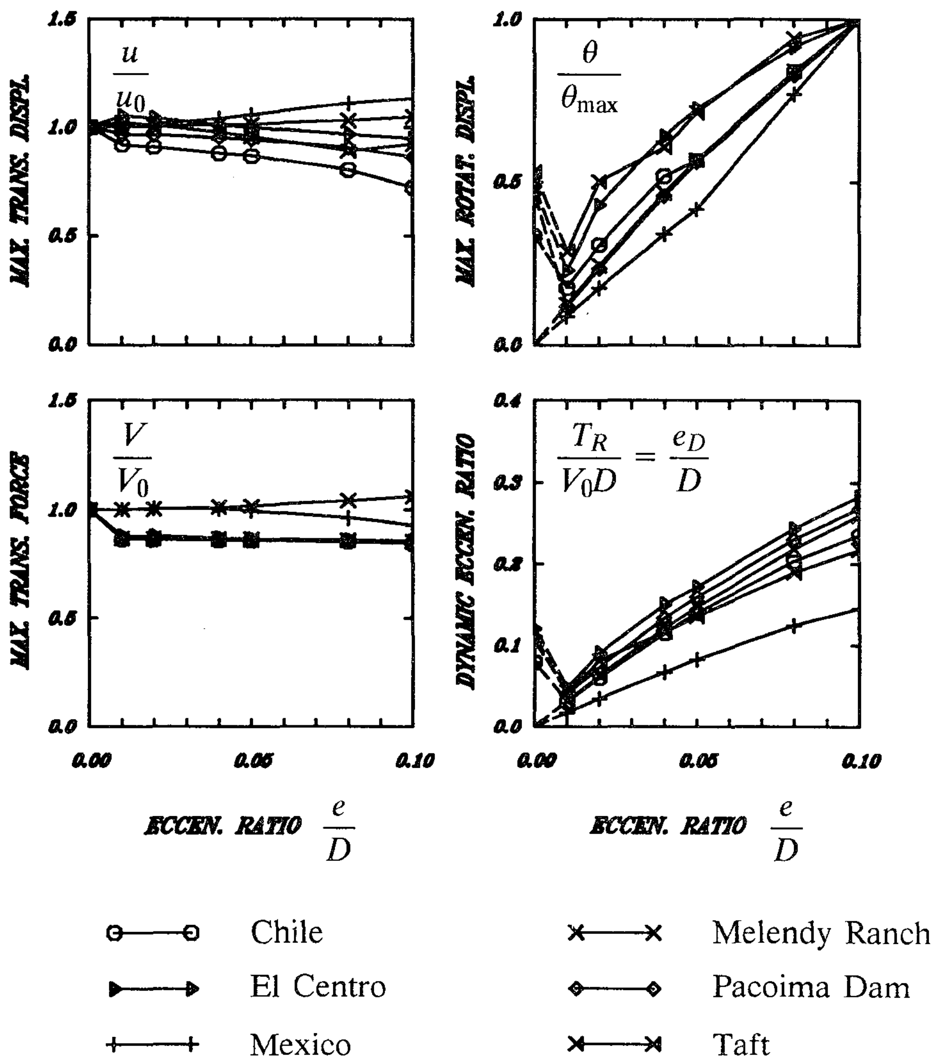

Figure 4–19 Maximum Response of One–Story 0.8 *Hz* System Subjected to Earthquake Ground Motion of 0.1g

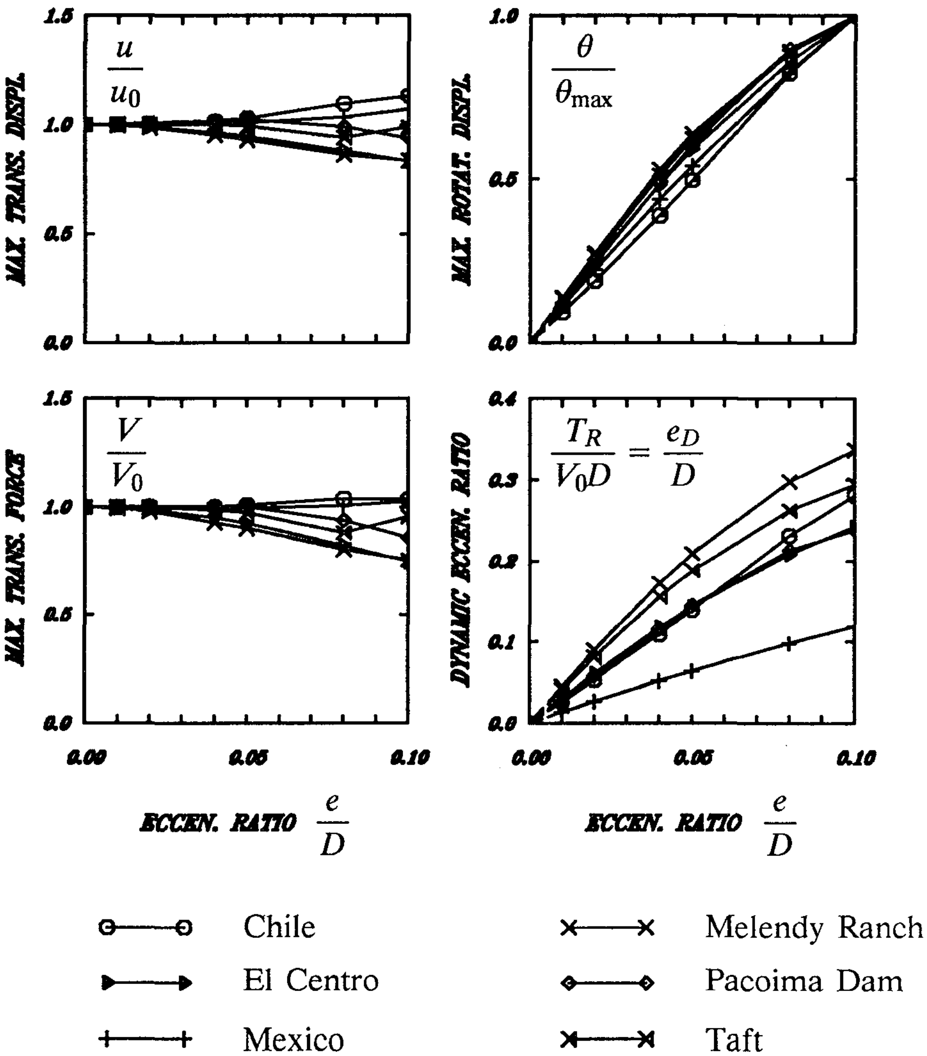

Figure 4–20 Maximum Response of One–Story 3.75 *Hz* System Subjected to Earthquake Ground Motion of 0.1g

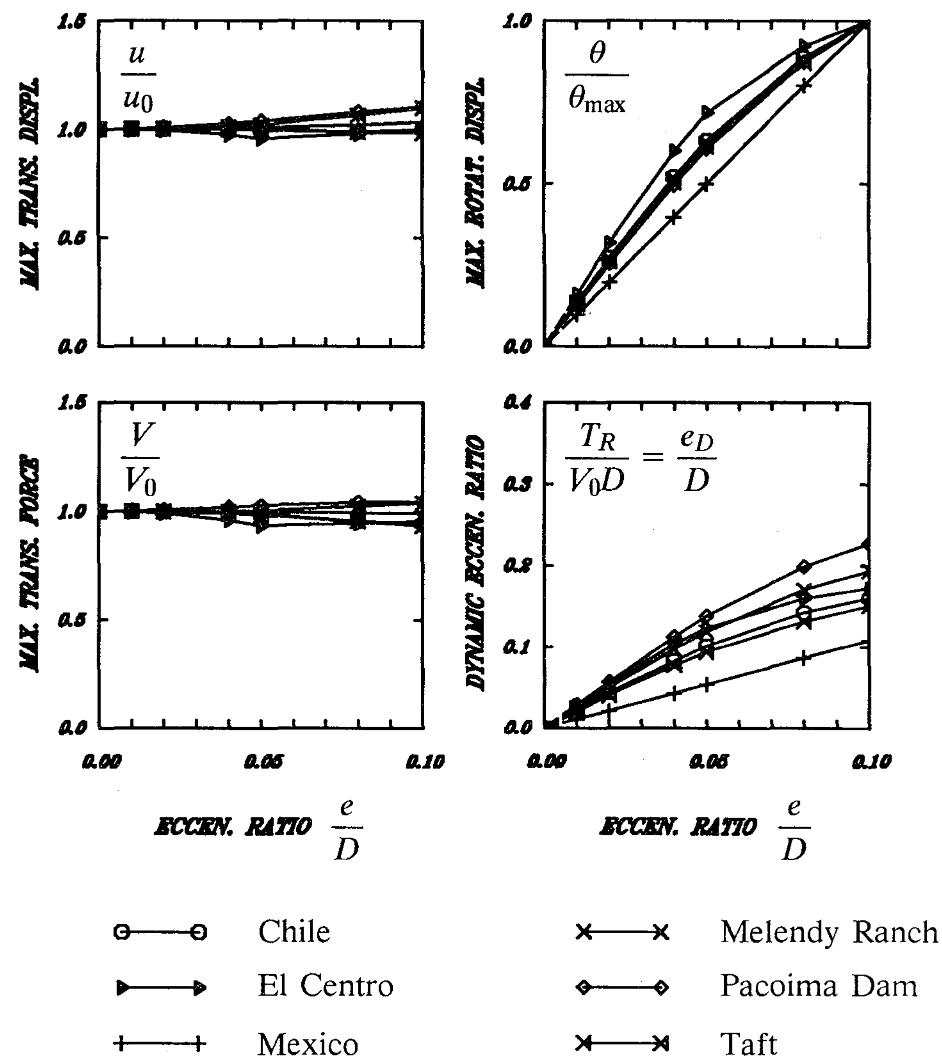

Figure 4–21 Maximum Response of One–Story 10.0 *Hz* System Subjected to Earthquake Ground Motion of 0.1g

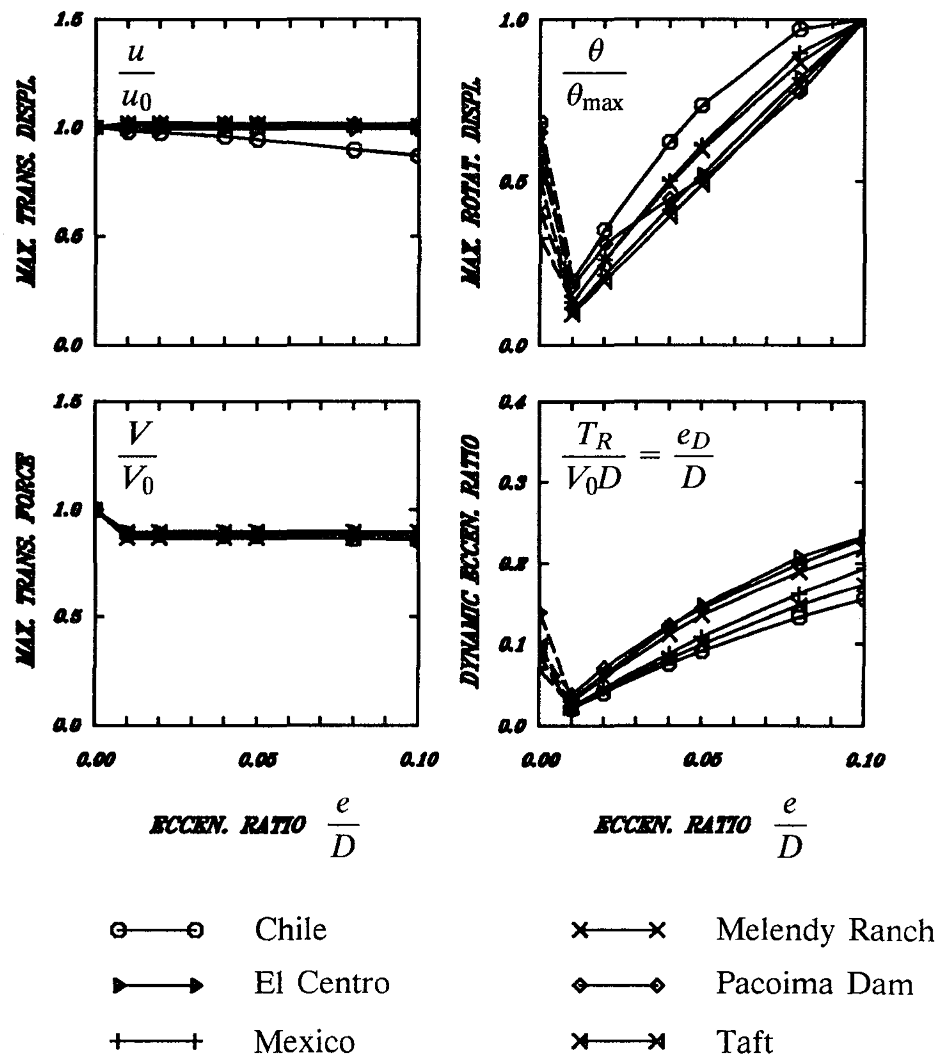

Figure 4–22 Maximum Response of One–Story 0.2 *Hz* System Subjected to Earthquake Ground Motion of 0.2g

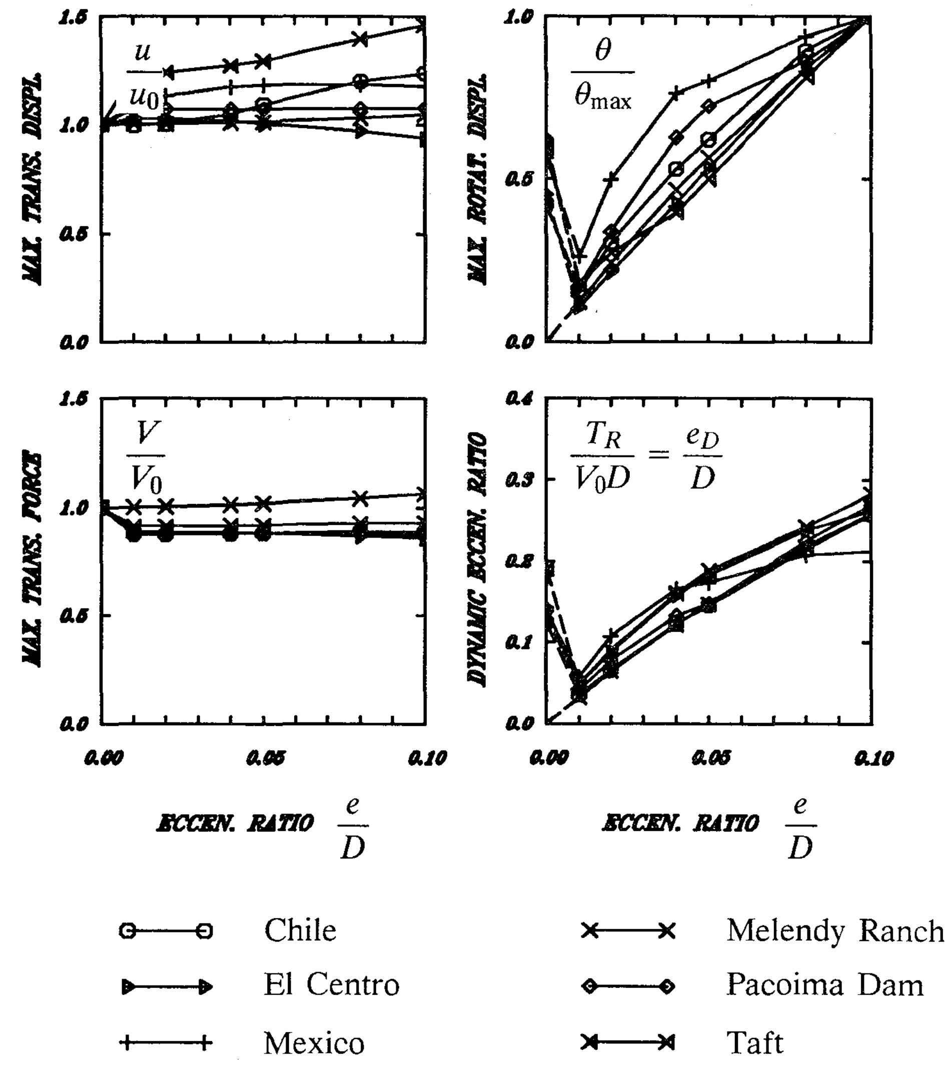

Figure 4–23 Maximum Response of One–Story 0.8 *Hz* System Subjected to Earthquake Ground Motion of 0.2g

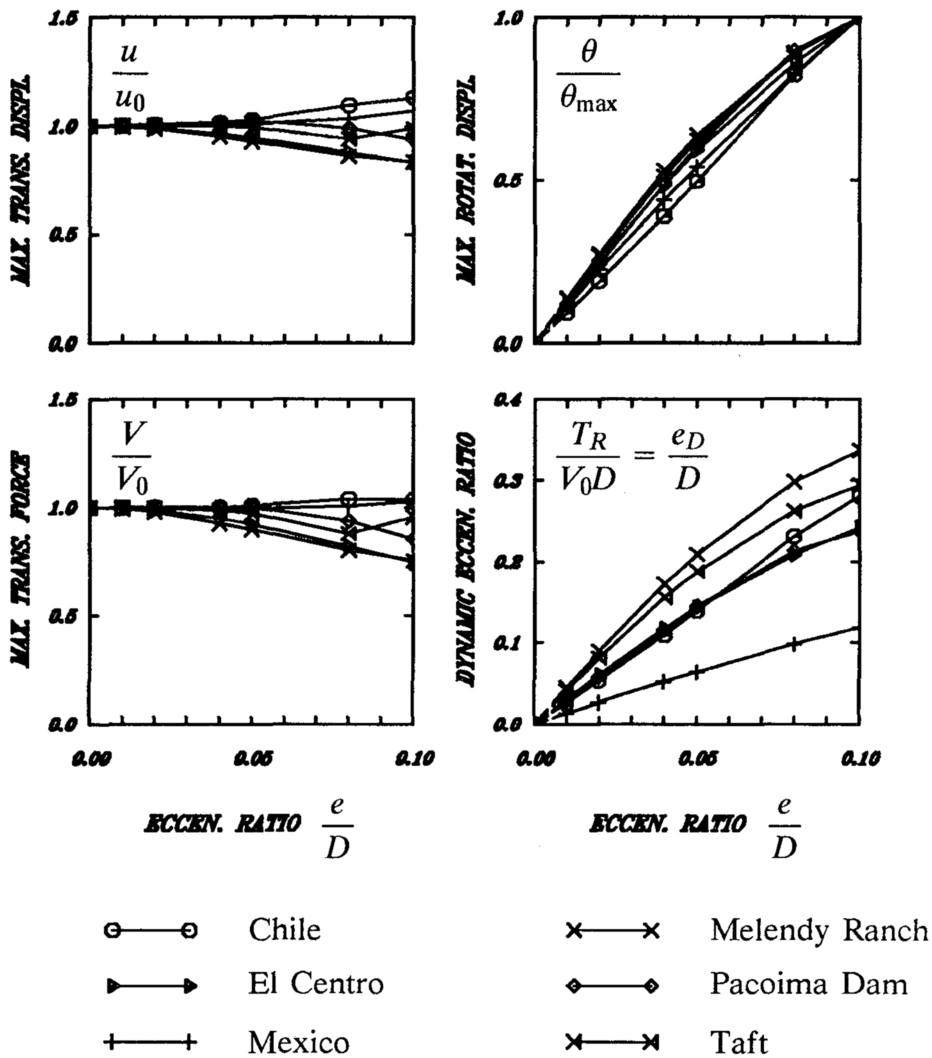

Figure 4–24 Maximum Response of One–Story 3.75 *Hz* System Subjected to Earthquake Ground Motion of 0.2g

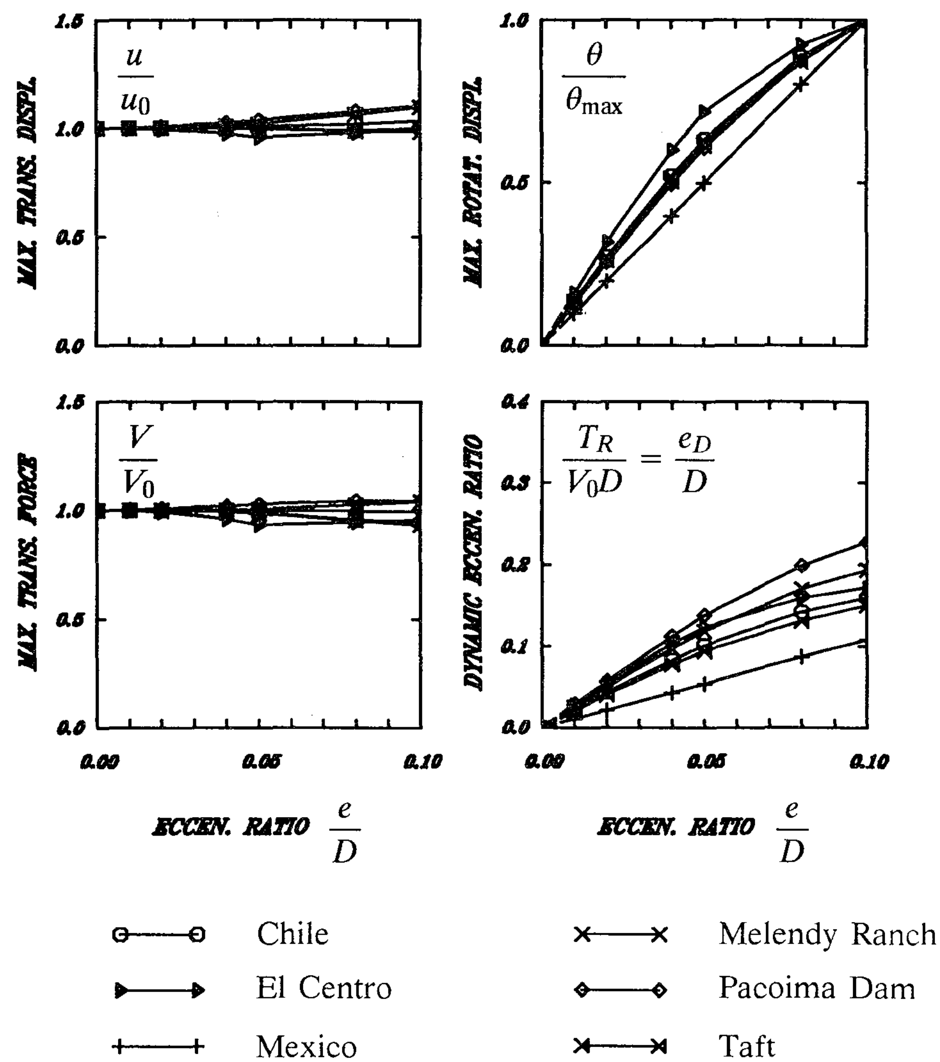

Figure 4–25 Maximum Response of One–Story 10.0 *Hz* System Subjected to Earthquake Ground Motion of 0.2g

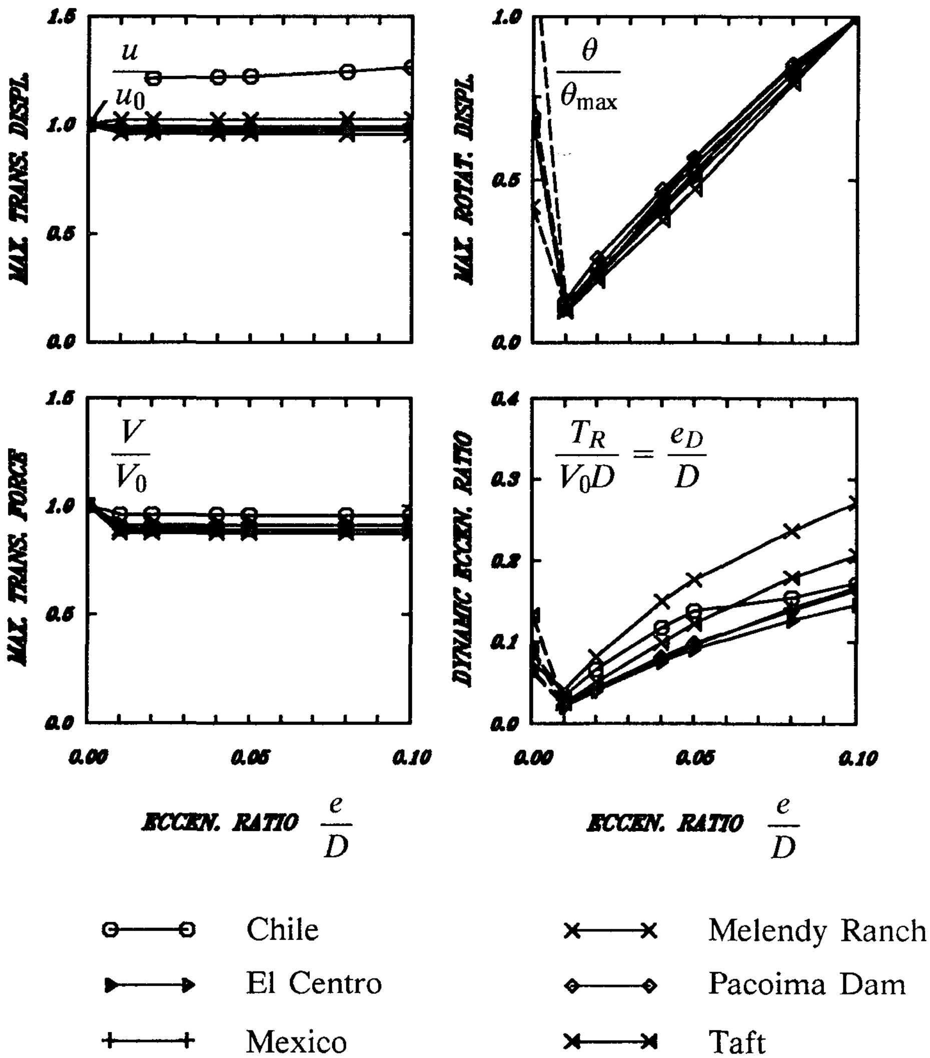

Figure 4–26 Maximum Response of One–Story 0.2 *Hz* System Subjected to Earthquake Ground Motion of 0.4g

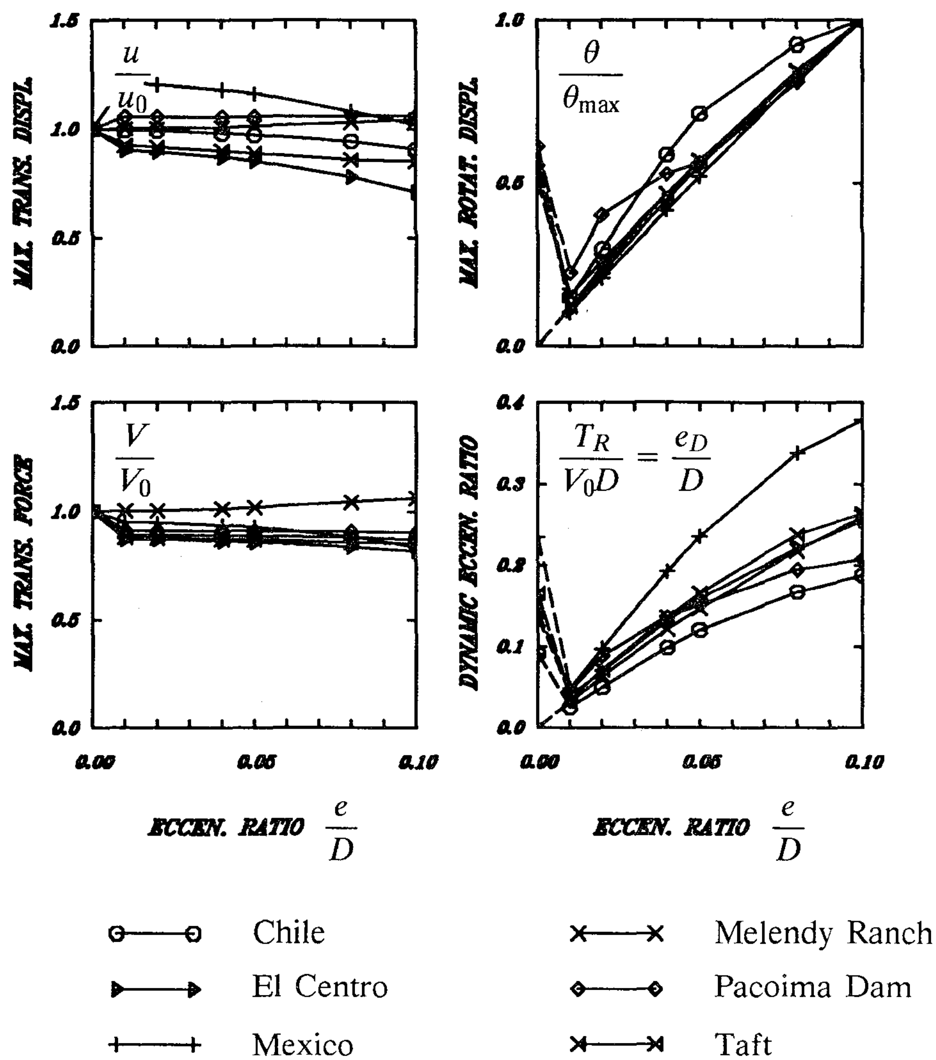

Figure 4–27 Maximum Response of One–Story 0.8 *Hz* System Subjected to Earthquake Ground Motion of 0.4g

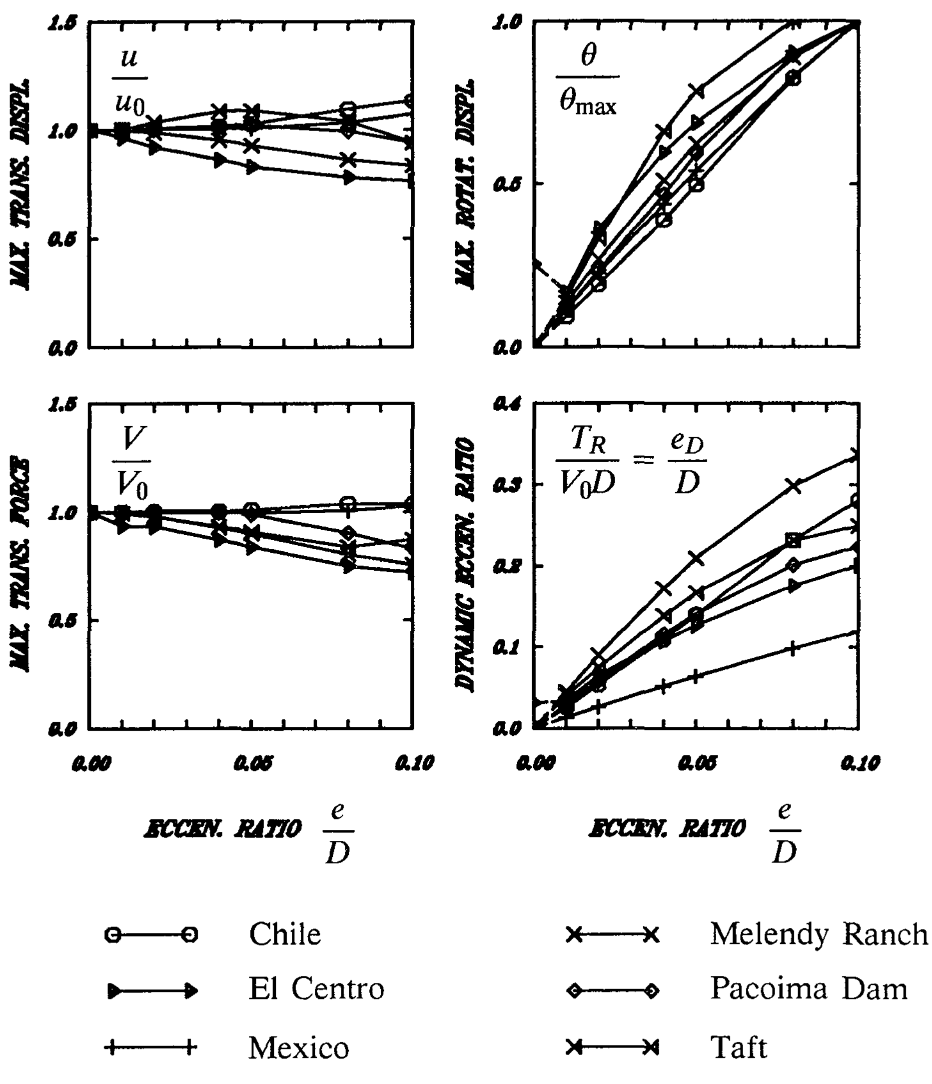

Figure 4–28 Maximum Response of One–Story 3.75 *Hz* System Subjected to Earthquake Ground Motion of 0.4g

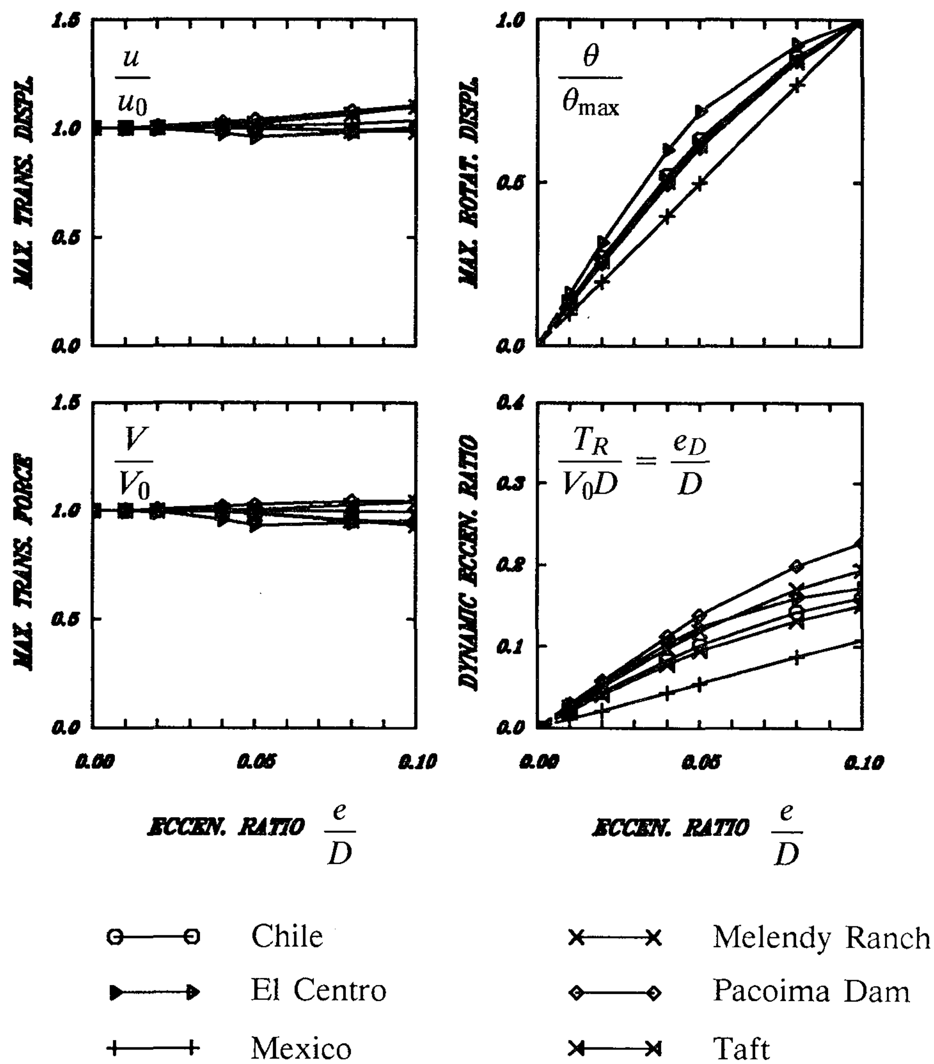

Figure 4–29 Maximum Response of One–Story 10.0 *Hz* System Subjected to Earthquake Ground Motion of 0.4g

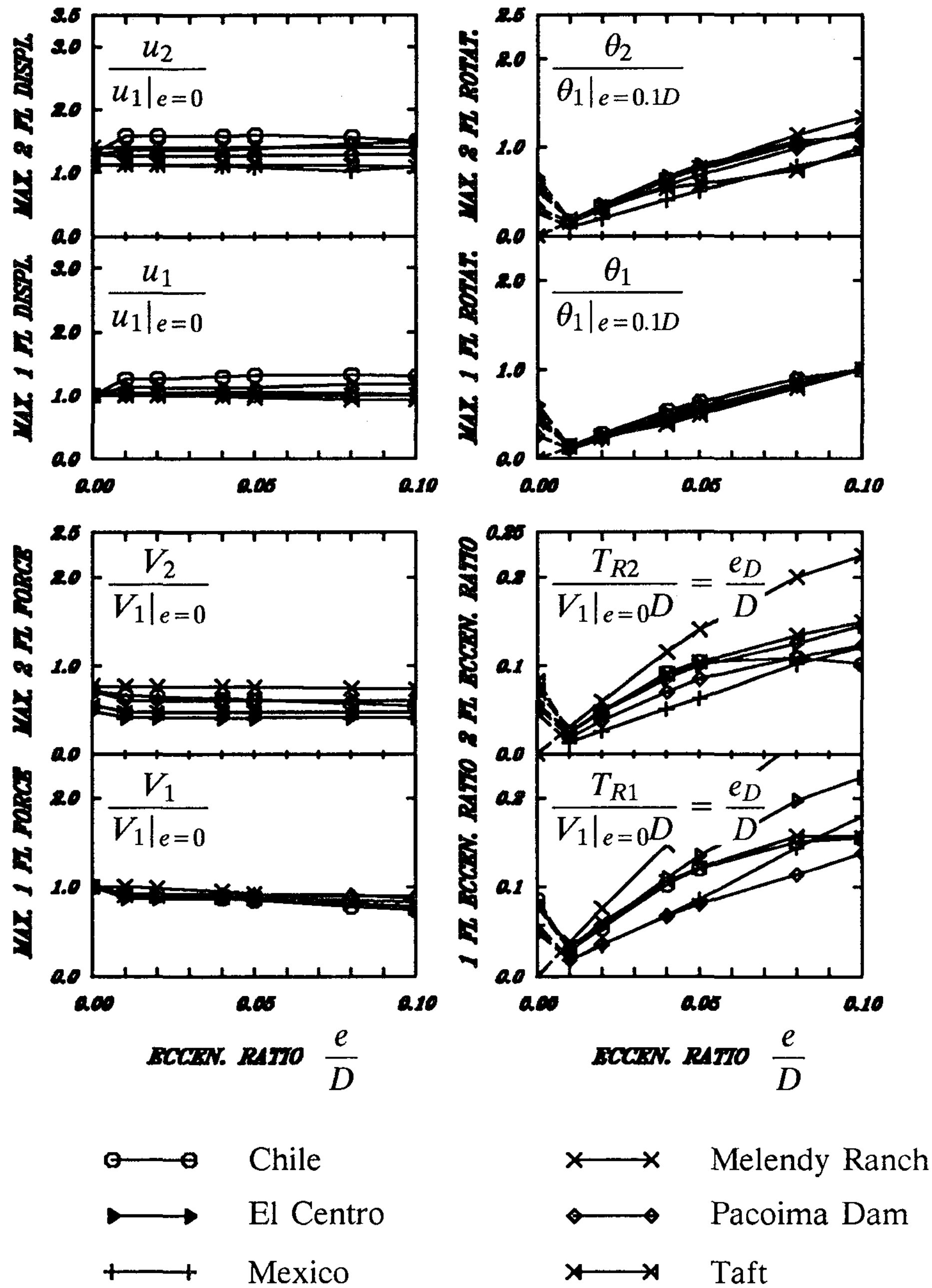

Figure 4–30 Maximum Response of Two-Story 0.2 *Hz* System Subjected to Earthquake Ground Motion of 0.1g

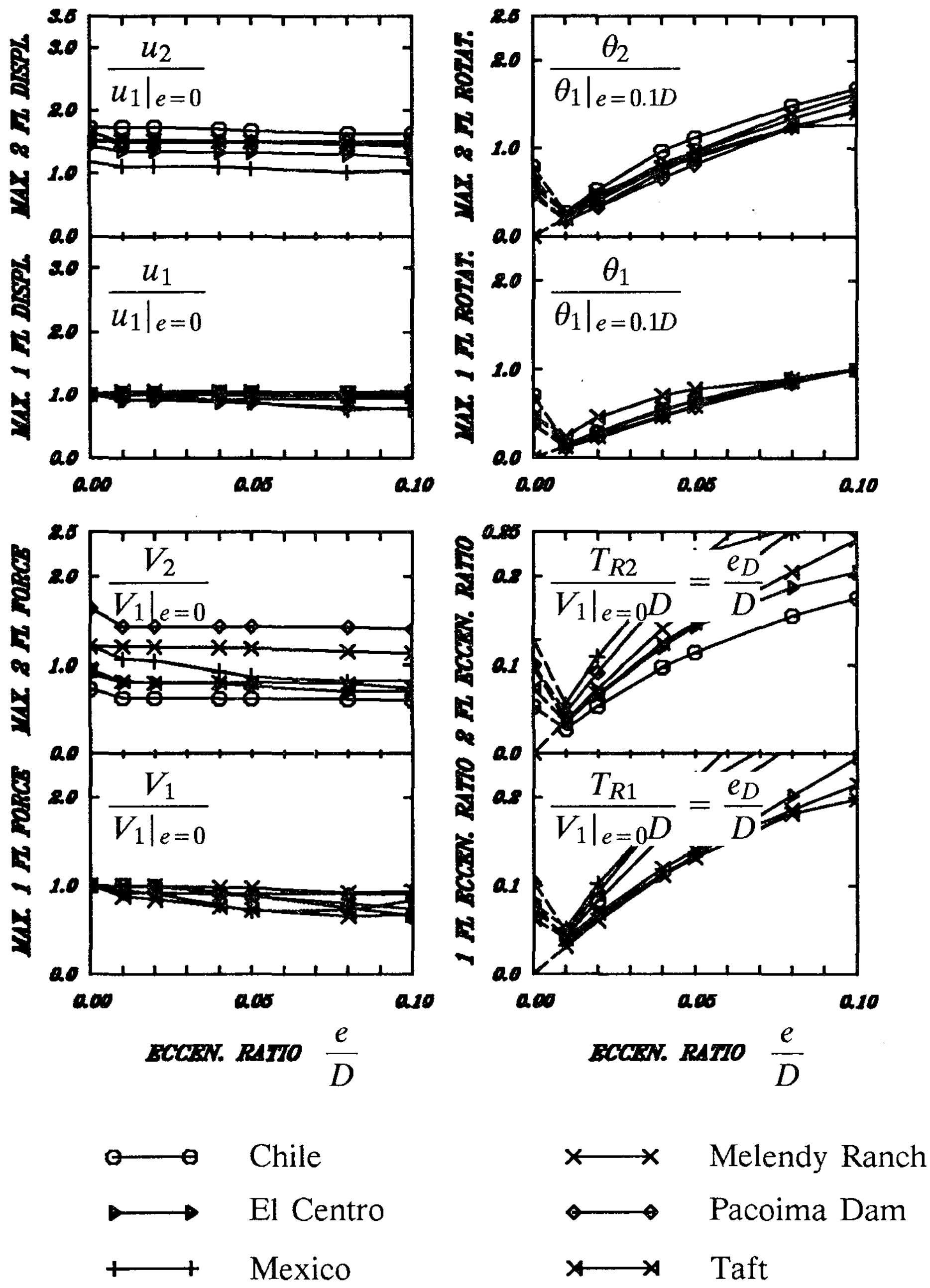

Figure 4–31 Maximum Response of Two–Story 0.8 *Hz* System Subjected to Earthquake Ground Motion of 0.1g

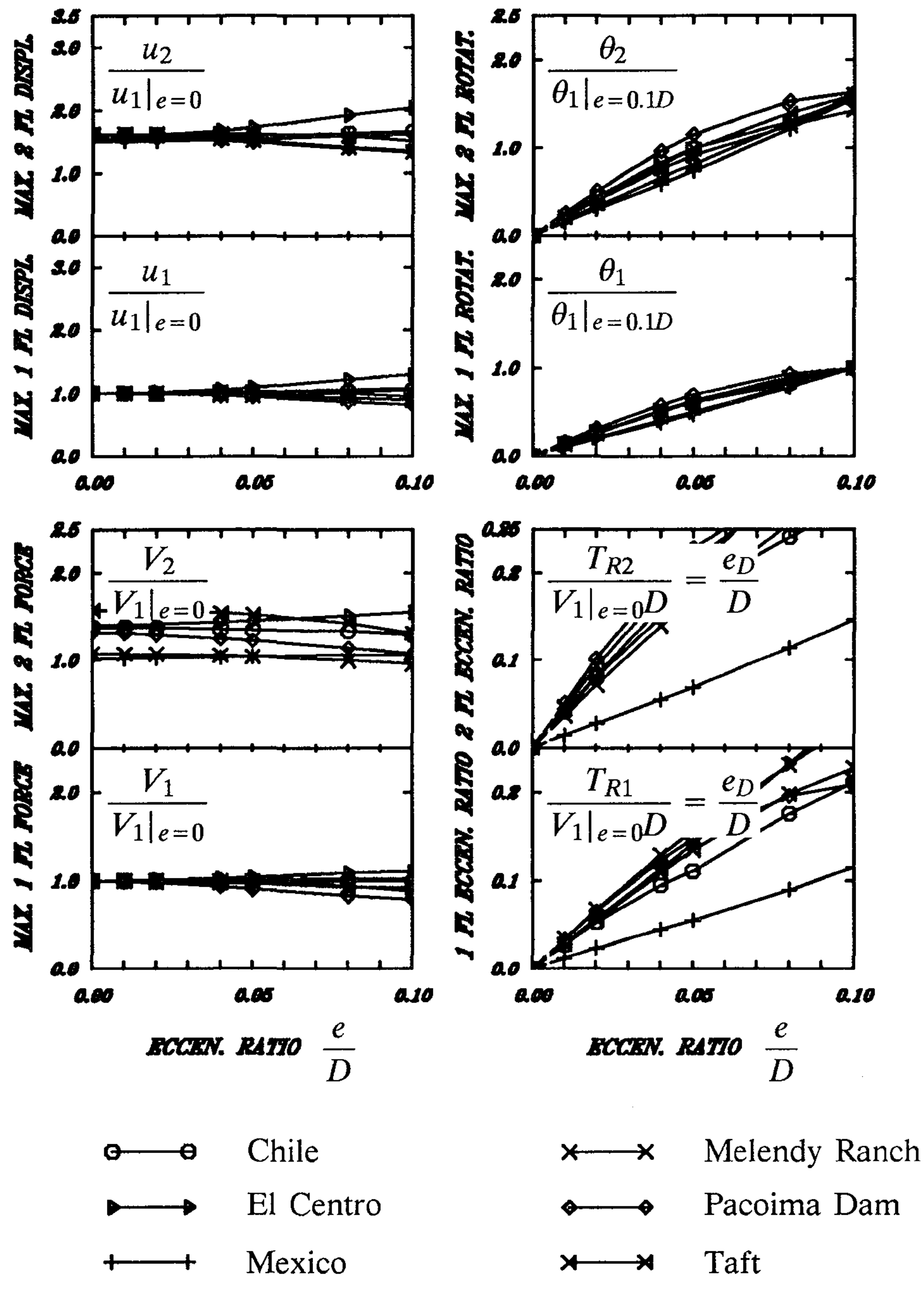

Figure 4–32 Maximum Response of Two–Story 3.75 *Hz* System Subjected to Earthquake Ground Motion of 0.1g

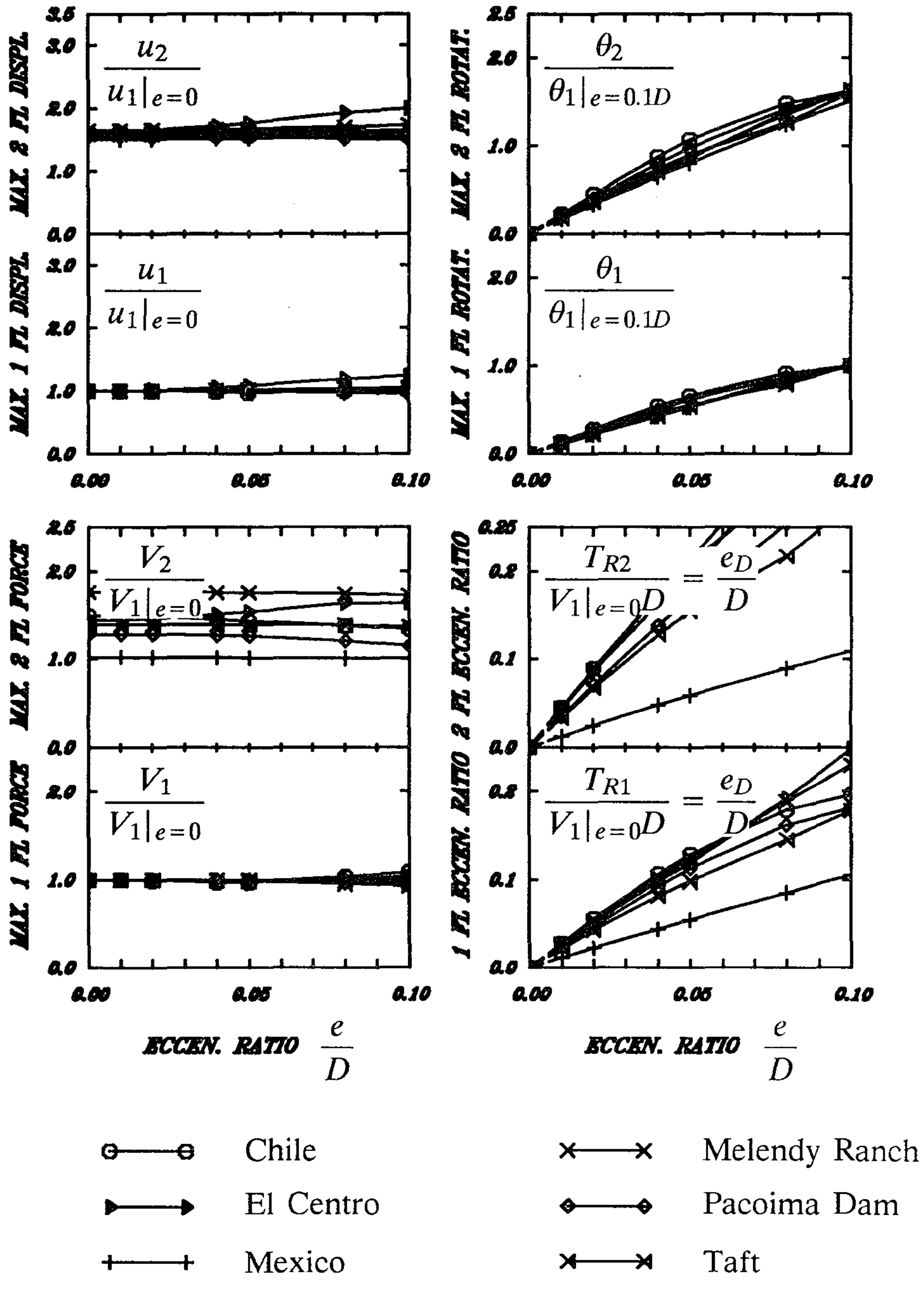

Figure 4–33 Maximum Response of Two–Story 10.0 Hz System Subjected to Earthquake Ground Motion of 0.1g

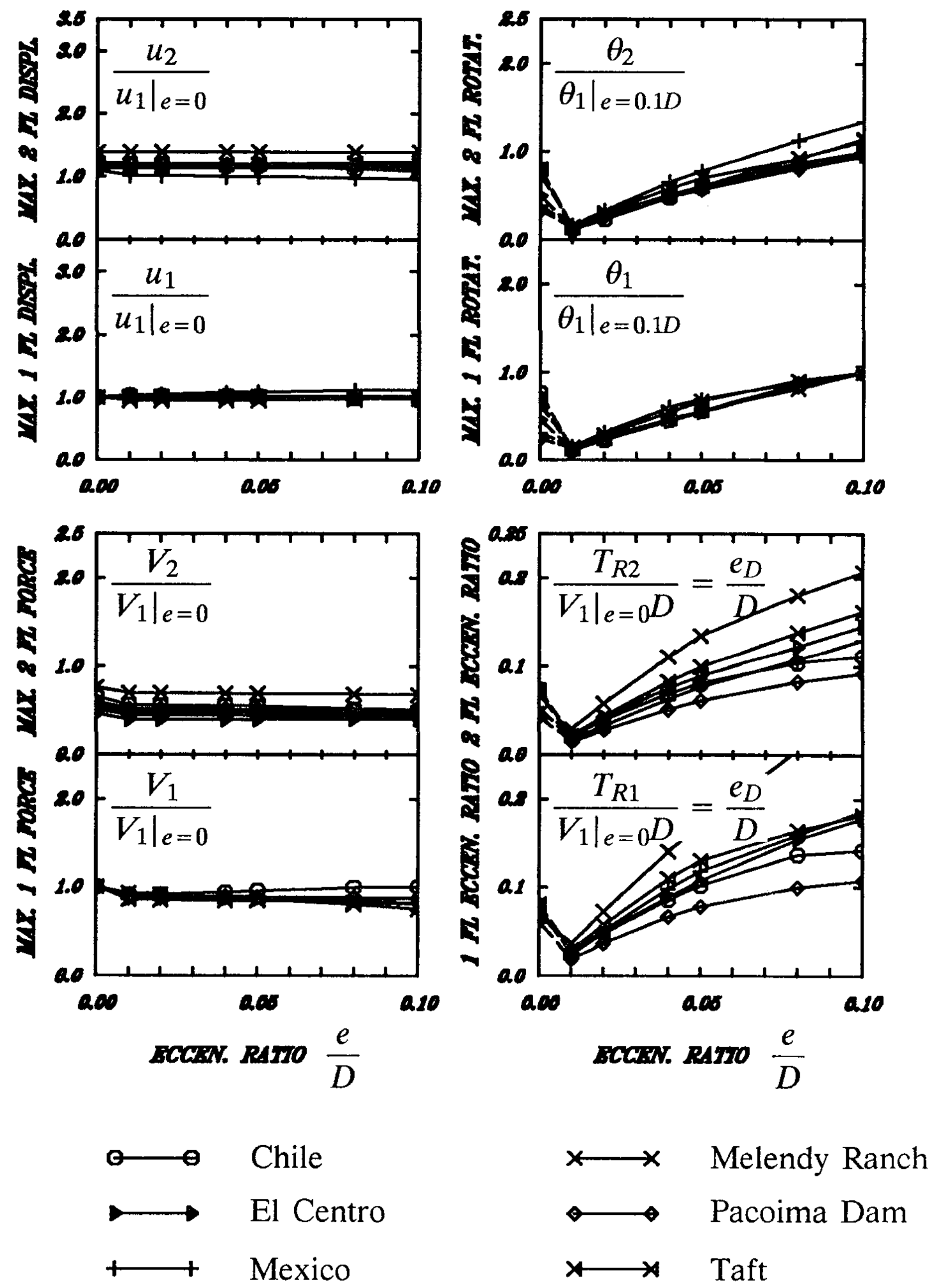

Figure 4–34 Maximum Response of Two-Story 0.2 *Hz* System Subjected to Earthquake Ground Motion of 0.2g

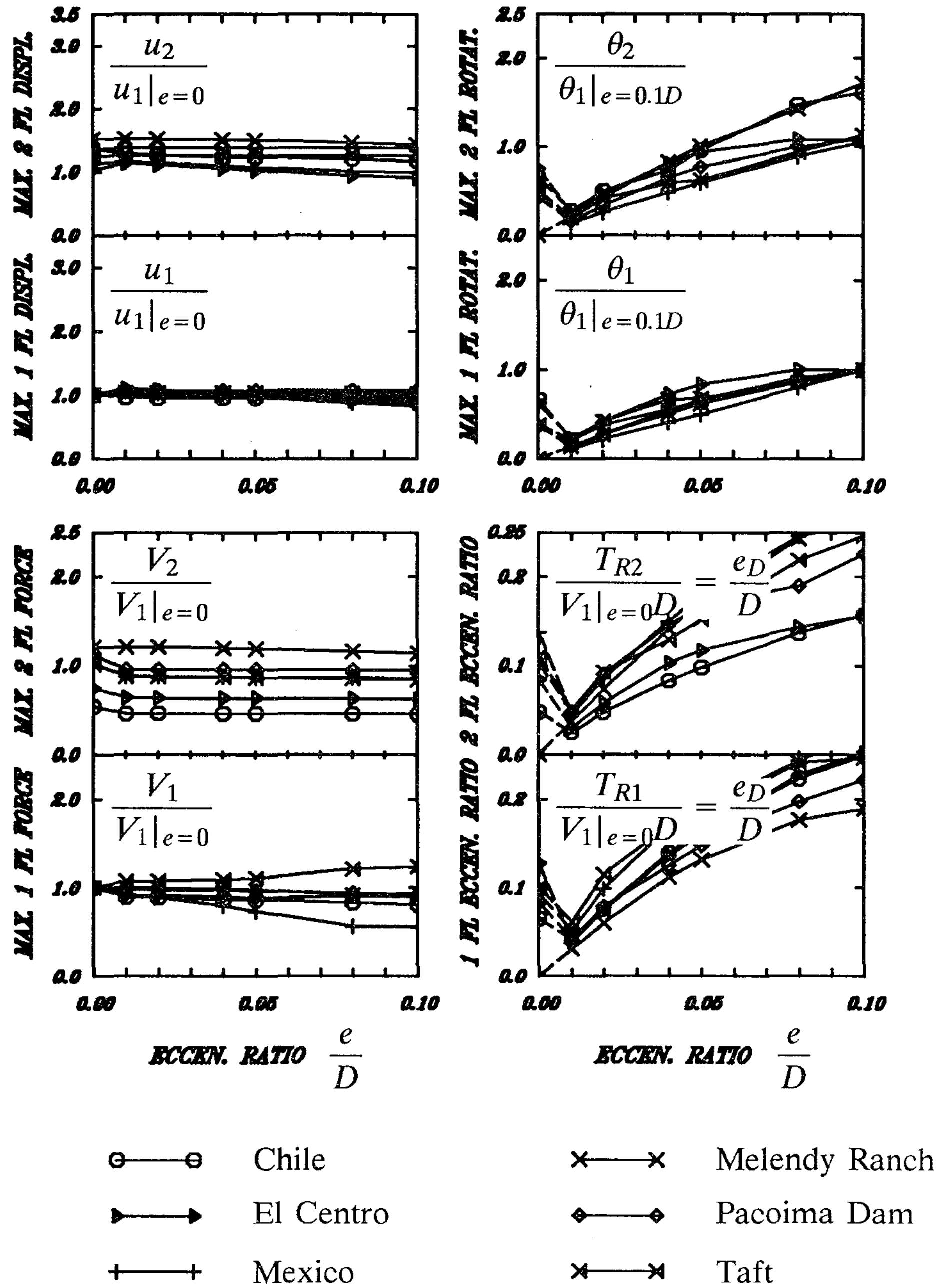

Figure 4–35 Maximum Response of Two-Story 0.8 *Hz* System Subjected to Earthquake Ground Motion of 0.2g

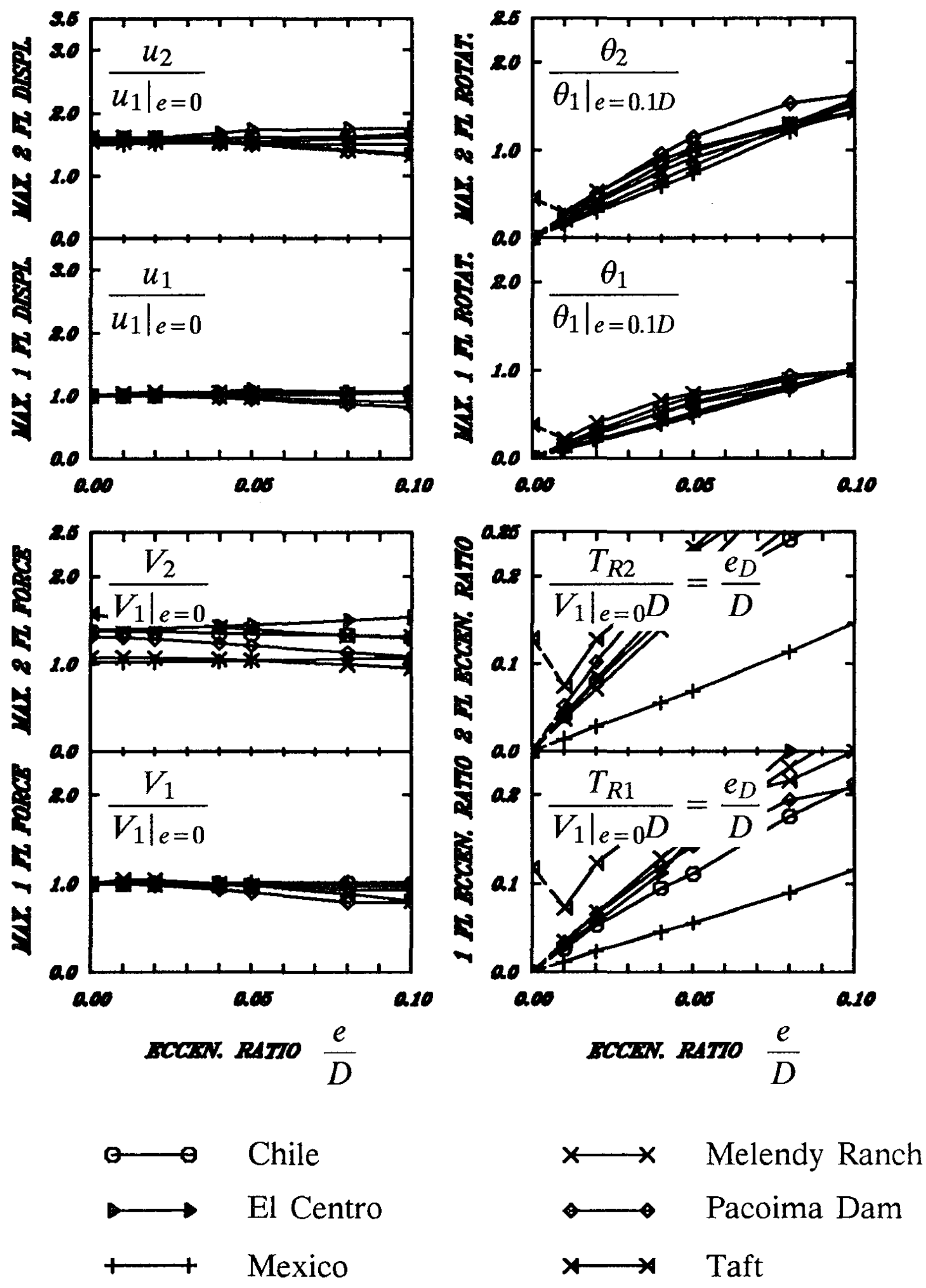

Figure 4–36 Maximum Response of Two-Story 3.75 Hz System Subjected to Earthquake Ground Motion of 0.2g

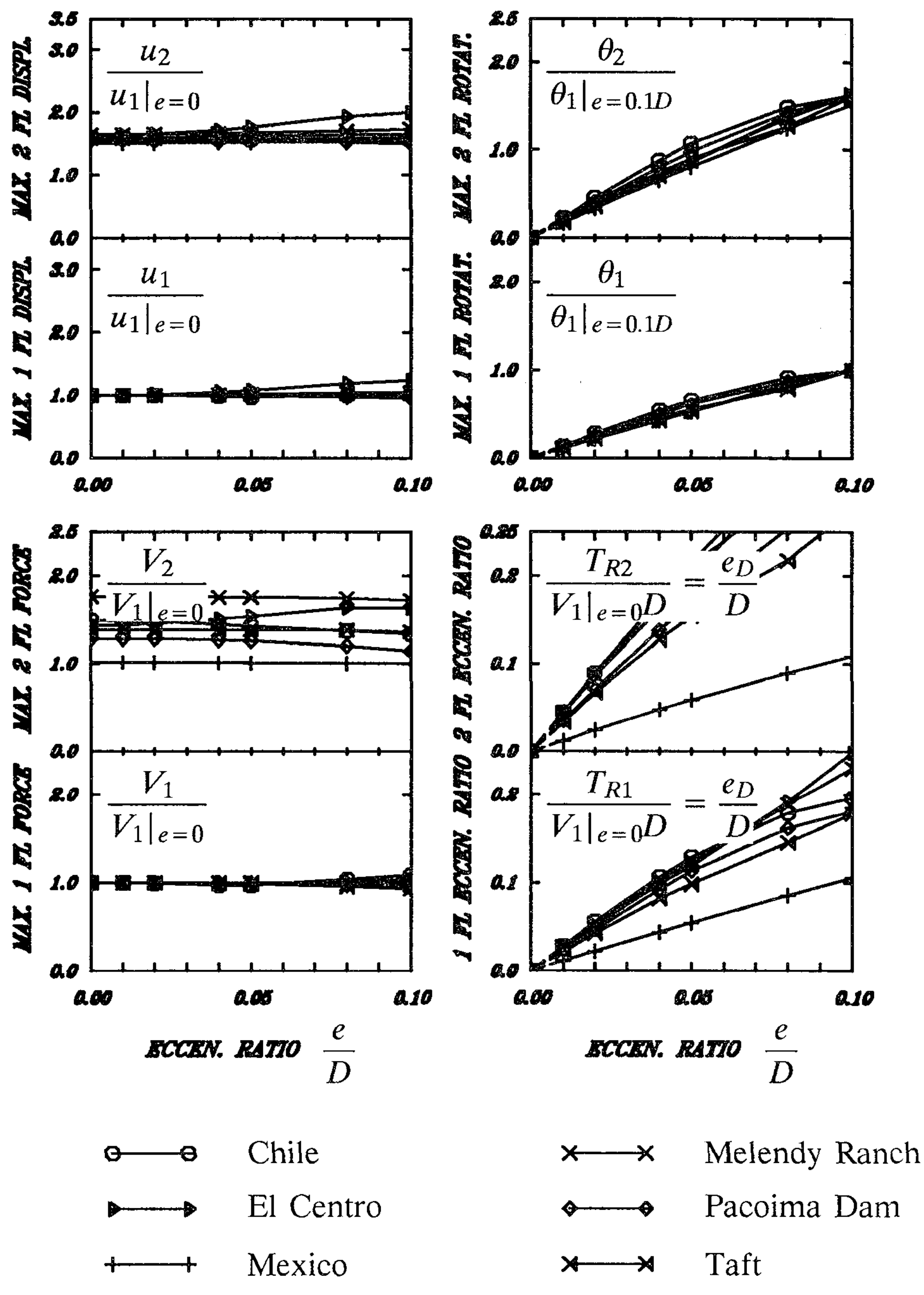

Figure 4–37 Maximum Response of Two–Story 10.0 Hz System Subjected to Earthquake Ground Motion of 0.2g

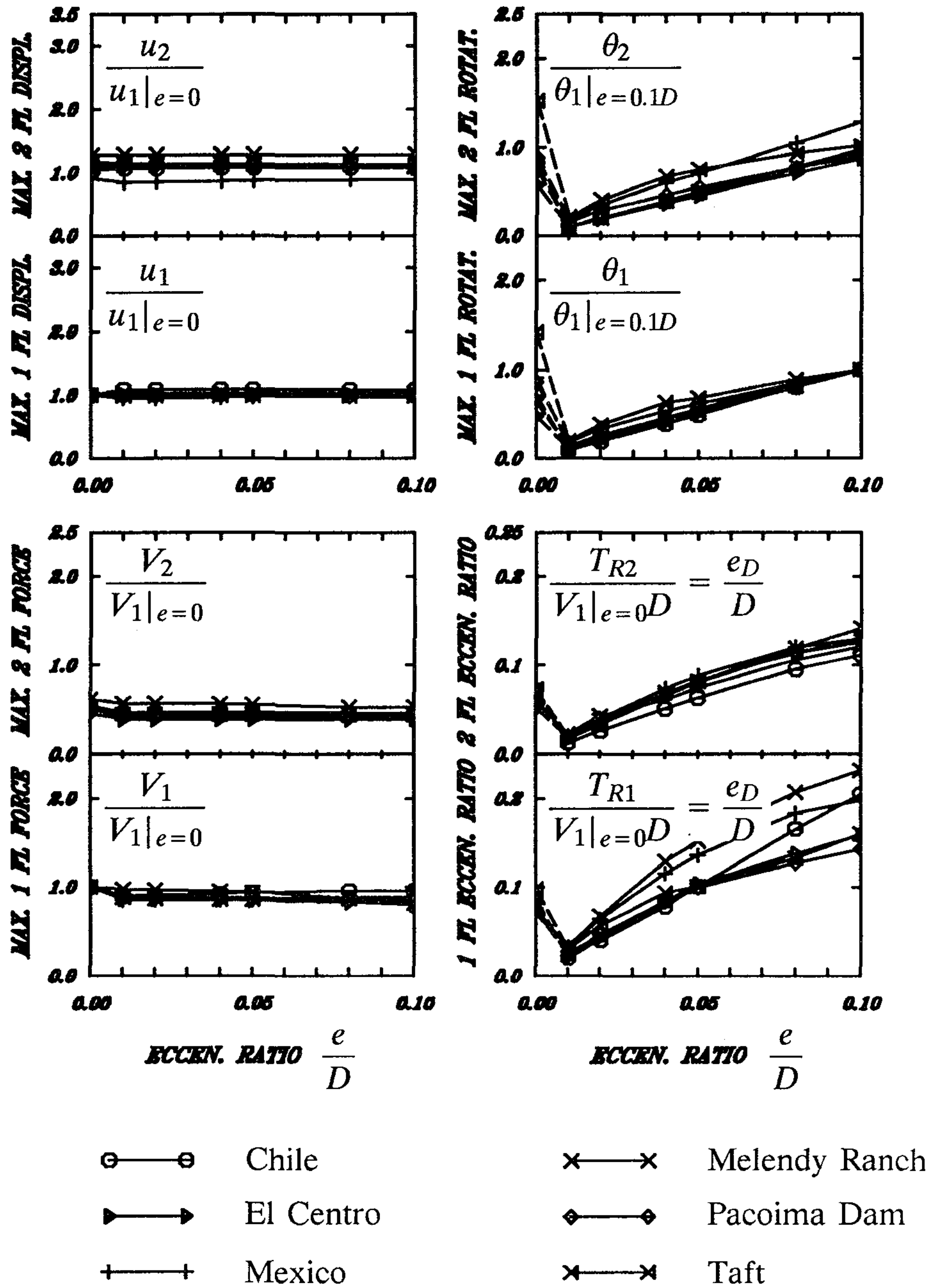

Figure 4–38 Maximum Response of Two-Story 0.2 *Hz* System Subjected to Earthquake Ground Motion of 0.4g

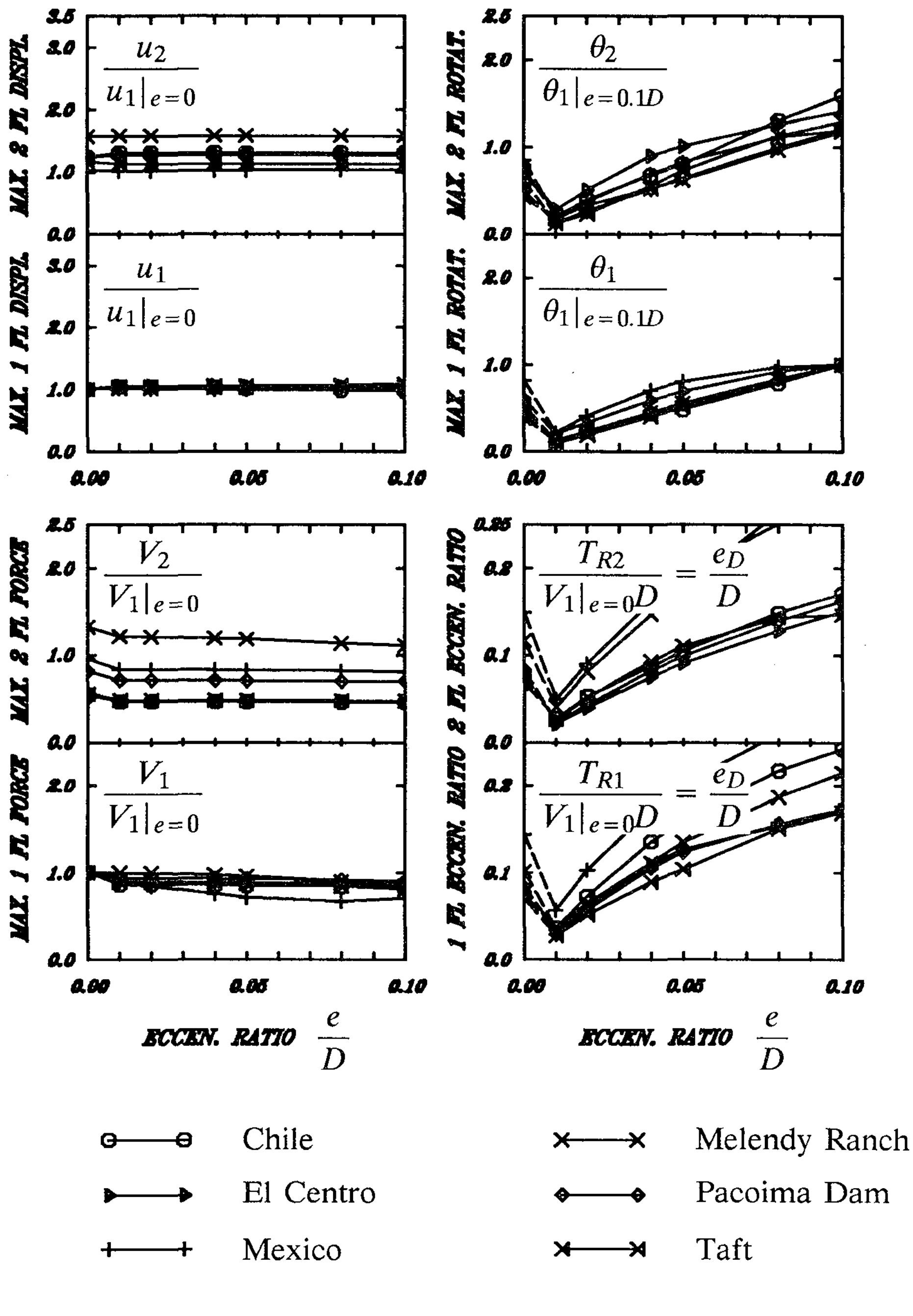

Figure 4–39 Maximum Response of Two-Story 0.8 *Hz* System Subjected to Earthquake Ground Motion of 0.4g

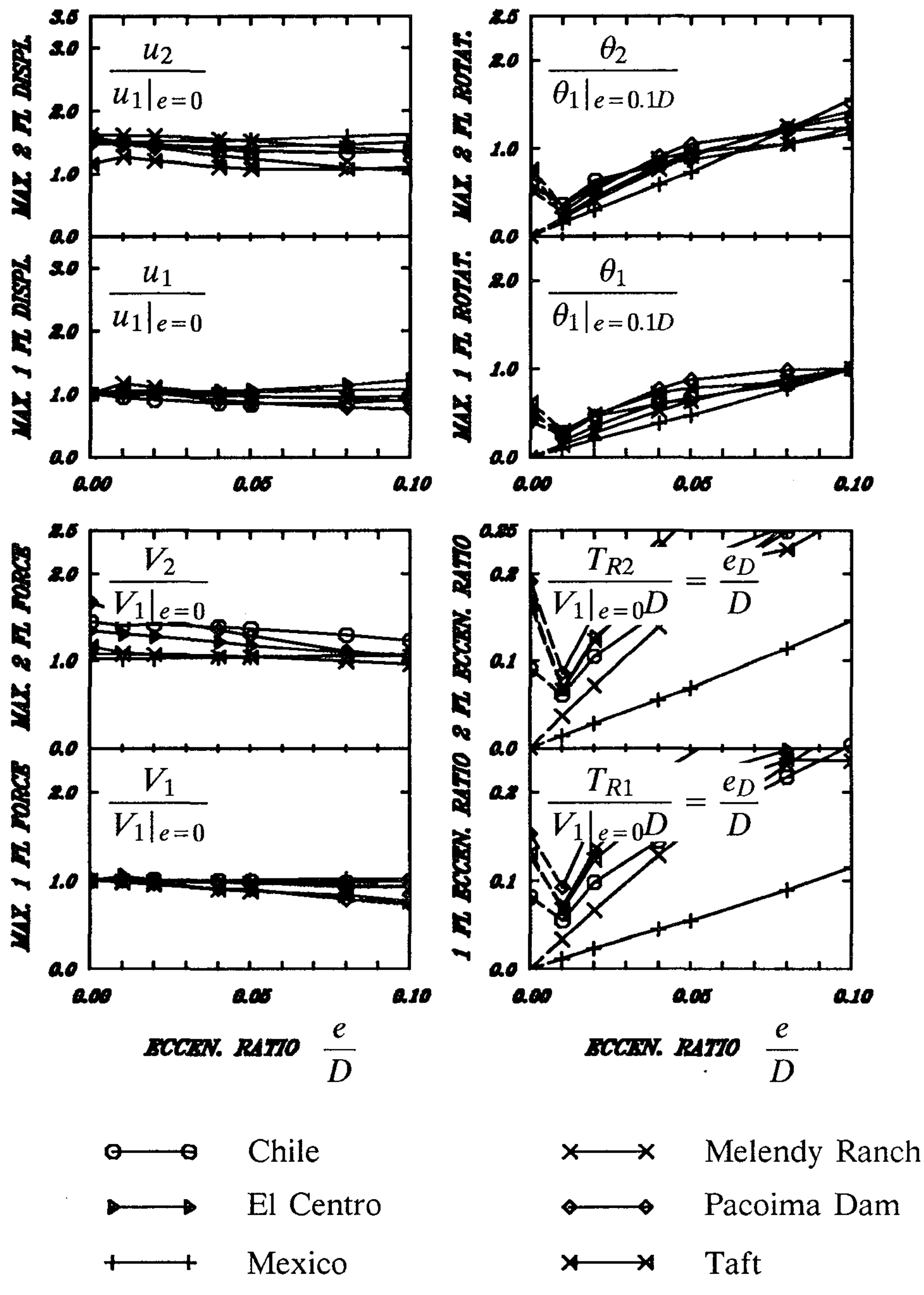

Figure 4–40 Maximum Response of Two–Story 3.75 *Hz* System Subjected to Earthquake Ground Motion of 0.4g

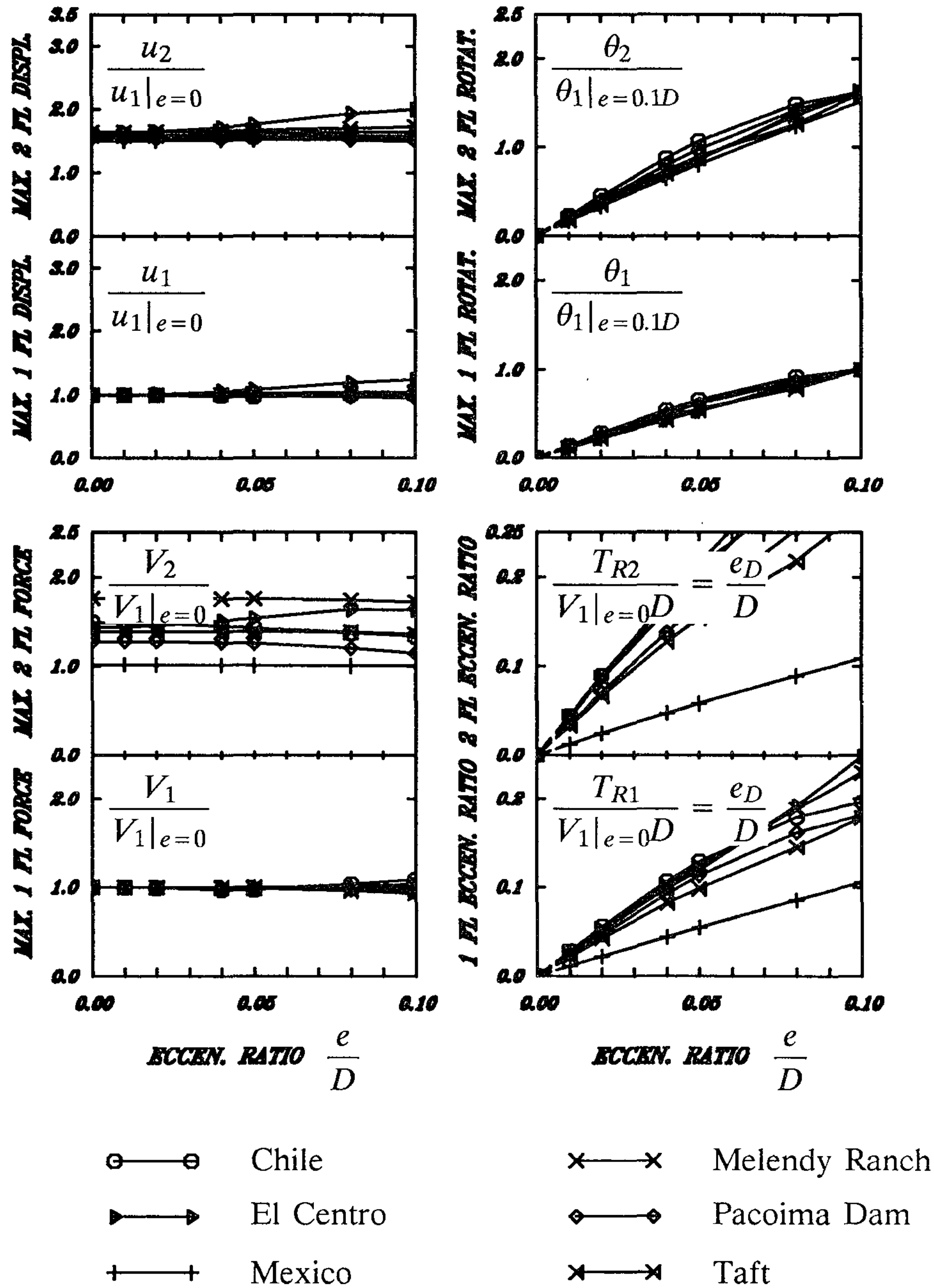

Figure 4–41 Maximum Response of Two–Story 10.0 Hz System Subjected to Earthquake Ground Motion of 0.4g

4.7 Summary

A limited parametric study of the effects of structural eccentricity on the overall maximum building response was performed. The maximum response of model structures with a frequency ratio of 1.225 subjected to selected ground motions has been presented for both the linear–elastic systems and inelastic systems. From the analysis results it appears that the maximum translational response is not severely affected by the torsional effects resulting from static eccentricity. This observation is valid for the asymmetric structural systems with an uncoupled frequency ratio of 1.225.

If a structure is designed to resist translational ground motion with sound engineering principles and judgement, the severity of torsional effects in structures subjected to strong ground motion depends largely on the building dimensions and the arrangement of lateral load–resisting stiffness and strength. Large torsional response in a structure subjected to strong ground excitation may cause its peripheral structural members to experience high deformation and force. Because of the distance between the members to the center of rigidity and the possible phase difference between the maximum translational and torsional response, however, a structure having relatively large maximum torsional response may not necessarily experience higher deformation and force than what was designed for translational resistance.

The maximum torsional response was observed to be nearly linearly proportional to the structural eccentricity. The current building codes however have not included as part of the design process the consideration of dynamic amplification of torsional moment. As shown by the analysis results, structural eccentricity directly affects the torsional response of buildings. The dynamic torsional moments at the floor levels are usually larger than the static torques determined by the dynamic translational forces at the mass center and the corresponding structural eccentricities. On the basis of the parametric study undertaken herein, the dynamic amplification factor for eccentricity should be taken as 2.5, in confirmation of the value suggested by Chopra and Newmark [7] some years ago.

This limited yet comprehensive investigation revealed the difficulty in determining the torsional effects of eccentricity on structural behavior during strong ground motion. As noted in the text it is suggested that the phasing effects receive additional study. Nevertheless, the observations and discussions in this chapter serve to aid placing in perspective the trends in the overall structural response, including torsional effects, resulting from ground motion excitation.

CHAPTER 5

LOW RISE BUILDING RESPONSE IN THE 1987 WHITTIER NARROWS EARTHQUAKE

5.1 General Remarks

The Whittier Narrows Earthquake on October 1, 1987, was of local Magnitude 5.9. This event was sufficiently significant in energy release to cause modest damage to engineered structures but smaller in size than that which would be expected to cause catastrophic damage. The inelastic deformations, and consequently the sustained damage to structural systems, in most engineered buildings was relatively minor from the Whittier Narrows Earthquake. Nonetheless a number of valuable records of building response were obtained during that event. This study, in part, is aimed at taking advantage of these data for the purposes of studying and evaluating the torsional response and behavior of two selected low–rise buildings.

Study of the data from the extensively instrumented buildings in the 1987 Whittier Narrows Earthquake suggests that torsional modes probably were excited in buildings that appear quite symmetric. Accordingly this study involves: (1) investigation of the observed response of two low–rise buildings in both the elastic and moderately inelastic domains, (2) comparison of such behavior with the results obtained from modeling studies, and (3) examination of the possible effects arising from stronger shaking. The study was directed towards attempting to provide a partial answer to the critical question as to whether or not the torsional response is important in the gross total response of these low–rise buildings, and to what extent torsional concepts should be considered in design. The numerical results, by employing the analytical model and analysis procedure in Chapter 3, were extrapolated to examine the survivability of the same buildings if subjected to a somewhat stronger earthquake. The ultimate goal was to contribute insight to the practical guidelines for design and analysis of low–rise buildings subjected to strong ground motion.

5.2 Descriptions of The Two Instrumented Buildings

The reasons for selecting the two buildings are (1) that they were fully instrumented during the 1987 Whittier Narrows Earthquake and the recorded data suggest that torsional modes were excited; (2) that the two buildings are low–rise structures of two to three stories; and (3) that each building has a relatively simple lateral load–resisting framework which enables research attention to be concentrated on the effects of torsion as contrasted to having to undertake an exhaustive structural modeling exercise. The two buildings are officially designated as the **Pomona Office Building (CSMIP–SN511)** and the **San Bernardino Office Building (CSMIP–SN516)**, respectively, for which structural data are available. The two buildings were fully instrumented and records were obtained in the 1987 Whittier Narrows Earthquake. The records are presented in Reference [44].

5.2.1 Pomona Office Building (CSMIP–SN511)

The **Pomona Office Building** is a reinforced concrete structure. It has two stories and a light–weight penthouse. The four facades of the rectangular building are composed of columns and glazing without any peripheral bearing or non–bearing wall. Piles were used in the foundation design; accordingly the base of the columns is assumed to be fixed in the following analysis. The typical floor plan of the building and sensor layout in the structure are shown in Figure 5–1.

The lateral load–resisting system consists of peripheral columns, crossing girders, and cast–in–place R/C slabs; it is a space moment frame designed to resist seismic loadings. The peripheral columns are designed to carry gravity loads and to provide seismic resistance, except for the four plain corner columns supplied for gravity loads. The columns in the rectangular building are symmetrically spaced and arranged. The girders are assumed to frame rigidly to the columns. To employ the analysis procedure presented in Chapter 3, a shear beam type of structural model is applied to represent the structure, and the masses are lumped at the floor levels with two lateral translational degrees of freedom and one corresponding rotational degree of freedom per story. The main properties of this building employed in the analyses are given in Appendix F.

There is a stairwell at the south end of the building which produces structural eccentricities; therefore it was anticipated that torsional effects would affect the response of the structure during an earthquake. Upon careful examination of the accelerograms obtained during the 1987 Whittier Narrows Earthquake, this assumption was proven to be the case. The stairs and stairwell walls were assumed to act as shear wall elements in the seismic analysis. Other than the stairwell walls, only light partitioning materials were used

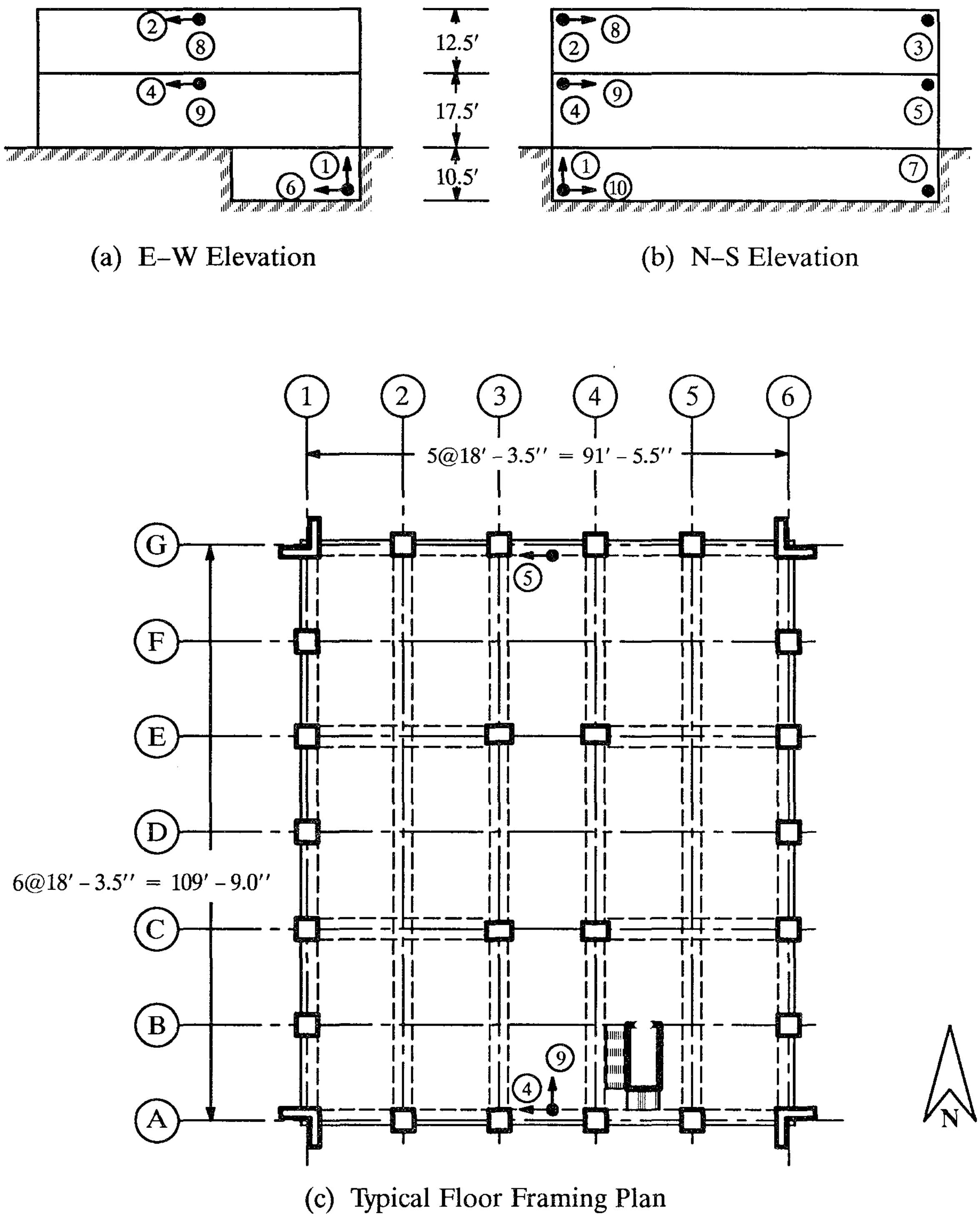

Figure 5–1 Sensor Layout and Floor Plan, Pomona Office Building

for interior functional usage, which in turn was assumed not to contribute to the stiffness for lateral resistance.

In this building, Channels 6, 7, and 10 of instrumentation are deployed in the basement with 6 and 10 at the South–East corner and 7 at the North–East corner. Channels 4, 5, and 9 are mounted at the second floor, and Channels 2, 3, and 8 at the roof at the same planar location as the second floor. The grouped Channels 4 and 9, and 2 and 8 are located on line A, while Channels 5 and 3 are on line G as shown in Figure 5–1. Channels 10, 9 and 8 are oriented in the North– South direction, and the rest of the paired channels are oriented in the East–West direction. In addition, Channel 1 grouped with Channels 6 and 10 in the basement is deployed to monitor the vertical component in the foundation motion.

5.2.2 San Bernardino Office Building (CSMIP–SN516)

This office building is a three–story frame structure as shown in Figure 5–2. From the available information, the building has glazing for the outside facades. This building was designed in conformation with the 1982 edition of the Uniform Building Code. No bearing wall was designed to carry gravity load or lateral loads, and only light materials were used as non–structural walls for partitioning purpose.

The structural frame is composed of structural steel columns and relatively flexible floors. The columns were designed to transmit gravity loads to the foundation and to resist lateral loadings. All columns were erected on concrete footings, and the peripheral footings were linked by a lightly reinforced concrete beam around the building. The outside columns are W14 prefabricated members, and the matrix of inside columns consists of lighter W8 members. Such arrangement of lateral resistant stiffness with strong members on the periphery provides the building with high rotational stiffness against any possible torsionally–induced loss of stiffness. The main properties of this building as used in the analyses are given in Appendix F.

The peripheral beams are composed of prefabricated W–shape structural steel members. For interior beams, relatively heavy W–shape structural steel beams are used in the E–W direction, and wood block beams in the other direction. The floor diaphragms are a combination of rather flexible trus–joists and plywood.

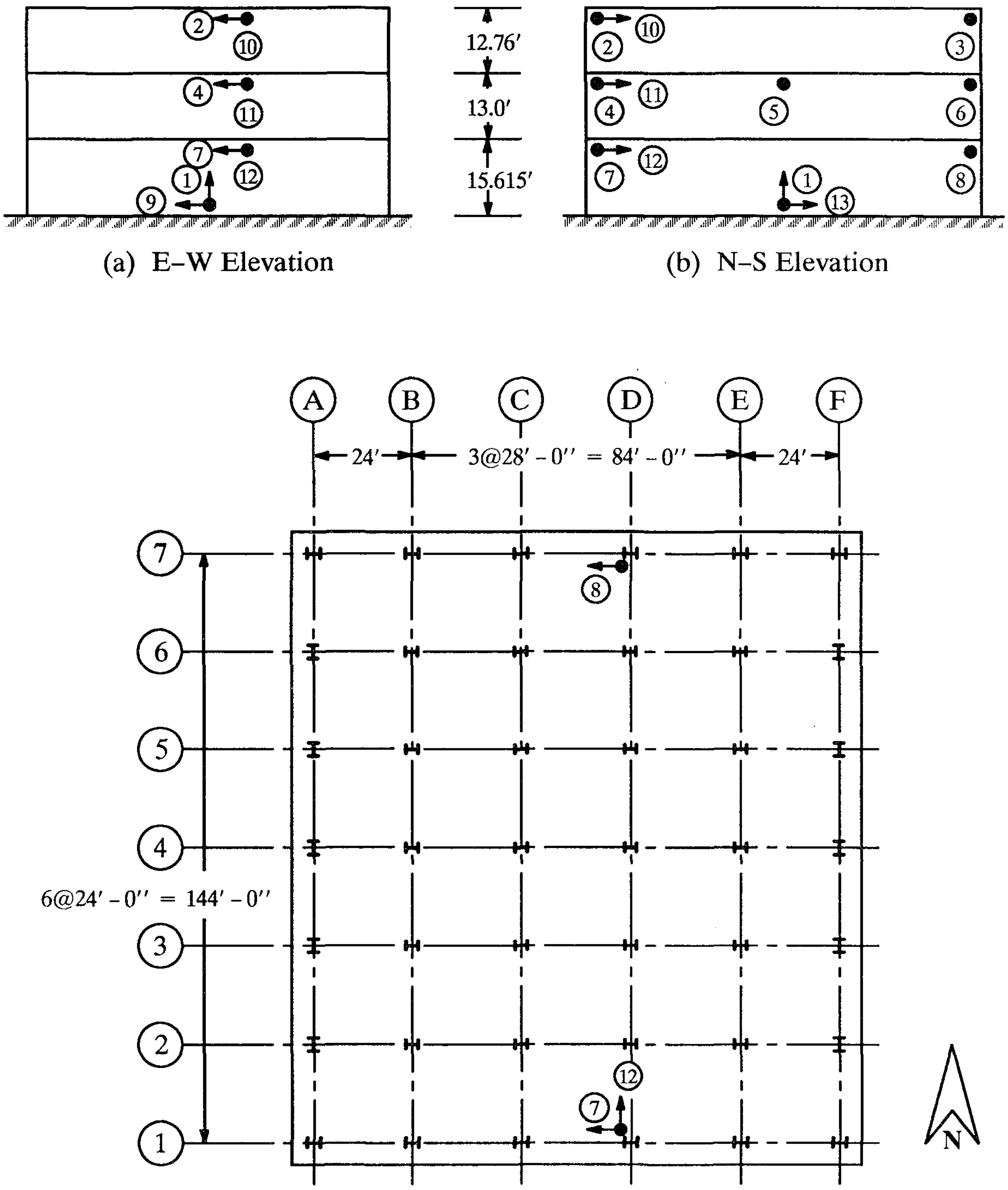

(a) E–W Elevation

(b) N–S Elevation

(c) Typical Floor Framing Plan

Figure 5–2 Sensor Layout and Floor Plan, San Bernardino Office Building

Thirteen instrumentation sensors are installed throughout the building as shown in Figure 5–2. Channels 1, 9, and 13 are mounted at the center of the ground floor with Channel 1 recording the upward motion component. Channels 7, 8, and 12 are at the second floor, Channels 4, 5, 6, and 11 are at the third floor with Channel 5 pairing with Channels 4 and 6 as a checking sensor, and Channels 2, 3, and 10 are deployed at the roof. The grouped Channels 7 and 12, 4 and 11, and 2 and 10 are located at the intersection of lines 1 and D, while Channels 8, 6, and 3 are located at the intersection of lines 7 and D. The checking Channel 5 at the third floor is situated at the intersection of lines 4 and D. Channels 13, 12, 11, and 10 are oriented in the North–South direction, and the rest of the pairing channels are oriented in the East–West direction.

5.3 Performance of The Buildings during The Earthquake

As described in the previous section, instrumentation sensors were installed to monitor the dynamic responses of the two buildings during an earthquake. Recorded are the translational responses of the structures to seismic motion. Some of the sensors are set up in pairs on various floors of the respective buildings. All sensors in each building are triggered at the same time, respectively. Therefore the rotational response of the buildings during the earthquake, which is the focus of this study, can be examined through the differential between the corresponding records at the paired sensors.

5.3.1 Examination of The Recorded Data for Rotational Motion

In order to examine the torsional(rotational) response that occurred, the differential responses of paired records are studied and the results reported below. The presence of torsion in the building responses will be demonstrated, then general observations will be discussed. The symbol in the figures, in/s/s, represents the unit of acceleration (in/s^2).

<u>Pomona Office Building (CSMIP–SN511)</u> From the paired sensors installed in the basement (Channels 6 and 7), there was no outstanding rotational component in the ground motion as reflected by the differential response in the recorded motions. The differences are shown in Figure 5–3.c by the differential between the records at Channels 6 and 7. Thus no rotational component of the ground motion, if there was any, is considered as ground motion input in later analysis of this building. The differential shown in Figure 5–3.b between the records at Channel 4 and 5 exhibits a certain amount

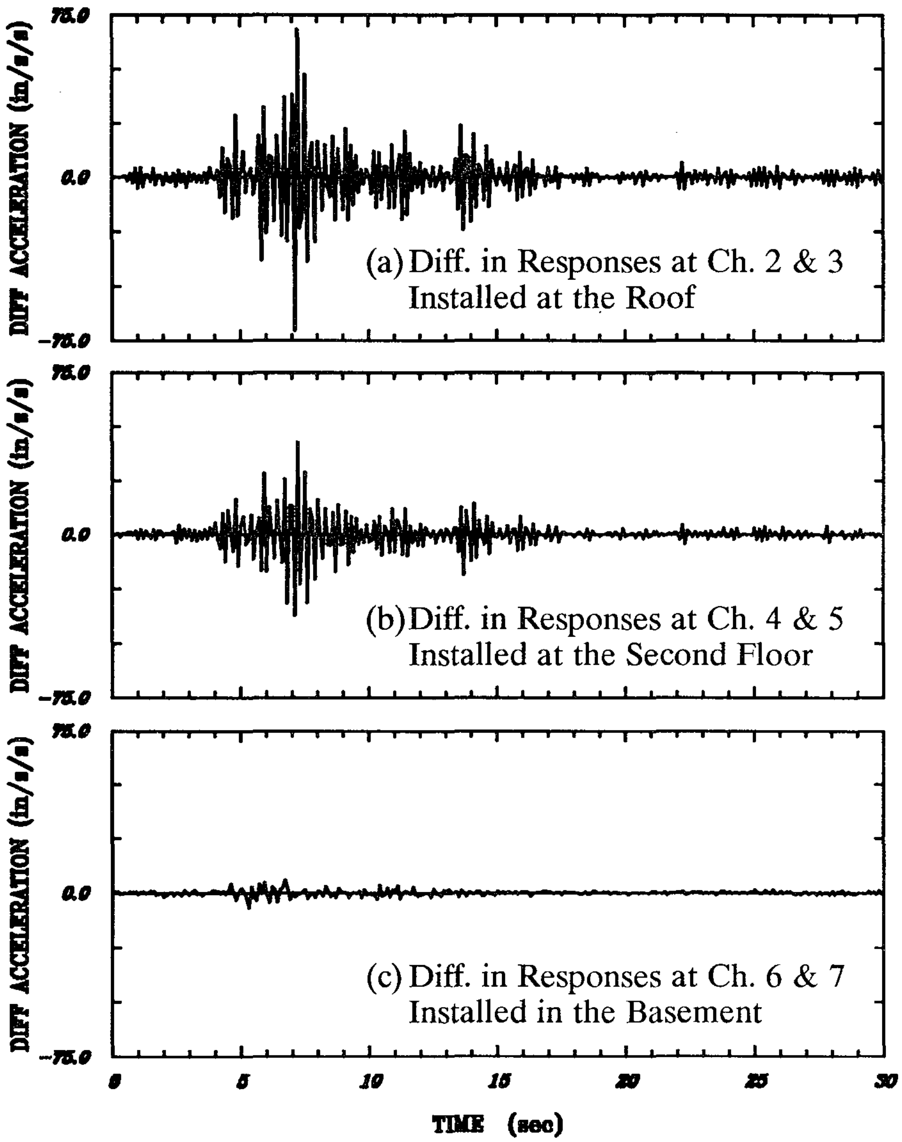

Figure 5–3 Differential in Recorded Responses of **CSMIP–SN511**

of rotational response, and the differential response recorded at the roof (Channels 2 and 3) shows relatively large torsional response, as shown in Figure 5–3.a.

San Bernardino Office Building (CSMIP–SN516) On the ground floor there is only one set of sensors, one channel along each principal direction, and thus no assessment of the rotational component of the ground motion input was obtained. Paired sensors are installed at the second floor (Channels 7 and 8), the third floor (Channels 4, 5, and 6), and the roof (Channels 2 and 3). The differences between the paired sensors are plotted in Figure 5–4. Significant torsional response at the respective floor levels, increasing with height in the building, can be observed by examining the differential of the corresponding records, especially at the roof of the building as shown in Figure 5–4.a. What is more, the beating phenomenon discussed in Chapter 2 may be noticed in the recorded data.

By way of the general observations, in these two buildings the observed torsional response could result from several sources. For Building **CSMIP–SN511**, the structural eccentricity between the centers of mass and rigidity at the various floors was the obvious cause. The structural eccentricities were created by the extra stiffness provided by, other than the lateral stiffness of the moment resisting frame, the stairs and stair–walls located at the south end of the building. The heavy mass located at the north–west corner also could have contributed to the torsional response because of the response interaction of all components in the building, even though the mass has been well isolated from the structure. For Building **CSMIP–SN516**, the relatively symmetric arrangement of lateral stiffness and the placement of the designed mass created very little structural eccentricity. However, the translational and torsional frequencies were close enough to each other to result in strong coupling, and thus provided a basis for torsional response to develop, as described in Chapter 2.

Because the building **CSMIP–SN511** had a certain amount of torsional response to begin with, the dynamic nature of the seismic response resulted in the dynamic amplification of the roof response. The maximum torsional response at the roof was about 1.65 times the maximum torsional response at the second floor. On the other hand, the maximum torsional response, as the result of strong coupling during beating at the roof of Building **CSMIP–SN516**, was about 1.35 times the maximum torsional response at the third floor and about 2.30 times that at the second floor. In addition, the biaxial effect from ground motion input in the two principal directions also may be a cause of the

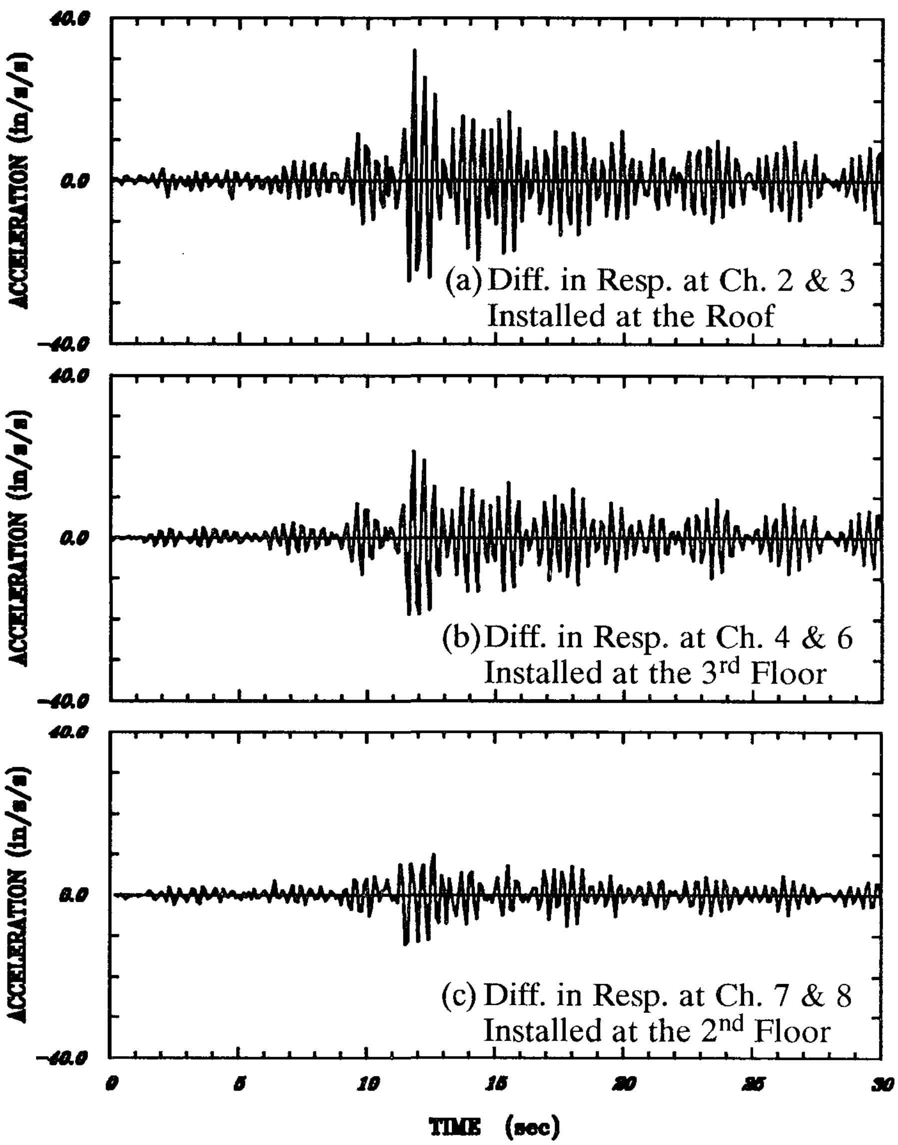

Figure 5–4 Differential in Recorded Responses of **CSMIP–SN516**

torsional response, resulting from the phase difference in the inputs from the two orthogonal directions. This topic is addressed later.

Originally, it was thought that possible timing differences in the paired channels when first triggered in data collection may have contributed to the observed differentials in the paired response records. However, from the telephone conversation with Dr. Mohjiz Huang at the Division of Mines and Geology, Sacramento, California, it was found that all the sensors are connected to one recorder, so the triggering time should be the same for all the channels. Any instrumental errors in triggering time can be ignored for practical purposes. This suggests that the torsional responses recorded by the paired sensors in the buildings are accurate and representative of the response during the earthquake.

5.3.2 Frequency Identification of The Buildings from Recorded Data

In that which follows the dominant frequencies are identified first and the engineering significance of these dynamic properties are discussed second. In order to identify the fundamental frequencies of the buildings, Fast–Fourier–Transform (FFT) analysis was performed on the data recorded in the buildings.

It is recognized that the records of the foundation responses are not truly free–field data and thus contain some structural response in them, but these are the best available information about the ground motion imparted into the buildings. The frequency contents of the records at the foundations and in the buildings have been studied, and it appears that there was no in–phase resonance effects in either of the buildings during the earthquake. Therefore the frequencies dominating the records at the foundations are taken as the major frequencies in the input ground motion, and the same frequencies in other records are excluded when studying the fundamental frequencies of the buildings. The building fundamental frequencies are determined as follows.

Pomona Office Building (CSMIP–SN511) The structure is relatively symmetric in the North–South direction with respect to mass and stiffness distribution. The responses recorded at Channels 10, 9, and 8 (see Figure 5–1) represent the response of the building from the basement to the roof in that direction. Because of symmetry, the motion in this direction is assumed not to be strongly coupled with the other motions in assessing the structural frequencies. Examination of the results of FFT analysis indicates that the dominant frequencies are quite narrowly banded at about 3.81 *Hz*, as shown in Figure 5–5.a for Channel 8. This leads to the conclusion that the fundamental frequency of the building in the North–South direction is about 3.81 *Hz* (period of 0.262 seconds).

Paired sensors are installed in the building in the East–West direction at the north and the south ends of the structure in the basement, at the second floor, and at the roof. Because of the existence of the torsional response (differentials between the records taken at the paired channels), the recorded data are considered to possess at least two fundamental frequencies, one for the motion in the East–West direction and the other for the torsional response. The results of FFT analysis of the records at the north end of the building (Channels 7, 5, and 3) show relatively narrowly–banded frequencies at the peaks. The FFT results of the records at the south end (Channels 6, 4, and 2), however, show that the dominant frequencies spread over quite a wide range as in Figure 5–5.b for Channel 2 at the roof. This observation confirms the original thought that there may well be at least two groups of dominant frequencies in these records.

Now the question is how to estimate the relevant frequencies with respect to the translational motion in the East–West direction and the torsional motion. It is difficult to extract directly the desired frequencies from the FFT results of the given data. An easier way might be to use the combinations of the paired records to see if it is possible to decouple the motions. Therefore, the sum of the paired records is used to represent the translational motion in the East–West direction, and the differential response between the paired records is used to evaluate the torsional motion. FFT analysis was performed on the combined records. The estimated frequencies are 3.30 *Hz* as depicted in Figure 5–5.c for translation in the East–West direction (period of 0.303 seconds) and 4.42 *Hz* for the second peak as shown in Figure 5–5.d for rotation (period of 0.226 seconds).

San Bernardino Office Building (CSMIP–SN516) In this building there exists little structural eccentricity because of the relatively symmetric placements of stiffness, strength and mass in the structure. The results of FFT analysis revealed the estimated fundamental frequencies of the building as being (1) 2.05 *Hz* in the North–South direction (period of 0.488 seconds) as shown in Figure 5–6.a for Channel 10 at the roof, (2) 2.20 *Hz* in the East–West direction (period of 0.455 seconds) as shown in Figure 5–6.b for the sum of the records at Channels 2 and 3 at the roof, and (3) 2.73 *Hz* in torsion (period of 0.366 seconds) as shown in Figure 5–6.c for the difference of the records at Channels 2 and 3.

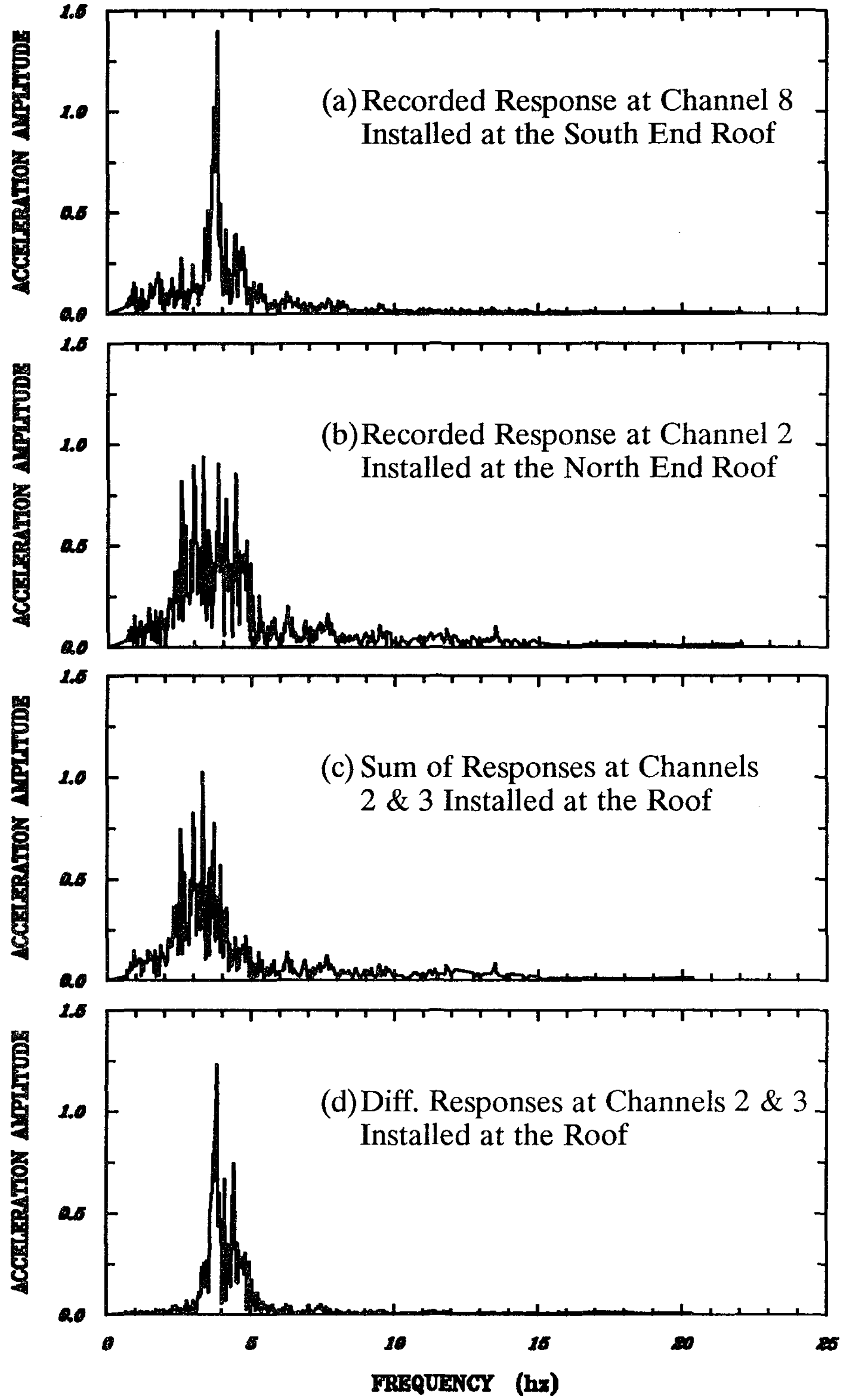

Figure 5–5 FFT Result of Recorded Response of CSMIP–SN511

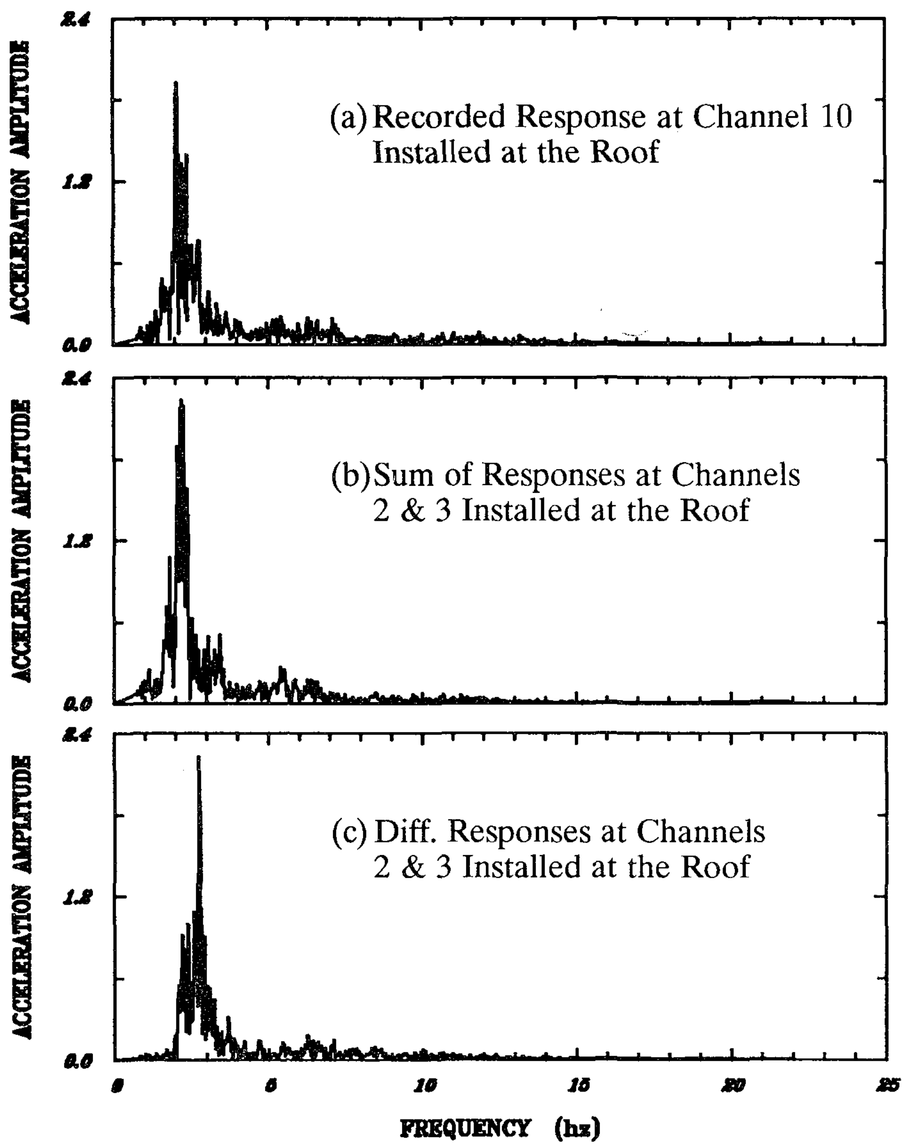

Figure 5–6 FFT Result of Recorded Response of **CSMIP–SN516**

In summary, the above identified frequencies for the two selected buildings have been estimated from the FFT analysis based on the data recorded during the earthquake. They represent the dominant frequencies in the recorded responses. These fundamental frequencies are taken as the coupled frequencies of the respective structures and as the basis of structural modeling in later analysis. In the following some factors that might have affected the foregoing estimates are discussed.

Special attention should be paid to certain artificially dominant frequencies when examining the results of FFT analysis. As a result of regular sampling intervals during data collection, an artificially dominant frequency could be created. During the correction and bandpass–filtering process of data records, the cut–off frequencies also could create some artificially dominant frequencies in the FFT results. The recorded responses of the two buildings supplied by the Division of Mines and Geology, State of California were the instrument–corrected and bandpass–filtered accelerations, velocities and displacements. The filter frequencies used were specified by the filter band 0.40–0.80 and 23.0–25.0 *Hz*.

The frequencies of the responses during the earthquake, shown in the results of FFT analysis, are a combined result of soil–structural interaction and structural response. In the following analysis of the two buildings, the bases of the structures are assumed to be fixed. Thus the foregoing estimated frequencies are assumed to be the fundamental frequencies of the structures. However, it is appreciated that the condition of the respective foundation would have affected the dominant frequencies in the response records; e.g., soft soil at the foundation would have decreased the frequencies, and hard rock under the foundation would have served to raise the frequencies. Also any possible nonlinear inelastic behavior in the structural system would have an effect on the shifting of the dominant frequencies.

In addition, the dominant frequencies in the records are affected by a possible concentration of imparted energy over some frequency bands in the ground motion. The ground motion input may well have excited the modes for which the frequencies are close, or nearly equal, to the dominant frequencies in the input motion. Therefore the peak amplitudes in the FFT results may correspond in some cases to the frequencies of those modes instead of the fundamental frequencies of the structure.

As a summary, in this section the torsional responses in the two selected buildings have been demonstrated by examining the differentials in the paired records. As the result of modal instability, as in beating phenomena, a noticeable amount of torsion and obvious beats were observed in the structure with close fundamental frequencies. Also some information about the dynamic properties of the structures, such as the fundamental frequencies of the buildings, has been determined from the field recordings through FFT analysis. These results are to be used in the next section as a basis for structural modeling.

5.4 Modeling of The Buildings

Both buildings are modeled as space frame structure with shear beam idealization. The bases of the two structures are assumed to be fixed. No soil–structural interaction is considered in the analysis herein.

The frequencies of a model structure are one of the most important factors in dynamic analysis. Without matching the fundamental frequencies of the models against respective buildings, any numerical computations of response–history of the buildings during the earthquake obviously would not be able to reflect what really occurred. Thus a considerable amount of effort was spent on identifying the fundamental frequencies of the structural models of the two buildings, in comparison with the estimated frequencies from the recorded data. As can be perceived, many factors play significant roles in this process. The effects of two major factors, each of which is important and representative in one particular building, are discussed in the following.

5.4.1 Effect of Wall Elements in Building CSMIP–SN511

In general, the inclusion of the wall rigidity in structural modeling changes the fundamental frequencies of the model by stiffening the structure, and in turn affects considerably the overall response of the structure to earthquake ground motion.

There is a set of stair walls located in the south end of this building. From the available information, there are no walls other than the glass walls (glazing) as window facades and some interior light partitioning. The building was first modelled as a space frame with rigid beams for its lateral load resistance. However, the structural frequencies based on such a model were too low, especially in the North–South direction. The calculated response at various locations in the structure to the ground motion was much higher than the corresponding records. When the stiffness provided by the walls around the stairwell was included in the analysis, the structural frequencies fell into the vicinity of the estimated frequencies from the recorded data, and the calculated response reached the same order of magnitude as the recorded data.

5.4.2 Effect of Flexibility of Beams in Building CSMIP–SN516

The basic assumption in the analysis procedure for this study was to model the buildings with shear beam idealization. In the beginning when formulating the models, rigid beams were used in the space frames. Later, it was noticed that not taking into account the flexibility of the slabs and beams made the structural models too stiff, especially when modeling Building **CSMIP–SN516**. Thus in order to retain the simplicity of the shear beam idealization, a factor was employed [5, 48] to modify the stiffness of the lateral resisting members to account for such effect.

The lateral stiffness of the resisting elements in the models was modified in accordance with the ratio of the flexural stiffness of columns and beams. The modification factor may be viewed as a compensation for the effect of frame action in the shear beam idealization. This factor can be relatively high for structural systems with flexible floor diaphragms. For example, the reduction for the lateral stiffness of some of the columns in the models was as high as 50 percent. With such modification, the computed responses of the structural models, respectively, to the recorded ground motion inputs are quite comparable to the field recordings. The comparison of the analysis results and the field recordings, and more importantly the interpretation of the structural responses during the earthquake, is presented in the following sections.

5.5 Interpretation of Response of The Two Buildings

The two buildings were analyzed using the procedure described in Chapter 3. In the analysis, the shear force interaction was considered with columns being the primary lateral force resisting elements. The recorded data at the basements were used as the ground motion input for the corresponding building. However, no upward recorded motion was included in the analysis, nor is any torsional component in the ground motion considered as input. The torsional component in the ground motion is relatively insignificant compared to the torsional response experienced by **CSMIP–SN511** (and no paired records existed at ground level for **CSMIP–SN516**). The ground motion records are presented in Figures 5–7 and 5–8. The seismic wave passage was assumed to be uniform throughout the corresponding building foundations.

In the following the analysis results, as well as the field recordings, are examined, in the light of the current design requirements in the Uniform Building Code (UBC–88) [18], the Recommended Lateral Force Requirements and Tentative Commentary (SEAOC– 88) [43], and the NEHRP Recommended Provisions for the Development of Seismic Regulations for New Buildings (NEHRP–85) [6].

5.5.1 Design Requirements

Both buildings are located in areas specified as seismic zone 4 (the highest seismic activity) according to the current design codes. The buildings were designed with flexural columns and beams as the special moment resisting space frame for their lateral load–resisting systems. The total design weight of **CSMIP–SN511** was estimated as 4190 kips, which includes the dead load of building materials, weight of permanent equipment, and the design live load. Weight of the roof, including the penthouse, was 2240 kips, and the weight of the second floor was 1950 kips. The total weight of **CSMIP–SN516** was estimated to be 1811 kips. The design weight of individual floors was as follows: 356 kips for the roof, 716 kips for the third floor, and 739 kips for the second floor.

Without regard to soil type and structural period, the upper limit of the design spectrum specified by the codes is used for both buildings, $C = 2.75$ in the UBC–88 Code and SEAOC–88 Code, and $C_s = 0.125$ in the NEHRP–85 Code.

For both buildings, the design base shear in both principal directions is calculated below in accordance with the UBC–88 Code and SEAOC–88 Code, which are the same:

$$V = \frac{Z\ I\ C}{R_w} W = \frac{0.4 * 1.0 * 2.75}{12} W = 0.0917W.$$

On the other hand, according to the NEHRP–85 Code the design base shear in both directions is required to be

$$V = C_s W = 0.125W.$$

The requirements for vertical distributions of design lateral force are similar in the current codes. Since the fundamental periods of the buildings are less than 0.7 seconds,

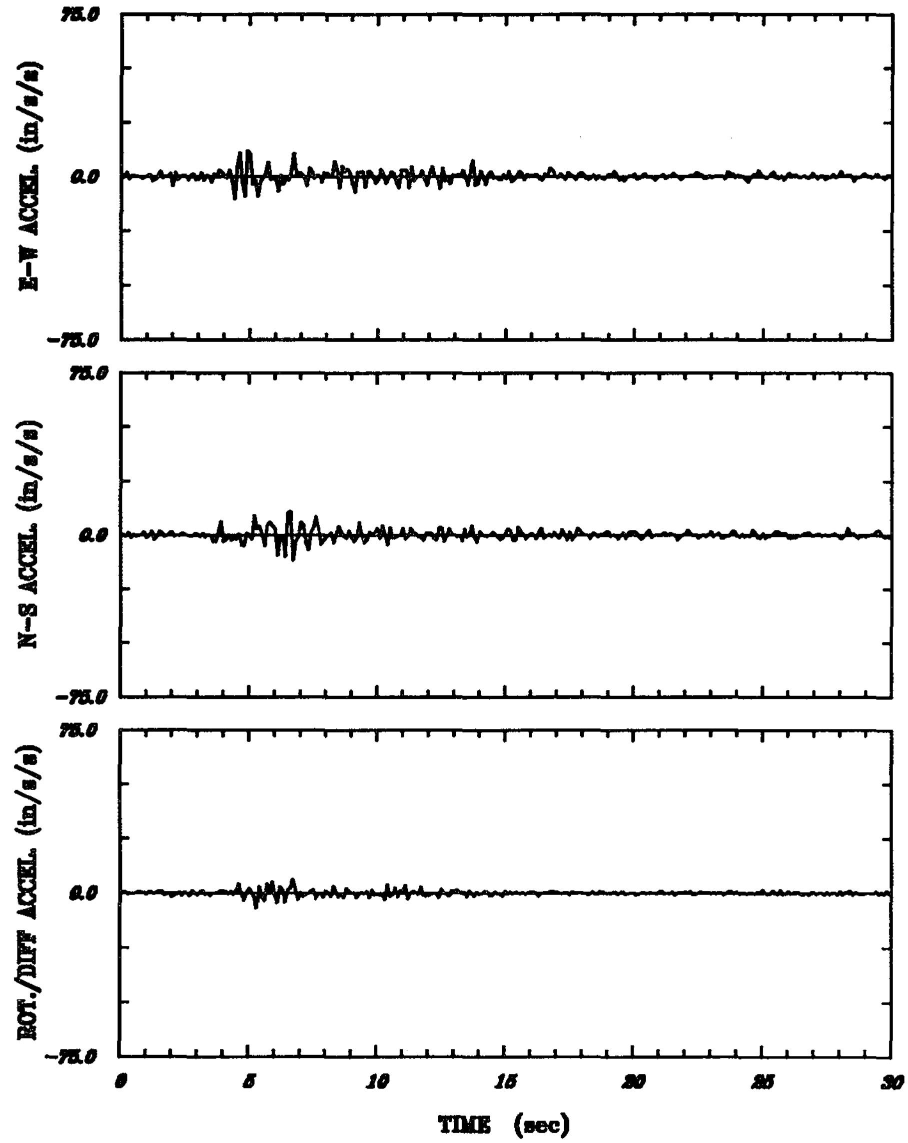

Figure 5–7 Recorded Ground Motion Input for CSMIP–SN511

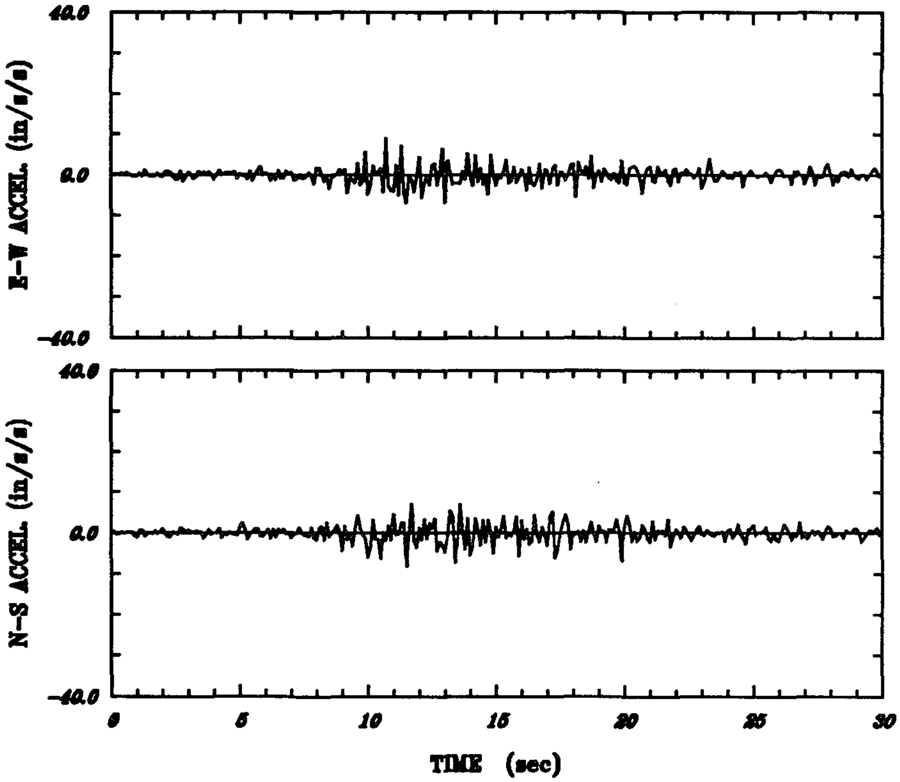

Figure 5–8 Recorded Ground Motion Input for **CSMIP–SN516**

the "whipping" force, or the concentrated force at the top, need not be considered for the two buildings. The calculated shear forces in each story are listed in Tables 5–1 and 5–2:

Table 5–1 Shear Forces in Building **CSMIP–SN511**

Story Level	Relative Shear Force (V)
2nd Story	0.663
1st Story	1.000

Table 5–2 Shear Forces in Building **CSMIP–SN516**

Story Level	Relative Shear Force (V)
3rd Story	0.315
2nd Story	0.753
1st Story	1.000

In order to determine the horizontal torsional moments in the two buildings, the "calculated" and "accidental" eccentricities are presented in Tables 5–3 and 5–4. The buildings' dimensions are 110 ft. in the N–S direction and 92 ft. in the E–W direction for Building **CSMIP–SN511**, and 144 ft. in the N–S direction and 132 ft. in the E–W direction for Building **CSMIP–SN516**, respectively. The torsional moments are the product of these eccentricities and the foregoing shear forces.

Table 5–3 Eccentricities in Building **CSMIP–SN511**

Story Level	North–South		East–West	
	"Calculated" e/D_x	"Accidental" e/D_x	"Calculated" e/D_y	"Accidental" e/D_y
2nd Story	0.083	0.050	0.000	0.050
1st Story	0.348	0.050	0.102	0.050

Table 5–4 Eccentricities in Building **CSMIP–SN516**

Story Level	North–South		East–West	
	"Calculated" e/D_x	"Accidental" e/D_x	"Calculated" e/D_y	"Accidental" e/D_y
3rd Story	0.000	0.050	0.000	0.050
2nd Story	0.000	0.050	0.000	0.050
1st Story	0.000	0.050	0.000	0.050

The horizontal shear forces plus the effect of the horizontal torsions should be distributed to the various lateral elements in proportional to their rigidity for each story.

The story drift limits specified by the codes are given in Tables 5–5 and 5–6. It can be observed that the story drift limits are more restrictive in the UBC–88 and SEAOC–88 code than in the NEHRP–85 Code. One reason for this difference could be that the base shear in the former codes is less than in the latter code.

Table 5–5 Story Drift Limits for Building **CSMIP–SN511**

Story Level	Story Height H (ft.)	Story Drift Limit (in.) UBC–88 & SEAOC–88 $\min\{\frac{0.04}{R_W},\ 0.005\}\cdot H$	Story Drift Limit (in.) NEHRP–85 $0.015\cdot H$
2nd Story	12.50	0.500	2.250
1st Story	17.50	0.700	3.150

Table 5–6 Story Drift Limits for Building **CSMIP–SN516**

Story Level	Story Height H (ft.)	Story Drift Limit (in.) UBC–88 & SEAOC–88 $\min\{\frac{0.04}{R_W},\ 0.005\}\cdot H$	Story Drift Limit (in.) NEHRP–85 $0.015\cdot H$
3rd Story	12.76	0.510	2.297
2nd Story	13.00	0.520	2.340
1st Story	15.62	0.625	2.811

These design requirements presented above were evaluated with respect to the analysis results and the field recordings in later discussions.

5.5.2 Numerical Analysis

The current seismic building codes usually call for planar analysis on regular structures such as the two selected buildings. Subsequently the estimated torsional effects ("calculated" and "accidental") are added. In this chapter, however, analysis is made on the 3–dimensional structural models of the two buildings so that the combined torsional effects with the translational responses can be investigated. Numerical response–history analyses are performed on the buildings subjected to the recorded base motions. The purposes are: (1) to illustrate the effect of biaxial ground motion input on the overall structural response, (2) to compare the calculated responses with the field recordings, and (3) to examine the performance and behavior of the two buildings during the 1987 Whittier Narrows Earthquake.

As shown in Figures 5–1 and 5–2, paired sensors are installed in the East–West direction on the buildings, respectively, to monitor the structural torsional response to any ground motion. The actual recorded response data at the locations of some sensors are presented in Figures 5–9 and 5–12. In order to illustrate the effect of biaxial ground motion input on the structural response, the two selected buildings first were subjected to the East–West component of the recorded base motion. The numerical results are plotted in Figures 5–10 and 5–13. Next, the two buildings were subjected to both translational components of the recorded base motions shown in Figures 5–7 and 5–8. The calculated responses to biaxial ground motion inputs at the corresponding sensors are presented for the two buildings in Figures 5–11 and 5–14, respectively. Because these records, and the calculated results at the sensor locations, contain not only the translational but also the rotational responses, the torsional response is embedded in the records.

When comparing the calculated responses with respect to the field recordings, the general trends in these records are observed to be similar. For the response–history of **CSMIP–SN511** as shown in Figures 5–9, 5–10 and 5–11, it seems that the results from single component ground input provide reasonably close estimates of the actual response during the earthquake; the results from biaxial ground motion input give an even better match, especially as a function of time. From these response–histories, which show the building response in the direction where strong torsional coupling exists, the peaks of maximum response and the burst of energy concentrations appear to occur at about the same time. Larger responses are observed at the upper stories. For **CSMIP–SN516** whose responses are shown in Figures 5–12, 5–13 and 5–14, the numerical results are even more spectacular in terms of matching the actual recorded response data. For example, the numerical analysis has reproduced the occurrence of the beating phenomenon, and the differences between the maximum calculated responses and the corresponding maximum recorded responses are within the range of three to five percent of each other. This fortuitous level of agreement was totally unexpected, and did not result from "turning knobs and levers" to arrive at such agreement.

Because of the low amplitude and intensity of recorded and calculated response to the earthquake, it is believed that structural members in both buildings did not experience much inelastic deformation, if there was any damage at all. Based on the above observations, one can conclude that for linear-elastic systems the analysis procedure presented in Chapter 3 numerically calculates quite accurately the response of low-rise structures during an earthquake. As a result, the following assessment of the building deformations and the shear forces experienced by the two structures becomes meaningful.

Although not as obvious for the two low-rise buildings, the comparison, between the calculated responses (to single component input and to biaxial ground motion input) with respect to the field recordings, suggests that the biaxial input of ground motion sometimes is important in determining structural response in building systems, especially in buildings with strong coupling between the translational and torsional motions and with relatively large building dimensions. The main reason for such an effect is the strong coupling and response phase differences among the translational and rotational motions. As a result of possible phase differences in the building responses among the orthogonal translational motions and the torsional motion, the translational ground motion in one direction may cause relatively large "dynamic" eccentricity in the other direction. Or stated another way, the ground motion input in the other direction definitely could enhance the overall building response, especially the torsional moments and deformations, for the several reasons outlined earlier in this report. With the presence of structural torsion arising from whatever sources, therefore, biaxial ground motion inputs affect the dynamic behavior of structures and play a significant role in their overall response. Thus in modeling structural response with respect to field recordings, it is important to perform a 3-dimensional analysis on the structural model in addition to the combination of the planar analysis and the estimated torsional deformations, especially when there exists potential torsionally- induced loss of stiffness. In addition, the imparted energy to a structure from biaxial ground motion input is definitely different than the amount of imparted energy from a single component input.

In the following, the story deformation responses and the response-histories for lateral forces applying at the floor levels are examined in the light of the current building code requirements tabulated in the previous section.

The deformation responses at several representative sensor locations are plotted in Figures 5-15 and 5-16 with respect to time divided by the permitted story drift limits by the UBC-88 and SEAOC-88 codes. As perceived, the actual story drifts experienced by both buildings are rather small, compared to the drift limits permitted for the corresponding stories. In addition, the shear forces for each story (story shear divided by the weight above the story) are presented in Figures 5–17 and 5–18 with respect to time. In these figures the horizontal torque at the rigidity center as computed in the response–history analysis is normalized by the nominal torsional moment. The nominal torsional moment here is defined as the sum of products of the maximum shear force and the corresponding eccentricity required by the codes.

The shear forces experienced by the two low–rise buildings as shown during the earthquake are less than ten percent of the corresponding weight of the stories above, which is smaller than the code requirements. For example, at the second floor of the **San Bernardino Office Building (CSMIP–SN516)**, in the North–South direction, one observes in Figure 5–18.b a peak value of story shear force divided by the weight above of 0.07; the code limit can be calculated as $0.753V$ divided by the weight above (356 kips + 716 kips, or 1072 kips), which is $0.753*0.0917W$ ($0.753*0.0917*1811$ kips) divided by 1072 kips for a ratio of 0.117. Also it is noticed that despite torsional deformations there was no outstanding torsional moments in the **San Bernardino Office Building (CSMIP–SN516)**, because of the symmetrical placement of mass and stiffness.

Therefore, the response of the two buildings stayed primarily in the linear–elastic range during this earthquake. This conclusion confirms the assumption made earlier in determining the dynamic properties of the buildings. Also it may be well to point out that both the reinforced concrete structure (**SN511**) and the steel structure (**SN516**) performed well during the earthquake of relatively small magnitude.

From the building responses presented in this section, strong beating phenomena may be observed. This is attributed to the effects of closely spaced fundamental frequencies of the two structures, as discussed in Chapter 2. The two selected buildings have the special moment resisting frames for their lateral force resisting system with the translational and torsional stiffness rather uniformly arranged. In such system, the fundamental periods for the translational motions and the rotational motion are relatively close to each other, so that beating effects are likely to take place and the imparted energy from the seismic ground motion is transferred back and forth among the translational and torsional motions. For instance, there is little eccentricity in the **San Bernardino Office Building (CSMIP–SN516)** so significant torsional response would not be expected. As a result of modal instability, however, torsional response and strong beating effects were observed. Even though not much additional shear force resulted from the torsional response, an unfavorable amount of rotational deformation could have damaged some non-structural members along the building peripheral.

5.6 Status of The Buildings after The 1987 Whittier Narrows Earthquake

The seismic design of the buildings and the connection designs of the two buildings appeared to be well detailed in the available design plans. Although some masonry walls in the **Pomona Office Building (CSMIP-SN511)** were distressed slightly in the numerical computations when subjected to the ground motion input recorded at its basement, there is no apparent change of the primary frequency in the records for either of the buildings. On the basis of the examination presented in the preceding section on deformations and shear forces experienced by the two low-rise buildings during the 1987 Whittier Narrows Earthquake, the response of the structures was primarily in the linearly elastic range. It seems that the seismic lateral forces induced from this earthquake were at the level of about ten to fifteen percent of the calculated lateral strength of the structures. Thus one can conclude that only ten to fifteen percent of the capacity of the structural members have been tested.

5.7 Survivability to Stronger Earthquakes

In order to examine whether or not the selected buildings will survive future stronger earthquakes, analysis was made on the structural models subjected to more intensive ground motions. The records during the 1987 Whittier Narrows Earthquake were scaled up to have the peak acceleration of $A_a = 0.4g$ (about 8.40 times for **CSMIP-SN511** and 15.1 times for **CSMIP-SN516**, respectively, larger than for the Whittier Narrows Earthquake) to meet the seismic regulations by the foregoing mentioned codes. The response-histories at several sensor locations in the two buildings when subjected to the higher level earthquake are presented in Figures 5-19 and 5-20, respectively. Strong beating is evident.

The calculated responses of the two selected buildings to such scaled ground motion records suggest that the expected lateral strength and capacity of both structures may be exceeded, especially for the **Pomona Office Building (CSMIP-SN511)**. The numerical analysis permitted five to ten percent of strength hardening in the structural members. The base shear force and the lateral forces on the structures were computed to be almost eleven times the design base shear strength required by the current codes, and the base shear level was computed to be about 1.8 times the calculated base shear strength and capacity of the corresponding structure. Therefore a small to at best moderate amount of inelastic behavior should be anticipated in case an earthquake with the noted intensity strikes the area. These data are shown herein.

The story deformations from the aforementioned computations are plotted against the corresponding drift limits in Figures 5–21 and 5–22. It is noticed that at the peaks in the response–histories (Figures 5–21.b and 5–22.c), the deformations in the first story would have been about fifty percent higher than the drift limits specified by the current building codes. On the basis of the analysis and the above observations, the two buildings would suffer moderate damage in case of the assumed earthquake. The buildings would not be expected to collapse so long as the detailing and connection constructions meet the specifications and requirements in the corresponding design. However, through damage to key structural elements it is possible that the torsional response might be accentuated in the later stages of excitation.

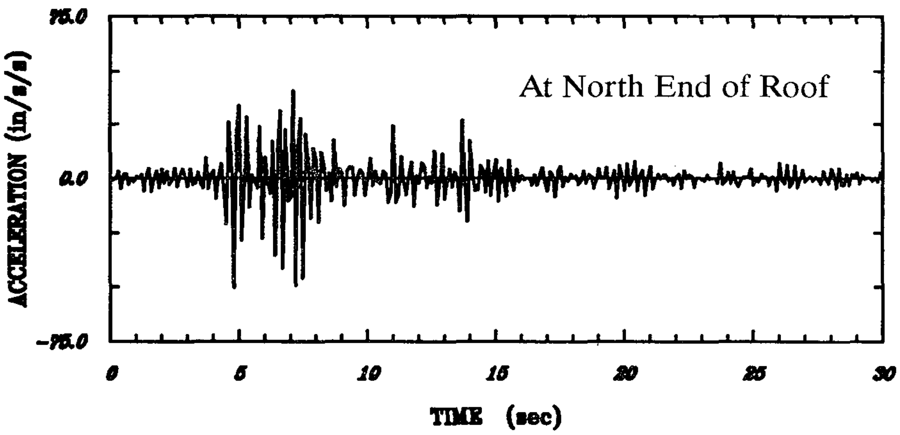

Figure 5–9.a Recorded Response at Channel 3 of **CSMIP–SN511**

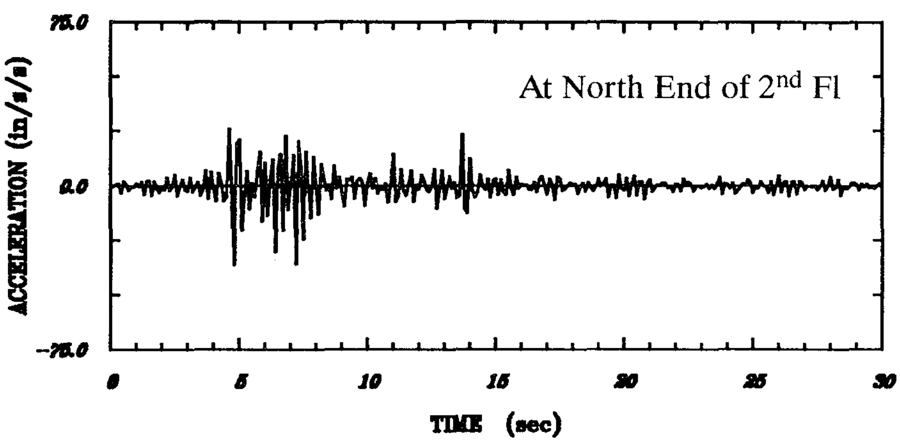

Figure 5–9.b Recorded Response at Channel 5 of **CSMIP–SN511**

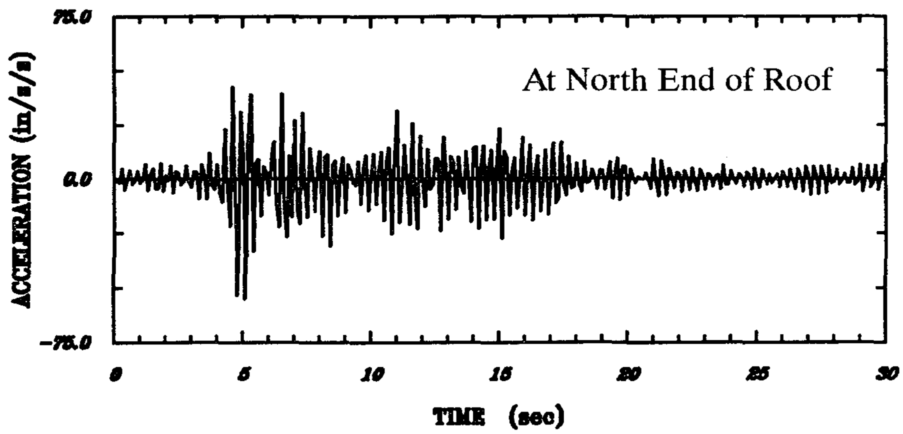

Figure 5–10.a Cal. Resp. at Channel 3 of **CSMIP–SN511** to E–W Base Motion

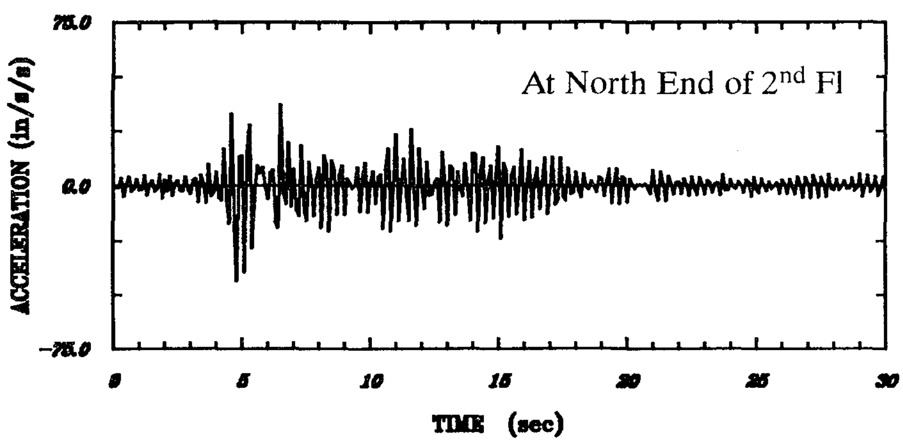

Figure 5–10.b Cal. Resp. at Channel 5 of **CSMIP–SN511** to E–W Base Motion

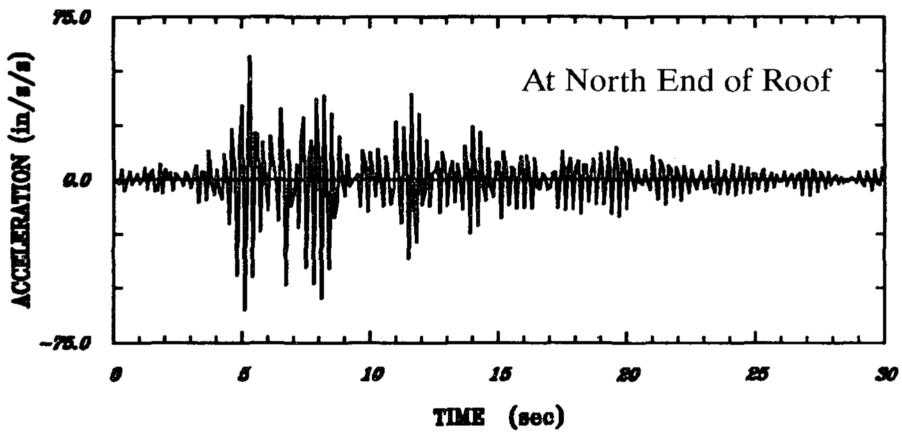

Figure 5–11.a Cal. Resp. at Channel 3 of **CSMIP–SN511** to Biaxial Base Motion

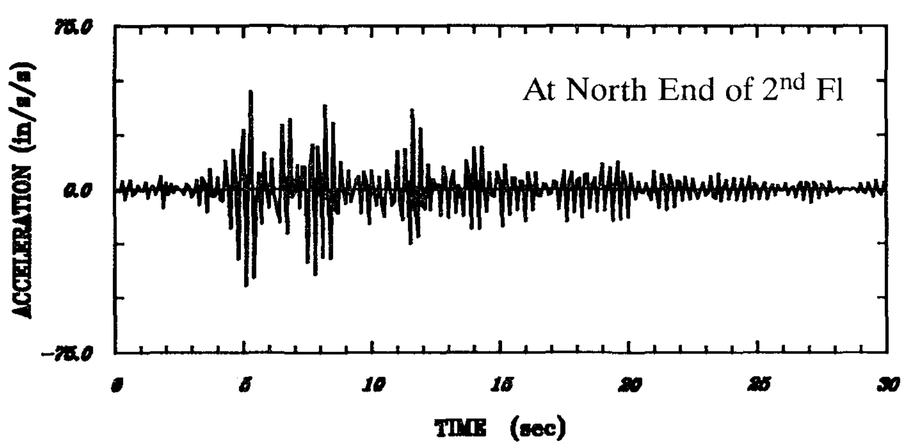

Figure 5–11.b Cal. Resp. at Channel 5 of **CSMIP–SN511** to Biaxial Base Motion

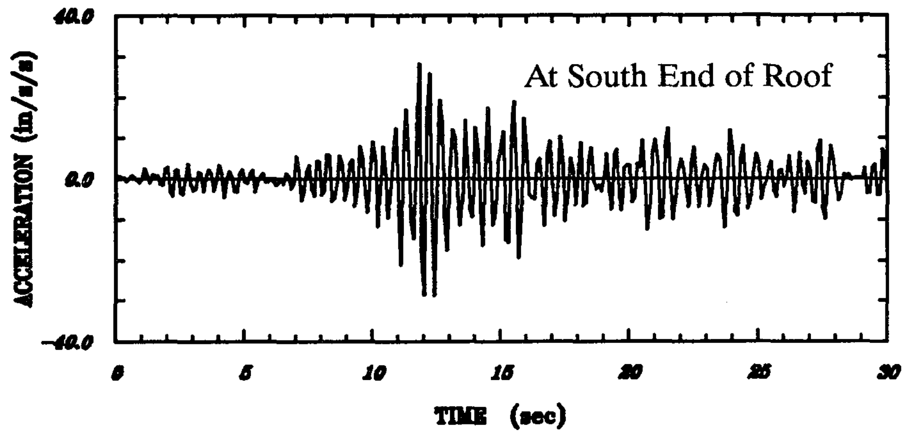

Figure 5–12.a Recorded Response at Channel 2 of **CSMIP–SN516**

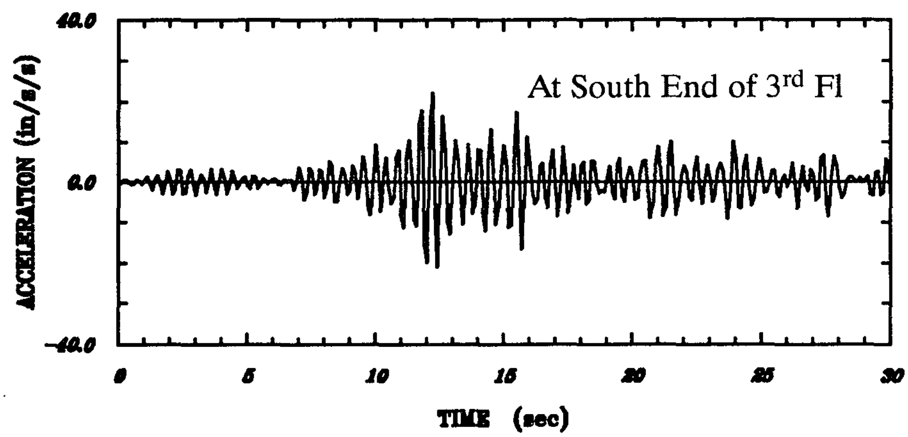

Figure 5–12.b Recorded Response at Channel 4 of **CSMIP–SN516**

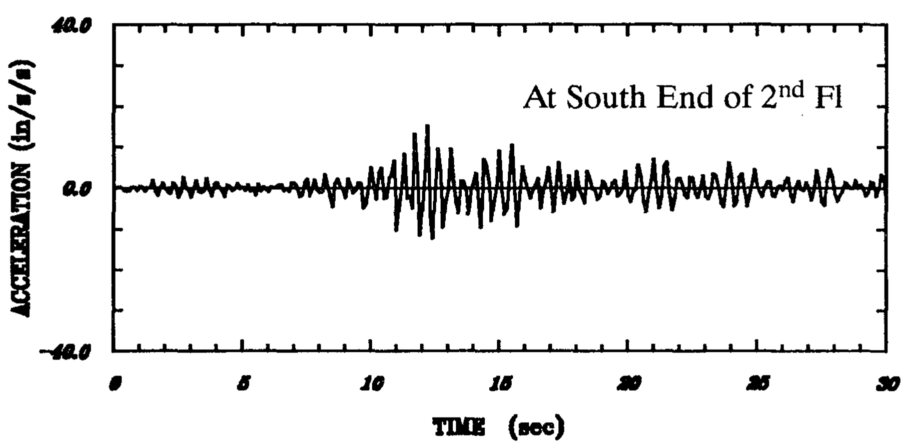

Figure 5–12.c Recorded Response at Channel 7 of **CSMIP–SN516**

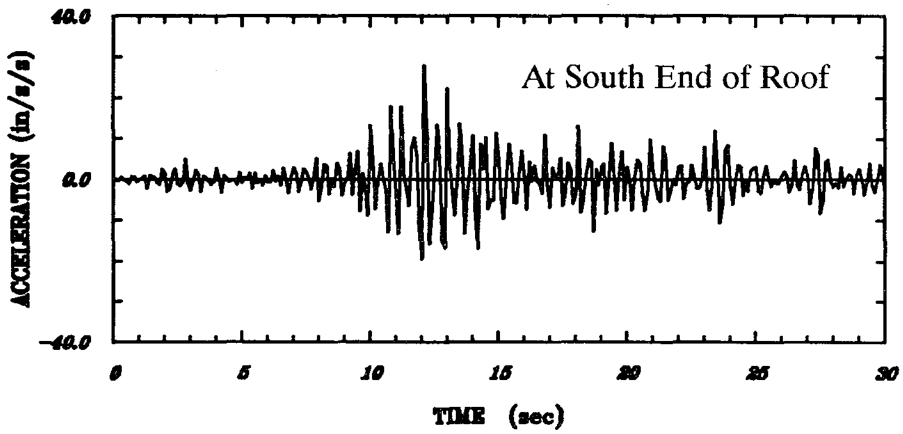

Figure 5–13.a Cal. Resp. at Channel 2 of **CSMIP–SN516** to E–W Base Motion

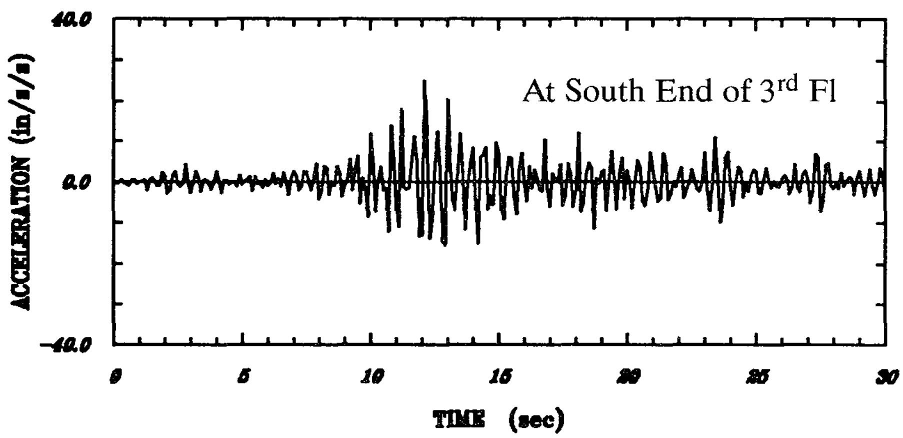

Figure 5–13.b Cal. Resp. at Channel 4 of **CSMIP–SN516** to E–W Base Motion

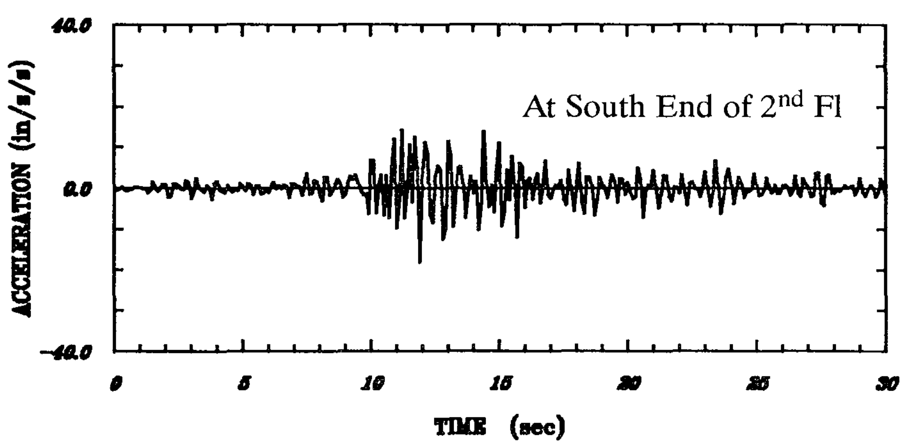

Figure 5–13.c Cal. Resp. at Channel 7 of **CSMIP–SN516** to E–W Base Motion

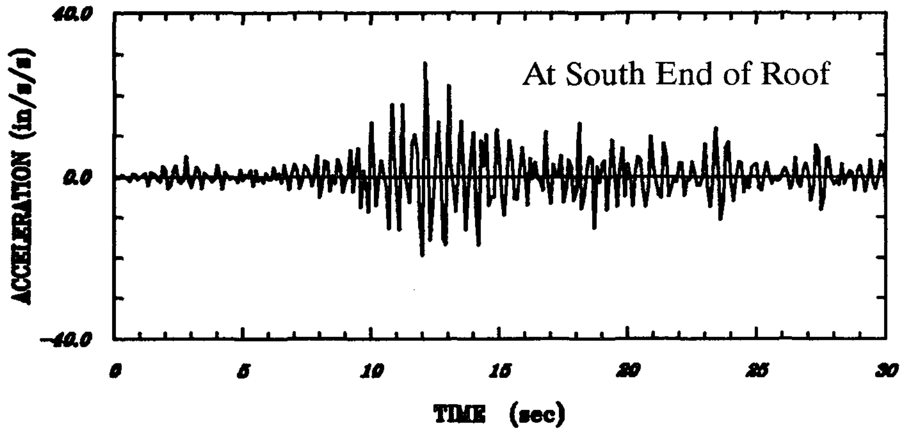

Figure 5–14.a Cal. Resp. at Channel 2 of **CSMIP–SN516** to Biaxial Base Motion

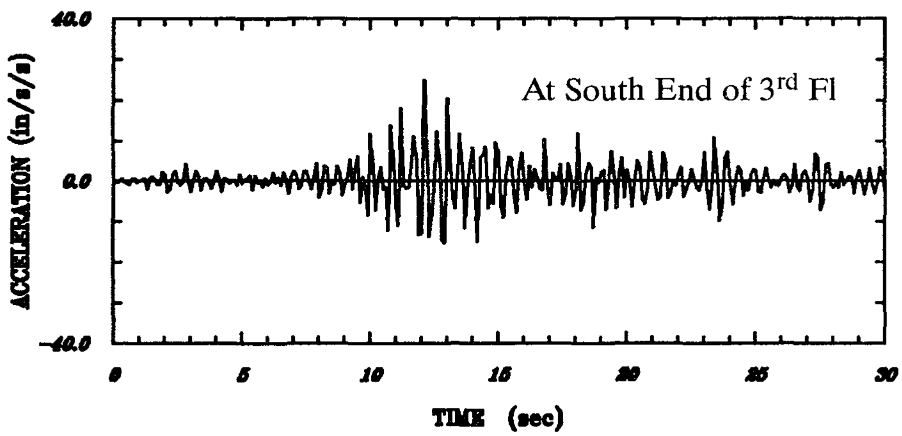

Figure 5–14.b Cal. Resp. at Channel 4 of **CSMIP–SN516** to Biaxial Base Motion

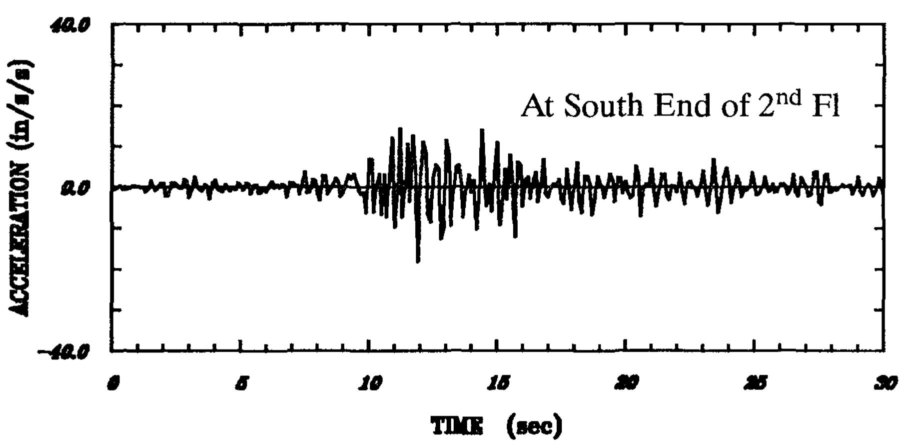

Figure 5–14.c Cal. Resp. at Channel 7 of **CSMIP–SN516** to Biaxial Base Motion

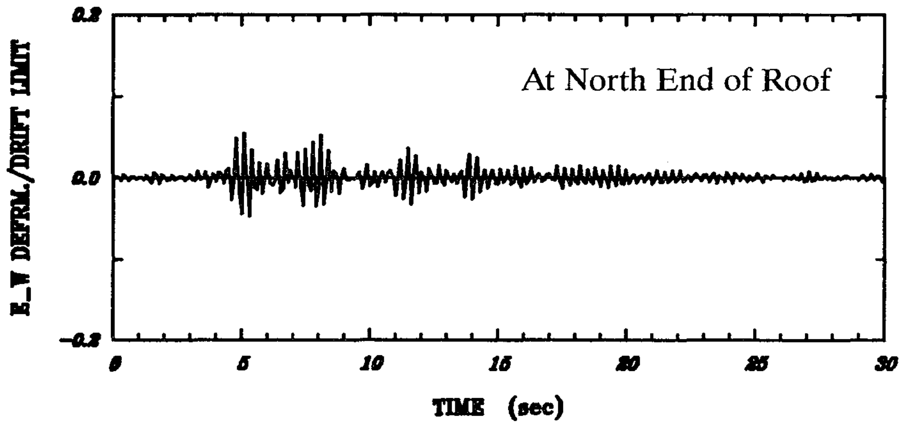

Figure 5-15.a 2nd Story Deformation at Channel 3 of **CSMIP-SN511**

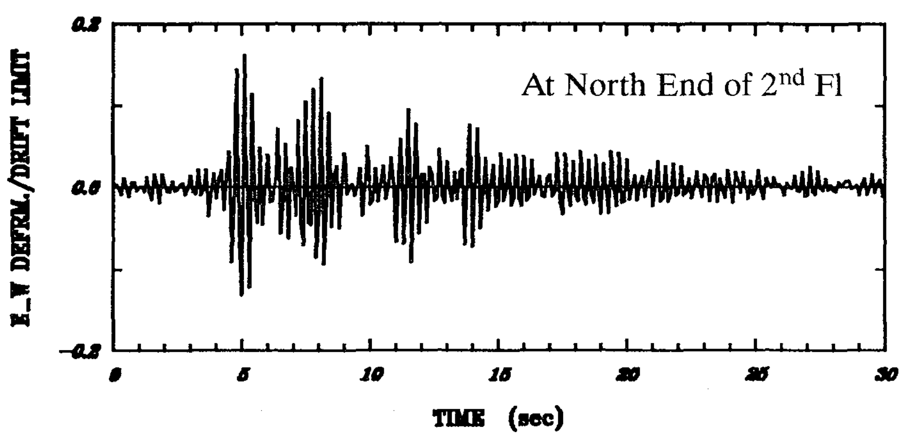

Figure 5-15.b 1st Story Deformation at Channel 5 of **CSMIP-SN511**

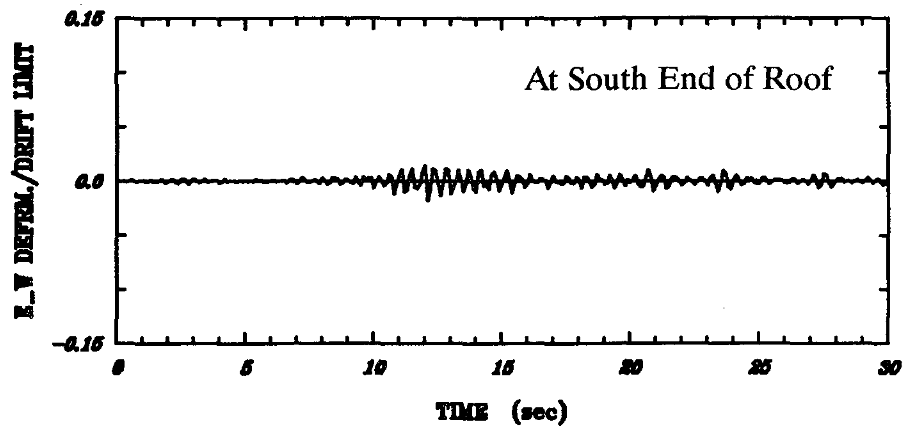

Figure 5–16.a 3rd Story Deformation at Channel 2 of CSMIP–SN516

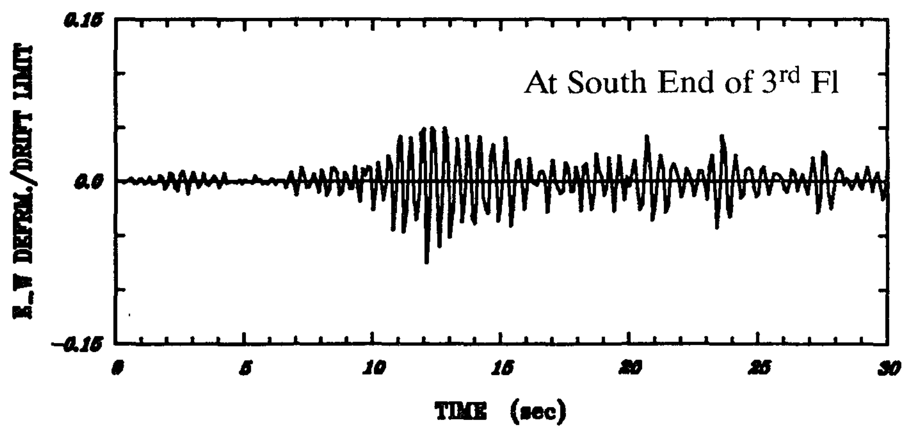

Figure 5–16.b 2nd Story Deformation at Channel 4 of CSMIP–SN516

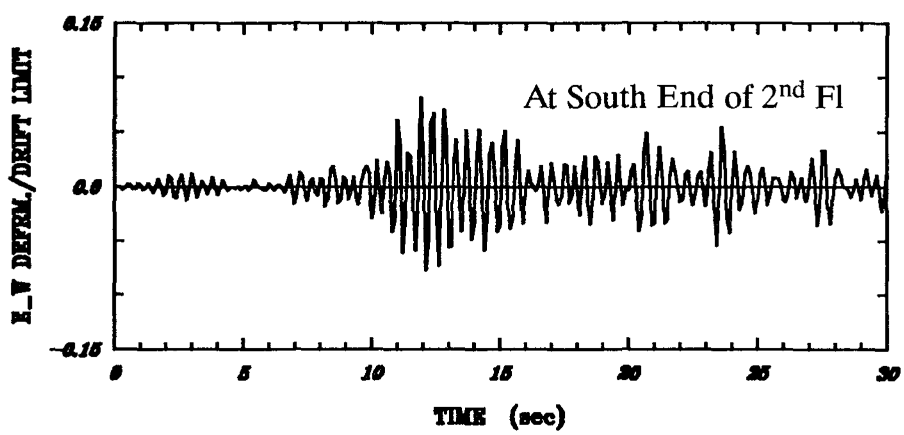

Figure 5–16.c 1st Story Deformation at Channel 7 of CSMIP–SN516

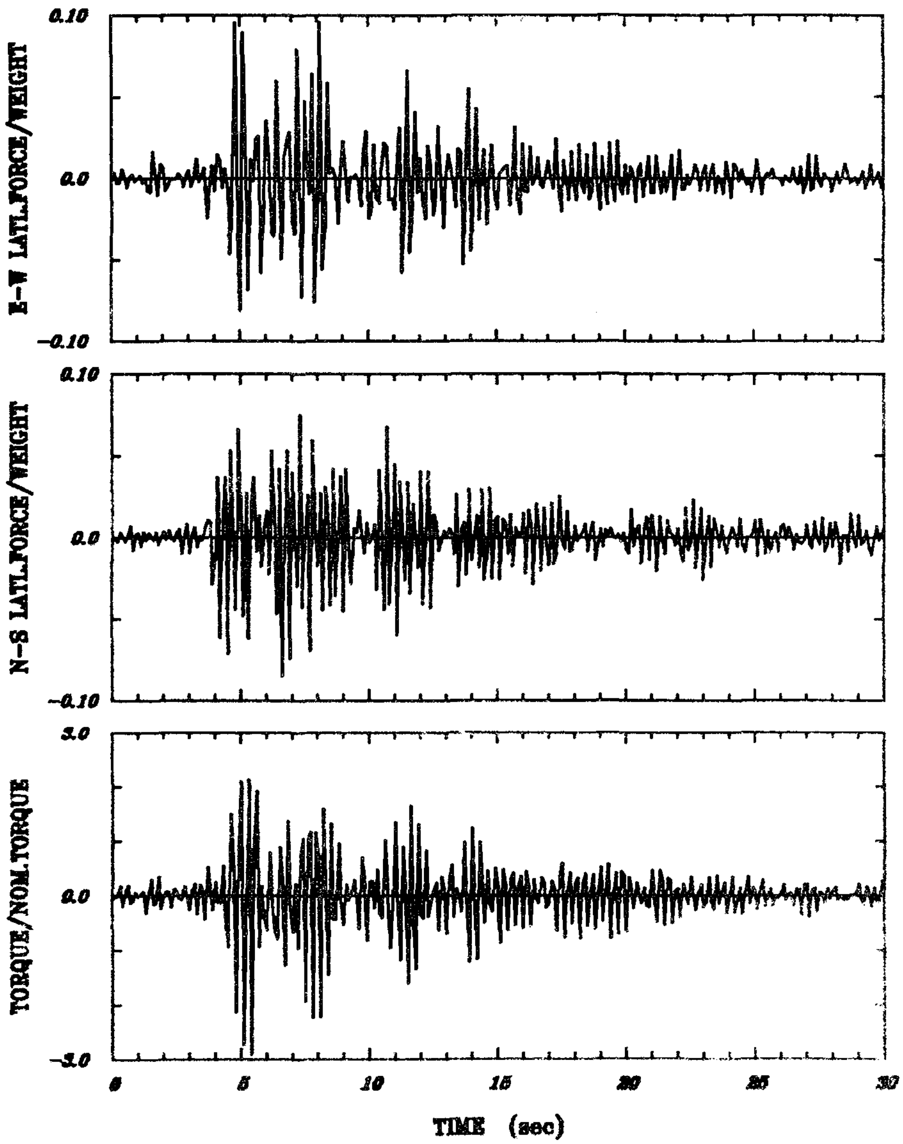

Figure 5-17.a Shear Forces at the 2nd Floor of CSMIP-SN511

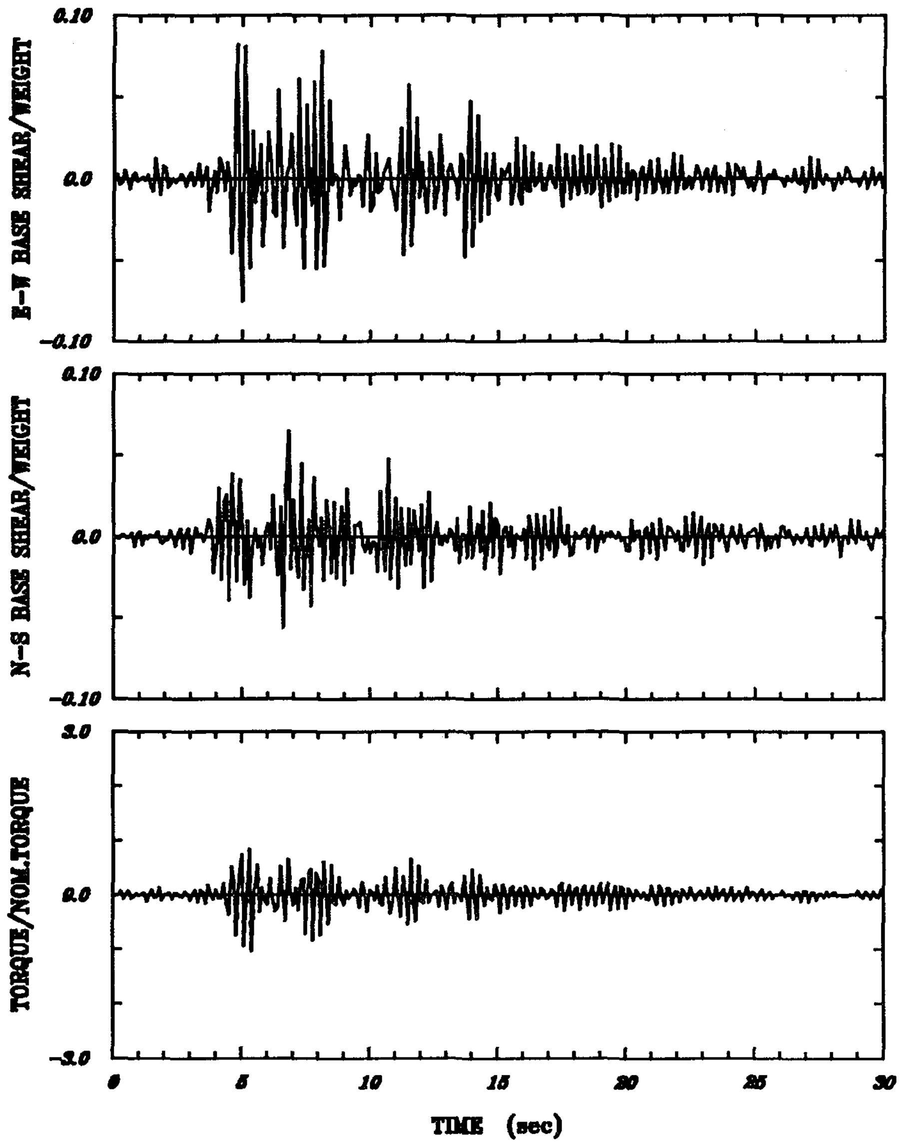

Figure 5–17.b Shear Forces at the 1st Floor (Base Shear) of CSMIP–SN511

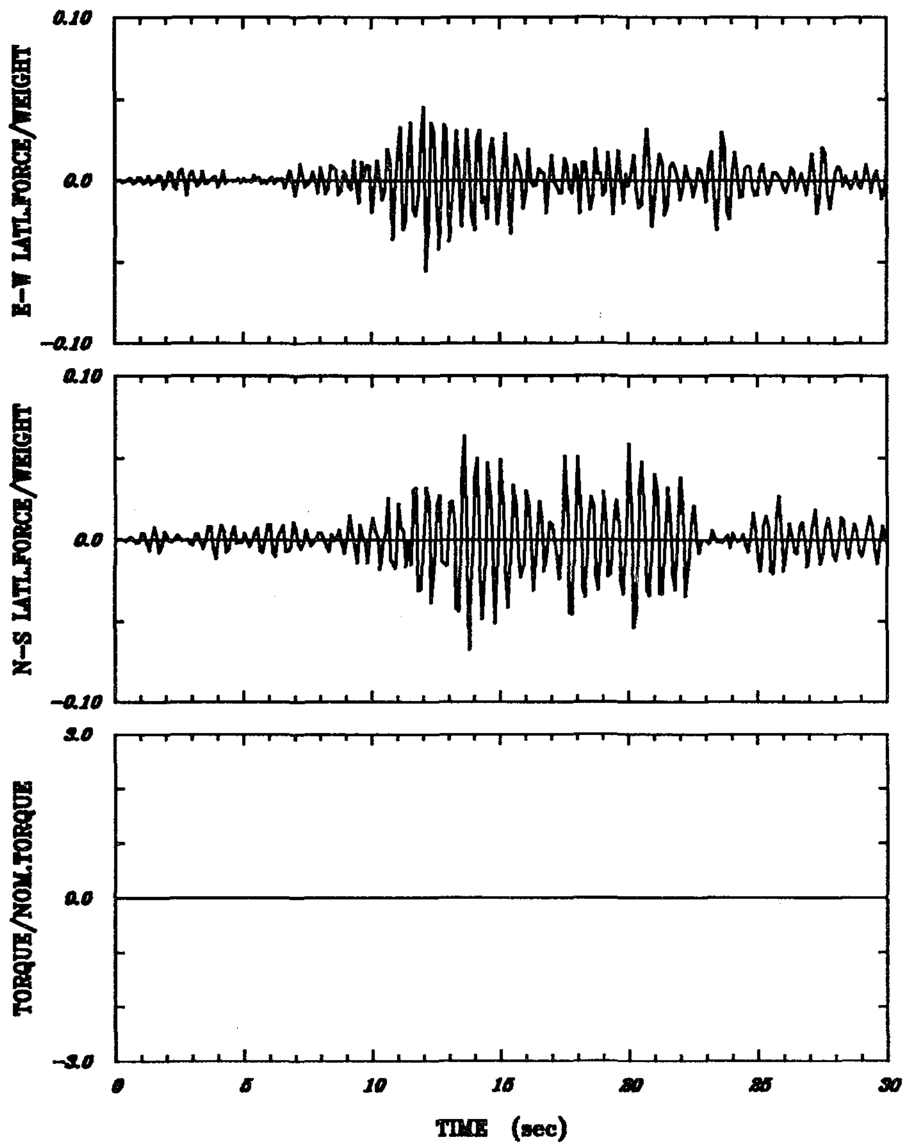

Figure 5–18.a Shear Forces at the 3rd Floor of CSMIP–SN516

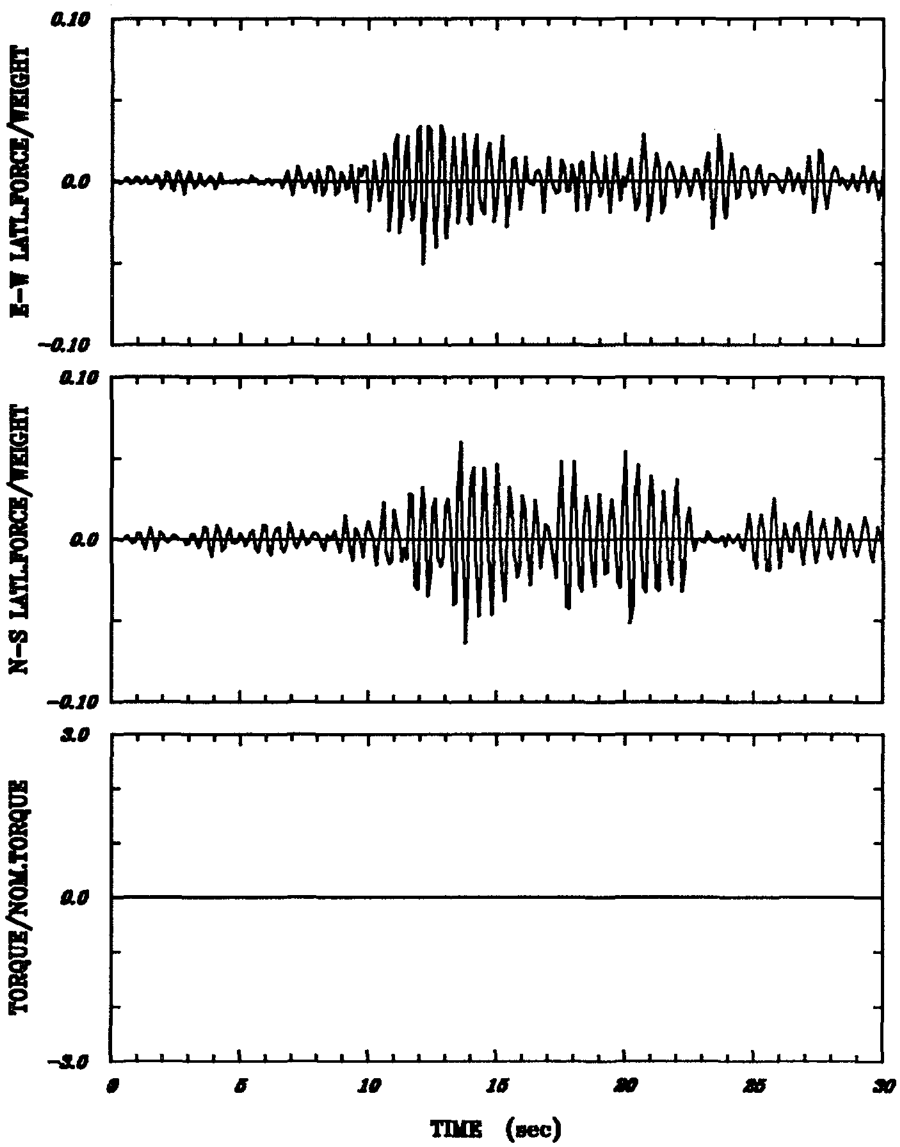

Figure 5–18.b Shear Forces at the 2nd Floor of **CSMIP–SN516**

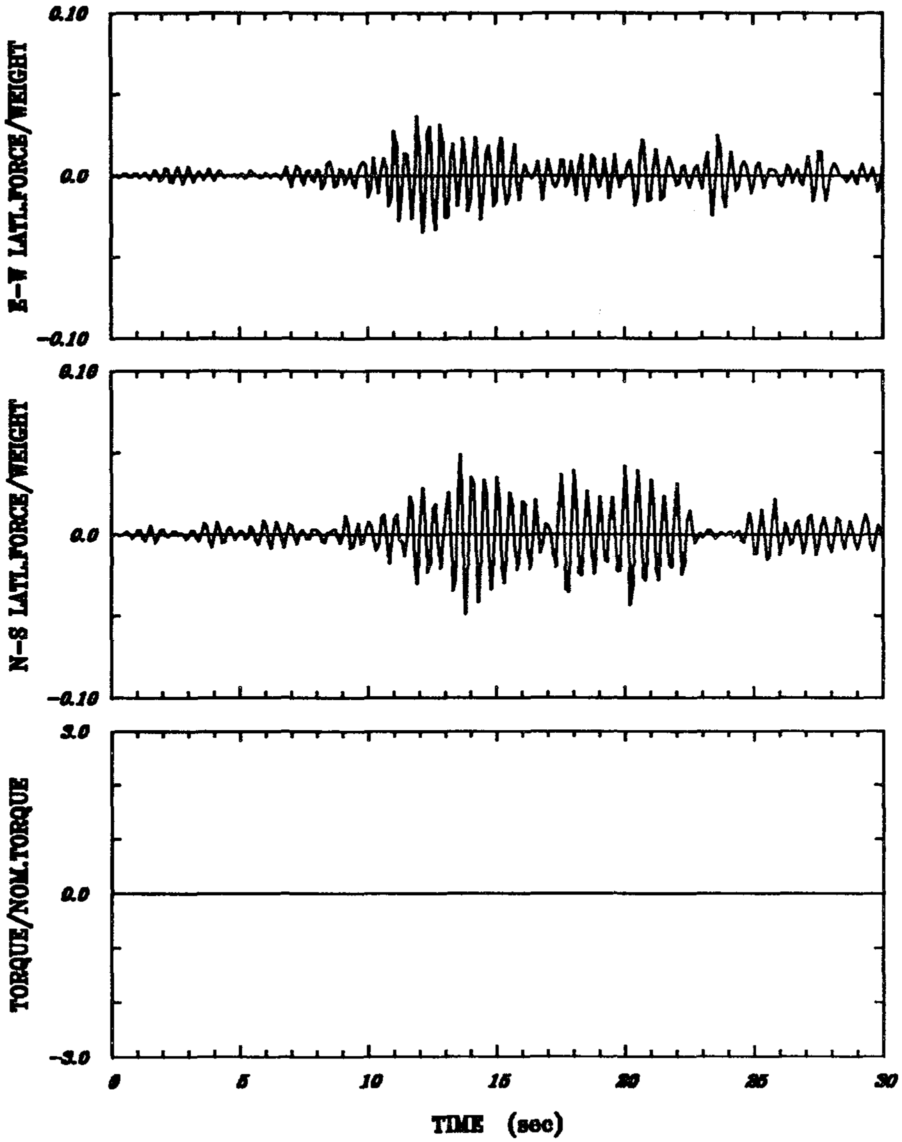

Figure 5-18.c Shear Forces at the 1st Floor (Base Shear) of CSMIP-SN516

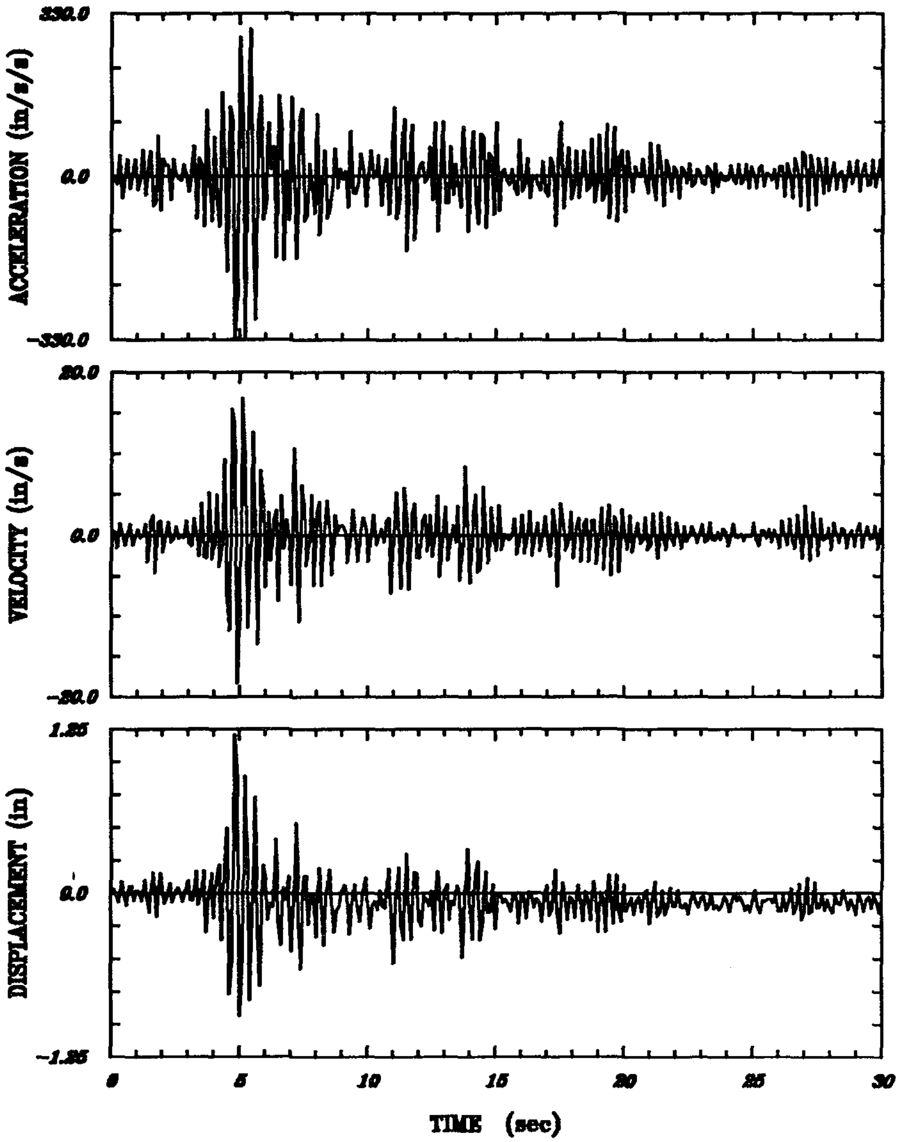

Figure 5–19.a Cal. Resp. at Channel 3 Installed at the North End of Roof of **CSMIP–SN511** to Base Motion $A_a = 0.4g$

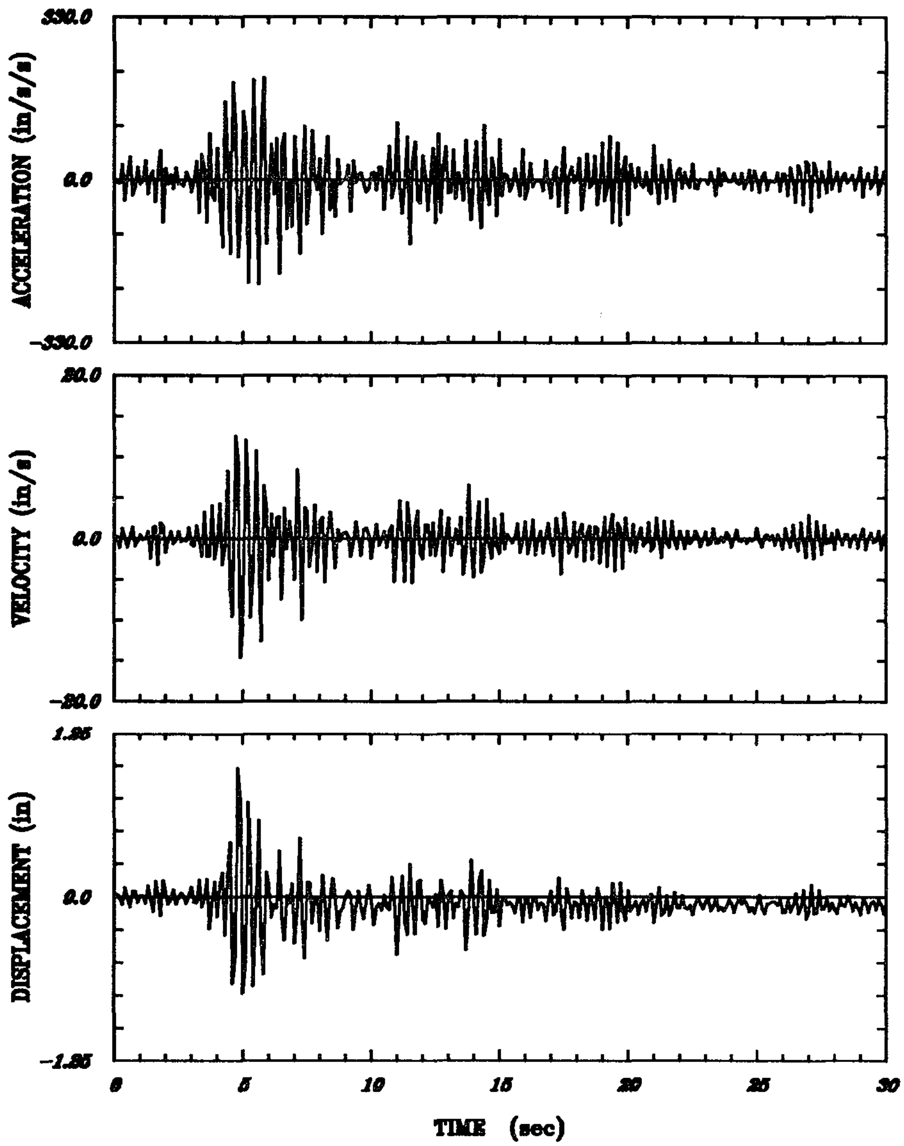

Figure 5–19.b Cal. Resp. at Channel 5 Installed at the North End of 2nd Floor of **CSMIP–SN511** to Base Motion $A_a = 0.4g$

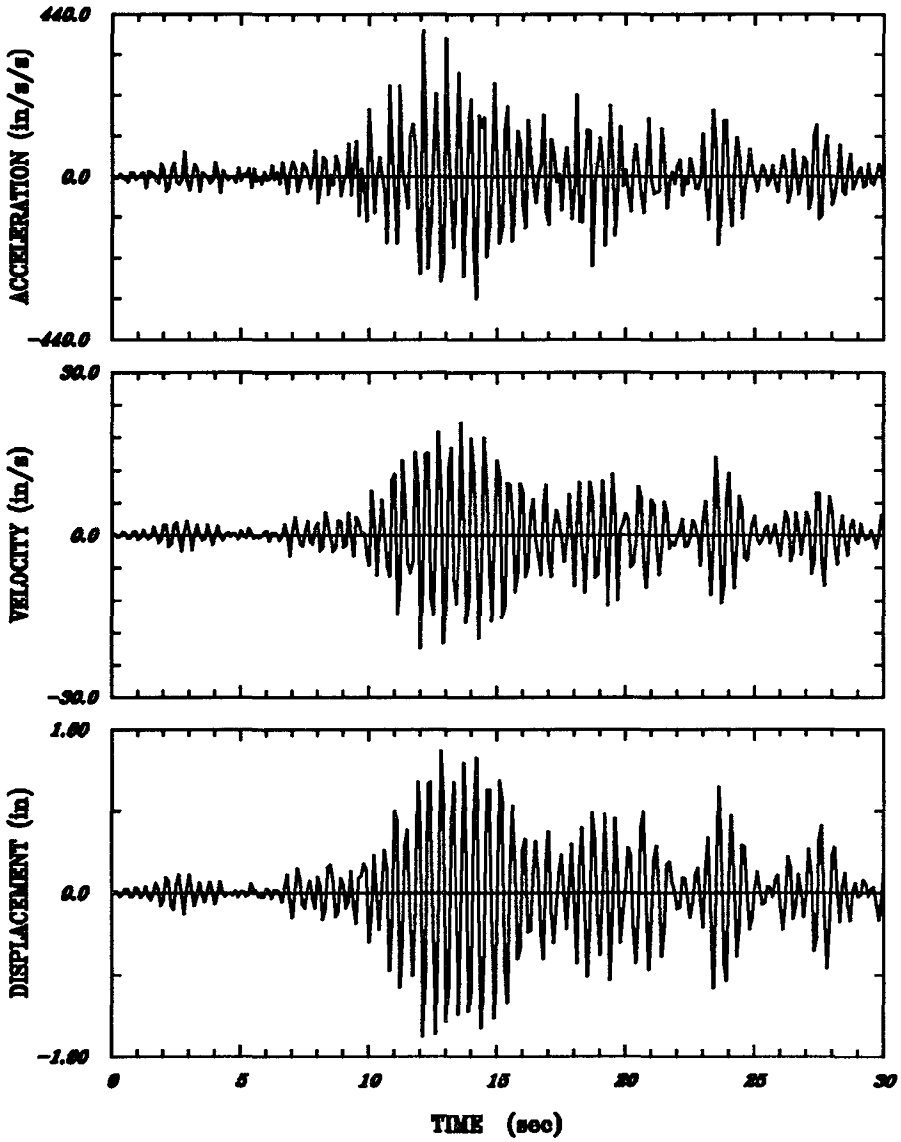

Figure 5–20.a Cal. Resp. at Channel 2 Installed at the South End of Roof of **CSMIP–SN516** to Base Motion $A_a = 0.4g$

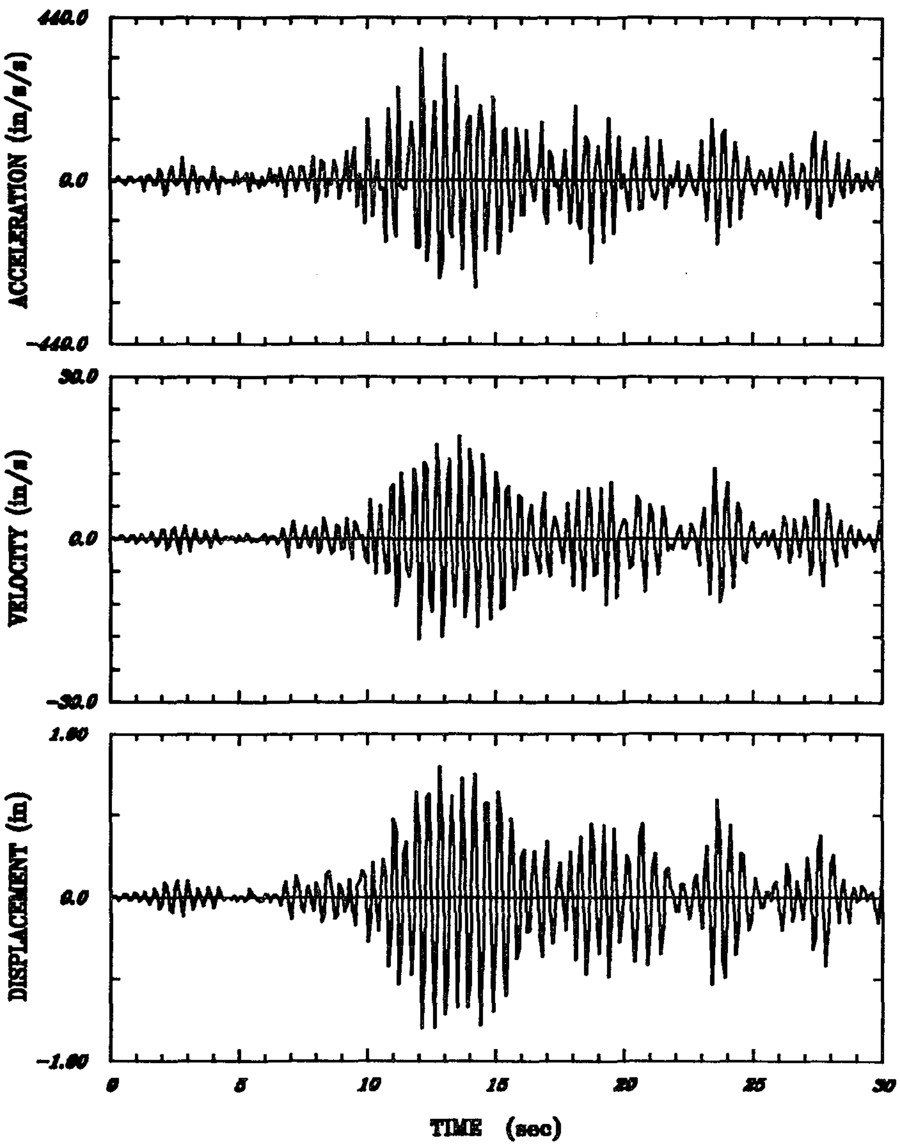

Figure 5–20.b Cal. Resp. at Channel 4 Installed at the South End of 3rd Floor of **CSMIP–SN516** to Base Motion $A_a = 0.4g$

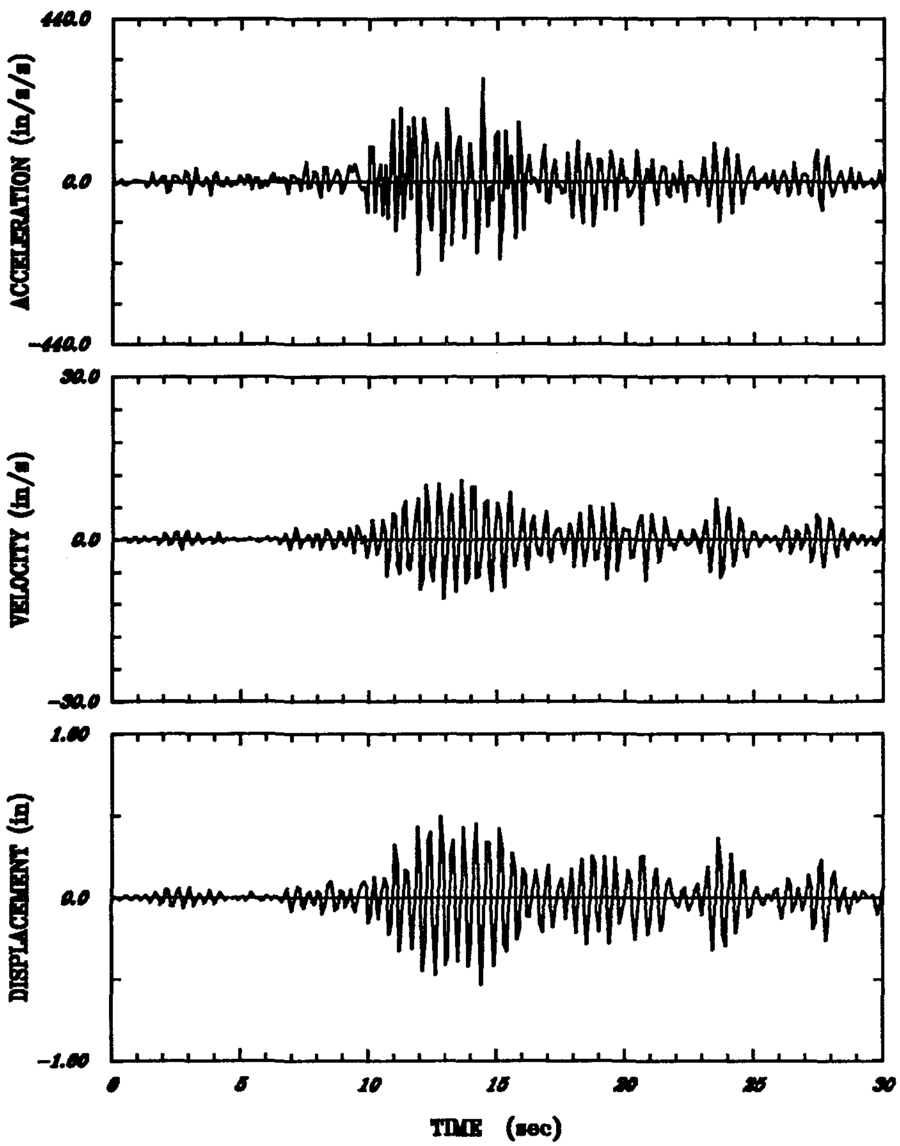

Figure 5-20.c Cal. Resp. at Channel 7 Installed at the South End of 2nd Floor of **CSMIP-SN516** to Base Motion $A_a = 0.4g$

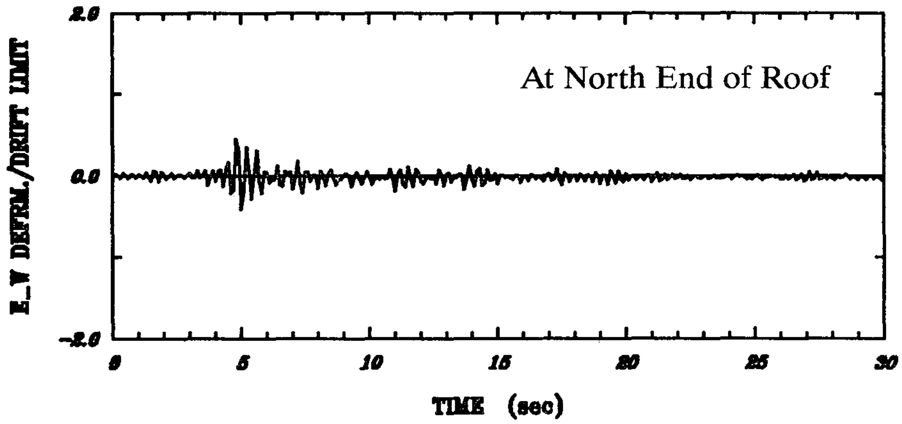

Figure 5–21.a 2nd Story Def. at Chnl. 3 of **CSMIP–SN511** to Base Motion $A_a = 0.4g$

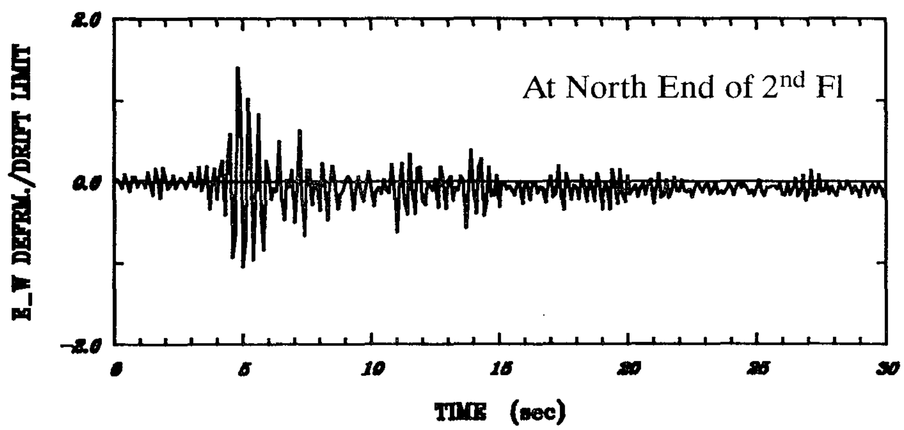

Figure 5–21.b 1st Story Def. at Chnl. 5 of **CSMIP–SN511** to Base Motion $A_a = 0.4g$

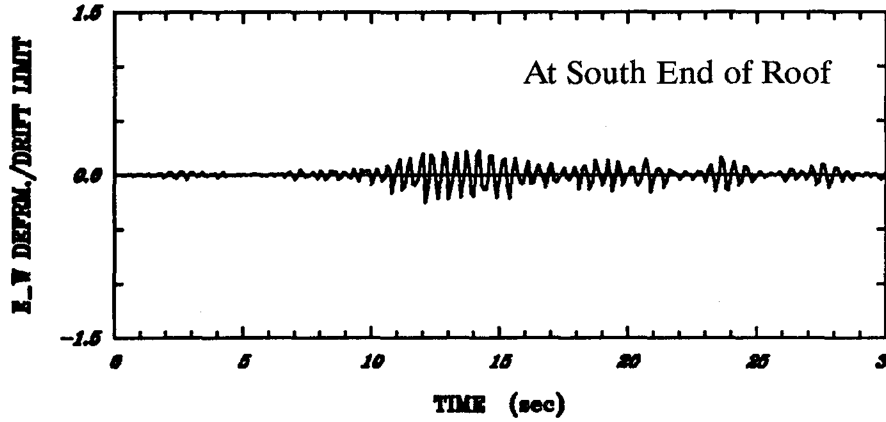

Figure 5–22.a 3rd Story Def. at Chnl. 2 of **CSMIP–SN516** to Base Motion $A_a = 0.4g$

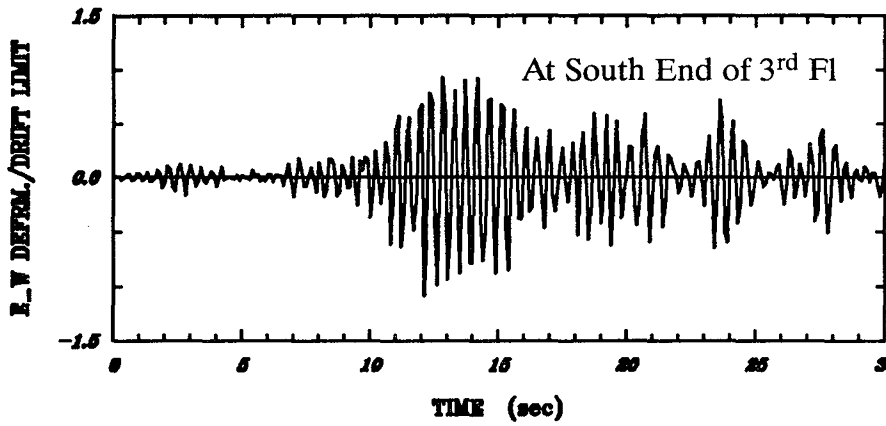

Figure 5–22.b 2nd Story Def. at Chnl. 4 of **CSMIP–SN516** to Base Motion $A_a = 0.4g$

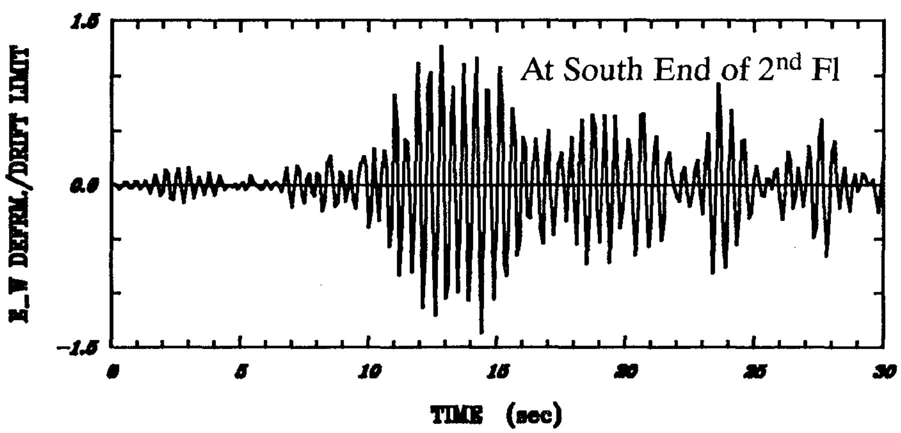

Figure 5–22.c 1st Story Def. at Chnl. 7 of **CSMIP–SN516** to Base Motion $A_a = 0.4g$

CHAPTER 6

SUMMARY AND CONCLUSIONS

6.1 Summary

The dynamic characteristics and torsional response of structures during strong ground motion have been investigated in this report. The purpose of this study was to increase the understanding of torsional effects in the structural response to strong seismic ground motion. As torsion is not known to be the primary cause of structural failures, this research also was directed towards attempting to answer the critical question of whether or not the torsional response is important in the gross response of buildings.

The first part of this investigation (Chapter 2) has contributed to the understanding of the severe coupling between translational and torsional response of structures with closely spaced torsional and translational frequencies. Such strong coupling (and consequently the beating phenomenon arising from modal instability) was demonstrated herein as being theoretically possible; it is believed to be the first conclusive theoretical demonstration of the beating phenomenon arising in the manner noted. Energy transfer was observed from the primary translational response to the torsional motion of single–mass systems when subjected only to translational base excitation. This study has shown the existence of significant torsional response in regular structures with small static eccentricity, in which a relatively low amplitude of torsional response normally would be expected. Moreover the recorded response in the buildings studied (Chapter 5), showed such beating.

The second phase of this research (Chapter 3) involved the formulation and development of a generalized nonlinear material model in the force–displacement space, based on the theories of classical plasticity to account for the force interactions and material strength hardening in the lateral load–resisting members. The procedure for integrating the equations of motion, Newmark's β method, combined with this extended mathematical model has been presented for numerical modeling of elastic and inelastic behavior of structures under earthquake excitation. Parametric studies of static eccentricity have been performed (Chapter 4) by using this procedure. The structural models in the parametric studies were a special class of systems with the uncoupled frequency ratio of 1.225. The reported results have demonstrated the dynamic amplification of torsional response of structures to ground excitation. The amplification factor for static eccentricity to account for such dynamic behavior, which is not considered in any of the current building codes, is about 2.5.

Although the foregoing research was directed towards providing a better understanding of torsional behavior in general, it did not address any building in particular. To comprehend the torsional effects in low–rise structures subjected to ground excitation, two buildings that were extensively instrumented during the 1987 Whittier Narrows Earthquake were studied. The recorded structural responses and analysis results of these buildings have been examined (Chapter 5) in the light of the seismic requirements in the current building codes. The behavior and response of the two structures were observed to be somewhat different from that envisioned and assumed by the direct design procedure employed by the codes.

6.2 Conclusions and Design Implications

On the basis of this study, the following general conclusions may be drawn along with their implications for engineering design practice.

1. When the translational and torsional frequencies are closely spaced, strong coupling effects in the translational and torsional response of structures may arise not only from the static eccentricity but also from modal instability. The latter effect does not receive mention in any of the current building codes.

2. In structures with little static eccentricity, the occurrence of a beating phenomenon in the response to translational base excitation is the result of modal instability when the translational and torsional frequencies are closely spaced. As a result, the torsional motion can reach unexpectedly high magnitudes. The imparted energy from the ground motion is transferred back and forth among the coupled motions without much loss in systems with relatively low damping, which can lead to excessive deformations in the peripheral members in buildings of large dimensions. Fortunately, such coupling effects are limited to a rather narrow range of *frequency ratios* roughly between 0.9 to 1.1. Therefore, structures should be so designed that their fundamental translational and torsional frequencies do not coincide. The

differences among the *frequencies* themselves should be on the order of 10 percent to avoid strong beating effects.

3. The coupled translational and torsional responses could be as much as 90 degrees out of phase between the response maxima, especially during strong torsional coupling associated with beating. The conditions leading to definitive phase differences needs to be studied further. The traditional rules for combining the modal maxima (e.g., the Square–Root–of–Sum–of–Squares rule and the Complete–Quadratic–Combination rule) employed to estimate the true maximum response may lead to significant inaccuracies in predicting maximum effects. These rules will need to be reviewed in the future.

4. Building dimensions are an important parameter when the torsional response is excited. Large torsional response in a structure may not necessarily result in large deformations experienced by the structural members. Torsional response has most severe effects on the members far away from the centers of rigidity. Therefore, torsional effects in buildings with small dimensions are much less important than in buildings with large dimensions.

5. Static eccentricity in structures affects the translational–torsional coupling. The maximum torsional response of structures is almost linearly proportional to their eccentricity. On the basis of the study undertaken herein, the dynamic amplification for the maximum torsional response of regular structures is about 2.5 times the static estimates. This torsional dynamic behavior is not considered in the current codes.

6. Static eccentricity in a class of structures with an uncoupled frequency ratio of 1.225 does not seem to significantly affect the maximum translational response. For this class of structures the common procedures in planar analysis of structures are adequate for estimating the envelope of translational response to strong ground motion.

7. Non–uniform arrangement of strength of the lateral load–resisting members could result in progressive torsionally–induced loss of stiffness if some inelastic behavior occurs during the structural response. In such a case, excessive inelastic torsional response may be controlled by increasing the yield strength of the structural members.

8. The study of the two low–rise buildings has shown that modeling of structural elements is an important part of accurate and meaningful analysis. Small changes in the structural frequencies, with respect to the frequency content of an earthquake, significantly affect the dynamic loadings onto the structure from the ground motion, and thus affect the dynamic response and behavior of the structure. Special attention should be paid to the distribution of mass and stiffness for each story. Also the out–of–plane flexibility of floor diaphragms should be taken into account.

9. The fundamental frequencies of moment–resisting–frame structures with uniformly arranged columns usually are not well separated, especially in structures with dimensional aspect ratios between 0.5 to two. Accordingly as discussed in connection with the beating phenomenon, and confirmed by the recorded response of the buildings during the 1987 Whittier Narrows Earthquake, torsion in such structures with quite symmetric layout of mass and stiffness is to be anticipated, especially in steel frame structures with relatively low damping values. Torsional analysis of structures with little static eccentricity should not be overlooked.

In summary, some comments and suggestions are presented for possible future improvements in building code provisions for the class of buildings studied. In cases where there is some degree of torsional response, the common procedures for planar analysis of structures seem to be adequate for estimating approximately the maximum translational response to strong ground motion. The reason for this observation is that in structures with their uncoupled frequencies well separated the maximum lateral response shows lack of sensitivity to the translational–torsional coupling. The reason for this insensitivity of translational response to the coupling is not precisely known but may be the result of phase differences in response, a subject that needs intensive study.

However, strong coupling, arising either from static eccentricity or from the beating phenomenon, may cause unexpectedly large torsional deformations in the peripheral members or in members located far away from the rigidity center, especially in structures with closely spaced frequencies and with large building dimensions. To fully account for the dynamic effect of torsion, an amplification factor of 2.5 for the static eccentricity may be employed to estimate the maximum torsional response for design purpose of regular structures subjected to strong ground motion.

In moment–resisting–frame structures of regular dimensional aspect ratios with uniformly arranged columns and symmetric layout of mass and stiffness, torsion should be anticipated in connection with the beating phenomenon. In order to avoid the effects of strong torsional coupling and to the extent possible to prevent damage caused by torsion, structures should be designed with their fundamental translational and torsional frequencies separated, even though such separation is difficult. It is rational to keep the translational frequency smaller in relation to the torsional frequency so that the fundamental mode is dominated by translational motion.

APPENDIX A

MODAL-ANALYSIS OF ONE-STORY MODEL

In the equations of motion for the linear-elastic system shown in Figure 2-1, If $[M]$ is the mass matrix, $[K]$ is the stiffness matrix, $\{F\}$ is the force vector of the external forces, and $\{U\}$ is the displacement vector of the degrees of freedom, then the condition of dynamic equilibrium, without considering damping forces, is expressed in terms of a set of simultaneous differential equations,

$$[M]\ \{\ddot{U}\}\ +\ [K]\ \{U\}\ =\ \{F\}. \tag{A.1}$$

The equations in the above expression are generally intercoupled. Upon selection of the natural coordinate system, the displacement variables in this set of equations are either dynamically or statically coupled. As in the example where the degrees of freedom are the displacements at the center of stiffness, the above equations are dynamically coupled, and the mass matrix will be a full matrix while the stiffness matrix is a diagonal matrix. When the degrees of freedom are chosen at the center of mass, these equations become statically coupled, and the mass matrix is diagonal while the stiffness matrix is full. The coordinates in this study originate from the center of mass. Therefore, the equations of motion are statically coupled.

One of the most common methods in solving this set of equations is modal analysis, in which the equations are decoupled by transforming the natural coordinates into a set of generalized coordinates. The basic procedure may be described as follows.

a) find the modal frequencies and mode-shapes, which are the eigensolutions associated with the properties of the system;
b) set up the uncoupled and independent equations of motion in terms of the generalized coordinates, by taking advantage of the orthogonal property of the mode-shapes and by computing the participation factors of the external forces applying in each mode;
c) solve the series of equations of the single-degree-of-freedom systems; and then transform the results back to the original natural coordinates.

The standard procedure of modal analysis can be found in textbooks on dynamics. In the following the procedure is developed for the linear-elastic system shown in Figure 2-1.

The eigen–equation for Equation A.1 is $[K]\{U\} = \omega^2[M]\{U\}$, in which

$$[K] = \begin{bmatrix} k_u & k_u e \\ k_u e & k_\theta \end{bmatrix}, \qquad [M] = \begin{bmatrix} m & 0 \\ 0 & J \end{bmatrix}, \qquad \{U\} = \begin{Bmatrix} u \\ \theta \end{Bmatrix},$$

k_u = translational stiffness of the system,

k_θ = torsional stiffness with respect to the center of mass,

e = static eccentricity between the centers of mass and stiffness,

m = mass,

J = rotational mass moment of inertia with respect to the mass center, and

ω^2 = square of circular natural frequency.

If the uncoupled translational frequency is $\omega_u = \sqrt{k_u/m}$ and the uncoupled torsional frequency is $\omega_\theta = \sqrt{k_\theta/J}$, then the modal frequencies of the system can be expressed as

$$\omega_{\substack{1\\2}}^2 = \frac{1}{2}(\omega_u^2 + \omega_\theta^2) \mp \sqrt{\frac{1}{4}(\omega_u^2 - \omega_\theta^2)^2 + \frac{k_u^2\, e^2}{mJ}}\,. \tag{A.2}$$

The two mode–shapes are, respectively,

$$\begin{Bmatrix} u \\ \theta \end{Bmatrix} = \begin{Bmatrix} 1 \\ a_1 \end{Bmatrix} = \begin{Bmatrix} 1 \\ \frac{1}{e}(\frac{\omega_1^2}{\omega_u^2} - 1) \end{Bmatrix} \quad \text{and} \quad \begin{Bmatrix} u \\ \theta \end{Bmatrix} = \begin{Bmatrix} 1 \\ a_2 \end{Bmatrix} = \begin{Bmatrix} 1 \\ \frac{1}{e}(\frac{\omega_2^2}{\omega_u^2} - 1) \end{Bmatrix}, \tag{A.3}$$

where a_1 and a_2 are variables defining the mode shapes. The modal transformation matrix is

$$[V] = \begin{bmatrix} 1 & 1 \\ a_1 & a_2 \end{bmatrix}. \tag{A.4}$$

Let $\{G\} = \{g_1, g_2\}$ represent the generalized degrees of freedom, then the transformation relationship becomes

$$\{U\} = [V]\ \{G\}. \tag{A.5}$$

With these relationships, the equations of motion Equation A.1 can be converted easily into the generalized coordinates, and then the results can be converted back into the original natural coordinates. The solutions for the linear–elastic system in free vibration and forced vibration are presented in the following.

Free Vibration Analysis

For free vibration analysis, the external applied force vector $\{F\}$ in Equation A.1 is assumed to be zero. With the initial conditions of $\{u_0, \theta_0\}$ and $\{\dot{u}_0, \dot{\theta}_0\}$, the solution of free vibration of the system is given as follows,

$$\begin{Bmatrix} u \\ \theta \\ \dot{u} \\ \dot{\theta} \end{Bmatrix} = \begin{bmatrix} \sin\omega_1 t & \cos\omega_1 t & \sin\omega_2 t & \cos\omega_2 t \\ a_1 \sin\omega_1 t & a_1 \cos\omega_1 t & a_2 \sin\omega_2 t & a_2 \cos\omega_2 t \\ \omega_1 \cos\omega_1 t & -\omega_1 \sin\omega_1 t & \omega_2 \cos\omega_2 t & -\omega_2 \sin\omega_2 t \\ a_1\omega_1 \cos\omega_1 t & -a_1\omega_1 \sin\omega_1 t & a_2\omega_2 \cos\omega_2 t & -a_2\omega_2 \sin\omega_2 t \end{bmatrix} \begin{Bmatrix} (\ a_2\dot{u}_0 - \dot{\theta}_0)/(a_2 - a_1)\omega_1 \\ (\ a_2 u_0 - \theta_0)/(a_2 - a_1) \\ (-a_1\dot{u}_0 + \dot{\theta}_0)/(a_2 - a_1)\omega_2 \\ (-a_1 u_0 + \theta_0)/(a_2 - a_1) \end{Bmatrix}, \quad \text{(A.6)}$$

where the dot represents the derivative of variables with respect to time.

Forced Vibration Analysis

If the external force vector $\{F\}$ is zero, the result for free vibration analysis constitutes the homogenous part of the general solution for Equation A.1. The particular part of the general solution depends upon the form of the external forces. Closed form solutions can be found only for a small family of external loadings. For most of the engineering problems, numerical procedures may be employed to find the approximated solutions.

For a single–degree–of–freedom (SDOF) system subjected to general dynamic loading, the Duhamel integral can be used to evaluate the response. In the case of arbitrary loadings the evaluation will have to be performed numerically. By means of modal analysis, the equations of motion (Equation A.1) are transformed into a series of SDOF equations. Then the results are combined to give the total response of the system.

When the system shown in Figure 2–1 is subjected to an uniaxial base excitation, $\ddot{u}_g$, the total response of the system is

$$u = -\frac{m}{m_1^* \ \omega_1} \int_0^t \ddot{u}_g(\tau) \sin \omega_1 (t-\tau) d\tau - \frac{m}{m_2^* \ \omega_2} \int_0^t \ddot{u}_g(\tau) \sin \omega_2 (t-\tau) d\tau \qquad \text{and}$$

$$\theta = -\frac{a_1 \ m}{m_1^* \ \omega_1} \int_0^t \ddot{u}_g(\tau) \sin \omega_1 (t-\tau) d\tau - \frac{a_2 \ m}{m_2^* \ \omega_2} \int_0^t \ddot{u}_g(\tau) \sin \omega_2 (t-\tau) d\tau, \tag{A.7}$$

where m_i^* = modal mass which equals $(m + Ja_i^2)$,

ω_i^2 = modal circular frequencies determined in Equation A.2,

a_i = quantities defined in Equation A.3, and

i = 1 or 2 to indicate the mode sequence.

The inertial force V_I applying at the center of mass is generated from both the base motion and the floor deformation relative to the base. This force equals the base shear for the single–story system. On the other hand, the torsional moment T_I response at the mass center is the result of rotational deformation of the system. These response are computed as follows,

$$V_I = m \ (\ddot{u}_g + \ddot{u}) \qquad \text{and} \qquad T_I = J \ \ddot{\theta} \ . \tag{A.8}$$

Equations A.7 and A.8 also can be normalized so that the normalization factors will demonstrate the dynamic amplifications of structural response to base motion through modal instability, resulting from close fundamental uncoupled frequencies as in the beating phenomenon. This phenomenon is discussed in Chapter 2.

APPENDIX B

RESPONSE DURING HARMONIC BASE MOTION

The steady-state response of a single-degree-of-freedom system to an arbitrary loading can be obtained by using the Duhamel integral. If the loading on the undamped system is generated from harmonic base motion, i.e., $\ddot{u}_g = \mathrm{a} \sin \Omega t$ where a and Ω are the amplitude and frequency of the base motion, the system response given in Equations A.7 and A.8 become

$$
\begin{aligned}
u &= \frac{m\ \mathrm{a}}{m_1^*\ (\Omega^2 - \omega_1^2)} (\sin \Omega t - \frac{\Omega}{\omega_1} \sin \omega_1 t) + \frac{m\ \mathrm{a}}{m_2^*\ (\Omega^2 - \omega_2^2)} (\sin \Omega t - \frac{\Omega}{\omega_2} \sin \omega_2 t) \\
\theta &= \frac{m\ \mathrm{a}\ a_1}{m_1^*\ (\Omega^2 - \omega_1^2)} (\sin \Omega t - \frac{\Omega}{\omega_1} \sin \omega_1 t) + \frac{m\ \mathrm{a}\ a_2}{m_2^*\ (\Omega^2 - \omega_2^2)} (\sin \Omega t - \frac{\Omega}{\omega_2} \sin \omega_2 t)
\end{aligned}
\tag{B.1}
$$

and

$$
\begin{aligned}
V_I &= m\ \mathrm{a} \left[\frac{m}{m_1^*} \frac{\omega_1^2}{(\Omega^2 - \omega_1^2)} (-\sin \Omega t + \frac{\Omega}{\omega_1} \sin \omega_1 t) + \frac{m}{m_2^*} \frac{\omega_2^2}{(\Omega^2 - \omega_2^2)} (-\sin \Omega t + \frac{\Omega}{\omega_2} \sin \omega_2 t) \right] \\
T_I &= m\ J\ \mathrm{a} \left[\frac{a_1\ \Omega^2}{m_1^*(\Omega^2 - \omega_1^2)} (-\sin \Omega t + \frac{\omega_1}{\Omega} \sin \omega_1 t) + \frac{a_2\ \Omega^2}{m_2^*(\Omega^2 - \omega_2^2)} (-\sin \Omega t + \frac{\omega_2}{\Omega} \sin \omega_2 t) \right],
\end{aligned}
\tag{B.2}
$$

in which m_i^* is the modal mass equaling $(m + Ja_i^2)$. It is obvious from the above equations that the responses illustrate certain beating characteristics when similar terms are collected.

APPENDIX C

ENERGY FLOW IN A FREE VIBRATING SYSTEM

With the initial conditions of $\{U\} = \{u_0, 0\}$ and $\{\dot{U}\} = \{0, 0\}$, the system response is expressed in Equation 2.5,

$$\begin{Bmatrix} u \\ \theta \\ \dot{u} \\ \dot{\theta} \end{Bmatrix} = \begin{bmatrix} \cos\omega_1 t & \cos\omega_2 t \\ a_1\cos\omega_1 t & a_2\cos\omega_2 t \\ -\omega_1\sin\omega_1 t & -\omega_2\sin\omega_2 t \\ -a_1\omega_1\sin\omega_1 t & -a_2\omega_2\sin\omega_2 t \end{bmatrix} \begin{Bmatrix} a_2 u_0/(a_2 - a_1) \\ -a_1 u_0/(a_2 - a_1) \end{Bmatrix}. \tag{C.1}$$

Hence, the kinetic energy associated with translational motion of the system can be computed as follows,

$$T_u = \frac{1}{2}\, m\, \dot{u}^2$$

$$= \frac{m}{2}\left(-\frac{a_2\omega_1}{(a_2 - a_1)}\; u_0\; \sin\omega_1 t + \frac{a_1\omega_2}{(a_2 - a_1)}\; u_0\; \sin\omega_2 t\right)^2$$

$$= \frac{m\;u_0^2}{2}\;\frac{a_2^2}{(a_1 - a_2)^2}\left(\omega_1\sin\omega_1 t - \frac{a_1}{a_2}\omega_2\sin\omega_2 t\right)^2$$

$$= \frac{m\;u_0^2}{2}\;\frac{a_2^2}{(a_1 - a_2)^2}\left[(\omega_1^2 + \frac{a_1^2}{a_2^2}\omega_2^2) - 2\omega_1\omega_2\frac{a_1}{a_2}\cos(\omega_1 - \omega_2)t\right]\sin^2\!\left(\frac{\omega_1 + \omega_2}{2}t + \psi_u\right), \tag{C.2}$$

in which ψ_u = phase angle defined by

$$\tan\psi_u = \frac{(\omega_1 a_2 + \omega_2 a_1)}{(\omega_1 a_2 - \omega_2 a_1)}\;\tan\!\left(\frac{\omega_1 - \omega_2}{2}t\right).$$

If one defines Y_u as the amplitude or "envelope" of the kinetic energy associated with translational motion with the period of $2\pi/(\omega_2 - \omega_1)$, then from Equation C.2,

$$Y_u = \frac{m\;u_0^2}{2}\;\frac{a_2^2}{(a_1 - a_2)^2}\left[(\omega_1^2 + \frac{a_1^2}{a_2^2}\omega_2^2) - 2\omega_1\omega_2\frac{a_1}{a_2}\cos(\omega_1 - \omega_2)t\right]. \tag{C.3}$$

By substitution Equation C.2 becomes

$$T_u = Y_u \sin^2\left(\frac{\omega_1 + \omega_2}{2} t + \psi_u\right) . \tag{C.4}$$

Similarly, the kinetic energy associated with rotational motion of the system is listed below.

$$\begin{aligned} T_\theta &= \frac{1}{2} J \dot{\theta}^2 \\ &= \frac{J}{2} \left(-\frac{a_1 a_2 \omega_1}{(a_2 - a_1)} u_0 \sin\omega_1 t + \frac{a_1 a_2 \omega_2}{(a_2 - a_1)} u_0 \sin\omega_2 t \right)^2 \\ &= \frac{J u_0^2}{2} \frac{a_1^2 a_2^2}{(a_1 - a_2)^2} (\omega_1 \sin\omega_1 t - \omega_2 \sin\omega_2 t)^2 \\ &= \frac{J u_0^2}{2} \frac{a_1^2 a_2^2}{(a_1 - a_2)^2} [(\omega_1^2 + \omega_2^2) - 2\omega_1\omega_2 \cos(\omega_1 - \omega_2)t] \sin^2\left(\frac{\omega_1 + \omega_2}{2} t + \psi_\theta\right) , \end{aligned} \tag{C.5}$$

in which ψ_θ = phase angle defined by

$$\tan\psi_\theta = \frac{(\omega_1 + \omega_2)}{(\omega_1 - \omega_2)} \tan\left(\frac{\omega_1 - \omega_2}{2} t\right) .$$

If Y_θ is defined as the amplitude or "envelope" of the kinetic energy associated with rotational motion with the period of $2\pi/(\omega_2 - \omega_1)$, then from Equation C.5,

$$Y_\theta = \frac{J u_0^2}{2} \frac{a_1^2 a_2^2}{(a_1 - a_2)^2} \left[(\omega_1^2 + \omega_2^2) - 2\omega_1\omega_2 \cos(\omega_1 - \omega_2)t\right] . \tag{C.6}$$

By substitution Equation C.5 becomes

$$T_\theta = Y_\theta \sin^2\left(\frac{\omega_1 + \omega_2}{2} t + \psi_\theta\right) . \tag{C.7}$$

It is apparent from Equations C.3 and C.6 that the envelope of kinetic energy in translation reaches its maximum and the envelope of kinetic energy in torsion hits its minimum at the same time when $\cos(\omega_1 - \omega_2) = 1$, and similarly that the envelope in translation reaches its minimum and in torsion its maximum at the same time when $\cos(\omega_1 - \omega_2) = -1$.

Since the energy possessed by an undamped free–vibrating system is constant, it is interesting to examine the ratio of maximum of the energy envelopes in both the translational and torsional motions. This ratio represents the percentage of the kinetic energy in translation transferred into the torsional motion. Based on Equations C.3, C.4, C.6, and C.7 it is defined that

$$\begin{aligned} \varrho &= \frac{T_{\theta\,\max}}{T_{u\,\max}} \\ &= \frac{Y_{\theta\,\max}}{Y_{u\,\max}} \\ &= \frac{J}{m}\; a_1^2 a_2^2\; \frac{(\omega_1+\omega_2)^2}{(\omega_1 a_2 - a_1\omega_2)^2}\;. \end{aligned} \tag{C.8}$$

By the definition for measuring the difference of uncoupled frequencies given in Equation 2.7, it can be shown that

$$\begin{aligned} \varrho &= \frac{m\ e^2}{J}\cdot\frac{1}{\left(1+\sqrt{\dfrac{\omega_\theta^2}{\omega_u^2}-\dfrac{m\ e^2}{J}}\right)^2}\cdot\frac{\left(1+\dfrac{\omega_\theta^2}{\omega_u^2}\right)+2\sqrt{\dfrac{\omega_\theta^2}{\omega_u^2}-\dfrac{m\ e^2}{J}}}{\left(1+\dfrac{\omega_\theta^2}{\omega_u^2}\right)-2\sqrt{\dfrac{\omega_\theta^2}{\omega_u^2}-\dfrac{m\ e^2}{J}}} \\ &= \frac{m\ e^2}{J}\cdot\frac{1}{\left(1+\sqrt{1-\dfrac{m\ e^2}{J}+\dfrac{\epsilon}{\omega_u^2}}\right)^2}\cdot\frac{\left(2+\dfrac{\epsilon}{\omega_u^2}\right)+2\sqrt{1-\dfrac{m\ e^2}{J}+\dfrac{\epsilon}{\omega_u^2}}}{\left(2+\dfrac{\epsilon}{\omega_u^2}\right)-2\sqrt{1-\dfrac{m\ e^2}{J}+\dfrac{\epsilon}{\omega_u^2}}}\;. \end{aligned} \tag{C.9}$$

The definitions of the parameters are given in Equations 2.2 and 2.3.

APPENDIX D

INTEGRATION OF EQUATIONS OF MOTION

The equations of motion for a system subjected to dynamic loading can be expressed as follows,

$$[M]\{\ddot{U}\} + [C]\{\dot{U}\} + \{Q\} = \{P\} , \tag{D.1}$$

where $[M]$ = diagonal mass matrix of the system,

$[C]$ = damping matrix of the system,

$\{Q\}$ = restoring force vector of the system,

$\{U\}$ = displacement vector of the degrees of freedom,

$\{P\}$ = external force vector applying onto the system, and

the dots represent the derivative of variables with respect to time.

Mathematically, Equation D.1 represents a set of differential equations of second order. In principle, the solution can be obtained by using standard procedures for linear–elastic systems with constant coefficient. However, the standard procedures for the solutions of general differential equations can be very complex, time consuming, and expensive to carry out.

The integration procedure adopted in this study is Newmark's β method which is a numerical step–by–step procedure. Therefore, instead of trying to satisfy the dynamic equilibrium equation D.1 at any time t, it is aimed to satisfy the equilibrium at discrete time intervals Δt apart. If one assumes that all response quantities at time t are known, the equations of motion at time $t + \Delta t$ becomes,

$$[M]\ {}^{t+\Delta t}\{\ddot{U}\} + [C]\ {}^{t+\Delta t}\{\dot{U}\} + {}^{t}\{Q\} + {}^{t}[K]\{\Delta U\} = {}^{t+\Delta t}\{P\} , \tag{D.2}$$

where ${}^{t}\{Q\}$ = restoring force vector of the system at time t,

${}^{t}[K]$ = tangent stiffness matrix of the system at time t,

$\{\Delta U\}$ = incremental displacement vector during the time interval Δt,

${}^{t+\Delta t}\{P\}$ = external force vector applying onto the system at time $t + \Delta t$,

${}^{t+\Delta t}\{U\}$ = displacement vector of the degrees of freedom at time $t + \Delta t$, and the dots represent the derivative of variables with respect to time.

Newmark's β method assumes,

$$
\begin{aligned}
{}^{t+\Delta t}\{\dot{U}\} &= {}^{t}\{\dot{U}\} + (1-\gamma)\cdot\Delta t\cdot{}^{t}\{\ddot{U}\} + \gamma\cdot\Delta t\cdot{}^{t+\Delta t}\{\ddot{U}\} \quad \text{and} \\
{}^{t+\Delta t}\{U\} &= {}^{t}\{U\} + \Delta t\cdot{}^{t}\{\dot{U}\} + \left(\frac{1}{2}-\beta\right)\cdot\Delta t^2\cdot{}^{t}\{\ddot{U}\} + \beta\cdot\Delta t^2\cdot{}^{t+\Delta t}\{\ddot{U}\} \ ,
\end{aligned}
\tag{D.3}
$$

where γ and β are parameters for numerical integration stability and convergence. With this formulation the solution to the linear or nonlinear system can be numerically, step–by–step, carried out in the time domain. By applying Equation D.3, one can easily convert the equations of motion in the form of Equation D.2 into the familiar form of the static equilibrium equation, in the following iterative incremental form,

$$
[K^*]\{\Delta U\}^{(i)} = \{P^*\} \ , \tag{D.4}
$$

where $[K^*] = \dfrac{1}{\beta\Delta t^2}[M] + \dfrac{\gamma}{\beta\Delta t}[C] + {}^{t}[K]$,

$$
\begin{aligned}
\{P^*\} = {}&{}^{t+\Delta t}\{P\} - {}^{t+\Delta t}\{Q\}^{(i-1)} \\
&- [M]\left[\frac{1}{\beta\Delta t^2}\left({}^{t+\Delta t}\{U\}^{(i-1)} - {}^{t}\{U\} \right) - \frac{1}{\beta\Delta t}{}^{t}\{\dot{U}\} - \left(\frac{1}{2\beta}-1\right){}^{t}\{\ddot{U}\}\right] \\
&- [C]\left[\frac{\gamma}{\beta\Delta t}\left({}^{t+\Delta t}\{U\}^{(i-1)} - {}^{t}\{U\} \right) + \left(1-\frac{\gamma}{\beta}\right){}^{t}\{\dot{U}\} + \left(1-\frac{\gamma}{2\beta}\right)\Delta t\ {}^{t}\{\ddot{U}\}\right] ,
\end{aligned}
$$

$$
\begin{aligned}
{}^{t+\Delta t}\{U\}^{(i)} &= {}^{t+\Delta t}\{U\}^{(i-1)} + \{\Delta U\}^{(i)} \ , \\
{}^{t+\Delta t}\{Q\}^{(i)} &= {}^{t+\Delta t}\{Q\}^{(i-1)} + {}^{t}[K]\{\Delta U\}^{(i)} \ , \\
{}^{t+\Delta t}\{U\}^{(0)} &= {}^{t}\{U\} \ , \quad \text{and} \\
{}^{t+\Delta t}\{Q\}^{(0)} &= {}^{t}\{Q\} \ .
\end{aligned}
\tag{D.5}
$$

Corresponding to the stiffness matrix in static analysis, the effective stiffness matrix $[K^*]$ in dynamic analysis involves the mass and damping matrices. In the same way, the effective load vector $\{P^*\}$ in dynamic analysis contains the response quantities at the beginning of the time step and the property matrices of the system. It is observed that no iteration is needed for solutions to linear systems. Generally several iterations are required for solutions to a nonlinear system in order to achieve certain accuracy within the desired tolerance(s), because the method approximates the system response during a time interval as assumed in Equation D.3.

When employing the integration scheme, special attention should be paid to the selection of time interval size and the assignment of various computation tolerances in order to insure the stability and convergence of the response solutions. The three basic tolerance criteria in computation are force, displacement, and energy balance tolerances. Selection of these criteria in calculation depends on the behavior and nature of the structural system in hand. In addition, a proper representation of the external applied loadings should be considered when discretized input data are used. Although the numerical procedure is unconditionally stable for linear systems, the method could become unstable for nonlinear systems when large time steps are used. Therefore, tighter control should be placed on the computational tolerances to minimize the effect of solution inaccuracy in analyzing inelastic structural systems.

It is noticed in Equation D.5 that the tangent stiffness ${}^t[K]$ at the beginning of a time step is used, and the incremental restoring forces $\{\Delta Q\}$ are approximated by the tangential increments ${}^t[K]\{\Delta U\}$. Unlike in static analysis, the mass matrix $[M]$ in dynamic analysis contributes significantly to the effective stiffness matrix $[K^*]$ as the inertial forces play a major role in balancing the structural motion, especially when the time step is very small as shown in the expression for $[K^*]$. Some advantage can be taken here of the fact that the dynamic analysis of structures is relatively insensitive to the update of the stiffness matrix ${}^t[K]$. If the tangent stiffness is updated too frequently, it will result in significantly expensive computational cost. On the other hand, because nonlinear response is highly path-dependent, any error admitted in a particular time step affects the solution of the remaining analysis. Therefore, the balance between solution accuracy and cost effectiveness must be considered carefully.

APPENDIX E

PLASTIC MODULUS FOR BILINEAR MODEL

The plastic modulus k is expressed as the ratio of the equivalent force increment d_eQ_{ij} to the equivalent deformation increment $d_eD^p_{ij}$, as defined in Chapter 3. This plastic modulus is assumed to be constant throughout a time interval, and is determined from the specified uniaxial force-deformation curve. In this appendix, the plastic modulus is obtained for structural members with a bilinear shear resisting relationship.

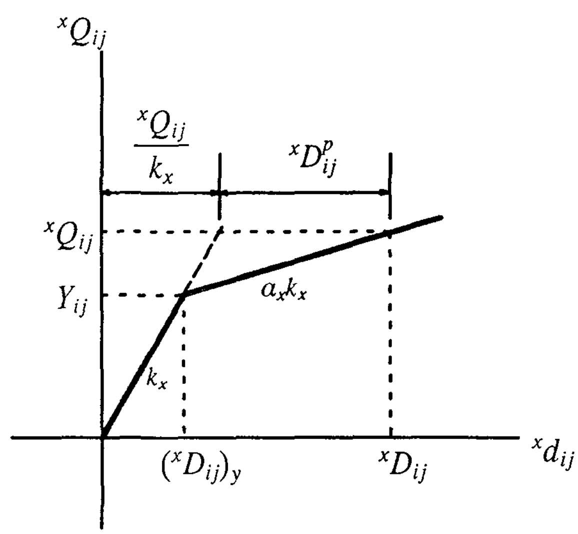

Figure E–1 Bilinear Shear Resisting Member i of Story j

The bilinear force–deformation curve for shear resisting element i of story j is illustrated in Figure E–1. In the figure k_x is the elastic stiffness of the member in the x–direction; a_x is the hardening coefficient; Y_{ij} is the yield force; $(^xD_{ij})_y$ is the yield deformation in the x–direction; $^xQ_{ij}$ and $^xD_{ij}$ are the current shear force level and deformation in the x–direction, respectively; and $^xD^p_{ij}$ equals the plastic deformation in the x–direction. It is understood that the plastic modulus k is calculated for each individual member. Thus the subscript ij will be omitted in the following derivation for the purpose of clarity and brevity without any confusion.

In the case of a uniaxial test of a structural member, neglecting the effect of Poisson's ratio,

$$\begin{cases} {}^{x}Q = {}^{x}Q \\ {}^{y}Q = 0 \end{cases} \text{, and} \qquad \begin{cases} {}^{x}D^{p} = {}^{x}D^{p} \\ {}^{y}D^{p} = 0 \end{cases} . \tag{E.1}$$

In the plastic range, it is observed in Figure E–1 that

$$\begin{aligned} {}^{x}Q &= Y + [{}^{x}D - ({}^{x}D)_{y}\ ]\ a_{x}\ k_{x} \\ &= Y + [\ \frac{{}^{x}Q}{k_{x}} + {}^{x}D^{p} - ({}^{x}D)_{y}\ ]\ a_{x}\ k_{x} \\ &= Y + a_{x}\ {}^{x}Q + a_{x}\ {}^{x}D^{p}\ k_{x} - a_{x}\ ({}^{x}D)_{y}\ k_{x} \\ &= (1 - a_{x})\ Y + a_{x}\ {}^{x}Q + a_{x}\ {}^{x}D^{p}\ k_{x}\ . \end{aligned} \tag{E.2}$$

Hence,

$$(1 - a_{x})\ {}^{x}Q = (1 - a_{x})\ Y + a_{x}\ k_{x}\ {}^{x}D^{p}\ . \tag{E.3}$$

By differentiating both sides of Equation E.3,

$$(1 - a_{x})\ d^{x}Q = a_{x}\ k_{x}\ d^{x}D^{p}\ . \tag{E.4}$$

Thus, from Equations E.1 and E.4,

$$k = \frac{d_{e}Q}{d_{e}D^{p}} = \frac{d^{x}Q}{d^{x}D^{p}} = \frac{a_{x}\ k_{x}}{(1 - a_{x})}\ . \tag{E.5}$$

APPENDIX F

SELECTED PROPERTIES OF THE TWO BUILDINGS

The selected properties employed in the analyses of the two low–rise buildings in Chapter 5 are listed in this appendix. The typical floor plans and the nominal dimensions of both buildings have been presented in Figures 5–1 and 5–2, respectively, in Chapter 5. The two buildings were designed with flexural columns and beams as the special moment resisting space frames for their lateral load–resisting system.

Pomona Office Building (CSMIP–SN511)

The total design weight of this building was estimated to be 4190 kips, which included the dead load of building materials, weight of permanent equipment, and the design live load. The weight of the roof, including the penthouse, was 2240 kips, and the weight of the second floor was 1950 kips.

The design dimensions and reinforcement schedules of the seismic frame columns are listed in Table F–1 and Figure F–1. The non–seismic frame columns on C–3, E–3, C–4, and E–4 have the design column sizes of 18–in by 25–in. The reinforcement schedule is shown in Figure F–2 with #3 tie bars at 18–in spacing for the first story and #3 tie bars at 14–in spacing for the second story. The non–seismic columns at the four corners A–1, G–1, A–6, and G–6 are detailed in Figure F–3 with #3 tie bars at 10–in spacing. In addition, the design thickness of the stair walls is 9–in.

San Bernardino Office Building (CSMIP–SN516)

The total design weight of this office building was estimated to be 1811 kips. The weight of individual floors was estimated as follows: 356 kips for the roof, 716 kips for the third floor, and 739 kips for the second floor.

The structural frame is composed of structural steel columns and relatively flexible floors. All the exterior columns are W14x176 prefabricated members. The interior columns on lines B and E are W8x31 steel members, and the interior columns on lines C and D are W8x35. The beam sizes are listed in Table F–2.

Table F-1 Seismic Frame Column Schedule for Building **CSMIP-SN511**

FLOOR \ COL NO	A-2 , G-2	A-3 , G-3	A-4, G-4, A-5, G-5	B-1, D-1, F-1, B-6, D-6, F-6	C-1, E-1, C-6, E-6
ROOF					
2nd FLR	25 X 25 b = 8" #11 #11 #9	25 X 25 b = 8" #11 #11 #11	25 X 25 b = 7" #11 #11 #11	25 X 25 b = 8" #11 #11 #7	25 X 25 b = 12" #10 #10 #7
1st FLR	25 X 25 b = 12" #11 #11 #9 #9	25 X 25 b = 12" #9 #11 #11 #11	25 X 25 b = 12" #9 #11 #11 #11	25 X 25 b = 12" #11 #11 #7	25 X 25 b = 12" #10 #10 #7
BUNDLE GROUP	1 2	1 2	1 2	1 2	1 2
BUNDLE PATTERN	COL SIZE TIE SPACING	COL SIZE TIE SPACING	COL SIZE TIE SPACING	COL SIZE TIE SPACING	COL SIZE TIE SPACING

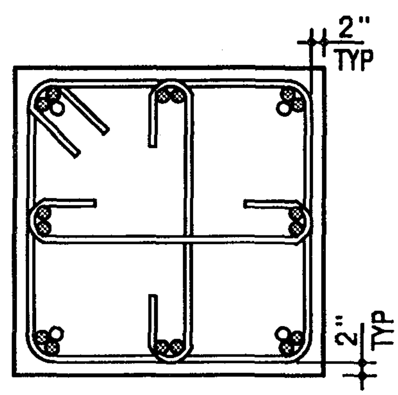

Figure F-1 Seismic Tie Detail

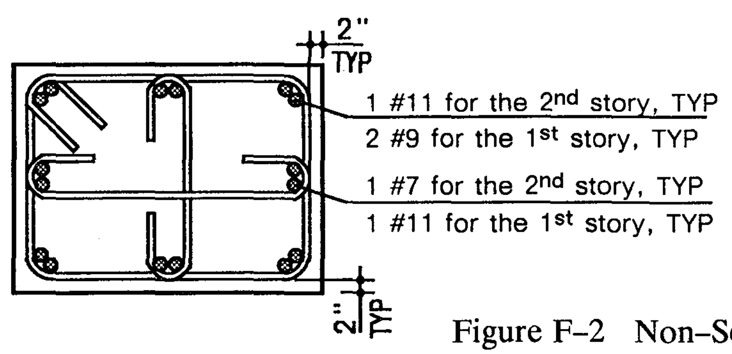

Figure F-2 Non-Seismic Column Detail

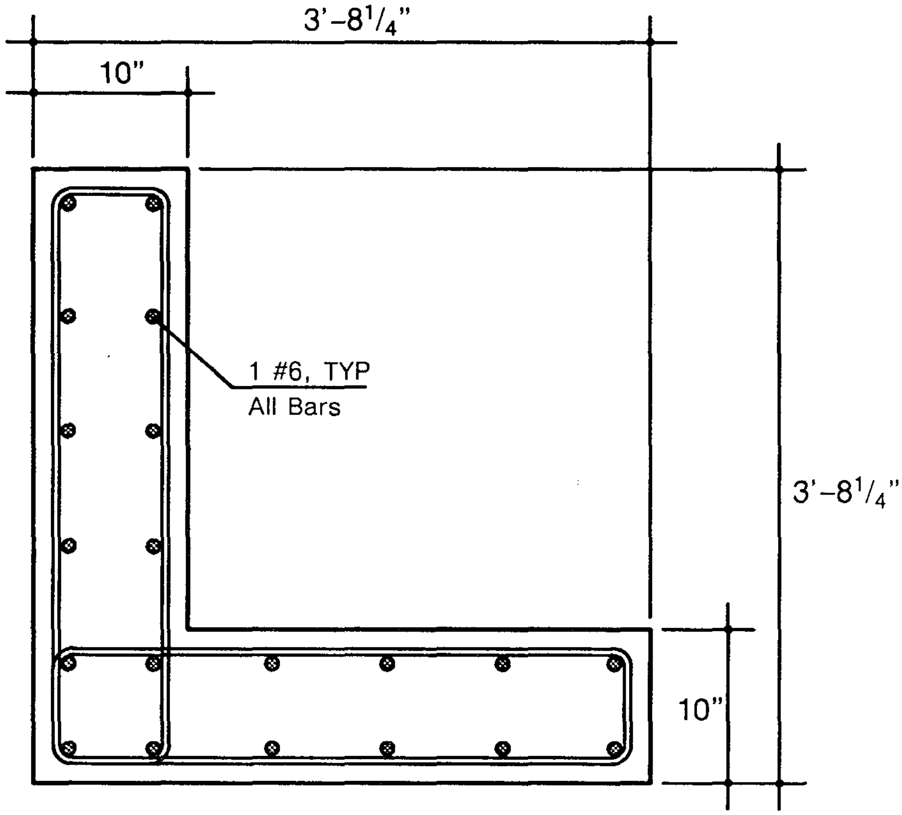

Figure F–3 Non–Seismic Column Detail

Table F–2 Beam Sizes for Building **CSMIP–SN516**

Story Level	Exterior Beams	Interior Beams (N–S Direction)	Interior Beams (E–W Direction)
Roof	W16x36	4x12 Block	$5^1/_8$ x $31^1/_2$ GLB
3	W24x68	4x14 Block	W18x40 (24' span) W21x50 (28' span)
2	W30x99	4x14 Block	W18x40 (24' span) W21x50 (28' span)

REFERENCES

1. Applied Technology Council, Tentative Provisions for the Development of Seismic Regulations for Buildings, ATC 3-06, U.S. Government Printing Office, Washington, D. C., June 1978, 505pp.

2. Ayre, R. S., "Interconnection of Translational and Torsional Vibrations in Buildings," Bulletin of the Seismological Society of America, Vol. 28, 1938, pp 89–130.

3. Bathe, K. J., Finite Element Procedures in Engineering Analysis, Prentice-Hall, New Jersey, 1982, 735pp.

4. Batts, M. E., G. V. Berg, and R. D. Hanson, "Torsion in Buildings Subjected to Earthquakes," Report No. UMEE 78R4, Department of Civil Engineering, University of Michigan, Ann Arbor, Michigan, November 1978, 151pp.

5. Blume, J. A., N. M. Newmark, and L. H. Corning, Design of Multistory Reinforced Concrete Buildings for Earthquake Motions, Portland Cement Association, Illinois, 1961, 318pp.

6. Building Seismic Safety Council, NEHRP Recommended Provisions for the Development of Seismic Regulations for New Buildings, 1985 Edition, 3 Volumes, Federal Emergency Management Agency/Earthquake Hazards Reduction Series 17 (129pp.), 18 (200pp.), and 19 (142pp.), Washington, D. C., February 1986.

7. Chopra, A. K. and N. M. Newmark, "Analysis," Chapter 2 in Design of Earthquake Resistant Structures, edited by E. Rosenblueth, John Wiley & Sons, New York, 1980, pp 27–53.

8. Class notes, "Nonlinear Analysis in Structure Mechanics," by Professors J. Ghaboussi and D. A. Pecknold in Department of Civil Engineering at the University of Illinois at Urbana-Champaign, Urbana, Illinois, Fall Semester of 1987.

9. Clough, R. W. and S. B. Johnston, "Effect of Stiffness Degradation on Earthquake Ductility Requirements," Proceedings of Japan Earthquake Engineering Symposium, Tokyo, Japan, October 1966, pp 227–232.

10. Clough, R. W. and J. Penzien, Dynamics of Structures, McGraw-Hill, New York, 1975, 634pp.

11. Dempsey, K. M. and H. M. Irvine, "Envelopes of Maximum Seismic Response for a Partially Symmetric Single Story Building Model," Earthquake Engineering and Structural Dynamics, Vol. 7, 1979, pp 161–180.

12. Dodds, R. H., "Numerical Techniques for Plasticity Computations in Finite Element Analysis," Computers & Structures, Vol. 26, No. 5, 1987, pp 767–779.

13. Erdik, M. O., "Torsional Effects in Dynamically Excited Structures," Ph.D. Thesis, Rice University, Houston, Texas, May 1975, 133pp.

14. Erdik, M. O., "Nonlinear, Lateral–Torsional Response of Symmetric Structures Subjected to Propagating Ground Motions," Proceedings of the 6th European Conference on Earthquake Engineering, Vol. 2, Dubrovnik, Yugoslavia, September 1978, pp 93–100.

15. Hejal, R. and A. K. Chopra, "Earthquake Response of Torsionally-Coupled Buildings," Report No. UBC/EERC 87/20, Earthquake Engineering Research Center, University of California, Berkeley, California, December 1987, 328pp.

16. Hoerner, J. B., "Modal Coupling and Earthquake Response of Tall Buildings," Ph.D. Thesis, Report No. EERL 71-07, California Institute of Technology, Pasadena, California, May 1971, 157pp.

17. Housner, G. W., "Limit Design of Structures to Resist Earthquakes," Proceedings of the 1st World Conference on Earthquake Engineering, Berkeley, California, June 1956, pp 5-1 to 5-13.

18. International Conference of Building Officials, Uniform Building Code, 1988 Edition, International Conference of Building Officials, Whittier, California, May 1988, 926pp.

19. Irvine, H. M. and G. E. Kountouris, "Inelastic Seismic Response of a Torsionally Unbalanced Single-story Building Model," Publication No. R79-31, Department of Civil Engineering, Massachusetts Institute of Technology, Cambridge, MASS, 1979, 163pp.

20. Irvine, H. M. and G. E. Kountouris, "Peak Ductility Demands in Simple Torsionally Unbalanced Building Models Subjected to Earthquake Excitation," Proceedings of the 7th World Conference on Earthquake Engineering, Vol. 4, Part I, Turkey, 1980, pp 117–120.

21. Jennings, P. C., R. B. Matthiesen, and J. B. Hoerner, "Forced Vibration of a 22-Story Steel Frame Building," Report No. EERL 71-01, Earthquake Engineering Research Laboratory, California Institute of Technology, Pasadena, California, February 1971, 99pp.

22. Kan, C. L. and A. K. Chopra, "Coupled Lateral torsional Response of Buildings to Ground Shaking," Report No. EERC 76/13, Earthquake Engineering Research Center, University of California, Berkeley, California, May 1976, 167pp.

23. Kan, C. L. and A. K. Chopra, "Effects of Torsional Coupling on Earthquake Forces in Buildings," Journal of the Structural Division, ASCE, Vol. 103, No. ST4, 1977, pp 805-819.

24. Kan, C. L. and A. K. Chopra, "Elastic Earthquake Analysis of a Class of Torsionally Coupled Buildings," Journal of the Structural Division, ASCE, Vol. 103, No. ST4, 1977, pp 821-838.

25. Kan, C. L. and A. K. Chopra, "Linear and Nonlinear Earthquake Responses of Simple Torsionally Coupled Systems," Report No. EERC 79/03, Earthquake Engineering Research Center, University of California, Berkeley, California, February 1979, 102pp.

26. Kan, C. L. and A. K. Chopra, "Torsional Coupling and Earthquake Response of Simple Elastic and Inelastic Systems," Journal of the Structural Division, ASCE, Vol. 107, No. ST8, 1981, pp 1569-1588.

27. Kan, C. L. and A. K. Chopra, "Simple Model for Earthquake Response Studies of Torsionally Coupled Buildings," Journal of the Engineering Mechanics Division, ASCE, Vol. 107, No. EM5, 1981, pp 935-949.

28. Kung, S-Y and D. A. Pecknold, "Effect of Ground Motion Characteristics on the Seismic Response of Torsionally Coupled Elastic Systems," Civil Engineering Studies, Structural Research Series No. 500, University of Illinois, Urbana, Illinois, June 1982, 325pp.

29. Lin, S. C. and A. S. Papageorgiou, "Demonstration of Torsional Coupling Caused by Closely Spaced Periods-1984 Morgan Hill Earthquake Response of the Santa Clara County Building," Earthquake Spectra, Vol. 5, No. 3, August 1989, pp 539-556.

30. McCabe, S. L. and W. J. Hall, "Assessment of Seismic Structural Damage," Journal of Structural Engineering, ASCE, Vol. 115, No. 9, September 1989, pp 2166–2183.

31. Morgan, J. R., W. J. Hall, and N. M. Newmark, "Response of Simple Structural Systems to Traveling Seismic Waves," Civil Engineering Studies, Structural Research Series No. 467, University of Illinois, Urbana, Illinois, September 1979, 114pp.

32. Newmark, N. M., "A Method of Computation for Structural Dynamics," Journal of the Engineering Mechanics Division, ASCE, Vol. 85, No. EM3, 1959, pp 67–94.

33. Newmark, N. M., "Torsion in Symmetrical Buildings," Proceedings of the 4th World Conference on Earthquake Engineering, Vol. 2, Santiago, Chile, 1969, pp A3–19 to A3–32.

34. Newmark, N. M. and W. J. Hall, "Seismic Design Criteria for Nuclear Reactor Facilities," Proceedings of the 4th World Conference on Earthquake Engineering, Vol. 2, Santiago, Chile, 1969, pp B4–37 to B4–50.

35. Newmark, N. M. and W. J. Hall, Earthquake Spectra and Design, Engineering Monographs on Earthquake Criteria, Structural Design, and Strong Motion Records, EERI, 1982, 103pp.

36. Newmark, N. M. and E. Rosenblueth, Fundamentals of Earthquake Engineering, Prentice–Hall, New Jersey, 1971, 640pp.

37. Nigam, N. C., "Inelastic Interactions in the Dynamic Response of Structures," Ph.D. Thesis, EERL Report, California Institute of Technology, Pasadena, California, June 1967, 195pp.

38. Ortiz, M., "Topics in Constitutive Theory for Nonlinear Solids," Ph.D. Dissertation, Department of Civil Engineering, University of California, Berkeley, California, 1981, 146pp.

39. Pecknold, D. A., "Inelastic Structural Response to 2D Ground Motion," Journal of the Engineering Mechanics Division, ASCE, Vol. 100, No. EM5, 1974, pp 949–963.

40. "Research Agenda: Learning from the 19 September 1985 Mexico Earthquake," National Research Council, January 1986, 34pp.

41. Rosenblueth, E. and J. Elorduy, "Response of Linear Systems to Certain Transient Disturbance," Proceedings of the 4th World Conference on Earthquake Engineering, Vol. 1, Santiago, Chile, 1969, pp A1–185 to A1–196.

42. Rosenblueth, E., et al. editors of "The Mexico Earthquake of September 19, 1985," Earthquake Spectra, EERI, Vol. 4, No. 3, Vol. 4, No. 4, and Vol. 5, No. 1, 1989.

43. Seismology Committee, Recommended Lateral Force Requirements and Tentative Commentary, 1988 Edition, Structural Engineers Association of California, San Francisco, California, June 1988, 61pp. and 133pp.

44. Shakal, A. F., et al., "CSMIP Strong-Motion Records from the Whittier, California Earthquake of 1 October 1987," Report No. OSMS 87–05, California Strong Motion Instrumentation Program, October 1987, 198pp.

45. Shiga, T., "Torsional Vibrations of Multi–storied Buildings," Proceedings of the 3rd World Conference on Earthquake Engineering, Vol. 2, Auckland and Wellington, New Zealand, 1965, pp 569–584.

46. Shiga, T., A. Shibata, and J. Onose, "Torsional Response of Buildings to Strong Motion Earthquakes," Proceedings of Japan Earthquake Engineering Symposium, Tokyo, Japan, October 1966, pp 209–214.

47. Simo, J. C. and R. L. Taylor, "Consistent Tangent Operators for Rate– Independent Elastoplasticity," Computer Methods in Applied Mechanics and Engineering, Vol. 48, 1985, pp 101–118.

48. Sozen, M., "Old–time Recipe for Converting A Frame into a Shear–Beam," private communication.

49. Tso, W. K., "Induced Torsional Oscillations in Symmetrical Structures," Earthquake Engineering and Structural Dynamics, Vol. 3, 1975, pp 337–346.

50. Tso, W. K. and Y. Bozorgnia, "Effective Eccentricity for Inelastic Seismic Response of Buildings," Earthquake Engineering and Structural Dynamics, Vol. 14, No. 3, 1986, pp 413–427.

51. Tso, W. K. and K. M. Dempsey, "Seismic Torsional Provisions for Dynamic Eccentricity," Earthquake Engineering and Structural Dynamics, Vol. 8, 1980, pp 275–289.

52. Tso, W. K. and A. W. Sadek, "Inelastic Seismic Response of Simple Eccentric Structures," Earthquake Engineering and Structural Dynamics, Vol. 13, No. 2, 1985, pp 135–280.

53. Veletsos, A. S., M. O. Erdik, and P. T. Kuo, "Response of Structures to Propagating Ground Motions," Structural Research Report No. 22, Department of Civil Engineering, Rice University, Houston, Texas, April 1975, 14pp.

54. Wilkins, M. L., "Calculation of Elastic–Plastic Flow," Methods of Computational Physics, Vol. 3, Academic Press, New York, 1964, pp 211–264.

55. Wood, S. L., J. K. Wight, and J. P. Moehle, "The 1985 Chile Earthquake – Observations on Earthquake–Resistant Construction in Vina Del Mar," Civil Engineering Studies, Structural Research Series No. 532, University of Illinois, Urbana, Illinois, February 1987, 176pp.

56. Wyllie, L. A. et al., "The Chile Earthquake of March 3, 1985," Earthquake Spectra, Vol. 2, No. 2, April 1986, pp 249–512.

57. Yamazaki, Y., "Inelastic Torsional Response of Structures Subjected to Earthquake Ground Motions," Report No. EERC 80/07, Earthquake Engineering Research Center, University of California, Berkeley, California, April 1980, 131pp.

58. Zahrah, T. F. and W. J. Hall, "Seismic Energy Absorption in Simple Structures," Civil Engineering Studies, Structural Research Series No. 501, University of Illinois, Urbana, Illinois, July 1982, 207pp.

59. Zeevaert–Wiechers, A. and A. E. Zeevaert–Wolff, "Observations on the September 19, 1985 Earthquake in Mexico City," Earthquake Engineering Research Institute Newsletter, May 1987, Vol. 21, No. 5, pp 1–6.